PICOSECOND EXCITATION AND QUANTUM BEATS OF MOLECULES IN SUPERSONIC MOLECULAR BEAMS

Thesis by

William Roger Lambert

In Partial Fulfillment of the Requirements

for the Degree of

Doctor of Philosophy

California Insititute of Technology

Pasadena, California

1983

(Submitted November 5, 1982)

ACKNOWLEGEMENTS

I would like to thank my research advisor, Professor Ahmed Zewail, and the Caltech community for their encouragement and support during my graduate studies.

This work was supported by the National Science Foundation under grants DMR 8015034 and CHE 8211356.

ABSTRACT

An understanding of the mechanisms responsible for intramolecular vibrational redistribution in polyatomic molecules has important implications for the efficacy of mode selective laser chemistry. In this thesis the application of picosecond laser excitation and supersonic molecular beam techniques to the investigation of the intramolecular dynamics of large polyatomic molecules is presented. Specifically, the first investigations on quantum interference effects observed in the energy and time resolved fluorescence following coherent picosecond laser excitation to intermediate excess energies in the first excited singlet state manifold are reported. The observation of quantum beats in anthracene and trans-stilbene indicates that at moderate excess energies, the effective density of rotational and vibrational states is quasi-discrete, even though the predominant relaxation dynamics reflect properties associated with the statistical limit. The relationship of internal temperatures and vibronic level structure to the quantum beats is investigated. The potential for using quantum interference effects as a probe of intramolecular energy and phase redistribution is emphasized.

The design and construction of a supersonic molecular beam apparatus developed for the application of pulsed picosecond excitation and fluorescence detection are also presented. In as much as the free jet expansion conditions perturb the internal dynamics of the diluent molecules, an understanding of the hydro- and thermodynamics of the expansion is essential. The influence of the expansion conditions on intermolecular collisional processes complex formation, and internal temperatures is discussed with respect to the intramolecular dynamics of anthracene.

TABLE OF CONTENTS

1. *INTRODUCTION*

The subject of intramolecular energy and phase redistribution (IVR) in large polyatomic molecules is of considerable current interest, particularly with respect to the implications for effecting mode selective laser chemistry (1-5). Implicit in developing an understanding of intramolecular dynamics is the description of the nature of the states which are optically prepared, the effective energy level structure, and the mechanisms responsible for intra-state coupling. To a large extent, the investigation of these phenomena in large molecules has been obviated by the rapid time scale on which these processes occur, and upon the spectral congestion arising from the large number of vibrational and rotational states which are populated at finite temperatures. In recent years, considerable progress toward understanding IVR has resulted from the application of laser spectroscopy to supersonic free jet expansion techniques (6,7). Supersonic free jet techniques enable the production of isolated molecules with vibrational and rotational temperatures on the order of 50 °K and 1 °K, respectively, thereby reducing the consequences of spectral congestion. In previous studies, laser excitation has been provided by pulsed YAG and nitrogen pumped dye lasers, the temporal resolution has necessarily been restricted to a time range greater than 5 nanoseconds, and therefore, manifestations of IVR are discussed in terms of spectral features associated with the energy resolved fluorescence and fluorescence excitation spectra.

On the other hand, direct time resolved measurements have been obtained with picosecond laser systems and gas bulb samples (8,9).The general conclusion following from these studies has been that IVR prodeeds on at least a subnanosecond time scale in large polyatomic

molecules. Aside from the inherent time resolution afforded by picosecond laser systems, the nearly transform limited pulse enables the coherent preparation of a well defined spectral bandwidth, thus, the potential for observing coherence effects is apparent.

In view of this background, it has been our intention to extend time resolved laser spectroscopy of supersonic free jet expansions to the picosecond time domain. To this end, the objective of this thesis has been the design and construction of a supersonic free jet apparatus, and application of time resolved picosecond laser excitation to the study of intramolecular energy and phase redistribution of large, isolated polyatomic molecules. Specifically, the work has focused on the investigation of quantum interference effects in the energy and time resolved fluorescence, following coherent picosecond excitation to intermediate excess energies in the first electronic singlet state manifold

With consideration of the precepts of IVR, one would expect to observe the manifestations of specific vibrational redistribution channels in large molecules at intermediate excess energies. Upon excitation to the general region between 500 and 2000 cm^{-1} above the first singlet state, the energy resolved fluorescence is characterized by both relaxed and unrelaxed components. This reflects the fact that specific states are identified by means of the respective dipole matrix elements for emission. In view of the quasi-discrete level structure implied by the resolved fluorescence spectra, the initial preparation of the states is crucial for defining the subsequent redistribution and relaxation. The direct manifestation of IVR would be the observation of multi-exponential relaxation rates, indicative of selective mode redistribution. Nevertheless, despite the fact that within the coherence width and bandwidth of the picosecond

laser excitation a large density of vibrational and rotational states is spanned, quantum interference effects were observed for the first time in large molecule (anthracene and trans-stilbene) in the energy and time resolved fluorescence upon excitation to moderate excess energies in the first excited electronic singlet manifold.

Quantum interference effects are well known in atomic systems (10). Recently, quantum beats have been observed in molecular systems cooled in free jet expansions (11-16). The interference effects in these systems arise from the mixed singlet-triplet and rovibronic character of the molecular eigenstates as confirmed by magnetic field effects on the quantum beat pattern (11). As a consequence, interference effects are observed only at low excess energies, and in the spectrally integrated fluorescence.

At high excess energies the level structure is complicated by the large density of states and upon first consideration one might not expect to observe relaxation properties of specific eigenstates. The observation of quantum beats in anthracene and trans-stilbene on the other hand is restricted to specific laser excitation and fluorescence detection energies. This indicates that at intermediate energies there exist regions in the level stucture where the effective density of states is small whereas the overall density of states reflects properties associated with the statistical limit.

The general design criteria of a supersonic molecular beam apparatus intended for use with a picosecond laser system and time correlated photon counting method of detection are discussed in section 2. The specific features of our particular nozzle, chamber and vacuum design, laser system and electronics are presented in section 4.2.

Efficient signal acquisition in the picosecond time domain is afforded by the high repetition rate, UV doubled cavity dumped picosecond dye laser and sensitive photon counting method of detection. The effectiveness and versatility of the apparatus is attested to by the wide variety of molecular systems and problems in intramolecular energy dynamics which have so far been investigated in this laboratory (11,16,17-21).

Since the present understanding of the mechanisms responsible for cooling the internal degrees of freedom of large polyatomic molecules in free jets, formation of van der Waals complexes and intermolecular dynamics within the isentropic core are not understood in detail, these features must be evaluated before conclusions regarding the intramolecular dynamics can be advanced. Furthermore, since the ground state population of the molecular states are determined by the expansion conditions, changing the carrier gas and backpressure provides a convenient means of modifying the intramolecular vibrational and rotational temperatures. A discussion of these properties is presented in sections 4.4,4.5 and 4.6, specifically with respect to the intramolecular dynamics and coherence effects in anthracene.

The investigation of quantum interference phenomena in anthracene and trans-stilbene is discussed in sections 4 and 5, respectively. Quantum beats not only serve to identify the intermediate level stucture of these molecules, but can serve as a probe of the internal energy and phase dynamics. A fundamental question regarding the observation of quantum beats is the nature of the interfereing states. The projection of a finite number of molecular eigenstates by means of dipole matrix elements has important implications for the efficacy of mode selective laser chemistry. To this end, quantum beats are used to investigate factors which deter-

mine the nature of IVR. A discussion of the current conceptual understanding of IVR in large polyatomic molecules is presented in section 4.7. These perturbations include; 1) the influence of the laser excitation conditions (section 4.9.2), 2) the influence of the conditions for fluorescence detection (section 4.9.2), 3) the effect of vibrational and rotational temperatures on the characteristic relaxation rates (section 4.9.4), and 4) the application of external fields (section 4.10).

Whereas quantum interference effects in anthracene are only observed for a single excitation energy, quantum beats in trans-stilbene are observed in the unrelaxed component of the energy resolved fluorescence for excitation to a number of transitions from 500 to 1200 cm^{-1} of excess vibrational energy in the first excited singlet state. Aside from the widespread distribution of interference effects, a remarkable feature is that, despite the relatively wide excess energy range in which quantum beats appear, the beat frequency remains essentially constant. The interference effects, vibrational spectroscopy and a discussion of possible explanations for the persistence of the beat frequency, particularly with respect to association of the quantum beats with specific vibrational motion,are presented in section 5.

As the seminal investigation of quantum interference effects in large molecules at intermediate excess energies, not only are new features associated with IVR presented, but many new questions are raised. The discussion provided herein should establish a basis for further investigations into the nature of coherence effects in large polyatomic molecules, and their use as a means to probe the dynamics of intramolecular energy and phase redistribution. Furthermore these studies demonstrate the efficacy of using the combination of picosecond excitation and free jet

techniques to the study of the dynamics of intramolecular processes.

REFERENCES

1. K.F. Freed and A. Nitzan, J. Chem. Phys., **73,** 4765 (1980).

2. W. Rhodes, J. Phys. Chem., **86,** 2657 (1982).

3. S. Mukamel and J. Jortner, in *The World of Quantum Chemistry*, ed. R. Daudel and B. Pullman, Reidel, Dordrecht, 1974, p. 145.

4. S.H. Lim, in *Radiationless Transitions*, ed. S.H. Lin, Academic Press, New York, 1980, p. 363.

5. K.F. Freed, in *Radiationless Processes in Condensed Phases*, ed. F.K. Fong, Springer-Verlag, New York, 1976.

6. R.E. Smalley, L. Wharton and D.H. Levy, Acc. Chem. Res., **10,** 139 (1979).

7. D.H. Levy, L/ Wharton and R.E. Smalley, in *Chemical and Biological Applications of Lasers*, V.2, ed. C.B. Moore, Academic Press, San Francisco, 1977.

8. R.C. Sharp, E. Yablonovitch and N. Bloembergen, J. Chem. Phys., **76,** 2147 (1982).

9. N. Halberstadt and A. Tramer, J. Chem. Phys., **73,** 6343 (1980).

10. S. Haroche, in *High Resolution Spectroscopy*, ed. K. Shimoda, Springer-Verlag, New York, 1976.

11. P.M. Felker, W.R. Lambert and A.H. Zewail, Chem. Phys. Lett., **89,** 309 (1982).

12. J. Chaiken, M. Gurnick and J.D. McDonald, J. Chem. Phys., **74,** 106 (1981); Ibid., **74,** 117 (1981); Ibid., **74,** 123 (1981).

13. W. Sharfin, M. Ivanco and S.C. Wallace, J. Chem. Phys., **76,** 2095 (1982).

14. S. Okajima, H. Saigusa and E.C. Lim, J. Chem. Phys., **76,** 2096 (1982).

15. B.J. van der Meer, H. Th. Jonkman, G.M. ter Horst and J. Kommandeur, J. Chem. Phys., **76,** 2099 (1982).

16. W.R. Lambert, P.M. Felker and A.H. Zewail, J. Chem. Phys., **75,** 5958 (1981).

17. W.R. Lambert, P.M. Felker and A.H. Zewail, J. Chem. Phys., **74,** 4732 (1981).

18. P.M. Felker, W.R. Lambert and A.H. Zewail, J. Chem. Phys., **77,** 1603 (1982).

19. J.A. Syage, W.R. Lambert, P.M. Felker, A.H. Zewail and R.M. Hochstrasser, Chem. Phys. Lett., **88,** 266 (1982).

20. P.M. Felker, J.A. Syage, W.R. Lambert and A.H. Zewail, accepted Chem. Phys. Lett.

21. W.R. Lambert, J.W. Perry and A.H. Zewail, to be published.

2. *PICOSECOND LASER SPECTROSCOPY OF FREE JET EXPANSIONS*

§2.1 *Introduction*

During the last several years the combination of supersonic free jet techniques and laser spectroscopy has found wide application for the investigation of electronic and vibrational redistribution in large polyatomic molecules. Whereas intermolecular collisions can be effectively eliminated in well designed gas bulb experiments, thermal congestion prevents the realization of single vibronic level excitation. Thermal congestion becomes a particularly insidious problem when large molecules with low vapor pressures are to be studied, to the extent that quantitative gas bulb experiments are prevented. These difficulties are to a large extent obviated by using supersonic free jet techniques to produce effectively isolated molecules with substantially reduced rotational and vibrational temperatures. It is not unusual to produce expansions of large polyatomic molecules with corresponding vibrational and rotational temperatures of 0.1 °K and 50°K, respectively.

The hydrodynamics and thermodynamics of molecular beam expansions has been the subject of several recent reviews (1,2). Specifically, with regard to the investigation of intramolecular energy and phase dynamics in isolated large molecules it is important to accomplish the maximum degree of cooling of the internal degrees of freedom and to produce mean collision free conditions. As the carrier gas and seed molecule are expanded into a vacuum chamber, collisions transfer energy from the intramolecular degrees of freedom to the translational coordinate. The terminal temperatures are determined by the collisional cross sections for particular intramolecular coordinates and by the

number of collisions which occur before the transition from hydrodynamic to free molecular flow is reached. The number of collisions is in turn proportional to the backpressure of the carrier gas and the diameter of the nozzle orifice (i.e. the molecular density). The limitation imposed upon the degree of cooling is determined by the propensity of the carrier gas to form clusters and to produce condensation complexes with seed molecules. The formation of van der Waals (vdW) complexes is dependent upon the nature of the carrier gas and the seed molecule. In practice, a suitable choice of expansion conditions is empirically determined such that the degree of rotational and vibrational cooling is maximized and the formation of vdW complexes is minimized. Measurement of intramolecular temperature is readily accomplished with high resolution laser absorption (fluorescence excitation) spectroscopy, generally requiring spectral resolution on the order of 0.3 cm^{-1} for large polyatomic molecules. The rotational temperature has been found to closely parallel the translational temperature (3), and therefore, in lieu of direct measurement of the rotational temperature, characteristic rotational temperatures within the expansion can be determined theoretically. In general, expansion conditions can be found which satisfy the requirements of efficient intramolecular cooling.

The determination of the collisional isolation in the expansion, however, is more difficult. Investigators in the field of intramolecular dynamics generally establish the absence of collisions from the lack of collisionally relaxed transitions in the energy resolved fluorescence and by the absence of multiexponential decays. Calculations of the intermolecular collision rate based upon hard sphere cross sections support the absence of collisions on experimentally important time scales. Whereas this

approach is adequate for describing intermolecular dynamics on the nanosecond time scale where conclusions are based upon qualitative features of energy resolved fluorescence spectra and nanosecond decay rates, one can expect subtleties to arise when one probes not only intramolecular energy but also phase dynamics on a picosecond time scale. It is now possible that collision dynamics can no longer be adequately described by the sudden freeze model (1,2). The questions of transverse velocity effects and background gas intrainment are not well understood at the present time and form an active area of current research in rarefied gas dynamics. Furthermore, since exact theories and experimental evidence has been obtained for pure simple gas expansions (1,2), it is probable that these studies have little bearing on the expansion dynamics of large polyatomic molecules. A precise understanding of intermolecular dynamics is requisite for careful studies of intramolecular processes on a subnanosecond time scale. Optimization of expansion conditions, however, is currently largely an empirical process. This will become apparent when we discuss the measurement of the total dephasing time obtained from quantum beat measurements (section 4). One can also envision different molecular subsystems as exhibiting different relaxation rates. In fact, differences in population and dephasing cross sections in free jet expansions have been determined for biacetyl (4) and for anthracene (section 4.9).

§2.2 *Vacuum System*

The design of a supersonic free jet apparatus is established by a number of criteria including; 1) the vacuum system, 2) the excitation source, and 3) the method of detection. Fluorescence detection and mass spectral analysis are the primary detection methods used to

investigate intramolecular dynamics of large polyatomic molecules in molecular beams. Clearly, the incorporation of a mass analyzer requires a differentially pumped vacuum system where pressures on the order of 10^{-8} torr can be achieved in the chamber in which the mass spectrometer is installed (5). In the first chamber a small portion of the expansion is selected by a skimmer, and the subsequent reduction in the transverse velocity component technically establishes the criteria for a supersonic free jet. The design of the system for fluorescence detection, on the other hand, requires only a single expansion chamber. Optimal signal conditions will maximize 1) the molecular density, 2) the solid angle of detection, and 3) the cooling of the intramolecular degrees of freedom on the diluent molecule. Since the maximum cooling conditions as well as the fluorescence signal are determined by the molecular density of the expansion, proportional to the backpressure of the carrier gas times the pinhole diameter, D , the design of the vacuum system should seek to maximize the throughput. It is desirable to use as large a diameter pinhole as possible in order to maximize the intramolecular cooling which is proportional to, $P \times D$, and the expansion density, proportional to, $P \times D^2$.

§2.3 *Design Considerations*

The parameter which one would therefore like to maximize in the design of a vacuum system for purposes of application to free jet expansions is the pumping throughput. The pump throughput can either be defined in terms of the mass flow rate through the intake aperture, $Q = \frac{G}{t}$ (gms/sec), or in terms of the volume, $Q = P + \frac{V}{t}$ (torr-l/sec) where P is the intake pressure of the volume, V. The pumping speed is related to the throughput by $Q = P \times S$. The actual pumping speed is

modified by the intermediate insertion of tubulation, angles, valves, baffles, traps, etc.. The effective pumping speed, S_{eff} is related to S by, $\frac{1}{S_{eff}} = \frac{1}{S} + \frac{1}{L}$ where L is the is the total conductance of the system. The total conductance is determined by the specific values of the individual vacuum components in series;

$$\frac{1}{L} = \frac{1}{L_1} + \frac{1}{L_2} + \ldots\ldots \frac{1}{L_n} \qquad (2.1)$$

The conductance of a vacuum component varies greatly depending upon the flow characteristics (i.e. continuous flow or molecular flow) and therefore on the pressure. Whereas conductances for flow through straight and bent tubulation can be directly calculated, conductances for baffles, cold traps and valves must be determined empirically. Conductances for these components are usually given in the respective technical literature.

The conductance for a straight tube appropriate for laminar, Knudsen, and molecular flow is given by;

$$L = 180\,\frac{d^4}{l}P + 12.1\,\frac{d^3}{l}\,\frac{1 + 256\,d\,P}{1 + 316\,d\,P} \qquad l/sec \qquad (2.2)$$

where d is the inner diameter of the tube in cm, l is the tube length in cm, and $P = \frac{P_1 + P_2}{2}$, the average of the pressures in torr at the tube entrance and exit. Equation 2.2 is exact for $l \geq 10\,d$. In the transition flow regime, $10^{-2} < d\,P < 5\times10^{-1}$ torr-cm, the complete Knudsen formula, equation 2.2 must be used. In the case of laminar flow, ($d \cdot P > 5 \cdot 10^{-1}$ torr-cm), $L = 180 \cdot \frac{d^4}{l}P$, (l/sec), and for molecular flow ($d \cdot P < 1 \cdot 10^{-2}$ torr-cm);

$$L = 12.1 \cdot \frac{d^3}{l} \qquad (l/sec) \qquad (2.3)$$

For short tubular sections;

$$L = \frac{1}{6} 2\pi R \frac{T^{1/2}}{m} \cdot \frac{d^3}{l} \tag{2.4}$$

where T is the source temperature and m is the molecular weight. The conductance of an aperature is calculated in terms of the surface area, F, in (cm^2);

$$L = 76.6 \cdot \delta^{0.712} \cdot (1 - \delta^{0.298})^{1/2} \cdot \frac{F}{1 - \delta} \tag{2.5}$$

where δ is the pressure ratio, $\frac{P_2}{P_1}$. For the case of molecular flow;

$$L = 11.6 \cdot F \qquad (l/sec) \tag{2.6}$$

The above equations are appropriate for air and therefore the general equations should be consulted when operating with other gases (6,7).

The influence of bends in the conductance can be accounted for by considering a greater effective tube length;

$$L_t < L_{eff} < L_t + 2.66 \cdot n \cdot r \tag{2.7}$$

where L_t is the total length of the tube (cm), n is the number of bends, r is the radius of the tube and L_{eff} is the effective tube length. In general, the design of the vacuum system should be such as to make connections as short as possible, minimizing the number of bends, and using tubes which have the same cross section as the inlet of the pump.

In addition to the general design bearing directly upon the pumping requirements on the vacuum system one must also consider the hydrodynamics of the free jet expansion. As the gas expands from a nozzle source, intermolecular collisions cause relaxation of the gas to a local thermodynamic equilibrium state, including both internal degrees of freedom and translational velocity. A point is reached at a distance from

the source where collisions no longer serve to equilibrate the gas thermodynamics and a transition is made from continuum to free molecular flow. This distance, generally termed the freezin distance, is defined by (8);

$$Z_c = \frac{D\cdot(n_s\ Q\ D)^1}{\gamma} = (\frac{D}{\lambda_s})^{\frac{1}{\gamma}} \qquad (2.8)$$

where D is the pinhole diameter, n_s the moleuclar density of the source, Q is the collision cross section for momentum transfer averaged over the Maxwellian velocity distribution, and γ is the heat capacity ratio, $\gamma = \frac{C_p}{C_v}$ of the gas. $\frac{\gamma_s}{D}$ is the Knudsen number. The gas expands freely along collisionless streamlines until background residual gas becomes entrained within the free jet expansion to produce a shock front which disrupts the free molecular flow. The axial shock front, termed the Mach disk appears at a distance empirically determined to be $z_m = \frac{2}{3}D\,(\frac{P_0}{P})^{\frac{1}{2}}$ where P_0 and P are the nozzle and chamber pressures, respectively. Clearly, the degree to which the background gas penetrates the free jet expansion depends upon the reciporical of the chamber pressure. The isentropic core is defined within the confines of the boundaries established by the freezin distance, the Mach disk and the shock structure. This region is pertinent for the purposes of investigating the intramolecular dynamics of internally cooled and isolated molecules. The extent to which the molecules can be considered isolated in this region is of particular relevance and will be discussed later.

In view of the many interrelated parameters associated with the design of a free jet apparatus for fluorescence detection, and the compromises implied therein for achieving a maximally efficient system,

perhaps the best concept of an appropriate design can be accomplished by comparison with similar systems. In this spirit, we present the design of our free jet apparatus and indicate the specific characteristics of its operation.

A 12" diameter stainless steel expansion chamber 36" long was evacuated with a 12" bore ring jet booster diffusion pump (Edwards 18B4A). The diffusion pump has a speed of 4000 l/sec below 10^{-2} torr. The diffusion pump was backed with a 150 cfm roughing pump (Kinney KT150). The 6" diameter PVC roughing line was approximately 20 feet long. In addition to the degree of vibration isolation afforded by the roughing pump, the long roughing line insured that vibrations were not transmitted to the expansion chamber. The expansion chamber was mounted in a horizontal configuration and attached to the diffusion pump by means of a 12" bore, pneumatically actuated right angle-valve (Vac-U-Torr Products). The free jet expansion propagated along the horizontal axis. The chamber pressure was always maintained below 10^{-1} torr in order to minimize back streaming of pump oil and to ensure isentropic expansion characteristics. When the chamber pressure was above 10^{-3} torr, there was evidence for significant intrusion of the shock structure within 5 mm from the source. Adequate expansion conditions were realized with a 45 psi backpressure of nitrogen and a pinhole diameter of 150 microns. The mass flow rate at the aperature given by;

$$J_0 = n_0 V_0 = \left(\frac{2}{\gamma + 1}\right)^{\frac{1}{\gamma - 1}} \left[\frac{2\gamma K T_s}{m(\gamma + 1)}\right]^{\frac{1}{2}} n_s \qquad (2.9)$$

calculated for the indicated conditions is 56 gms/M^2-sec. Converting to units of pressure and volume using $P \cdot V = G \cdot R \cdot \frac{T}{m}$, the nozzle throughput is 1300 torr-l/sec. Visualization of an iodine expansion provided a

convenient method for determining the macroscopic features of the free jet. The observation of individual streamlines resulting from Doppler shifted transitions upon excitation with a single mode (~20 MHz) ring dye laser indicated the long term stability of the expansion. The freezin zone was extimated to be located approximately 1 mm from the nozzle based upon the observation of fluorescence lifetimes indicative of hard sphere collision processes.

§2.4 *Nozzle Design*

The effective pumping speed of a vacuum system can be greatly increased by using a pulsed nozzle source. Endeavors along these lines have generated two principal pulsed nozzle designs, the Gentry-Geise (9,10,11,12) and the solenoid (13,14,15,16) valves. The performance characteristics of the valves are, for a Gentry-Giese: rep. rate = 5 Hz, pulse width = 10 μsec, and for the solenoid valves: rep. rate = 60 Hz pulse width = ~ 300 μsec. Although these valves are routinely used, the present designs intrinsically suggest technical difficulties. It would also seem that by incorporation of moving components in the nozzle throat, that expansion instabilities would be greater than for cw conditions. Nevertheless, in conjunction with the use of low repetition rate nitrogen of YAG pumped dye lasers (40 Hz), the signal will not be compromised and the pumping requirements can greatly be reduced, thereby enabling larger diameter pinholes to be used. Furthermore, the efficient use of heavier gases such as argon at low pressures (~100 torr) have been demonstrated to provide effective cooling of polyatomic molecules (17). A further advantage is the fact that in view of the low duty cycle, valuable samples will not as readily be consumed.

Clearly, for application with high repetition rate picosecond or cw lasers, a continuous nozzle source is indicated. The increased pumping speed required is balanced by the increased signal acquisition efficiency. Aside from being much simpler to design, due to the absence of electrical and dynamic mechanical components, the nozzle can be heated to much higher temperatures. This is especially important for samples with low vapor pressures. We have found that sample vapor pressures on the order of 1 torr are convenient for efficient signal acquisition. The specific design and operation of our cw nozzle is discussed in section 4.2.3.

§2.5 *Internal Cooling*

For the purposes of accomplishing spectroscopy of large polyatomic molecules in free jet expansions it is important to understand the processes which influence the cooling of the intramolecular degrees of freedom and, the intermolecular collisional processes which persist in the region of the isentropic core. Despite the thorough work done by McClelland et al. (3) regarding vibrational and rotational relaxation of iodine in a seeded supersonic beam, the practical choice of experimental conditions for application to other molecules is largely empirical. Current theoretical treatments are generally based upon inert gas expansions, and are therefore adequate for only a cursory understanding of polyatomic molecule free jets. Based upon the numerous moleucles studied in this laboratory, it has been our experience that optimal expansion conditions are highly dependent upon the molecules of interest. In general, however, we have found that the trend (3,18) regarding the vibrational and rotational cooling of large molecules which follows the order; helium < neon < nitrogen < argon, is valid. The converse order indicates the propensity for complex formation. For experimental conditions appropriate

for our free jet apparature (3 atm backpressure, 150 micron diameter pinhole), neon expansions produce the best compromise between efficient internal cooling and the absence of complex formation.

The cooling of the rotational degrees of freedom in polyatomic molecules has been demonstrated to be a very efficient process (3,17,19,20,21) such that for the heavier carrier gases, for example, neon, nitrogen and argon, the rotational temperature is determined by the terminal translational temperature. Assuming for the moment the validity of the sudden freeze model (1,2) wherein the thermodynamic parameters are considered to be defined at the freezin distance (eqn.2.8), the terminal translational temperature is related to the temperature of the source, T_0 and the terminal Mach number by (1,22);

$$T_{trans} = T_0 [\, 1 + \tfrac{1}{2} (\gamma - 1) M_{at}^2 \,]^{-1} \qquad (2.10)$$

where $\gamma = \frac{C_p}{C_v}$ is the specific heat capacity ratio, and, M_{at}, is the terminal Mach number;

$$M_{at} = F(\gamma) \frac{Kn_0}{\varepsilon}^{-\frac{(\gamma - 1)}{\gamma}} \qquad (2.11)$$

defined by the Knudsen number, Kn_0, and the fractional change in the mean random velocity per collision, ε. The Knudsen number, determined by the ratio of the mean free path to the nozzle diameter at the nozzle orifice is defined by;

$$Kn_0 = R \frac{T_0}{P_0 D Q} \qquad (2.12)$$

where T_0 is the source temperature, P_0, is the backpressure of the carrier gas, D is the diameter of the nozzle orifice and Q is the hard sphere collision cross section. The collisional cross section (23), $Q = \pi r_0^2$ where

r_0

is the length parameter in the Lennard-Jones potential, $v(r) = 4\varepsilon\left(\frac{r_0}{r}\right)^{12} - \left(\frac{r_0}{r}\right)^{6}$ for the particular carrier gas can be found in reference 23. $F(\gamma)$ is an empirically determined parameter which depends upon the heat capacity (2);

$$F(\gamma) = 2^{\left(\gamma - \frac{1}{\gamma}\right)} \gamma \left\{ \left[\pi\gamma(\gamma - 1)\right]^{\left(\gamma - \frac{1}{\gamma}\right)} \times \left[\tfrac{1}{2}(\gamma - 1) A^2(\gamma)\right]^{\frac{1}{\gamma}} \right\}^{-\frac{1}{2}} \qquad (2.13)$$

where $A(\gamma)$ is an empirically determined constant (22).

Equations 10-13 are successful in predicting the rotational temperature of diluent molecules in free jet expansions when heavier carrier gases are used (3,17). The initial collisions of the lighter carrier gas serve to accelerate the heavier diluent molecules. At low backing pressures and for lighter carrier gases, the translational velocity will not become equilibrated, and as a result, the local translational temperature will lag behind that of the carrier gas. The rotational temperature will be determined by the local translational temperature. This phenomena has been described as the velocity slip effect (24,25,26) and has been documented for the lighter carrier gases, helium, D_2, and H_2 (2,22).

A description of the vibrational temperature in a free jet expansion is considerably more complicated. In general, the vibrational cooling of polyatomic molecules in free jet expansions is found to be very efficient. Experimental measurements (3) indicate, that in contrast to the conventional Landau-Teller (27) mechanism for describing collisionally induced vibrational relaxation, the vibrational cooling cross section exhibits an inverse temperature dependence. Furthermore, the vibrational relaxation cross sections are too large to reconcile with impulsive collision

potentials. Although the exact mechanisms responsible for the dramatic vibrational cooling are not understood in detail, a number of mechanisms, in addition to hard sphere V-T transfer, have been suggested which involve the formation and dissociation of weakly bound complexes. The low translational temperatures achieved in a free jet expansion favor the formation of weakly bound complexes. Since condensation complexes formed prior to the freezin zone persist within the region of the isentropic core, the translational temperature and hence the vibrational and rotational effective collisional cross section will evolve with the laser to nozzle distance. Therefore, efficient collisional dynamics in the free jet expansion can be rationalized despite the low molecular density. The orbiting resonance complex model (22,28,29,16) has been proposed as contributing to vibrational relaxation. Within the centrifugal barrier, subsequent impact with the repulsive walls redistributes energy among the exit translational and rotational channels of each molecule. An alternative mechanism considers the vibrational predissociation of van der Waals complexes (30,31, 32,33). In essence, the complexes decay by means of vibrational to translational energy transfer, and their longevity indicates their efficiency for inducing relaxation. The observation that complex formation is initiated subsequent to expansion conditions required for efficient vibrational cooling supports the vibrational predissociation mechanism. A final cooling mechanism is possible for polyatomic carrier gases, for example, nitrogen or oxygen. Energy transfer between the diluent and the carrier gas species by means of $V \rightarrow R + T$ and $V \rightarrow V$ mechanisms (27) may contribute to the vibrational relaxation. In this case, not only will the translational exit channel serve as the thermodynamic sink for internal energy relaxation, but the vibrational and rota-

tional degrees of freedom of the polyatomic carrier gas will also participate.

The formation of vdW complexes in free jet expansions not only serve to increase the spectral congestion, but also influence the intramolecular dynamics of large polyatomic molecules. Therefore, for the purposes of investigating IVR in isolated molecules, vdW complex formation is to be avoided and can generally be achieved using appropriate expansion conditions. Since complex formation is perceived as being an extension of the factors which contribute to efficient vibrational relaxation, cooling of the internal degrees of freedom can be achieved in the absence of vdW complexes. Hence, the formation of vdW complexes is favored by high backing pressures and heavy (argon) and polyatomic (nitrogen) carrier gases. Since the formation of complexes requires three body collisions, the condensation occurs during the initial stages of the expansion where the molecular density is greatest and where velocity slip effects are of most significance. Helium is much less likely to form vdW complexes since it is unable to support a stable diatomic complex, and since the velocity slip effect is greatest. VdW complexes are readily distinguished for fluorescence excitation spectra by the appearance of spectral features up to ~350 cm^{-1} to the low energy side of the 0-0 origin. The vdW complexes can exhibit broad (34) or sharp transitions (35), the intensities of which reflect a P^{2n} dependence, where P is the backing pressure and n is the coordination number. As discussed in the previous section, the appropriate choice of the expansion conditions to effect vibrational cooling in the absence of vdW complex formation is dependent upon a number of factors including the pumping system and the particular polyatomic molecule of interest, and hence is a largely empirical decision. Therefore,

prior to any interpretation of intramolecular dynamics, a characterization of the expansion composition is imperative. It has oftentimes proven advantageous to use binary carrier gas mixtures to optimize the expansion conditions. For example, an argon-helium (ratio 20:80) mixture would increase the cooling efficiency while minimizing vdW complex formation.

Provided adequate spectral resolution is available, the direct measurement of the vibrational and rotational temperature from fluorescence excitation can usually be accomplished in a straightforward manner. Accurate rotational temperatures can be determined from comparison of experimental profiles with calculated rotational contours (see section 4.6 and references 20 and 36). Transitions associated with vdW complexes can be most easily distinguished by noting the pressure dependence of the intensities for the fluorescence excitation features in the region of the S_1 origin. Van der Waals complexes generally are found to appear to the red of the 0-0 origin.

§2.6 *Intermolecular Collisions in the Isentropic Core*

The description of the intermolecular dynamics in the region of the isentropic core is essential if one is to understand intramolecular dynamics of polyatomic molecules in free jet expansions. Subsequent to the freezin zone, the gas travels along axial streamlines and further collisions serve to increase the intramolecular temperatures. Since the stream velocity is inconsequential to the argument, the isentropic jet is treated as a bulk gas (2,18,37), such that $z_c = n\,\sigma\,\bar{v}\,(2)^{\frac{1}{2}}\,(1)$. The temperature at a point in the jet is given by (2,37);

$$T = T_0 \left[1 + \tfrac{1}{2}(\gamma - 1)\, M_{eff}^2 \right]^{-1} \qquad (2.14)$$

where γ is the heat capacity ratio $\frac{C_p}{C_v}$, T_0 is the source temperature and M_{eff} is the local Mach number. M_{eff} is dependent upon the distance from the nozzle, x, and has been empirically derived to be (22);

$$M = A\left(\frac{x - x_0}{D}\right)^{\gamma - 1} - \tfrac{1}{2}\left(\frac{\gamma + 1}{\gamma - 1}\right) / A\left(\frac{x - x_0}{D}\right)^{\gamma - 1} \qquad (2.15)$$

x_0 and A are variable parameters which depend upon γ. This equation reduces to;

$$M_{eff} = 3.26\left(\frac{x}{D} - 0.075\right)^{0.67} - 0.61\left(\frac{x}{D} - 1.075\right)^{-0.67} \qquad (2.16)$$

for a monoatomic gas and;

$$M_{eff} = 3.65\left(\frac{x}{D} - 0.4\right)^{0.4} - 0.82\left(\frac{x}{D} - 0.4\right)^{-0.4} \qquad (2.17)$$

for a diatomic gas. In analogous fashion to equation 2.15 the

$$n = n_0\left[1 + \tfrac{1}{2}(\gamma - 1) M_{eff}^2\right]^{\frac{-1}{(\gamma - 1)}} \qquad (2.18)$$

where n_0 is the density of molecules at the source. Combining equations 2.14 and 2.18, the collision rate in the isentropic core is;

$$Z_c = (2)^{\frac{1}{2}} n_0 \sigma \bar{v}_0 \left[1 + \tfrac{1}{2}(\gamma - 1) M_{eff}^2\right]^{\frac{-(\gamma + 1)}{2(\gamma - 1)}} \qquad (2.19)$$

where $\bar{v}_0$ is the mean molecular velocity within the source appropriate for a Maxwellian velocity distribution;

$$\bar{v}_0 = \left(\frac{8 K T}{\pi M}\right)^{\frac{1}{2}} \qquad (2.20)$$

Using a reasonably liberal hard sphere collision cross section of 100 A° and standard expansion conditions ($\frac{x}{D}$=33, T_0 = 450 °K, M_{N_2} = 28, P = 45 psi, γ = 7/5), a collision rate of 10^6 collisions/sec is calculated. Using equation 2.19, and within the limits of one's knowledge of the cross sec-

tion, the approximate collision rate can be calculated in the isentropic core. A realistic estimate for the collisional cross section is complicated by the fact that scattering cross sections generally vary as the inverse power of the initial relative velocity, thereby effectively increasing the collision frequency in a supersonic beam. The calculation of hard sphere collision rates in effusive beams and supersonic beams is discussed in reference 18.

Although concern regarding the extent to which free jet expansions can be considered to exhibit collsion free conditions is generally expressed, the typical approach has been to calculate intermolecular collision rates based upon the previous hydrodynamic equations which have been derived for pure molecular expansions. This may be a reasonable approach when intramolecular dynamics of large polyatomic molecules are to be interpreted by means of general spectral features associated with the energy resolved fluorescence and the excess energy dependence of fluorescence decay rates. However, for high resolution resolved fluorescence, and picosecond time scales, subtle effects of weak collisions in the isentropic core can be expected to become apparent. As discussed in section 4.4, the persistence of collisional effects in a nitrogen-anthracene expansion despite the low molecular density which effectively obviates hard sphere collisional processes indicates that quasi-resonant or vdW complex induced relaxation mechanisms play an important role in modifying intramolecular dynamics. We see that these weak elastic collisions are mediated through interaction with an ensemble of states rather than by means of a specific interaction.

§2.7 Picosecond Laser Spectroscopy of Free Jet Expansions

The application of picosecond laser spectroscopy to free jet expansions has been shown, as a consequence of our studies, to be an efficient means of obtaining both spectrally and temporally resolved spectra by means of fluorescence detection. The relatively low pulse energy of 35 njoules (as compared to the ~50 mjoule pulse energies characteristic of nitrogen and YAG pumped dye laser systems) is compensated by the high repetition rates. The high repetition rates are in turn ideally suited for fluorescence detection by sensitive time correlated single photon counting techniques. The repetition rate of the picosecond system should be variable in order to accomodate the measurement of molecular species with long lifetimes. The high peak powers (~2 KW) of commercial picosecond systems enable efficient second harmonic generation (39) with the use of appropriate frequency doubling crystals (40). Of particular importance to the study of intramolecular dynamics is the near transform limited properties of the picosecond pulse (~0.5 a° bandwidth, 310 psec pulse width) which reflects a coherence width of ~3 cm^{-1}. This property allows the coherent preparation of a spectrally defined set of molecular eigenstates, thereby enabling the investigation of phase redistribution and coherence effects of molecular systems. Although temporal resolution was limited in our experiments by the response time of the photomultiplier tube (~250 psec), the application of pump-probe techniques or streak camera detection is indicated for improved temporal resolution. The details of our picosecond laser system, fluorescence detection and the data acquisition are presented in section 4.2.5..

An additional experimental consideration which was found to have an important influence on our temporal measurements, and which has not

been previously addressed in the literature, is the effect of the expansion propagation perpendicular to the fluorescence collection optics. When the fluorescence is resolved by means of a finite aperture it is important to realize the contribution of the transit time for the fluorescing molecules across the object field. The relative impact of the transit time effect will be determined by a) the slit width, b) the magnification of the imaging system, and c) by the velocity of the molecules in the free jet expansion. The slit width and imaging response remain constant in time while the object defined by the fluorescing molecules is traveling with a perpendicular velocity of $\sim 10^5$ cm/sec. Since our optical system matches f/1 collection optics to an f/6.5 monochromator, the implicit magnification contributes to transit time effects. The result of convoluting the transit time of fluorescing molecules across the object field with the temporal fluorescence relaxation will be manifest as a non-exponential, artificially truncated decay. Although these effects can be eliminated by increasing the slit width spectral resolution is reduced. A more convenient method for minimizing transit time effects is to use heavier carrier gases such as neon or nitrogen. Assuming that the molecules in the beam achieve a velocity commensurate with the terminal expansion velocity given by (41); $V_T = (2\, C_p\, \frac{T_s}{M})^{1/2}$ where C_p is the heat capacity of the expanding gas, T_s is the source temperature, and M is the molecular weight, the velocity is seen to depend upon $M^{-1/2}$. The fluorescence lifetime of anthracene in a free jet expansion varies from 24 - 5 nsec. Whereas helium expansions showed the result of transit time effects, single exponential decays on these time scales could be obtained when lifetime experiments were performed using neon or nitrogen as the carrier gas.

REFERENCES

1. J.B. Anderson, R.P. Anderson and J.B. Fenn, Adv. Chem. Phys., **10,** 275 (1966).

2. J.B. Anderson in *Molecular Beams and Low Density Gas Dynamics*, P.P. Wegener, Ed., Marcel Dekker, New York, 1974.

3. G.M. McClelland, K.L.Saenger, J.J. Valentini and D.R. Hershbach, J. Phys. Chem., **83,** 947 (1979).

4. W. Henke, H.L. Selzle, T.R. Hays, S.H. Lin and E.W. Schlag, Chem. Phys. Lett., **77,** 448 (1981).

5. See for example M.P. Casassa, D.S. Bomse and K.C. Janda, J. Chem. Phys., **74,** 5044 (1981).

6. A. Roth, *Vacuum Technology*, North Holland, New York, 1976.

7. G.L. Weissler and R.W. Carlson, ed., *Vacuum Physics and Technology*, Academic Press, New York, 1979.

8. J.B. Anderson and J.B. Fenn, Phys. Fluids, **8,** 780 (1965).

9. W.R. Gentry and C.F. Giese, Rev. Sci. Instr., **49,** 595 (1978).

10. N. Inoue and T. Uchida, Rev. Sci. Instr., **39,** 1461 (1968).

11. M.G. Liverman, S.M. Beck, D.L. Monts and R.E. Smalley, J. Chem. Phys., **70,** 192 (1979).

12. R.L. Beyer and M.D. Duncan, J. Chem. Phys., **74,** 2174 (1981).

13. F.M. Behlen, N. Mikami, and S.A. Rice, Chem. Phys. Lett., **60,** 364 (1979).

14. C.E. Otis and P.M. Johnson, Rev. Sci. Instr., **51,** 1128 (1980).

15. A. Auerbach and R. McDiarmid, Rev. Sci. Instr., **51,** 1273 (1980).

16. J. Tusa, M. Sulkes and S.A. Rice, J. Chem. Phys., **70,** 3136 (1979).

17. A. Amirav, U. Even and J. Jortner, Chem. Phys., **51,** 31 (1980).

18. D.M. Lubman, C.T. Rettner and R.N. Zare, J. Phys. Chem., **86,** 1129 (1982).

19. S.M. Beck, D.E. Powers, J.B. Hopkins, and R.E. Smalley, J. Chem. Phys., **73,** 2019 (1980).

20. S.M. Beck, M.G. Liverman, D.L. Monts and R.E. Smalley, J. Chem. Phys., **70,** 232 (1979)

21. M. Gurnick, J. Chaiken, T. Benson and J.D. McDonald, J. Chem. Phys., **51,** 31 (1980).

22. H. Ashkenas and F.S. Sherman in *Rarefied Gas Dynamics*, 4^{th} Symposium, Vol. II, J.H. deLeeuw, Ed., Academic Press, New York, 1966, p. 85.

23. J.O. Hirschfelder, C.F. Curtiss and R.B. Bird, *Molecular Theory of Gases and Liquids*, Wiley, New York, 1954.

24. R. Camparque and J.P. Breton, Entropie, **42,** 18 (1971).

25. N. Abauf, J.B. Fenn and D.R. Miller, Rarefied Gas Dynamics, **5,** 1317 (1967).

26. R.A. Larsen, S.K. Neoh and D.R. Herschbach, Rev. Sci. Instr., **45,** 1511 (1974).

27. See for example J.D. Lambert, *Vibrational and Rotational Relaxation in Gases*, Clarendon Press, Oxford, 1977.

28. D.A. Micha, Phys. Rev., **162,** 88 (1967).

29. W. Sharfin, K.E. Johnson, L. Wharton and D.H. Levy, J. Chem. Phys. **71,** 1292 (1979).

30. G. Ewing, Chem. Phys., **29,** 253 (1978).

31. J.A. Beswick and J. Jortner, J. Chem. Phys., **69,** 512 (1978).

32. J.A. Beswick and J. Jortner, J. Chem. Phys., **74,** 6725 (1981).

33. J.A. Beswick and J. Jortner, Adv. Chem. Phys., **48,** 323 (1981).

34. T.R. Hays , W. Henke, H.L. Selzle and E.W. Schlag, Chem. Phys. Lett., **77,** 19 (1981).

35. D.H. Levy, Adv. Chem. Phys., **48,** 323 (1981).

36. W.E. Howard and E.W. Schlag, in *Radiationless Transitions*, Academic Press, New York, 1980, p. 81.

37. A. Kantrowitz and J. Grey, Rev. Sci. Instr., **22,** 328 (1951).

38. R.E. Smalley, L. Wharton and D.H. Levy, Acc. Chem. Res., **10,** 139 (1977).

39. A. Yariv, *Quantum Electronics*, Wiley and Sons, New York, 1975, p. 421.

40. Cleveland Crystals product literature.

41. L.D. Landau and E.M. Lifshitz, *Fluid Mechanics*, Pergammon, New York, 1959.

3. *FLUORESCENCE EXCITATION AND SINGLE VIBRONIC LEVEL FLUORESCENCE SPECTRA FOR THE $^1B_{2u}$+ STATE OF ANTHRACENE AND DEUTERATED ANTHRACENES IN FREE JET EXPANSIONS*

Abstract

Fluorescence excitation and frequency resolved fluorescence spectra of the $^1B_{2u}$ state of h_{10}-; 9-d_1- ; 9,10-d_2- and d_{10}-anthracene cooled in a supersonic free jet expansion are presented. The vibrational assignments for the ground and first excited singlet states are compared with previous experimental and theoretical results. Emphasis is placed upon the interpretation of the vibrations appearing around 1400 cm^{-1} of excess vibrational energy in the first excited singlet state where substantial vibronic coupling is apparent. In addition, the high resolution resolved fluorescence spectra reveal the presence of many transitions corresponding to the b_{1u} and b_{2u} symmetry species.

§3.1 *Introduction*

The study of large, isolated molecules in supersonic free jet expansions has revealed many new and important features of intramolecular vibrational redistribution processes. Among these studies, we have presented in a recent communication preliminary work on quantum beats in anthracene (1). For this molecule, quantum beats were observed upon picosecond laser excitation to 1380 ± 5 cm^{-1} of excess energy in the first excited electronic $^1B_{2u}$, singlet state for a number of transitions in the energy resolved fluorescence. A fundamental question arising from this work is the physical or quantum mechanical nature of the interacting states which are responsible for the appearance of this interference phenomenon. As an initial step toward understanding vibronic coupling in anthracene upon excitation to intermediate excess energies, as will be discussed in a subsequent paper, it is important to know the vibrational structure in both the ground and the excited electronic states as well as the relative Franck-Condon factors associated with the absorption and emission processes for specific vibrational modes in anthracene.

Although high resolution absorption and emission spectra have previously been obtained for h_{10}- and d_{10}- anthracene in mixed crystals (2-5) and in Shpolskii matrices (3), much of the inherent structure is masked by phonon coupling, and in the former case, especially by the presence of multiple lattice sites. Furthermore, the apparent Franck-Condon factors are likely to be perturbed by interactions with the matrix. The use of free jet techniques eliminates these problems, enabling the observation of much greater spectral detail as has been demonstrated in the case of, for example, naphthalene, by Smalley and coworkers (6). The ground state vibrational frequencies obtained by us for h_{10}- and d_{10}- anthracene com-

pare favorably with experimental results and calculated values based upon normal coordinate force field analysis.

In contrast, there is little information regarding the excited state vibrational frequencies in anthracene to be found in the literature. The best absorption spectra have been obtained in cryogenic matrices and reflect the inherent limitations of this technique, while there is an abscence of theoretical treatments of excited state vibrational frequencies. Furthermore, there is no experimental information on the vibrational analysis of the partially deuterated anthracenes. In this regard, an understanding of the influence of partial deuteration, specifically in the 9-d_1- and 9,10 d_2- positions would provide information on the influence of slight perturbations upon the vibrational properties of the isolated molecule.

In this paper we present a vibrational analysis for the ground and excited states of h_{10}-anthracene based upon fluorescence excitation and resolved fluorescence spectra obtained using free jet techniques. In addition we also present an analysis of the vibrational spectroscopy of the isotopic derivatives; 9-d_1- ; 9,10 d_2-, and d_{10}-anthracene.

§3.2 *Experimental*

The complete details of the experimental apparatus will be deferred to a subsequent publication (7) and therefore will only be outlined here. The free jet was created by passing 45 psi of an inert carrier gas over anthracene heated to 150 °C, and expanding the gas through a 150 micron pinhole into a vacuum chamber at 10^{-4} torr. Nitrogen was used as the carrier gas for the experiments reported in this paper. There was no change in the measured vibrational frequencies when either helium or neon was used, although, small differences in the relative Franck-Condon

factors were observed in the resolved fluorescence spectra. For example, the ratio of the 0-0 to the 1400 cm^{-1} mode was 2.0 and 1.6 when helium or nitrogen , respectively, was used as a carrier gas. For the fluorescence excitation spectra, there was no dependence in the calculated frequencies or relative amplitudes upon the nature or the pressure of the carrier gas (15-45 psi).

The focused laser beam crossed the free jet 5 mm from the pinhole. The fluorescence was collected with f/1 imaging optics, passed through a microprocessor controlled monochromator (dispersion 16 A°/mm) and focused onto a photon counting photomultiplier tube. Data was acquired on a multichannel scalar prior to transfer to a PDP 11/23 computer for analysis. Vacuum corrections have not been made and would result in a relative difference of only 1 cm^{-1} over the 3000 cm^{-1} range covered by the reported spectra. Vacuum correction would also result in an absolute shift of 7.5 cm^{-1} to lower energy for the reported origins.

Laser excitation was provided by a synchronously pumped mode-locked cavity dumped picosecond dye laser. The output pulses were frequency doubled with a 1 cm thick lithium iodate crystal. An intracavity 2-plate birefringent filter established a 2 A° laser bandwidth in the ultraviolet.

In order to obtain the resolved fluorescence spectra, the laser wavelength was tuned to the origin of the first excited singlet state of anthracene (3611.8 ± 0.3 A°, h_{10}-) and the fluorescence was resolved with 1 cm^{-1} resolution (2 micron slitwidth). To acquire fluorescence excitation spectra, the front slit was opened to 1 mm and the rear slit assembly was removed from the monochromator housing thereby producing an effective bandwidth of approximately 500 A° for fluorescence collection.

The laser was tuned manually by means of a micrometer drive attached to the birefringent filter. The standard micrometer was replaced with a 2 inch micrometer head with ten-thousandths of an inch gradations in order to enable accurate and reproducible step adjustments. The laser was tuned in 0.4 A° increments and the wavelength in the UV was noted every 15 steps in order to eliminate any major nonlinearity resulting from the tuning procedure. The phase matching angle of the lithium iodate frequency doubling crystal was adjusted to maximize the photon counting rate at each step. Peak heights of the spectra were measured to be reproducible to within 0.4 A°. The resolution of the fluorescence excitation spectra was therefore determined by the 2 A° laser bandwidth in the UV. The fluorescence excitation spectra have not been normalized for the laser power.

Fluorescence excitation spectra were also obtained for h_{10}-anthracene using a frequency doubled nitrogen pumped scanning dye laser. The dye laser output was frequency doubled with a phase matched, 1 cm^3 KDP crystal. The laser bandwidth was approximately 0.03 A°. The absolute laser wavelength was calibrated using the optogalvanic method (8).

H_{10}-anthracene (Aldrich) and d_{10}-anthracene (Aldrich) were zone refined (100 passes) prior to use. 9-d_1-anthracene and 9,10 d_2-anthracene were synthesized by acid-catalyzed deuterium-hydrogen exchange (9) from the respective brominated precursors: 9-bromoanthracene (Aldrich) and 9,10-dibromoanthracene (Kodak). Purification was accomplished upon repeated recrystallization from $CHCl_3$. The isotopic purity was determined by mass spectral analysis to be >95% .

§3.3 *Results*

3.3.1 Resolved Fluorescence- Ground State Vibrational Frequencies

Figures 1 and 2 present the frequency resolved fluorescence spectra for anthracene and the deuterated species upon excitation to the zero vibrational level of the $^1B_{2u}$+ excited state. The $^1B_{2u}$+ symmetry designation for the first excited singlet state of anthracene is appropriate for polarization along the short molecular axis (2,3) using Parsier's (10) notation. The spectra are dominated by progressions of the nine a_g fundamentals below 2000 cm^{-1}, although other planar vibrations belonging to b_{3g}, b_{1u} and b_{2u} symmetries also appear, but with less intensity. Strong progressions of the 1100 cm^{-1}, 1200 cm^{-1}, 1400 cm^{-1} and 1560 cm^{-1} vibrations appear, as well as the respective combination bands with the low frequency 390 cm^{-1} and 750 cm^{-1} vibrations. In tables 1-4, the vibrational frequencies obtained from our spectra are compared to both experimental and calculated frequencies. Assignments for the ground state vibrations were made on the basis of relative intensities, ability to form combination bands, and on comparison with published results. For h_{10}- and d_{10}-anthracene, the calculated frequencies agree very well with those measured from our spectra and assignments could be made with confidence. We have included assignments for strong combination bands based upon consideration of reasonable Franck-Condon progressions. In addition, we have included multiple assignments for some transitions where a definite assignment was ambiguous.

Except for a theoretical treatment of 9,10-d_1-anthracene (11), there is no documentation for the vibrational analysis of the partially deuterated anthracenes. Assignments for the a_g and b_{3g} modes were there-

fore based upon correlation with the frequencies and relative intensities for h_{10}- and d_{10}-anthracene. Table 5 presents a direct comparison of the a_g and b_{3g} vibrational frequencies for the isotopic anthracenes studied. With the exception of the vibrations corresponding to the b_{3g}, h_{10}-, 1100 cm^{-1} mode, all fundamental vibrations could be accounted for. Despite the reduction in symmetry of 9,d_1-anthracene from D_{2h} to C_s, the differences in frequencies compared with h_{10}-anthracene are only very slight, and nearly identical for the a_g symmetry group. As expected, upon deuterium substitution the vibrational frequencies for d_{10}-anthracene are substantially less than those of analogous vibrations in the fully protonated species. The difference is most notable for those modes which involve in-plane C-C-D bending motions. For reference, the vibrational mode classifications based upon potential energy distribution analysis (12) are given in the margins of table 5.

§3.3.2 *Fluorescence Excitation Spectra - Excited State Vibrational Frequencies*

Medium resolution fluorescence excitation spectra for anthracene and the deuterated species are presented in figure 3. As in the case for the resolved fluorescence, the spectra are dominated by the a_g and b_{3g} fundamentals and combinations thereof. However, there is a substantial difference in the relative intensities for transitions around 1400 cm^{-1} of excess energy for the different isotopic species. The unresolved background which appears at higher energies (>1000 cm^{-1}) is probably due to congestion resulting from overlapping resonances and the result of the wide excitation bandwidth. That the unresolved structure is not due to a substantial ground state population is supported by the 130:1 ratio of the 0-0 to hotband intensities for h_{10}-anthracene which corresponds to a

vibrational temperature of approximately 15 °K. The excitation spectra of d_1-anthracene, d_2-anthracene and d_{10}-anthracene exhibit spectral features which can be associated with incomplete deuteration and appear to the red of the origin and the 390 cm^{-1} transition. These features are most obvious in the hotband region and should only contribute to the unresolved background at higher excess energies.

Tabulation of the transition frequencies appearing in the fluorescence excitation spectra and the vibrational assignments for h10-; 9,d_1-; 9,10 d_2- and d_{10}-anthracene are presented in tables 6-8. Assignments for h_{10}- and d_{10}-anthracene were made by comparison with previous mixed crystal and Shpolskii matrix work (2,3). In view of the slight difference between the ground and the excited state vibrational frequencies for the dominant a_g vibrations, prominent transitions which could not be associated with combination bands were assigned as a_g and b_{3g} fundamentals. Based upon the similarity of the ground state frequencies for h_{10}-, d_1- and d_2-anthracene vibrations, assignments for the excited state vibrations of the deuterated species were made by comparing the frequencies and the relative intensities. A direct comparison of the excited state vibrational frequencies for the a_g and b_{3g} fundamentals is presented in table 9. It is likely that the 1286 cm^{-1}, a_g, transition in h_{10}-anthracene represents a vibrational fundamental from both the a_g and the b_{3g} symmetry groups. In the region around 1400 cm^{-1} there are a number of vibrations which do not directly correlate with the ground state frequencies, specifically, the 1373 cm^{-1} ground state vibration of h_{10}-anthracene. It appears that in this region, modes with b_{1u} and b_{2u} symmetries can gain appreciable oscillator strength in absorption by coupling with the strongly optically active a_g vibrations. Partial substitution at the 9 and 10

positions fails to significantly influence the vibrational frequencies as witnessed by comparing the results for h_{10}-, d_1- and d_2- anthracene. However, as is the case for the ground state frequencies, those vibrations which involve C-C-D bending motion are most influenced by total deuterium substitution. The b_{3g}, d_{10}-, 785, 822, and 902 cm^{-1} modes are influenced to the greatest extent. The large deuterium substitution effect for these specific vibrations implies that the corresponding motions involve considerable movement of the outer rings. This interpretation is supported by normal coordinate analysis (for example see reference 12).

§3.4 *Discussion*

The ground state symmetry of anthracene is D_{2h}. The symmetry is defined such that the *Z* axis is established perpendicular to the molecular plane and the *X* direction lies along the long molecular axis. Using this designation, the first excited singlet state is identified with $^1B_{2u}$+ symmetry (10). The normal vibrations are then distributed among the symmetry species according to : 12 a_g, 11 b_{3g}, 11 b_{1u}, 11 b_{2u}, 4 b_{1g}, 6 b_{3u}, 5 a_u. The a_g, b_{3g}, b_{1u}, and b_{2u} vibrations correspond to in-plane vibrations and are Raman and optically active (13), while the b_{1g}, b_{2g}, and b_{3u} vibrations are associated with out-of-plane motion and are infrared active(14). Based upon normal coordinate analysis, Ohno (12) has discussed the motional characteristics of the ground state vibrations for h_{10}- and d_{10}- anthracene. Using potential energy distribution analysis, the planar vibrations were classified according to the degree of C-H stretching, C-C stretching, C-C-H bending and C-H bending. Collective motion in benzoid rings can be classified further, the most important for our purposes being the designation of a Kekule' type C-C stretching motion wherein bond extension and compression alternates on adjacent

bonds. As will be discussed, vibrations corresponding to these motions are the most active accepting modes, and appear in the region around 1400 cm^{-1} of excess energy.

In both the absorption and emission spectra we observe vibrations which are associated with a_g and b_{3g} symmetry, and with less intensity, vibrations corresponding to b_{1u} and b_{2u} symmetries. These symmetry groups represent only planar vibrations. For strict D_{2h} symmetry of the excited state suface only, the a_g, b_{3g}, and b_{1g} vibrations should exhibit oscillator strength in electronic transitions. Whereas the non-planar vibrations of the b_{1g} group have not been identified in either our electronic spectra or those of other investigators, we can identify vibrations belonging to the b_{1u} and b_{2u} symmetry species, especially in the resolved fluorescence spectra. Therefore, it appears that the extent of the in-plane character of the vibrations dominates the degree of optical activity. In addition, we have already noted the near identity of both the vibrational frequencies and the relative intensities for h_{10}-anthracene and 9,d_1-anthracene, which further implies that characteristics of D_{2h} symmetry are not rigorously in force with regard to determining electronic optical activity. Since the $^1B_{2u}$ state is the lowest energy optically allowed singlet state (10,15), it is not likely that coupling with nearby electronic states is responsible for the breakdown of the symmetry rules as is the case for naphthalene (16).

For D_{2h} symmetry, vibronic transitions to the $^1B_{2u}$+ singlet state should rigorously be polarized according to B_{1u}, B_{2u} and B_{3u} transition moments. In absorption, therefore, one expects to observe vibronic transitions to a_g, b_{3g}, and b_{1g} modes. Whereas transitions to a_g and b_{3g} vibrational states are observed for our spectra, b_{1g} states are not

observed. In addition, almost all vibrations corresponding to b_{2u} and b_{3u} symmetry appear, albeit with weak intensity, in the fluorescence excitation spectra. The absence of b_{1g} vibrations indicates a distortion of the excited state electronic surface with respect to that of the ground state, while the oscillator strength exhibited by the b_{1u} and b_{2u} vibrations suggests the consequences of vibronic coupling. Upon excitation to the $^1B_{2u}$+ origin, energy resolved emission is primarily to modes of a_g symmetry, and with less intensity to b_{3g} vibrations. The dominant emission to a_g vibrations is anticipated considering the polarization determined by the B_{2u} electronic transition moment. Clearly, distortion of the excited state surface enables optical activity of the b_{3g} modes. Calculations (17,18) confirm that the fluorescence Franck-Condon factors of the b_{3g} modes are roughly one tenth that of the a_g vibrations. The optical activity of only planar modes in absorption and emission indicates that the type of bond motion is more important than symmetry in determining the radiative properties.

The general vibrational structure in both the ground and excited states of anthracene is characterized by combination bands of 390 cm^{-1} and 750 cm^{-1} built upon strong fundamentals at 1160 cm^{-1}, 1400 cm^{-1} and 1560 cm^{-1}. A major difference between the absorption and emission spectra is the greater intensity of the 1260 cm^{-1} (h_{10}-anthracene) mode in the resolved fluorescence. Whereas the overall vibrational structure of the resolved fluorescence for the various species is very similar in frequency and relative intensity (figure 1), there is a much larger difference in the overall characteristics of the fluorescence excitation spectra (figure 3), most notably in the relative intensities of the transitions around 1400 cm^{-1} for d_2- and d_{10}- anthracene. Corresponding differences

have been documented for 9-methylanthracene and 9,10-dimethylanthracene in Shpolskii matrices (19,20). In comparison with our fluorescence excitation spectra, the spectra of anthracene and 9-methylanthracene are very similar despite the reduction in symmetry imposed by the unsymmetrical methyl substitution. For 9,10-dimethylanthracene, however, the relative intensities of the 1460 cm^{-1} and 1500 cm^{-1} transitions become substantially reduced in comparison with the intensities of other transitions.

The fact that the ground and excited state vibrational frequencies are nearly identical implies that the corresponding potential energy surfaces are similar. For an effectively isolated molecule such as is produced in a free jet expansion, and in the absence of vibronic coupling and mode dependent nonradiative relaxation channels, one expects the Franck-Condon factors for the absorption and emisssion in a small energy region to be similar. The dramatic difference in the amplitudes of vibrational modes in the region of S_1+1400 cm^{-1} for absorption and emission is shown in figure 5. The assignments for the spectral features are given in table 10. The difference is seen to be most dramatic for the 1382 cm^{-1} mode. Although the main spectral features correspond to strongly optically active a_g and b_{3g} vibrations, several other fundamental and combination bands exhibit appreciable oscillator strength. As mentioned previously, many vibrations which appear in this region of the spectrum correspond to b_{1u} and b_{2u} fundamentals as well as combination bands. The anomalous intensities present a difficulty with regard to establishing vibrational assignments for the transitions. Our designation of the 1414 cm^{-1} mode as an a_g fundamental is based upon the following considerations. Table 1 indicates that the major progressions which appear in the

energy resolved fluorescence spectrum for h_{10}-anthracene are composed of a_g vibrations. It is therefore appropriate to assign the major transition at 1414 cm^{-1} as an a_g fundamental (figure 4). Comparison of the ground and excited state vibrational frequencies, Tables 5 and 10, show that the ground state frequencies of a_g fundamentals are less than the excited state frequencies by approximately 0-20 cm^{-1}. Assigning the excited state vibration which appears at 1382 cm^{-1} as an a_g fundamental (corresponding to the ground state frequency of 1414 cm^{-1}) would be in contradiction to the general expectation of higher excited state vibrational frequencies for large polyatomic molecules (21). The apparently low excited state oscillator strength of the 1414 cm^{-1} a_g fundamental is perhaps the result of dilution by means of Fermi resonance interaction with the b_{2u} fundamental at 11402 cm^{-1}, and various combination bands which appear in this region (figure 4), particularly the (385 + 1022) cm^{-1} band at 1421 cm^{-1}. Many combination bands in this region appear to be associated with a_g, b_{3g} and b_{2u} fundamentals of ~1175 cm^{-1} and the 237 cm^{-1} b_{1u} vibration. The large difference between the absorption and emission Franck-Condon factors for the 1380 cm^{-1} b_{3g} mode is a consequence of the different symmetries of the transition moments for absorption and emission (from the $^1B_{2u}$+ origin). The fact that the 1380 cm^{-1} vibration appears strongly in absorption but only weakly in fluorescence supports its assignment as a b_{3g} mode.

Table 10 presents a comparison of the vibrations in the region around 1400 cm^{-1} in both the ground and excited electronic states for the isotopic anthracenes. Corresponding assignments obtained from reference 12 have been included. A predominant feature of the vibrations at 1400 cm^{-1} of excess energy is the Kekule' type C-C stretching motion which charac-

terizes these modes (12). Kekule' type vibrations are indicated by symmetric in-plane C-C stretching motions such that extension and compression alternates between adjacent bonds. This motion tends to localize between electrons on specific C-C bonds, and consequently a modification in the resonance energies results. The corresponding change in electronic structure for these modes may explain the fact that the most active accepting modes found in the electronic spectra of polyacences occur at about 1400 cm^{-1}.

As in other regions of the spectra, we expect the a_g and b_{3g} vibrations to exhibit the largest oscillator strength. Considering first the resolved fluorescence spectra for h_{10}-anthracene we note that a single b_{1u} and two b_{2u} vibrations have substantial intensity. It is likely that the vibrations at 1402 cm^{-1} (b_{2u}, CC-K) and 1429 cm^{-1} (b_{1u}, CC-CCH-D) gain strength through coupling with the dominant 1414 cm^{-1} (a_g, CC-K) mode due to the similar nature of the motions involved. The frequencies and intensities of the six transitions noted here are very similar for h_{10}-, d_1- and d_2-anthracene, however, the frequencies are shifted to lower energy as anticipated for a deuterium isotope effect and as was observed for the ground state vibrations, such that the three peaks between 1397-1429 cm^{-1} are then observed as two peaks at 1384 cm^{-1} (b_{2u}, CC-K) and 1390 cm^{-1} (a_g, CC-K). The b_{2u}, b_{3g} and b_{1u} modes are probably shifted to lower energy as they involve C-C-H bending motion which is more susceptible to an isotope effect, and hence, no longer appear in this energy region. Likewise, other h_{10}-anthracene vibrations involving C-C-H bending motions are shifted to lower energy such that the 1345 cm^{-1} (b_{2u}, CCH-CC_K) and 1379 cm^{-1} (b_{3g}, CCH) vibrations are not observed within this energy region for d_{10}-anthracene. Other vibrations however, are shifted

into the energy region around 1400 cm^{-1} upon complete deuteration. These include the d_{10}- vibrations corresponding to 1421 cm^{-1} (CC_K, a_g), 1413 cm^{-1} (CC-D, b_{1u}) and 1405 cm^{-1} (b_{2u}, CC-K), the latter vibration gaining oscillator strength through coupling with the intense 1390 cm^{-1} vibration. Again, the 1405 cm^{-1} and 1390 cm^{-1} vibrations involve the same CC, Kekule' type stretching motion, thereby providing a mechanism for vibronic coupling.

Based upon the fact that the vibrational frequencies in the ground and excited states are nearly identical for h_{10}-anthracene, the excited state vibrations which appear around 1400 cm^{-1} for the deuterated species can be assigned with some degree of confidence. The analysis is presented in table 10. As anticipated, based upon symmetry arguments, the intense transitions at 1398-1410 cm^{-1} and 1492-1499 cm^{-1} are associated with totally symmetric a_g motions. Vibrations corresponding to b_{3g}, b_{1u} and b_{2u} symmetries can also be designated. As was the case for the ground state frequencies, the excited state vibrational frequencies and relative intensities for the d_1- and d_2- derivatives are the same as for h_{10}-anthracene. Complete deuteration shifts the vibrational frequences to lower energy by approxiamtely 50 cm^{-1} such that the totally symmetric vibrations subsequently appear at 1368-1374 cm^{-1} and at 1438 cm^{-1}, respectively.

The vibration which appears at 1379 cm^{-1} in the fluorescence excitation spectra of h_{10}-anthracene exhibits an anomalously large intensity when compared to mixed crystal and Shpolskii matrix work (2,3). On the basis of force field calculations (12), this vibration should be designated as a C-C-H bending mode with b_{3g} symmetry. Small(2) assigned the vibrational band at 1394-1396 cm^{-1} as a b_{3g} fundamental because it was polar-

ized more strongly along the *a'* rather than the *b* axis when anthracene was incorporated into a p-terphenyl matrix. However, a corresponding polarization dependence was not found for the 1399 cm^{-1} and 1374 cm^{-1} vibrations of anthracene in either fluorene or n-heptane matrices as reported by Bree and Katagiri (3). The 1374 cm^{-1} vibration was consequently assigned to an unspecified combination band by these authors. Bree et al. (4) have interpreted the complicated structure which appears in the absorption spectrum of d_{10}-anthracene near 1400 cm^{-1} in terms of strong vibrational interactions and Fermi resonances. These discrepancies emphasize the point that matrix interactions can substantially influence the relative intensities of specific vibrational symmetries of the impurity molecule. It is well documented however, that vibrational frequencies obtained using low temperature matrices agree very well with those determined from corresponding studies done in the gas phase. With further reference to the b_{3g} vibration at 1379 cm^{-1}, it is interesting to note that the vibration is ascribed to a C-C-H bending motion similar to that of the 1265 cm^{-1} vibration which reflects large amplitude in-plane motions of the protons on the outer rings, and which exhibits a weak emission Franck-Condon factor(12). It is reasonable to presume that this type of large amplitude peripheral vibration would be substantially influenced, and even inhibited by matrix interaction.

§3.5 *Conclusion*

In this paper we have presented the resolved fluorescence and the fluorescence excitation spectra of the $^1B_{2u} \leftarrow {}^1A_{1g}$ transition for h_{10}-; 9,d_1-; 9,10 d_2- and d_{10}-anthracene in a free jet expansion. This technique has enabled us to determine the vibrational structure of these molecules in much greater detail than has previously been reported. Assignments

for the ground and excited state vibrations have been based upon comparison with previous theoretical and experimental work. In the case of the vibrational assignments for h_{10}-anthracene and d_{10}-anthracene, the agreement is excellent. We have also presented the spectra and assignments for the partially deuterated species, 9,d_1-anthracene and 9,10 d_2-anthracene. The availability of high resolution spectra of isolated molecules obtained using free jet techniques should enable accurate force field calculations to be performed for the ground state vibrations of these molecules. Furthermore, the presentation of the excited state vibrational frequencies should provide a basis for theoretical modeling of the excited state electronic surface. It is clear from our results that the vibronic coupling in even a relatively structurally simple molecule such as anthracene is quite complicated. Symmetry considerations alone are insufficient to develop more than a qualitative interpretation of the overall vibrational structure for transitions to the first excited singlet state of anthracene.

This discussion of the vibronic spectroscopy of anthracene and the deuterated derivatives will be valuable in understanding vibronic relaxation properties at excess energies as obtained from resolved fluorescence spectra. As has been exemplified by the work of Smalley et al. (6), analysis of the resolved fluorescence as a function of excess excitation energy can reveal properties of intramolecular relaxation processes including vibrational redistribution rates. Details of our work on the lifetimes and excess energy dependence of the resolved fluorescence of h_{10}-; 9,d_1-; 9,10 d_2-; and d_{10}-anthracene as a function of excess vibrational energy will be presented in a subsequent publication (22).

Our recent observation of quantum beats in h_{10}-anthracene implies

the existence of specific intramoleuclar vibronic interactions at intermediate excess energies (1). With reference to the spectra presented in this paper the excess energy of excitation for which beats were observed was 1380 ± 5 cm^{-1} and corresponds to the energy of the strongly optically active b_{3g} mode. The fact that the b_{3g} vibrations have a much larger relative Franck-Condon factor for absorption as compared to emission may be a diagnostic for locating other transitions which exhibit quantum interference effects. The extent to which the adjacent vibrations are simultaneously excited by the laser bandwidth will be discussed in a forthcoming publication where the specific effects of laser excitation bandwidth, and laser excitation frequency on the interference pattern will be discussed (23). A major question arising form the observation of quantum beats in a large molecule such as anthracene, is the nature of the eigenstates responsible for the interference effect and the mechanism(s) responsible for the mode selective interference which the presence of beats at such high excess energies implies. This discussion of the vibrational properties of h_{10}-anthracene and the deuterated anthracenes will be an essential reference in developing an understanding of this manifestation of vibrational/rotational interaction.

REFERENCES

1. W.R. Lambert, P.M. Felker and A.H. Zewail, J. Chem. Phys., **75,** 5958 (1981).

2. G.J. Small, J. Chem. Phys., **52,** 656 (1970).

3. A.V. Bree and S. Katagiri, J. Mol. Spectrosc., **17,** 24 (1965).

4. A. Bree, S. Katagiri, and S.R. Stuart, J. Chem. Phys., **44,** 1788 (1966).

5. N. Kesri and R. Ostertag, Chem. Phys. Lett., **39,** 431 (1976).

6. S.M. Beck, D.E. Powers, J.B. Hopkins and R.E. Smalley, J. Chem. Phys., **73,** 2019 (1980); S.M. Beck, J.B. Hopkins, D.E. Powers and R.E. Smalley, J. Chem. Phys., **74,** 43 (1981).

7. W.R. Lambert, P.M. Felker and A.H. Zewail, to be submitted.

8. E.F. Zalewski, R.A. Keller and R. Engleman, Jr., J. Chem. Phys., **70,** 1015 (1979), and references therein.

9. J.L. Charlton and R. Agagnier, Can. J. Chem., **51,** 1852 (1973).

10. P. Parsier, J. Chem. Phys., **24** 24, 250 (1956).

11. B.N. Cyvin and S.J. Cyvin, J.Phys. Chem., **73,** 1430 (1969).

12. K. Ohno, J. Mol Spectrosc., **77,** 329 (1979).

13. A. Bakke, B.N. Cyvin, J.C. Whitmer, S.J. Cyvin, J.E. Gustavsen and P. Klaeboe, Z. Naturforsch., **34A,** 579 (1979).

14. G. Neerland, B.N. Cyvin, J. Brunvoll, S.J. Cyvin and P. Klaeboe, Z. Naturforsch., **35A,** 1390 (1980).

15. J.W. Sidman, J. Chem. Phys., **25,** 115 (1956).

16. For example, M.J. Robey, I.G. Ross, R.V. Southwood-Jones and S.J. Strickler, Chem. Phys., **23,** 207 (1977), and references therein.

17. K. Ohno, Chem. Phys. Lett., **70,** 526 (1980).

18. K. Ohno, Chem. Phys. Lett., **53,** 571 (1978).

19. Ch. Jung, A. Kawski and M.I. Zukowska, Z. Naturforsch., **34A** 105 (1979).

20. Ch. Jung, A. Kawski and M.I. Zukowska, Z. Naturforsch., **34A** 557 (1979).

21. G. Herzberg, *Molecular Spectra and Molecular Structure* , Van Nostrand Reinhold, New York, 1966.

22. W.R. Lambert, P.M. Felker and A.H. Zewail, to be submitted.

23. W.R. Lambert, P.M. Felker and A.H. Zewail, to be submitted.

24. N. Neto, M. Scorocco and S. Califano, Spectrochimica. Acta., **22,** 1981 (1966).

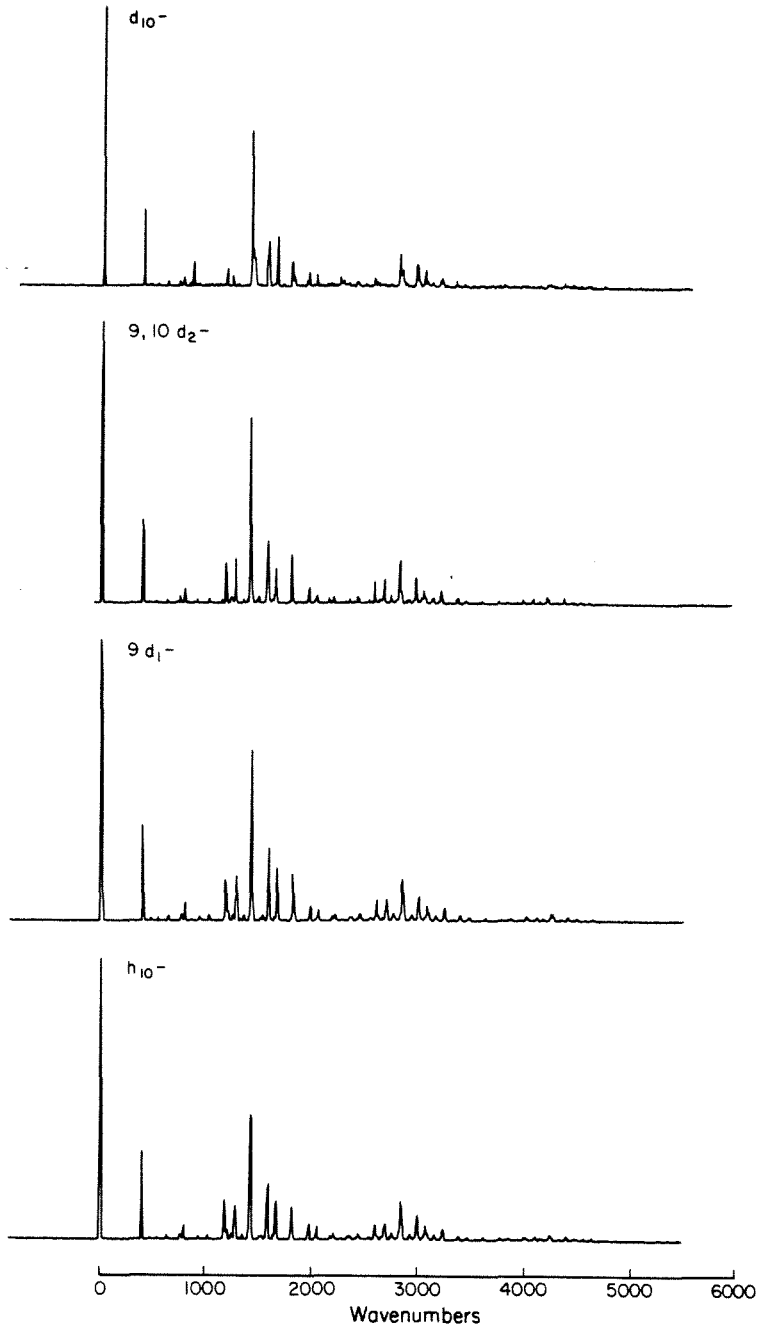

Figure 1.

Energy resolved fluorescence spectra of h_{10}-anthracene (*a*); 9,d_1-anthracene (*b*); 9,10 d_2-anthracene (*c*); and d10-anthracene (*d*). The frequency is relative to the excitation origins at 3611.8 A° (h_{10}-), 3610.0 A° (9,d_1-), 3608.5 A° (9,10 d_2-), and 3602.5 A° (d_{10}-). The relative magnitudes of the transitions appear in tables 1-4. The spectra were obtained with 3.0 cm^{-1} resolution.

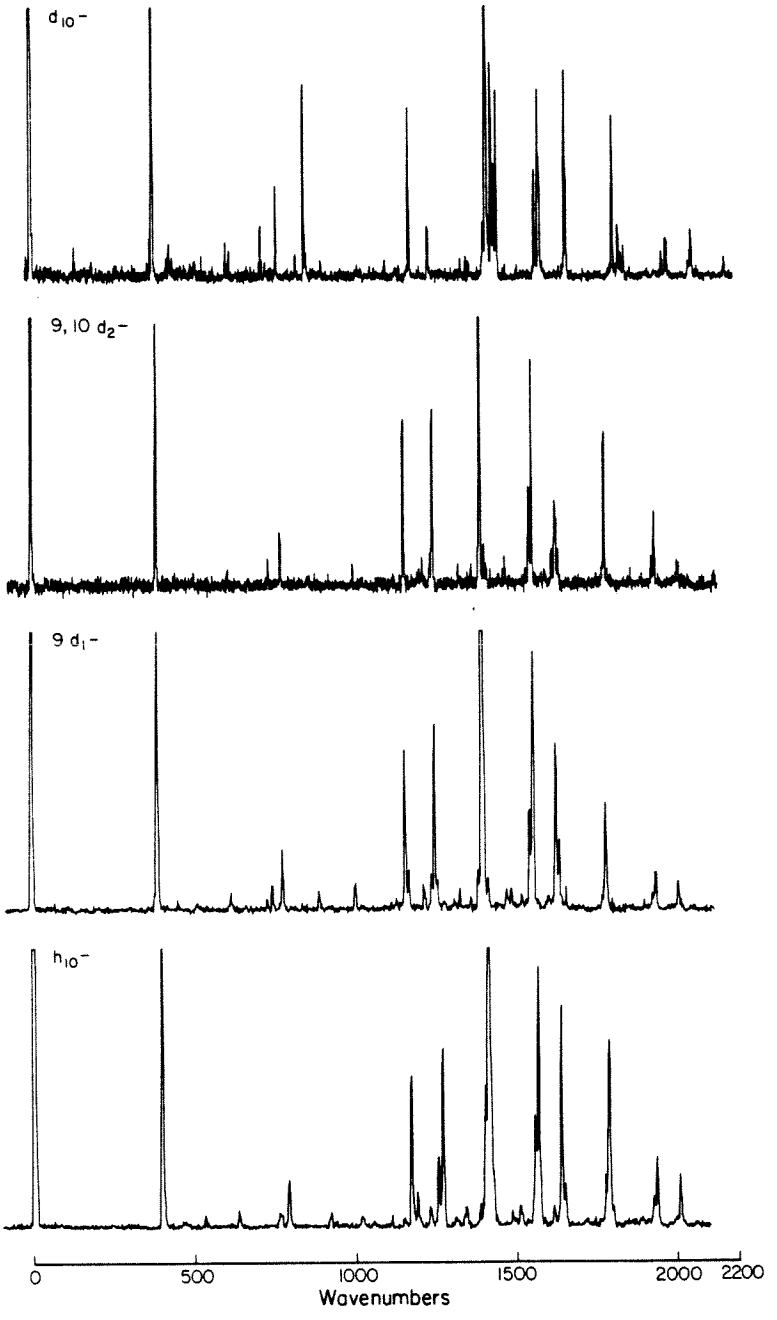

Figure 2.

Energy resolved fluorescence spectra of h_{10}-anthracene and the deuterated derivatives. The spectra are the same as those presented in figure 1 except that the amplitudes have been expanded in order to emphasize the less intense transitions.

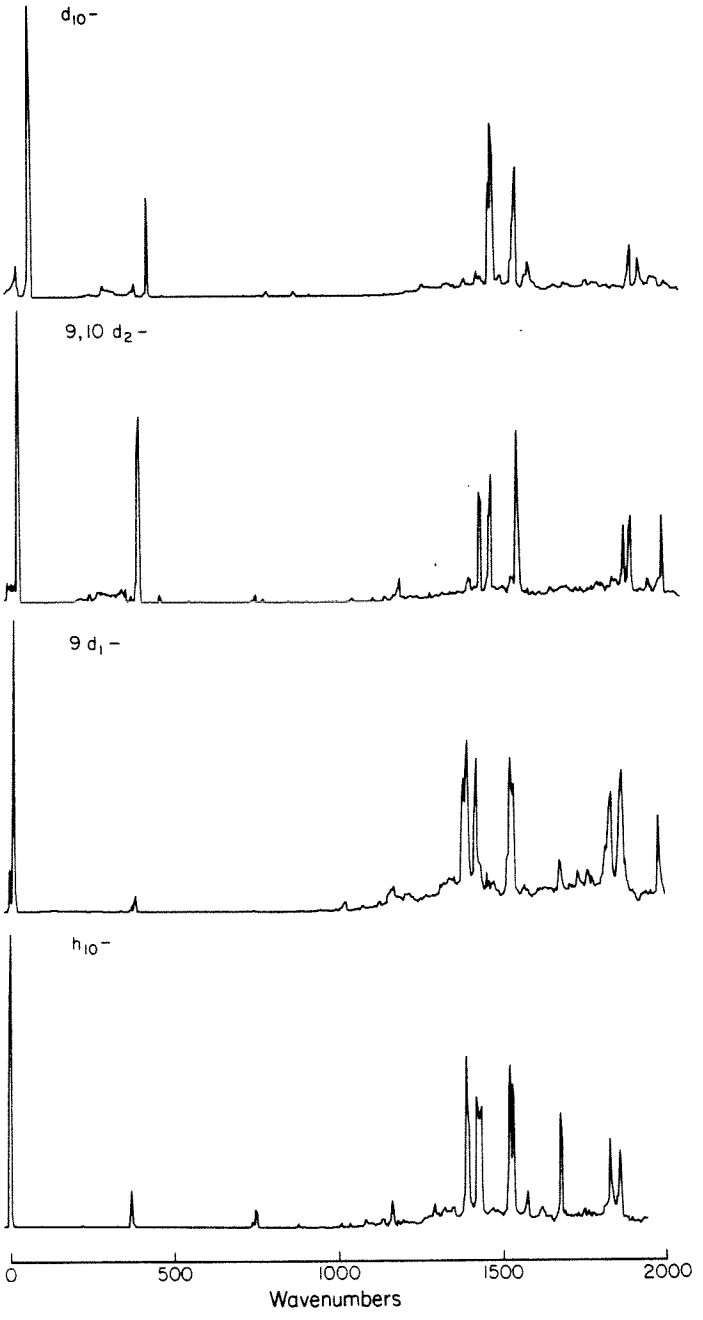

Figure 3.

Fluorescence excitation spectra of h_{10}-anthracene (*a*); 9,d_1-anthracene (*b*); 9,10 d_2-anthracene (*c*); and d_{10}-anthracene (*d*). The frequency is relative to the respective origins. The intensities have not been normalized to the excitation power, however the power was determined to be linear within 300 cm^{-1} intervals. The spectral resolution is approximately 0.3 cm^{-1}. The structure which appears to the red of the origin and the 390 cm^{-1} mode for d_1-, d_2- and d_{10}- anthracene is probably due to sample impurities.

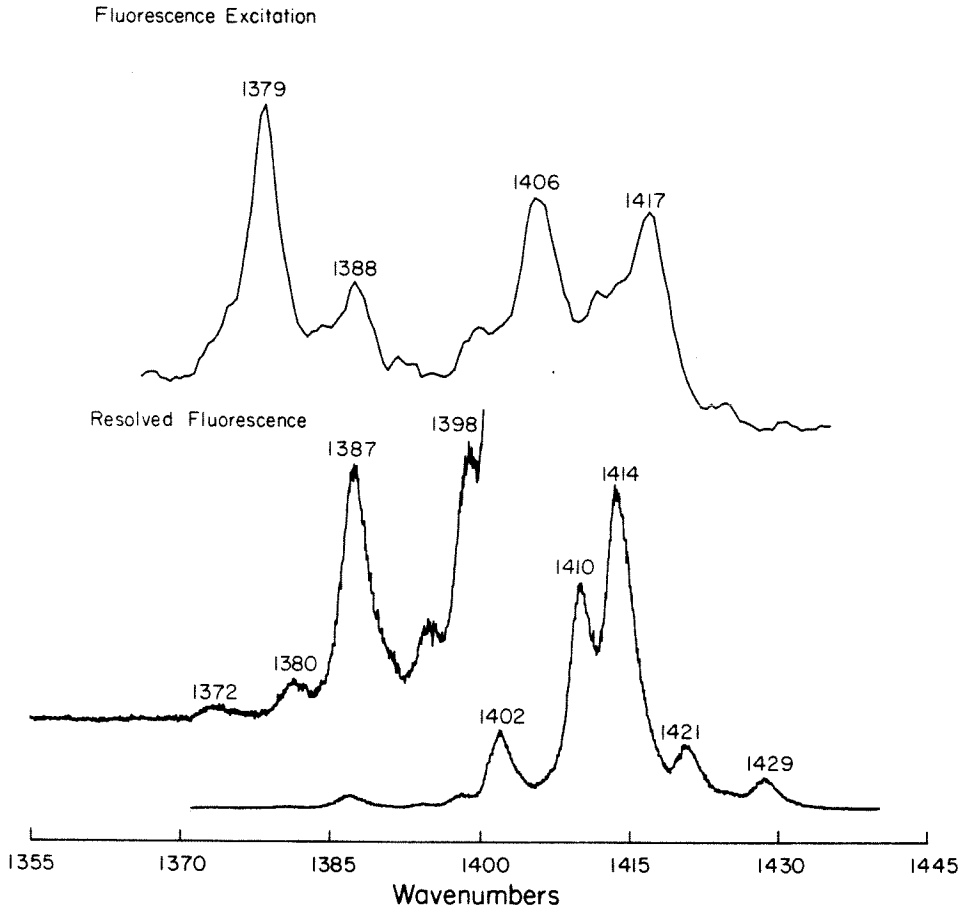

Figure 4.
The excited state and ground state vibrations of h_{10}- anthracene in the region around 1400 cm^{-1} above the S_1 origin. The assignments are given in table 10.

Table 1. Assignments for the single vibronic level fluorescence of h_{10}-anthracene upon excitation to the $^1B_{2u}$ singlet state origin at 3611.8±0.5 A°.

Energy, cm^{-1}	Intensity	Assignment	Expt. a.	Expt. b.	Theory c.	Theory d.	Theory e.
0	100	origin, 27686 cm^{-1}	--	--	--	--	--
387	45	b_{3g}	397	390	320	369	380
387	45	a_g	397	390	373	399	394
452	1	b_{1g}	--	--	--	--	--
519	1	b_{3g}	521	--	513	519	532
621	2	a_g	625	624	645	658	622
748	3	a_g	754	757	708	731	751
777	7	($_g$	2x387)	--	(779)	--	--
910	2	b3g	903	--	892	909	907
1006	2	a_g	1007	1008	881	1016	1005
1100	1	b_{3g}	1102	--	1023	1097	1112
1139	1	b_{1u}	1147	(1146)	1063	1127	1138
1162	22	a_g	1164	1163	1093	1170	1165
1180	3	b_{3g}	1187	1188	1170	1204	1184
1220	3	--	--	--	--	--	--
1246	4	b_{3g}	1273	(1246)	1237	1264	1275
1260	22	a_g	1264	1258	1145	1254	1260
1302	1	b_{1u}	--	--	--	1319	1309
1335	2	b_{2u}	1317	1320	1288	1359	1345
1382	2	b_{3g}	1433	--	--	1385	1379
1397	9	b_{2u}	1400	(1394)	--	1397	1397
1408	59	a_g	1412	1402s	1413	1390	1403
1424	8	b_{1u}	1448	1410	1449	1441	1447

1484	2	a_g	1480	--	1532	1481	1483
1508	2	(2×748)	--	--	--	--	--
1531	1	b_{2u}	1534	--	1563	1531	1532
1555	7	(1162+387)	--	(1552)	--	--	--
1566	31	a_g	1556	1561	1610	1562	1557
1617	2	b_{1u}	1620	--	1619	1616	1629
1640	20	b_{3g}	1632	(1647)	1681	1627	1626
1654	3	(387+1260)	--	--	--	--	--
1785	10	(2×387+1006)	--	--	--	--	--
1797	16	(387+1407)	--	--	--	--	--

Table 2. Assignments for the single vibronic level fluorescence of d_{10}-anthracene upon excitation to the $^1B_{2u}$ singlet state at 3620.0±0.5 A°.

Energy[f]	Intensity	Assignment	Experiment a.	Experiment b.	Theory c.	Theory d.	Theory e.
0	100	origin, 27762 cm^{-1}	--	--	--	--	--
376	31	b_{3g}	375	381	355	354	355
376	31	a_g	375	381	380	375	372
527	1	b_3g	--	--	501	492	494
599	1	a_g	--594	602	576	634	600
706	1	a_g	710	707	702	671	687
750	6	(2×376)	(750)	(761)	--	--	--
812	2	b_{3g}	--	806	804	794	812
837	12	a_g	834	844	824	789	822
844	2	a_g	--	--	834	--	844
883	2	b_{3g}	--	880	865	869	844
1083	1	b_{3g}	(1085)	(1096)	1058	1092	1026
1160	10	a_g	1154	1158	1164	1235	1164
1218	4	b_{3g}	(1208)	(1225)	1240	1278	1241
1382	4	b_{1u}	1384	--	1384	1385	1381
1390	46	a_g	1382	1388	1376	1324	1350
1405	14	b_{2u}	1401	(1401)	1390	--	--
1414	10	(2×706)	--	1419	--	--	--
1421	13	a_g	1421	--	1431	1418	1409
1480	2	b_{3g}	--	--	1550	1433	1499
1532	9	a_g	1529	1538	1526	1456	1534
1544	16	1539	b_{3g}	--	--	--	--
1547	10	(1159+376)	--	--	--	--	--
1623	17	b_{3g}	--	1616	1585	1572	1605

1765	13	(1389+376)	(1756)	(1770)	--	--	--
1782	5	(1405+376)	(1776)	--	--	--	--
1788	3	(2×706+376)	--	(1785)	--	--	--
1797	3	(1421+376)	(1796)	(1803)	--	--	--
1910	3	(1532+376)	(1904)	(1917)	--	--	--
1922	4	(837+706+376)	(1914)	--	--	--	--
1997	5	(1622+376)	--	(1997)	--	--	--

a. Reference 2. b. Reference 3. c. Reference 12. d. Reference 11. e. Reference 24. f. cm^{-1}

Table 3. Assignments for the single vibronic level fluorescence of 9,10-d_2-anthracene upon excitation to the $^1B_{2u}$+ singlet state origin at 3609.3 Å (27706 cm^{-1}).

Relative Frequency[a]	Intensity	Ref. 14	Assignment
0	100	--	0-0 origin
387	35	395	a_g, b_{3g}
503	2	500	b_{3g}
611	3	640	a_g
700	2	--	--
736	4	745	a_g
774	8	--	(2×387)
798	2	--	--
841	2	--	--
858	2	855	b_{3g}
881	3	898	b_{1u}
1002	4	1005	a_g
1159	13	1150	a_g
1219	3	1207	b_{3g}
1243	4	(505+736)	
1256	14	1250	a_g
1333	3	1336	b_{2u}
1374	3	1385	b_{3g}
1402	56	1397	a_g
1414	5	1398	b_{2u}
1421	3	1448	b_{1u}
1479	4	1480	a_g
1545	3	--	(1159+386)
1555	9	1574	b_{3g}

1563	19	1557	a_g
1605	3	--	(1219+387)
1626	4	1620	b_{1u}
1637	8	1629	b_{3g}
1639	7	--	(1251+387)
1646	4	--	(1159+505)
1791	13	--	(1402+387)
1807	1	--	(1414+387)
1874	3	--	(1479+287)
1941	4	--	(1555+387)
1950	7	--	(1563+387)
2021	3	--	(1636+387)

a. cm^{-1}

Table 4. Assignments for the single vibronic level fluorescence of 9-d_1-anthracene upon excitation to the origin of the $^1B_{2u}{}^{+2+}$ singlet state at 3610.0 A° (27701 cm^{-1}).

Relative Frequency, cm^{-1}	Intensity	Assignment
0	100	0-0 origin
390	32	a_g, b_{3g}
455	2	a_g
514	2	b_{3g}
621	3	a_g
730	2	a_g
747	3	a_g
779	7	(2×390)
895	3	b_{3g}
1008	4	a_g
1137	2	(747+390)
1162	16	a_g
1177	5	b_{3g}
1221	3	b_{3g}
1246	4	(2×620)
1256	18	a_g
1266	4	(514+746)
1288	2	(894+390)
1335	3	b_{2u}
1371	2	b_3g
1394	5	(1007+390), b_{2u}
1408	67	a_g
1425	4	b_{2u}
1482	4	(746+730)

1483	4	a_g
1497	3	(2×746)
1557	12	(1161+390),b_{3g}
1567	30	a_g
1638	18	b_{3g}
1649	9	(1256+390)
1796	18	(1407+390)
1954	8	(1567+390)
2027	6	(1638+390)

Table 5. Comparison of the ground state vibrational frequencies for h_{10}-; 9-d_1-; 9,10-d_2- and d_{10}-anthracene for the a_g and b_{3g} symmetry groups. The specific vibrational types according to reference 13 are presented in the margins.

	h_{10}	d_1	d_2	d_{10}	
a_g					
CC-CCC	387	389	387	376	CCC-CCC
CCC	621	621	611	599	CCC
CC	747	747	736	706	CC
CC	1006	1007	1002	837	CC-CCd
CCH	1162	1161	1159	1159	CCD
CC	1260	1256	1252	1159	CC
CC	1407	1407	1402	1389	CC
CC-CCH	1483	1483	1480	1421	CC
CC-CCC	1565	1565	1563	1526	CC
b_{3g}					
CCC	387	389	387	376	CCC
CCC	519	514	504	527	CCC
CCC	909	894	858	811	CCD
CCH-CC	1100	--	--	--	CCD-CCC
CCH	1179	1175	--	883	CCD
CCH	1246	1246	1219	1082	CCD
CCH	1381	1371	1374	1217	CC
CC	1565	1557	1555	1543	CC
CC	1640	1638	1638	1622	CC

Table 6. Excited state vibrational frequencies and assignments for h_{10}-anthracene.

Energy, cm^{-1}	Intensity	Ref. 3	Ref. 2	Assignment
0	VS	--	--	0-0 origin, 27722 cm^{-1}
390	S	389	385	a_g
590	W	590	590	b_{3g}
657	W	663	--	a_g
749	W	744	739	a_g
760	M	(778)	(770)	(2×390)
888	W	894	--	b_{3g}
1009	W	1005	--	a_g
1037	W	1030	1024	b_{3g}
1062	W	(1057)	--	(390+657)
1082	W	--	--	b_{3g}
1104	W	--	--	--
1134	W	(1133)	(1124)	(760+390)
1165	M	1166	1155	a_g
1190	W	1199	--	b_{3g}
1286	M	(1283)	--	a_g
1316	W	(1326)	--	(2×657)
1340	W	(1334)	--	(749+590)
1373	VS	(1374)	1388	b_{3g}
1398	VS	1399	1396	a_g
1410	VS	(1419)	(1409)	(1009+390)
1448	W	--	--	(1037+390)
1492	VS	--	(1484)	(2×749)
1499	VS	1503	1497	a_g

1543	M	(1546)	(1540)	a_g
1591	M	--	--	b_{3g}
1611	W	(1620)	--	(1037+590)
1639	S	--	--	b_{3g}
1681	W	(1672)	--	(2×390+888)
1696	W	(1693)	--	(1037+657)
1709	W	--	--	--
1764	S	(1774)	(1773)	(1373+390)
1791	S	(1788)	(1781)	(1398+390)

Table 7. Frequencies and assignments for the excited state vibrations of d_{10}-anthracene.

Frequency, cm^{-1}	Relative Intensity	Ref. 3	Ref.2	Assignment
0	S	--	--	Origin, 27790 cm^{-1}
173	W	205	--	--
217	W	205	--	--
328	W	335	--	b_{3g}
367	M	380	371	a_g
--	--	568	570	b_{3g}
--	--	690	695	a_g
725	W	--	--	a_g
745	W	(758)	(744)	(2×367)
785	W	789	--	b_{3g}
822	W	836	828	--
865	W	--	843	a_g
902	W	903	893	b_{3g}
921	W	944	(941)	(568+367)
1028	W	--	--	(690+328)
1045	W	--	--	(725+328)
1062	W	(1069)	(1066)	(690+367)
1082	W	--	--	(725+367)
1102	W	--	--	(3×367)
1160	W	(1169)	--	(785+367)
1176	W	--	--	a_g
1196	M	(1215)	(1199)	(822+367)
1230	W	--	--	b_{3g}
1258	M	(1260)	(1265)	(568+690)

1303	M	--	--	(568+725)
1336	M	(1320)	--	--
1368	M	--	--	--
1374	S	1389	1376	a_g
1394	M	1406	1391	(568+822)
1438	S	1441	1428	a_g
1473	M	1456	1433	a_g
1547	W	1524	1530	a_g
1577	W	--	(1574)	(902+690)
1638	W	--	--	b_{3g}
1652	W	--	(1656)	(1336+328)
1687	W	--	--	(1336+328)
1703	W	(1715)	--	(1374+328)
1738	M	--	(1747)	(1374+367)
1758	M	(1762)	(1748)	(1438+328)
1789	M	(1782)	(1799)	(1438+367)
1829	W	(1815)	--	(1473+367)

Table 8. Frequencies and assignments of the excited state vibrations for 9,10-d_2-anthracene and 9_1-anthracene.

d_2-anthracene Energy	d_1-anthracene Intensity	Assignment Energy	Intensity	Assignment
0	VS	0	VS	0-0 origin
--	--	123	W	--
219	W	218	W	--
385	VS	385	VS	a_g
452	W	--	--	b_{3g}
536	W	--	--	b_{3g}
571	W	--	--	a_g
748	M	746	M	a_g
768	MW	766	M	(2×385)
844	W	875	W	(452+385)
894	W	894	W	b_{3g}
945	W	957	W	(571+385)
1024	W	1025	M	a_g
1088	M	1080	M	a_g
1128	M	1127	M	(748+385)
1173	MS	1171	M	b_{3g}
1260	M	1265	M	(894+385)
1335	M	1337	M	b_{3g}
1366	M	1362	M	a_g
--	--	1373	S	a_g
1392	S	1403	VS	a_g
1420	S	1429	W	(1024+385)
1447	M	1429	W	--
1472	MS	1445	W	(1088+385)

1491	VS	1490	VS	a_g
1522	W	--	--	(2×385+748)
1535	W	1532	W	a_g
1555	W	1552	W	(1173+385)
1584	W	1585	W	--
1587	W	--	--	--
1630	W	1626	W	b_{3g}
1661	W	1654	W	(2×385+894)
1676	W	1677	M	--
1718	M	1713	M	(1335+385)
1754	M	1713	M	(1366+385)
1779	S	1760	S	(1392+385)
1795	S	1787	VS	(1420+385)
1837	M	1850	W	(1447+385)
1877	S	1872	S	(1491+385)

Table 9. Comparison of the excited state vibrational frequencies for h_{10}- ; 9,d_1- ; 9,10-d_2- ; and d_{10}- anthracene for the a_g and b_{3g} symmetry groups. Frequencies for which the assigments are questionable appear in brackets.

	h_{10}	d_1	d_2	d_{10}
a_g				
-	390	385	385	367
-	657	--	--	--
-	749	746	748	725
-	1009	1002	--	1102
-	1165	1171	1173	1176
-	1286	1265	1260	1258
-	1410	1403	1392	1374
-	1495	1490	1491	1438
-	1591	1585	1584	1547
b_{3g}				
-	390	385	385	367
-	590	--	--	--
-	888	894	894	785
-	1037	1025	1024	822
-	1082	1080	1088	902
-	(1286)	(1265)	(1260)	--
-	1380	1380	1420	1230
-	(1591)	(1585)	(1584)	1577
-	1639	1626	1630	1638

Table 10. Comparison of the ground and excited state vibrational frequencies in the region around 1400 cm^{-1} above the S_1 origin for h_{10}-, 9-d_1-, 9,10-d_2-, and d_{10}-anthracene.[a]

-	h_{10}	d_1	d_2	d_{10}
Ground State				
b_{2u}	1335	1334	1333	--
b_{3g}	1381	1371	1374	--
b_{2u}	1397	1394	1414	1384
a_g	1407	1408	1402	1390
b_{1u}	1424	1424	1422	1413
a_g	1483	1483	1480	1421
Excited State				
b_{2u}	1340	1337	1335	--
b_{3g}	1373	1373	1366	--
b_{2u}	1410	1403	1420	1374
b_{1u}	1448	1445	1472	1394
a_g	1495	1490	1491	1438

a. The accuracy is± 3 cm^{-1}.

4. *QUANTUM BEATS AND VIBRATIONAL REDISTRIBUTION IN ANTHRACENE*

§4.1 *Introduction*

Intramolecular vibrational redistribution in large polyatomic molecules is of fundamental importance with regard to establishing the criteria necessary to effect mode selective chemistry. Associated with this problem is the challenge of developing an appropriate description of the energy level structure and intrastate coupling mechanisms. From an experimental perspective, the evaluation of these properties in large molecules is complicated by the large vibrational and rotational density of states which exist at moderate excess energies, as well as the rapid temporal evolution of the internal energy redistribution. Fluorescence quenching (1), predissociation of van der Waal complexes (2), and direct temporal (3) measurements have indicated that IVR rates proceed on a time scale of less than at least a few hundred picoseconds. The combination of picosecond laser excitation and supersonic free jet techniques provides a means of investigating the rapid internal dynamics for isolated molecule conditions in the absence of spectral congestion.

In a recent communication (4) we have reported preliminary results on the observation of coherence effects in the time and energy resolved fluorescence of anthracene upon picosecond (~ 10 psec) excitation to the 1380 cm^{-1} vibronic level of the first excited singlet manifold. Despite the fact that the coherence width of the laser excitation (~ 3 cm^{-1}) spanned a large number of vibrational and rotational states at this excess energy, quantum beats appear on the resolved fluorescence for only a small number of spectrally resolved transitions. These features indicate that specific vibronic properties of the optically prepared molecular eigenstates are maintained despite the fact that the overall density of states reflects properties commensurate with the statistical limit.

Recently, interference phenomena have been used to probe the energy level structure and dynamics of excited population in the electronic ground state manifold (5).

A principal question arising from the initial observation of quantum beats in anthracene and high excess energies is the nature of the eigenstates which are responsible for the interference effects. Although the majority of energy deposited within the molecule is redistributed among the bath modes as evidenced by the dominant relaxed fluorescence component, energy can remain localized in specific states which are radiatively coupled to a common ground state. The mechanisms responsible for this process are fundamental to the concepts of IVR and hence indicate that the quantum beats can be used as a means to probe intramoleuclar dynamics.

The extent to which the distribution and coupling of the states which are quasi-energetic with the interfering states define energy redistribution can be investigated by monitoring the influence upon the quantum interference parameters (damping rate, beat frequency, modulation depth). The use of supersonic free jet techniques presents a convenient method of modifying the internal vibrational and rotational temperatures of the diluent molecule. However, since the processes responsible for the cooling of the internal degrees of freedom, complex formation, and intermolecular dynamics in the free jet, for large polyatomic molecules are not completely understood, it is important that these factors be systematically evaluated before drawing conclusions regarding intramolecular dynamics. The distribution of interacting states also depends upon the coherence width and bandwidth of the laser excitation. Previous examples of quantum beats in large molecules have reflected the mixed

singlet-triplet character of the prepared eigenstates. The nature of this interaction has been demonstrated by the application of an external magnetic field (6). In an analogous manner, the influence of the application of external fields on the quantum beat parameters in anthracene are investigated. As a final point, since the quantum beats appear only for specific detection conditions, an analysis of the vibronic structure of anthracene will indicate the symmetry and vibrational characteristics of the states which are efficiently projected out of the quasi-continuum by the respective dipole matrix elements.

REFERENCES

1. R.A. Coveleskie, D.A. Dolson and C.S. Parmenter, J. Chem. Phys., **72,** 5774 (1980).

2. M.P. Casassa, D.S. Bomse and K.C. Janda, J. Chem. Phys., **74,** 5044 (1981).

3. N. Halberstadt and A. Tramer, J. Chem. Phys., **73,** 6343 (1980).

4. W.R. Lambert, P.M. Felker and A.H. Zewail, J. Chem. Phys., **75,** 5958 (1981).

5. R.C. Sharp, E. Yablonovitch and N. Bloembergen, J. Chem. Phys., **76,** 2147 (1982).

6. P.M. Felker, W.R. Lambert and A.H. Zewail, Chem. Phys. Lett., **89,** 309 (1982).

§4.2 EXPERIMENTAL PROCEDURES

§4.2.1 Vacuum System

The 36" × 12" cylindrical stainless steel chamber was evacuated with a 12" bore ring jet booster diffusion pump (Edwards 18B4A) with a pumping speed of 4000 l/sec (< 10^{-2} torr). The diffusion pump was backed with a 150 CFM roughing pump (Kinney KT-150). The ultimate pressure obtained with this system is 10^{-5} torr. Under normal operating conditions, equivalent to using a 150 micron pinhole at 3 atm backpressure of nitrogen, the chamber pressure was less than 10^{-3} torr. The large distance (36") between the viewing windows and the diffusion pump prevented backstreaming from interfering with fluorescence collection. The diffusion pump was not baffled in order to take full advantage of the maximum throughput. The vacuum chamber could be isolated from the pumping system with a pneumatically actuated right angle valve (Vac-U-Torr Products) to provide easy access to the chamber between experiments.

§4.2.2 Chamber Design

The 36" × 12" cylindrical stainless steel vacuum chamber was mounted in a horizontal configuration. The inside of the chamber was covered with a flat black epoxy topcoat (Bostik). Large, 6" diameter, ports which were covered with either plexiglas or quartz (Quartz Scientific, Inc.) windows provided access to the nozzle assembly and enabled efficient fluorescence collection. Insert flanges enabled moving the window to within 1.5" of the horizontally mounted nozzle (figure 1). The laser beam passed vertically through 20" long entrance and exit baffles which reduced the scattered laser radiation. Various 2.5" access

ports accomodated electrical and water feedthroughs and vacuum gauges.

§4.2.3 *Nozzle Assembly*

A schematic of the nozzle assembly is presented in figure 2. The three dimension adjustable mount enabled accurate positioning of the free jet expansion with respect to the laser beam. The maximum dimensions of travel are 2 inches parallel to the laser propagation axis and 3 inches along the axial direction. Attached to the positioning mount is a stainless steel jacket wound with coax sheathed heater wire (Semco Inc.). The heater is divided into two sections in order to provide slightly higher temperatures at the front of the nozzle. Heat was transferred efficiently to the nozzle tip with a brass fitting to prevent condensation at the orifice. Extension of the nozzle tip away from the heater body increased the effective solid angle for fluorescence collection. The nozzle temperature was controlled with a DC power supply (Hewlett Packard 6253A) and monitored by thermocouples mounted on the heater body. A blackened shield was mounted around the assembly to prevent thermal radiation and scattered light from reaching the detector. This external shield also could be used as a convenient base on which to mount various assemblies such as Helmholtz coils and Stark plates. Electrical connections for the heater and thermocouples are brought through the shield perpendicular to the nozzle axis. Stainless steel shim stock was wrapped around the heater to minimize thermal loss to the shield.

Although stainless steel nozzles and metal pinholes were originally used, we have found that pyrex nozzles are more convenient for the present applications. Pyrex nozzles possess the following advantages: 1) organic compounds will not decompose on the surface at high

temperatures, 2) the tip can be viewed, and 3) the nozzles are easily cleaned. The overall length of the nozzle shown in figure 3 is 200 mm. The nozzle is divided into three sections: 1) a 1.5" length of 6 mm OD, 4 mm ID tubing,2) a 5.0" length of 16 mm OD, 14 mm ID tubing, and 3) a 1.5" length of 6 mm capillary tubing. The large OD center section provided a large resevoir in which to place solid samples. In order to form the pinhole, the capillary tube was drawn closed, and the tip subsequently ground with emery cloth to produce a round opening. The pinhole diameter and quality was determined by comparison with metal pinholes of known dimensions. The nozzle was held to a stainless steel rod with a double O-ring compression fitting. Below 200 °C, viton O-rings were sufficient, however, at higher temperatures, teflon, vespel or graphite seals could be used. The fitting was capable of holding a backpressure of 50 atm.

§4.2.4 *Expansion Conditions*

H_{10}-anthracene (Aldrich) and d_{10}-anthracene (Aldrich) were zone-refined (100 passes) prior to use. 9,d_1-anthracene and 9,10-d_2-anthracene were synthesized by acid-catalyzed deuterium-hydrogen exchange (1) from the respective brominated precursors, 9-bromoanthracene (Aldrich) and 9,10-dibromoanthracene (Kodak). Purification was accomplished upon repeated recrystallization from $CHCl_3$. The isotopic purity of 9,10-d_2- and 9-d_1-anthracene was determined from mass spectral analysis to be > 95 % .

Helium, neon and nitrogen at pressures up to 10 atmospheres were used as the carrier gas. Preliminary experiments with argon confirmed the propensity for complex formation, and as a consequence, argon was not used in these experiments. Argon-anthracene cluster formation was determined by the presence of structureless red shifted features

appearing in the energy resolved fluorescence (2). The observed fluorescence was also consistent with that expected for anthracene dimers (3). The nozzle was heated to 150 °C . The chamber pressure was continuously monitored with an ionization (Granville Phillips 224, Bayerd-Albert tube) or convectron (Granville Phillips 275 gauge and controller) gauge.

As the carrier gas and seed molecules are expanded through the pinhole into the vacuum chamber, a zone is reached termed the freezin distance, where intermolecular collisions no longer serve to transfer energy from the internal degrees of freedom to translational motion. The distance at which the intramolecular temperatures, to a first approximation, cease to evolve, is determined by (4); $x_c = D\,(n_s\,\sigma\,D)^{\frac{1}{\gamma}}$ where D is the pinhole diameter, n_s is the molecular density of the source, σ is the hard sphere collision cross section and γ is the heat capacity ratio of the carrier gas. At large distances from the nozzle, however, interaction of the free jet with the background gas leads to a collapse of the expansion shock structure. This distance is denoted as the Mach distance and is determined by (4); $x_m = D\,(0.67)\left[\frac{P_0}{P}\right]^{\frac{1}{2}}$ where D is the pinhole diameter, P_0 is the nozzled pressure and P is the pressure in the expansion chamber. Characteristic values for the freezin distance and the Mach distance for standard operating conditions (150 micron pinhole, 45 psi backpressure) are 4.7 cm and 48.5 cm, respectively. Between these two extremes, within the region of the isentropic core, the expanding gas travels along essentially collisionless streamlines. The time between hard sphere collisions in this region is calculated to be approximately 10^5 seconds (refer to section 4.3 for details). It is within this region that the dynamics of vibrationally and rotationally cold and isolated molecules

can be investigated. Since the experimental lifetimes, on the order of 10 nsec, are considerably shorter than the fluorescence lifetime, anthracene can be considered as isolated, at least with respect to hard sphere collisions, on this time scale. A complete discussion of collisional processes in the anthracene free jet expansion is the subject of section 4.3. The long term stability of our free jet is confirmed by visualizing persistent streamlines for an iodine expansion. The divergence of the jet is approximately 45 degrees from the centerline axis. Using a calculated value for the flow velocity of 10^5 cm/sec, and considering a viewing region 1 cm in length, the perpendicular Doppler width is estimated to be ~200 MHz while the axial velocity distribution is ~20 MHz. Further discussion of how the beam expansion conditions relate to, and influence the intramolecular vibrational and rotational temperatures, specifically with reference to anthracene can be found in sections 4.4, 4.5, and 4.6.

§4.2.5 *Picosecond Laser Excitation : Energy and Time Resolved Fluorescence*

For the energy resolved fluorescence and fluorescence decay measurements, excitation was provided by a synchronously pumped, mode-locked, cavity-dumped picosecond dye laser system (Spectra Physics 375, 342A, 344). A mode-locked argon ion laser (Spectra Physics 171) at 1 watt average power pumped the dye laser to generate 15 psec pulses with a bandwidth of 2 A°. The average power per pulse is 30 njoules. The repetition rate of the cavity-dumped picosecond pulses was variable and normally operated at 4 MHz. The extinction ratio between the dumped and non-dumped pulses was on the order of 500:1. The laser pulse duration (20 - 2 psec) and bandwidth (5.0 - 0.5 A°) could be varied by the insertion of various intracavity dye laser tuning elements (wedge, three plate

birefringent filter, fine tuning etalon and solid etalon). The laser dyes DCM and R6G (Exciton) were used to generate tunable laser power from 740 A° to 570 A°. The determination of the laser bandwidth was made with a scanning monochromator (0.25 A° resolution).

Precise mode-locking of the dye laser (accomplished by matching the argon ion laser and dye laser cavity lengths) was necessary to achieve minimum pulse widths and maximum laser power. Approximate adjustment could be determined by monitoring the average UV power produced by second harmonic generation, however, fine adjustment was accomplished upon maximizing the autocorrelation intensity.

The measurement of the temporal characteristics of the laser pulse was accomplished using zero background second harmonic generation (5). In this technique the dye laser beam is separated into two parts, the length for one of which is variable. The two noncollinear beams are focused onto a 0.2 mm thick $LiIO_3$ crystal to generate the second harmonic. A stepper motor driven translation stage (Micro-Controle M062-FC03) was used to vary the time delay between the arrival of the two pulses. The second harmonic generation signal is proportional to the autocorrelation function of the pulse intensity, $I(t)$, and given by;

$$G(\tau) = \frac{\langle I(t-\tau)\, I(\tau)\rangle}{\langle I^2(t)\rangle} \qquad (4.2.1)$$

where τ is the time delay between the pulses and the brackets indicate a time average. $G(\tau)$ is a maximum for simultaneous arrival of the two pulses, $\tau = 0$. The second harmonic is detected with a filtered photomultiplier. Phase sensitive detection (~300 MHz) was used to provide a large dynamic response range. The output of the lockin amplifier (PAR HR-8) was digitized with a voltage to frequency converter and temporarily stored in a multichannel analyzer (MCA, Tracor Northern TN1706). The

contents of the MCA were transferred to a PDP 11/23 computer for subsequent analysis.

For the purposes of investigating the dynamics of anthracene, the second harmonic of the picosecond dye laser was generated using 1 cm^3 phase matched lithium iodate crystals (Cleveland Crystals). Two crystals were required to produce tunable ultraviolet power over the range of interest: 1) $LiIO_3$ crystal cut for 0.610 micron fundamental, Θ_m = 69.40° with respect to the *C* axis, and 2) a crystal cut for the 0.690 micron fundamental, Θ_m = 54° with respect to the *C* crystallographic axis, *type* 1 phase matching. A 50 mm focal length lens focused the fundamental onto the doubling crystal to produce the second harmonic beam. Although the UV beam was elongated due to differences in the phase matching angle along the path of the tightly focused fundamental, maximum power was produced. The conversion efficiency was measured to be ~11 % .

The second harmonic was collimated, directed through a 100 cm long entrance baffle provided with three adjustable apertures, and focused onto the fee jet expansion 5 mm from the nozzle. The mirror which directed the laser beam through the free jet apparatus was antireflection coated, enabling the transmitted laser fundamental to be directed onto a fast photodiode which was then used to trigger the timing electronics. The laser beam exited the free jet expansion chamber through an additional 100 cm long light baffle.

Molecular fluorescence was collected with an f/1 lens and imaged with another lens onto the entrance slit of the monochromator. This simple two lens system, although not maximizing the collection efficiency , allowed versatility in the optical alignment. Scattered light was not found to be a problem in these experiments. The emission was resolved with a

microprocessor controlled, f/6.9, 0.5 meter monochromator (Spex Industries 1870 and CD2 microprocessor) with a grating dispersion of 16 A°/mm.

The energy and time resolved fluorescence measurements were made using single photon counting techniques. The time resolved emission was detected with an Amperex *XP2020Q* photomultiplier, and the output sent to a constant fraction differential discriminator (ORTEC moder 583). The inverted operating configuration was used in which the response signal provided the start pulse for the time-to-amplitude conversion (TAC, ORTEC model 457). When the response rate is less than the source repetition rate, this configuration provides an optimum data acquisition rate (6). The stop conversion signal from the TAC was generated from the laser fundamental by means of a fast photodiode (Hewlett-Packard, 5082-4203) and a constant fraction discriminator (ORTEC model 473A). The ratio of the response rate to the laser repetition rate was always less than 1 %. The output of the TAC was processed and temporarily stored in a Tracor-Northern TN1706 multichannel pulse height analyzer (MCA). For sampling energy resolved spectra, pulses were acquired in the multichannel scalar mode. For temporal measurements the time base was calibrated using the full laser repetition rate (80 MHz) based upon knowledge of the mode locking frequency. The instrument response function, obtained by scattering laser pulses from the nozzle, was determined to have a width of 250 psec. The spectra which were accumulated on the MCA were subsequently transferred to a PDP 11/23 computer for analysis.

§4.2.6 *Fluorescence Excitation Spectra - Nitrogen Laser*

A pulsed nitrogen pumped dye laser system (Molectron DL2) was used to produce fluorescence excitation spectra. The spectral bandwidth and

temporal pulse width were measured to be 0.5 cm^{-1} and 5.0±0.5 nsec, respectively. The dye laser grating was scanned with an externally driven stepper motor (Superior Electric). The absolute laser wave- length was calibrated using the optogalvanic method (7). The second harmonic was generated upon focusing the laser fundamental onto a 1 cm^3 KDP crystal, collimated, and subsequently focused onto the free jet expansion approximately 5 mm from the nozzle. Scattered light was reduced by passing the laser beam through baffles extending to either side of the expansion chamber. Fluorescence was collected with f/1 optics and passed through a monochromator before being focused onto the photomultiplier tube. The monochromator grating was either adjusted to zeroth order (grazing incidence) or centered to the red of the origin. In both configurations the slit width was 3 mm and neutral density filters were used if necessary to reduce the signal intensity. The latter method, although not collecting the total fluorescence, did reduce the amount of scattered light detected. The output of the photomultiplier was integrated with a boxcar averager (PAR 162/164). The averaged signal was digitized with a voltage-to-frequency converter and temporarily stored in a multichannel analyzer (Tracor Northern TN1706). The data was subsequently transferred to a PDP 11/23 computer for analysis. The fluorescence excitation spectra were not normalized with respect to the laser power.

REFERENCES

1. J.L. Charlton and R. Agagnier, Can. J. Chem., **51,** 1852 (1973).

2. T.M. Hayes, W. Henke, H.L. Selzle and E.W. Schlag, Chem. Phys. Lett., **7,** 69 (1981).

3. E.A. Chandross, J. Ferguson and E.G. McRae, J. Chem. Phys., **45,** 3546 (1966).

4. H. Ashkenas and F.S. Sherman in *Rarefied Gas Dynamics*, 4^{th} Symposium Vol. II, ed. J.H. de Leeuw, Academic Press, New York, 1976, p. 84.

5. E.P. Ippen and C.V. Shank in *Ultrashort Light Pulses*, Top. Appl. Phys., **18,** ed. S.L. Shapiro, Springer Verlag, Berlin, 1977.

6. G.R. Hansen, B.W. Wallin and F.E. Lytle, Rev. Sci. Inst., **50,** 64 (1979).

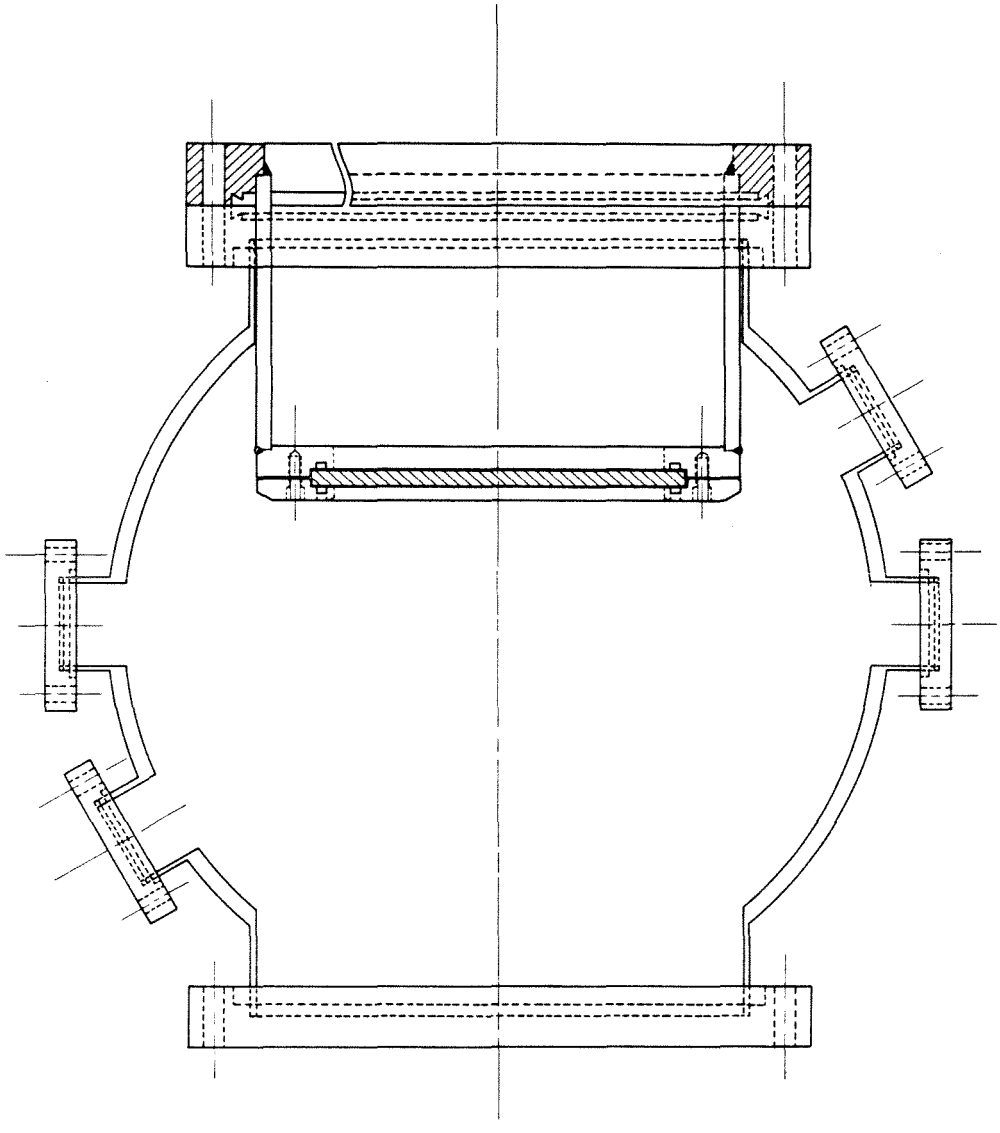

Figure 1.
Diagram of the expansion chamber as viewed along the nozzle axis. The 6" diameter quartz window is inserted into the chamber to improve the fluorescence collection efficiency. The laser beam passes vertically through the chamber and light baffles (not shown) which reduce scattered laser radiation.

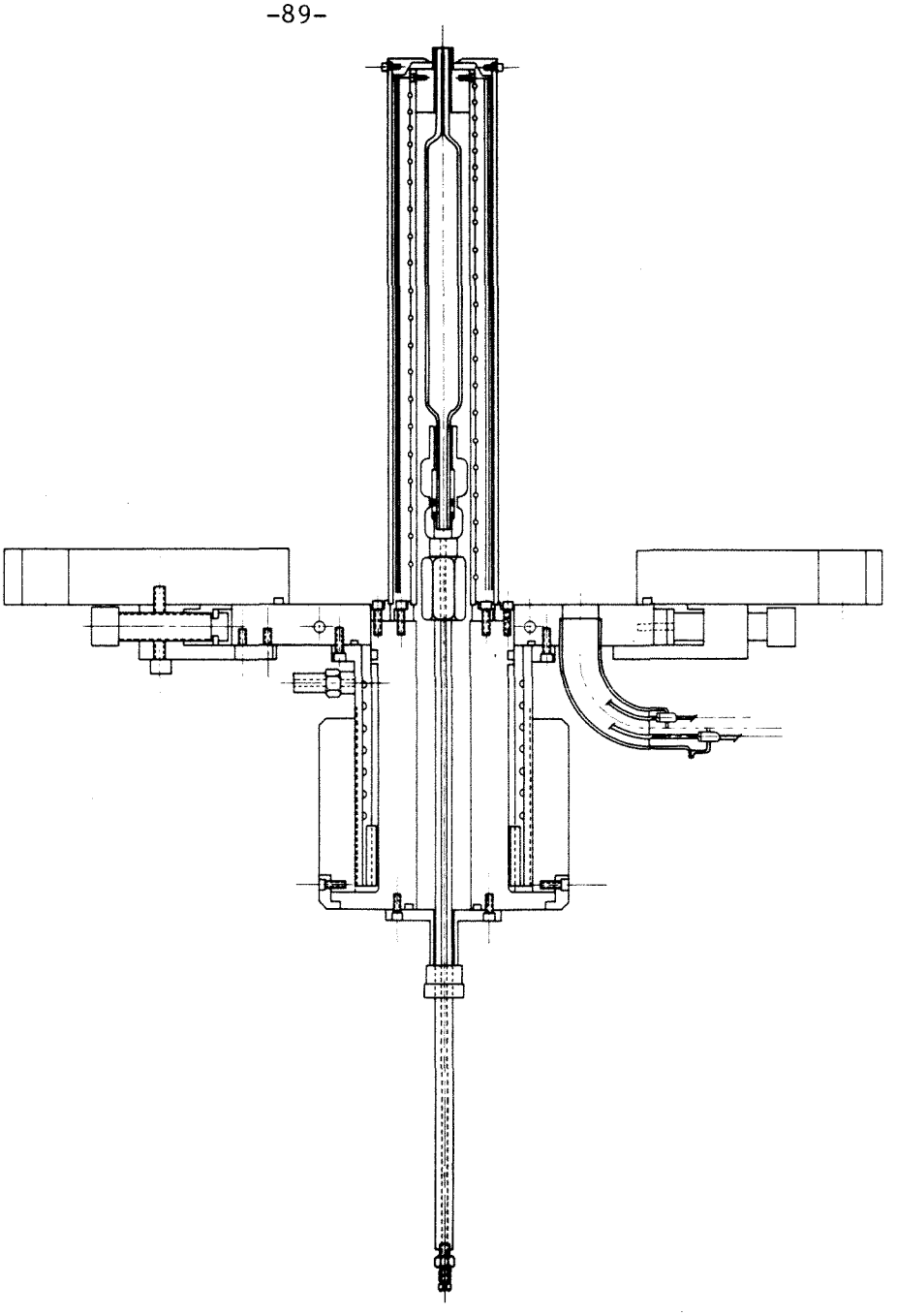

Figure 2.
Schematic of the nozzle assembly. The nozzle mounting plate is positioned perpendicular to the plane of the figure by means of adjustment bolts. The large nut enables 3" adjustment along the jet axis. Provision has been made in the design for water cooling of the positioning plate. Attached to the mounting plate are the heater and radiation shield. A pyrex nozzle is shown mounted to the inlet line. Further details are given in the text.

§4.3 METHODS OF ANALYSIS

§4.3.1 Fluorescence Lifetimes

The temporal width of the system response function, $F(t)$, was 250 psec and is primarily determined by the electron dispersion of the photomultiplier. Fluorescence decay curves which did not exhibit quantum beats were fit to a single exponential function of the form;

$$G(\tau) = A \exp^{\frac{-t}{\tau}} \tag{4.3.1}$$

where A and τ are adjustable parameters. For these cases the system response function was sufficiently short compared to the observed decay that analysis did not require deconvolution. The curve fitting was performed on a PDP 11/23 computer using a nonlinear least squares routine based on Marquardt's algorithm (1,2). The quality of the fits was determined by the reduced chi-squared (χ^2_v) and by inspection of the weighted residuals (2) and the residual autocorrelation function (3,4).

§4.3.2 Quantum Beats

Application of Fourier transform analysis to the fluorescence decays exhibiting quantum beats provided an estimation of the physical parameters associated with the interacting eigenstates. Spectra which exemplify the steps in the analysis of the quantum beats are shown in figure 1.

A convenient functional form which describes the temporal evolution of a coherently prepared set of molecular eigenstates is given by (5);

$$\rho_{ii}(t) = \rho_{ii}(0) \sum_j \left\{ \left[\exp \frac{(-\Gamma_{ji})}{\Lambda^2_{ji}} \right] \times \left[(\omega^2_{ji} + 2\hbar^{-2} |H'_{ji}|^2) + 2\hbar^{-2} |H'_{ji}|^2 \cos\Lambda_{ji}\, t \right] \right\} \tag{4.3.2}$$

where $\Lambda^2_{ji} = \omega^2_{ji} + 4\hbar^{-2} |H'_{ji}|^2$. The equation describes the decay of a

particular eigenstate $\rho_{ii}(t)$ which is coupled via $|H'_{ji}|^2$ to other eigenstates $\sum\rho_{jj}(t)$. $\rho_{ii}(t)$ is composed of an exponential term with a relaxation rate given by Γ_{ji} and a damped oscillatory term with frequency $\Lambda_{ji} = \frac{1}{h}(E_j - E_i)$. The oscillatory components can most easily be analyzed by Fourier transforming equation 4.3.1 to yield;

$$\bar{\rho}(\omega) = \int_{-\infty}^{+\infty} dt e^{-i\omega t} \frac{\rho_{nn}(t)}{\rho_{nn}(0)} = \sum_j \frac{2\Gamma_{ji}}{\Lambda_{ji}^2} \left\{ \frac{1}{\omega^2 + \Gamma_{ji}^2} + \frac{|H'_{ji}|^2}{h^2} \left[\frac{1}{(\omega - \Lambda_{ji}^2) + \Gamma_{ji}^2} + \frac{1}{(\omega + \Lambda_{ji}^2) + \Gamma_{ji}^2} \right] \right\} \tag{4.3.3}$$

Again, the first term arises from the single exponential decay and consists of a half Lorentzian term centered at zero frequency with a width determined by Γ_{ji}. The second term representing the interference component, establishes a Lorentzian Fourier lineshape with a maximum position given by $\frac{1}{h}(E_i - E_j) = \Lambda_{ji}$ and with a width of Γ_{ji}. With reference to equation 4.3.3, the positions of the Fourier transform peaks are equivalent to the energy difference between the two interfering states, the linewidth equivalent to half the total dephasing rate, Γ_{ji} (T_2^{-1}) and the area is proportional to the modulation depth. When the resolved spectra representing different total counts were compared, the areas were normalized, the correctness of this procedure being verified in an independent experiment.

Since the exponential term and the oscillatory component decay on a similar time scale, the direct Fourier transformation of the data will produce a frequency domain spectrum which is dominated by a half-Lorentzian centered at zero frequency. Therefore, in order to accomplish analysis of the quantum beats, it was first necessary to remove the

unmodulated exponential terms in equation 4.3.3. In order to analyze the time resolved fluorescence which exhibited quantum beats, the response of the system to the laser pulse, $F(t)$, was convoluted with the response function of the system $G(t-t')$,which was considered to be a single exponential of the form defined in equation 4.3.1, such that;

$$I(t) = \int_0^t dt'\ F(t')\ G(t-t') \qquad (4.3.4)$$

where $I(t)$ is the experimental fluorescence signal. Curve fitting was performed beginning ten data points (760 psec) to earlier time than the maximum intensity. The best least squares fit (1,2) to an average single exponential decay is subtracted from the experimental data to produce the residual, which in turn is composed only of the damped interference terms in equation 3. Fourier transformation of the residual generated the frequency domain spectrum, which in turn was analyzed to determine physical parameters associated with the interference terms. Fourier transformation was accomplished using a routine based upon the Cooley-Tukey fast Fourier transform algorithm (6,7).

When a single oscillatory term predominated, the Fourier transformation yielded frequency domain spectra which were relatively free of leakage and sidelobe interference. In these cases the spectral parameters of interest (peak position, FWHM, and area) were obtained upon fitting the single peak to a Lorentzian lineshape profile. On the other hand, the situation regarding the Fourier transformation of the spectra exhibiting multiple interference terms is more problematic. The Fourier transforms of the spectra generally produced several apparently unsymmetrical peaks in the frequency domain. The extent to which sidelobes and leakage contributed to these spectra can be determined upon appli-

cation of appropriate window functions to the data prior to transformation. The application of window functions (8) significantly removes sidelobes and leakage which result from the convolution of the rectangular sampling window in which the time domain data were acquired. The relative peak positions in the frequency domain are maintained, however artificial lineshapes are produced upon Fourier transformation which are broader than they otherwise would be (8,9). Application of a Hanning lag window (6,8) revealed that much of the asymmetry associated with the frequency domain peaks was the result of artifacts produced as the result of Fourier transformation of the truncated waveform. The frequency domain spectra generated from data to which the Hanning function had been applied therefore provided an indication of the number and relative positions of the peaks. In order to obtain reasonable estimates for the lineshapes of data exhibiting multiple oscillatory components, the direct Fourier transform of the residual data was fit to the appropriate number of Lorentzians based upon the previous application of a filter function. Lineshape analysis for a designated number of Lorentzians was accomplished using a nonlinear least squares routine based on Marquardt's algorithm (1). The program determined values for the peak positions, peak heights, widths, and areas of the frequency domain spectra. The single-parameter 80 percent confidence intervals are reported in this work.

The validity of the parameters obtained by Fourier analysis were verified by fitting the residual directly to a sum of damped sinusoids. The agreement of the values determined by the two methods was excellent.

§4.3.3 *Autocorrelation Measurements*

Autocorrelation traces of the dye laser pulses were obtained using zero background second harmonic generation (10). A stepper motor driven translation stage (Micro-Controle M062-FC03) was used to vary the time delay between the arrival of the two pulses at a 0.2 mm thick $LiIO_3$ crystal. The second harmonic generated by the two focused noncollinear beams was detected by a photomultiplier. Phase sensitive detection (~300 Hz) was used to provide a large dynamic response range. The output of a lockin amplifier (PAR HR-8) was digitized with a voltage-to-frequency converter and temporarily stored in a multichannel analyzer (Tracor Northern TN1706). The contents of the multichannel analyzer were transferred to a PDP 11/23 computer for analysis.

The temporal structure of synchronously pumped dye lasers have been shown to be adequately described (11,12) by the 'noise-burst' model as developed theoretically by Pike and Hersher (13). In this treatment, fluctuations of the cavity mode phases result in substructure in the pulse intensity envelope and consequently the pulse intensity function can be modeled as the product of an envelope function and a Gaussian distributed random variable describing thermal noise. The functional form of the pulse autocorrelation is given by (13);

$$G(\tau) = G_p(\tau)\,[1 + G_n(\tau)] \qquad (4.3.5)$$

where $G^p(\tau)$ is the autocorrelation function of the pulse envelope and the term in brackets describes the autocorrelation of the noise substructure. The functions $G_n(\tau)$ and $G_p(\tau)$ have been shown to approximate Gaussians with a FWHM of, $\delta\tau_n(\tau_p) = \sqrt{2}\delta\tau_c(\delta\tau_p)$ where t_c is the laser coherence time and t_p is related to the pulse duration. An example of the autocorrelation function obtained for the synchronously pumped cavity dumped dye laser is shown in figure 2. The trace purposely represents non-optimal mode

locking conditions in order to accentuate the difference between $G_p(t)$ and $G_n(t)$. In terms of relating the autocorrelation shown in figure 2 to the physical properties of the laser pulse, the broad base results from the temporal overlap of the pulse envelope, and the coherence spike is the consequence of the overlap of the substructure.

Considering that our application requires only a qualitative determination of the laser coherence time and temporal pulse width, the autocorrelation traces measured in this work were not fit to specific functional forms. In lieu of an exact analysis, τ_c and τ_p were obtained using the following prescription: *a*) if substructure was present in the autocorrelation trace; $\sqrt{2}\tau_c \approx \frac{3}{4}FH$ (full height). and $\sqrt{2}\tau_p \approx \frac{1}{4}FH$; *b*) if there was no evident substructure, $\sqrt{2}\tau_p \approx \sqrt{2}\tau_c \approx \frac{1}{2}FH$. Despite the ingenuousness of this approach the values obtained are not likely to be in error by more than 25 %.

REFERENCES

1. D.W. Marquardt, J. Soc. Ind. Appl. Math, **11,** 431 (1963).

2. P.R. Bevington, *Data Reduction and Error Analysis for the Physical Sciences* , McGraw Hill, New York, 1969.

3. A. Grinvald, Anal. Biochem., **75,** 260 (1976).

4. A. Grinvald and I.Z. Steinberg, Anal. Biochem., **59,** 583 (1974).

5. W. Henke, H.L. Selzle, T.R. Hays, S.H. Lin and E.W. Schlag, Chem. Phys. Lett., **77,** 448 (1981).

6. E.O. Brigham, *The Fast Fourier Transform* , Prentice Hall, New Jersey, 1974.

7. J.W. Cooley and J.W. Tukey, Math Computation, **19,** 297 (1965).

8. R.B. Blackman and J.W. Tukey, *The Measurement of Power Spectra* , Dover Publications, New York, 1958.

9. C.K. Yuen and D. Fraser, *Digital Signal Analysis* , Pittman, London, 1979.

10. E.P. Ippen and C.V. Shank, in *Ultrashort Light Pulses* , Top. Appl. Phys., 18, ed. S.L. Shapiro, Springer Verlag, Berlin, 1977.

11. D.P. Millar and A.H. Zewail, submitted Chem. Phys..

12. D.B. McDonald, J.L. Rossel and G.R. Fleming, IEEE J. Quant. Elec., *QE- 17*, 1134 (1981).

13 H.A. Pike and M. Hersher, J. Appl. Phys., *41*, 4562 (1970).

Figure 1.

Representative data presented for different stages of the analysis of fluorescence decays exhibiting a single or multiple oscillatory components. a) The top figures show the time resolved fluorescence decay which contains both exponential and oscillatory components. b) Subsequent to deconvolution of the system response function and subtraction of the single exponential components, the residual which contains only damped oscillatory terms is generated. The parameters determined upon direct Fourier transformation are compared to those obtained by fitting the residual to a sum of damped sinusoids. c) The residual is Fourier transformed to produce the frequency domian spectrum. d) Comparison of the spectrum obtained upon direct Fourier transformation with that obtained by first multiplying the residual with a Hanning window prior to transformation indicates the amount of leakage and side lobe formation as a consequence of the truncation.

SINGLE FT COMPONENT

MULTIPLE FT COMPONENT

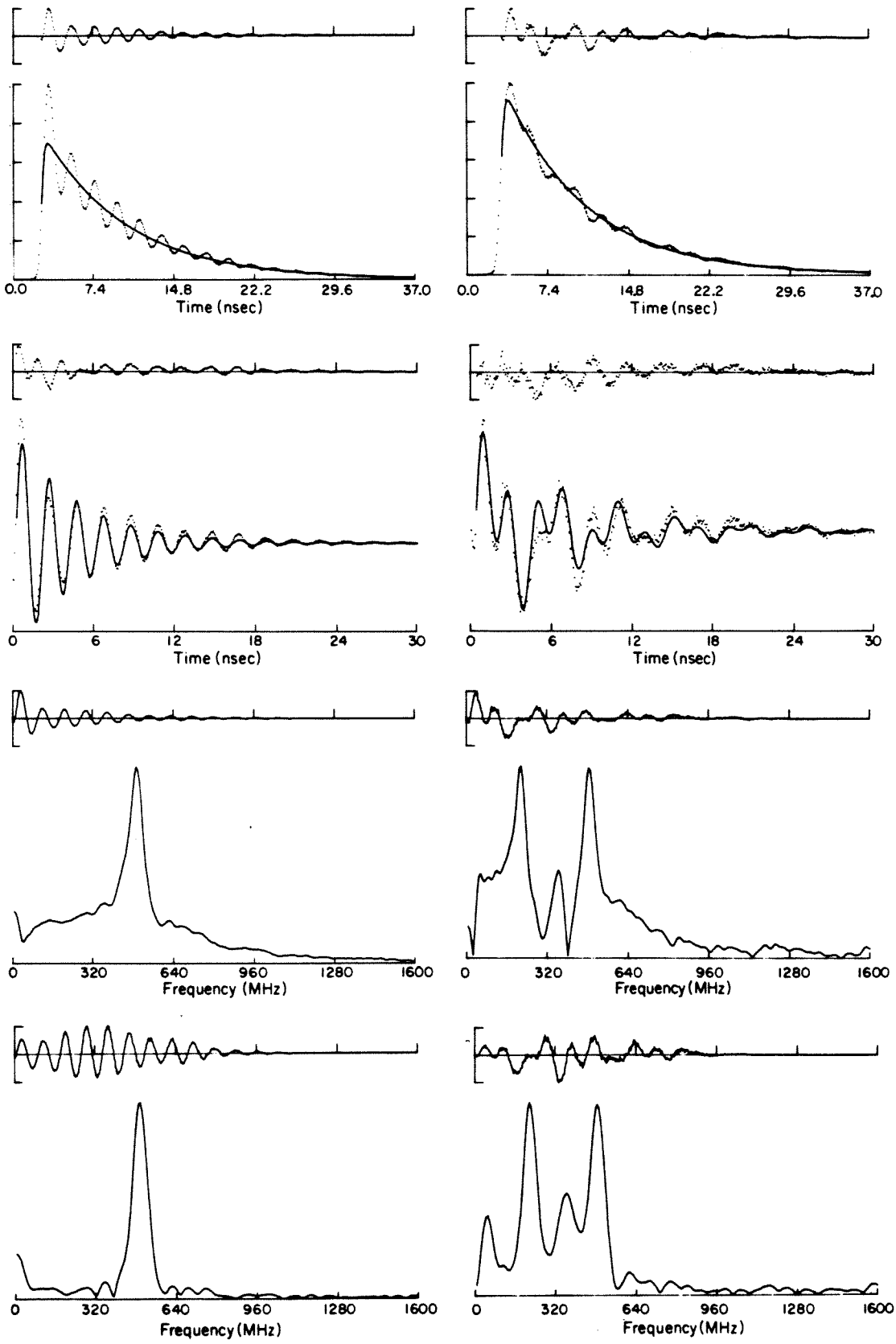

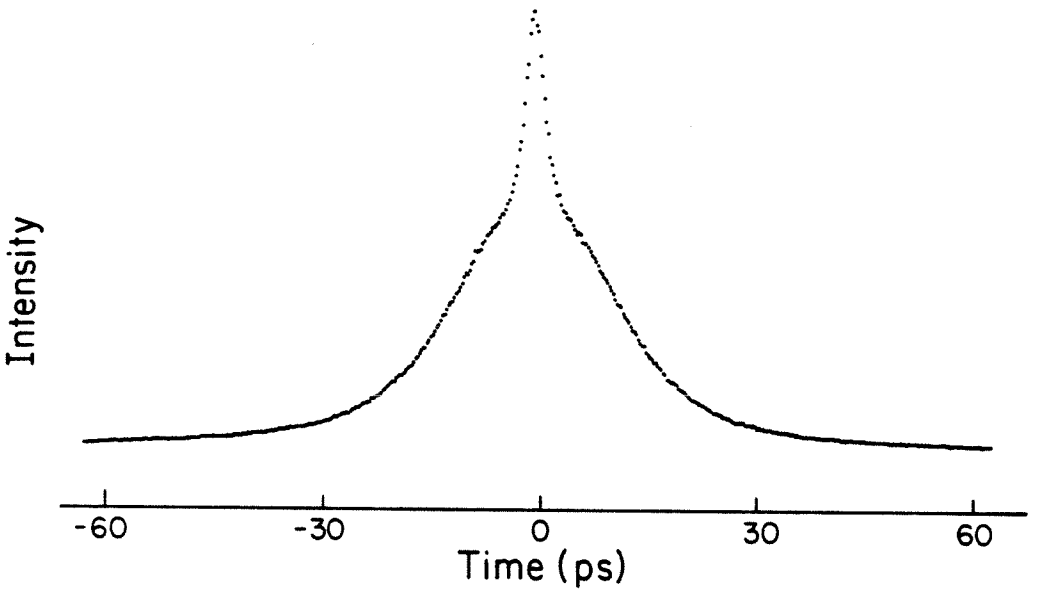

Figure 2.
An example of an autocorrelation trace. The laser is not optimally modelocked in order to emphasize the coherence spike and the envelope of the pulse substructure. The coherence time and the pulse duration, measured as indicated in the text, are τ_c = 2.7 psec and τ_p = 27 psec .

§4.4 *COLLISIONAL PROCESSES IN THE FREE JET EXPANSION AND EVIDENCE FOR COMPLEX FORMATION*

§4.4.1 *Introduction*

An understanding of intermolecular collisional processes in a free jet expansion is essential for determining the physics of intramolecular energy and phase dynamics. In this section we are not so much concerned with collisions which occur prior to the freezin zone (the distance from the nozzle orifice at which the terminal thermodynamic parameters of the expanding gas are established and which are responsible for the cooling of the intermolecular degrees of freedom), but rather with collisions between the carrier gas and the diluent molecule which occur downstream of the source in the region of the isentropic core. The collisions in this region influence the intramolecular dynamics by serving to thermalize the intramolecular energy and phase distribution by the introduction of additional relaxation pathways. Despite the fact that hard-sphere, inelastic collisional processes have been used to study vibrational relaxation of molecules seeded in a free jet expansion (1) and that quenching collisions have been used to reveal properties of intramolecular dynamics (2), the intermolecular interactions which occur in the region of the isentropic core of a free jet expansion are not understood in detail. Complications and subtleties arise when one considers that interaction cross sections change throughout the expansion and more importantly, that free jet expansions have a propensity for generating weakly bound species, such as are exemplified by van der Waal (vdW) complexes (3) and orbiting resonances (4). As the translational temperature of the expanding gas is reduced in the free jet expansion a situation

is produced in which the normal thermodynamics of gas mixtures are no longer rigorously valid. For example, the efficient vibrational relaxation of I_2 cannot be accounted for by considering solely impulsive Landau-Teller energy transfer between collision partners, and as a consequence the importance of quasi-resonant or vdW complex formation in determining the thermodynamics of the free jet expansion has been advanced (5).

In terms of energy and phase redistribution in large molecules, the subtleties of long range collisional cross sections and quasi-resonant complexes may become manifest through the perturbation of the bath manifold of vibrational and rotational states. These elastic collisions would not alter the total energy distribution in the molecular electronic states (in contrast to inelastic collisions which would induce, for example, singlet-triplet mixing), but lead to relaxation and redistribution of the molecualr rotational and vibrational energy. Elastic, intermolecular dephasing collisions have been studied directly in gas phase systems using coherent transient spectroscopy (6). Recently, the analysis of quantum beats for biacetyl in a fee jet expansion (7) has enabled the measurement of specific relaxation cross sections. In a helium-biacetyl expansion, the collisional cross section (inelastic) was determined to be 25 $A^{\circ 2}$ whereas the dephasing cross section (elastic) was measured to be 100 $A^{\circ 2}$.

For a three level system the linewidth associated with the Fourier transform of the quantum beat pattern reflects the homogeneous linewidth of the transitions (see section 4.7). For a multiple level system, as is reflected in large molecules such as anthracene, the association of the linewidth with specific intramolecular energy dynamics is potentially much more complicated but, intrinsically, can possess a higher information content. Since the primary motivation of this research is to under-

stand intramolecular dynamics, it is essential that the contribution of intermolecular processes be understood in detail, before definitive conclusions can be advanced. The fact that the damping rate of the quantum beats is dependent upon elastic or dephasing perturbations, whether of inter- or intramolecular origin, makes the characterization of collisional processes in the expansion even more imperative.

Several theoretical treatments have specifically addressed the degree to which molecules are isolated in a free jet expansion (8). These studies deal with collisional rates in the isentropic region based upon hard sphere collision cross sections. In practice, the influence of inelastic collisions can be determined by observing buildups in the time resolved spectra. On the other hand, models for elastic collisional processes have not been developed largely because elastic processes can only be observed indirectly or qualitatively by analysis of absorption lineshapes and energy resolved fluorescence. The influence of intermolecular interactions can be qualitatively evaluated by change in the expansion conditions of the free jet which include, 1) the backpressure of the carrier gas, 2) the distance from the nozzle at which the expansion is probed, and 3) the carrier gas can be changed. Furthermore, by associating the damping rate of the quantum beats with the homogeneous linewidth, the influence of the expansion conditions on the elastic relaxation and redistribution processes can be evaluated. In this section the manifestation of collisional processes in the time and frequency resolved spectra of anthracene is discussed, and their influence upon the quantum beats are indicated.

§4.4.2 Collisional Dynamics in a Free Jet Expansion

In a free jet expansion the carrier gas and seed molecules are expanded through a pinhole into a vacuum chamber. As the gas undergoes isentropic free wall expansion, the temperature and density, and hence the intermolecular collision rate decrease with increasing distance from the jet source. As the collision rate decreases, a point is reached where a transition from continuum to molecular flow occurs (characterized by the Knudsen number, $Kn_s = \frac{\lambda_s}{D}$, where λ_s is the mean free path between collisions at the nozzle orifice, and D is the diameter of the source), and the axial velocity distribution and Mach number (the ratio of the stream velocity to the local speed of sound) no longer change as a function of distance from the source. This 'freezing- in' distance is defined by (9);

$$x_s = D\,(\,n_s\,Q\,D\,)^{\frac{1}{\gamma}} \qquad (4.4.1)$$

where D is the pinhole diameter, Q, the hard sphere collisional cross section, and n_s is the molecular density at the source. γ is the heat capacity ratio given by $\gamma = \frac{C_p}{C_v}$. Subsequent to this distance, to a first approximation, the gas travels along directed axial streamlines. The isentropic core is surrounded by a shock boundary which at large distances from the source collapses to form a shock front, known as the Mach disk, which originates from collisions with the background gas. The distance from the source at which the Mach disk appears is given by (9);

$$x_c = D\,(\,0.67\,)\left(\frac{P_0}{P}\right)^{\frac{1}{2}} \qquad (4.4.2)$$

where P_0 is the nozzle backing pressure and P is the pressure of the

expansion chamber. Calculated values for the distances of the freezin zone and the Mach disk for our typical expansion conditions (D=150 microns, P_0=45 psi, P= 10^{-4} torr, Q_{N_2} = 43 × 10^{-16} cm^2, T_0=450 °K) are; x_m = 4.7 cm and x_c = 48.5 cm , respectively. The flow structure of the free jet expansion was also evaluated empirically. The freezin zone was found to be located approximately 1 mm from the source based upon our observation of non-exponential fluorescence decays and vibrational mode-selective relaxation at this distance (10). The absence of shock structure for an axial distance at least 5 cm from the source was verified by visualizing persistent streamline flow characteristics of an I_2 expansion using a single mode cw ring laser (11). With a backing pressure of 5 atm, the jet expanded in a well defined cone with an angular spread of approximately 90 degrees implying that a certain degree of density collimation occurred in the jet beyond the general $\cos^2\Theta$ angular dependence given by (9);

$$\rho = \rho_0 (0.16) \left(\frac{X}{D} \right)^{-2} \cos^2\Theta \qquad (4.4.3)$$

Using a typical flow velocity of 1 × 10^5 cm/sec, an axial velocity distribution of 200 MHz is calculated for this divergence, 5 mm from the source.

In the isentropic core the gas expansion is characterized by flow along well defined streamlines which exhibit characteristic translational temperatures and intermolecular collision rates. It is the expansion characteristics in this region that are important for interpreting the results on quantum beats and intramolecular energy and phase redistribution in anthracene. The translational temperature is related to the distance form the source by (12);

$$T = T_0 [1 + \tfrac{1}{2}(\gamma - 1) M_{eff}^2]^{-1} \qquad (4.4.4)$$

where M_{eff} is the local Mach number defined by (9);

$$M_{eff} = A\left(\frac{\gamma}{D}\right)^{\gamma-1} - \tfrac{1}{2}\frac{(\gamma+1)}{(\gamma-1)}\left\{\left(\frac{A\,x}{D}\right)^{\gamma-1}\right\}^{-1} \qquad (4.4.5)$$

where the variable A was determined empirically and depends on the heat capacity ratio of the carrier gas, being 3.26 for a monatomic and 3.65 for a diatomic gas. This expression for the temperature is not to be confused with that for the terminal Mach number presented in section 4.6. The terminal Mach number which establishes the intermolecular temperatures in the expansion in the absence of collisions is defined at the freezing zone. After the freezing zone, intermolecular collisions are no longer effective in transferring energy from the intramolecular degrees of freedom to the translational coordinate. Subsequent collisions, however, serve to perturb the internal energy distribution of the molecule.

Since the molecular flow in the isentropic region of the expansion is adiabatic, the velocity of the gas in this region will be related to the molecular velocity within the source in a manner analogous to that for the temperature given in equation 4.4.4. Since the effective Mach number, defined as the ratio of the bulk flow velocity, V , to the speed of sound, C, is given by ;

$$M_{eff} = V\left(\frac{M}{\gamma K T}\right)^{\frac{1}{2}} \qquad (4.4.6)$$

the stream velocity in terms of the Mach number, and using equation 4.4.4 is;

$$V = V_0\left\{1 + \tfrac{1}{2}(\gamma-1)\,M_{eff}^2\right\}^{-\frac{1}{2}} \qquad (4.4.7)$$

The number of collisions per molecule along an axial flow vector is given, for a Maxwellian velocity distribution by (8);

$$z = n\,Q\,V\,2^{1/2} \tag{4.4.8}$$

where Q is the collisional cross section, and n is the molecular density. The molecular density at a distance downstream from the source is (8,13);

$$n = n_0 \left\{ 1 + \tfrac{1}{2}(\gamma-1)\, M_{eff}^2 \right\}^{-1/2} \tag{4.4.9}$$

combining equations 4.4.7, 4.4.8, and 4.4.9, the collisional frequency in terms of the effective Mach number is derived;

$$z = 2^{1/2}\, n_0\, V_0\, Q \left\{ 1 + \tfrac{1}{2}(\gamma-1)\, M_{eff}^2 \right\}^{\frac{-(\gamma+1)}{2(\gamma-1)}} \tag{4.4.10}$$

§4.4.3 Results and Discussion

Calculations for hard sphere collision rates as a function of the axial distance from the source for typical expansion conditions in our free jet apparatus are presented in figures 1-3. Values for the hard sphere collision cross section of the carrier gases were obtained from the work of McClelland et al. (5) and were assumed to remain constant throughout the expansion. Since the cross sections in reference 5 relate specifically to collisions with I_2, it should be emphasized, that collisional cross sections are dependent upon the specific molecules of the collisional pair. Hence the values which are used here will serve as a relative estimate. The typical distance from the source at which the laser crossed the free jet expansion was 5 mm. For standard expansion conditions the collision rate in the expansion is approximately 10^5 Hz regardless of the carrier gas (figure 1). Therefore, considering that the radiative relaxation rate of anthracene in the free jet is between 5.6 and 24.0 nsec., it is unlikely that hard sphere collisions would influence the intramolecular dynamics of

anthracene during the experimental observation time. As shown in figure 2, changing the backpressure of the carrier gas over the range of pressures employed in these experiments does not appreciably alter the calculated collison rate. The most difficult parameter in the calculation of the collision rate to estimate is the cross section for the specific collision induced interaction. In figure 4.4, Q has been varied over two orders of magnitude using estimates for the vibrational (1.5 $A^{\circ 2}$) , rotational (43 $A^{\circ 2}$) and orbiting resonance (200 $A^{\circ 2}$) cross sections estimated in reference 5, and again the hard sphere collision rate remains much less than the fluorescence relaxation rate of anthracene.

Despite the low probability that hard sphere collisions influence the intramolecular dynamics of anthracene for typical expansion conditions, spectral features consistent with collisionally relaxed transitions were observed upon excitation to intermediate excess energies (S_1+1380 cm^{-1}) when nitrogen was used as the carrier gas (figure 4). The amplitudes of the progressions built upon the 0-0 transition at 3611.8 A° reached a maximum value at a nitrogen backpressure of 100 psi (figure 5). Although transitions were observed at 3611.8 A° with low intensity when either neon or helium was used as a carrier gas, the amplitudes did not change as a function of the carrier gas backpressure (figure 4). Collisionally relaxed transitions were easily distinguished upon measurement of the radiative lifetime (figure 6). The radiative lifetime of the relaxed, 0-0 transition, for 30 psi of nitrogen backpressure was 21.7 ± 0.3 nsec compared to the approximately 9.0 nsec lifetime for the strong spectral features associated with transitions built upon the (1,1) origin. The lifetime of 21.7 nsec obtained at λ_{det}=3611.8 A° for λ_{ex}=3439.6 A° ($\delta\nu$ = 1380 cm^{-1}) is in close agreement with the 23.5 ± 0.8 nsec fluorescence lifetime

obtained for excitation to the S_1 origin at 3611.8 A°. The lifetime for the feature at 3619.5 A° in figure 6 is 11.6 nsec, slightly longer than that for the pressure independent transitions. Since the amplitude of this transition is pressure dependent, the longer lifetime is explained by the partial contribution of a collisionally relaxed transition. Therefore, in addition to the usual progressions associated with anthracene fluorescence at this excitation energy (refer to section 4.7), strong collisionally relaxed features appear for example at 21 cm^{-1}, 47 cm^{-1} and 63 cm^{-1} from the 0-0 origin. The energies of these transitions correspond to resonances observed in the fluorescence excitation spectra of helium-anthracene and nitrogen-anthracene expansions. As discussed in section 4.3, it is possible that these transitions correspond to van der Waals complexes. Evidence for collisionally relaxed transitions are also observed upon excitaton to a number of vibronic levels between 992 cm^{-1} and 1520 cm^{-1} of excess vibrational energy (figures 7a and b). In this region, collisionally relaxed transitions are observed as resonances appearing at 0 cm^{-1} relative frequency.

Several observations lead us to the conclusion that it is unlikely for these relaxed features to be the direct consequence of hard sphere nitrogen-anthracene collisions in the free jet expansion. First, both the time and frequency resolved spectra were relatively insensitive to variations in the laser to nozzle distance, except when the laser was located approximately 1 mm from the source. Only in this region of the expansion where buildups in the time resolved fluorescence observed (14) as is predicted theoretically for inelastic collisions (15) and as is observed experimentally in other molecular systems (1a). Calulations using a cross section of 200 A°, characteristic of orbiting resonances (7), provide colli-

sion rates of approximately 10^6 Hz for a laser to nozzle distance of 5 mm (figure 3). Although many approximations are incorporated into calculations of collision rates, especially with regard to estimates of the destruction cross section for the specific interaction, in free jet expansions, the theoretical values for collision rates would need to be increased by over two orders of magnitude in order for hard sphere collision processes to compete with the radiative relaxation processes in anthracene. A point to be made in this regard is the evidence for mode selective collisionally induced processes subsequent to excitation to intermediate excess energies. The influence of selective mode preparation is most easily seen by comparing the resolved fluorescence spectra in figure 7. Between 992 cm^{-1} and 1520 cm^{-1} of excess vibrational energy there appear several transitions which exhibit a collisionally relaxed peak at 0 cm^{-1} (relative frequency). Again, these features do not appear when helium or neon is used as a carrier gas. That these transitions correspond to emisssion from collisionally relaxed vibrational modes is confirmed by the longer lifetime (by $\sim$ 50 %) for these transitions compared with that for other features appearing in the fluorescence spectra. When the laser is within 1 mm from the source, a temporal buildup in the time resolved fluorescence decays is observed for all vibrational modes, regardless of the excess energy of excitation. This observation is consistent with hard sphere collisions being the predominant relaxation mechanism during the initial stages of the expansion. This collisional relaxation is also dependent upon the nature of the carrier gas (10).

Further evidence for the absence of hard sphere collisions in the free jet comes from the fact that, whereas the intensity of the relaxed transition appearing at 3611.8 A° upon excitation to 3439.6 A° (figure 4) is pres-

sure dependent, variation of the laser to nozzle distance (figure 8) does not influence the amplitude. The distance of the laser from the nozzle was varied between 13 mm and 3 mm without observing a change in the relative magnitude of the 0-0 transition. The evolution of thermodynamic parameters associated with cooling of the intramolecular degrees of freedom cease at the freeze-in zone. If hard sphere collisions subsequently persisted in the expansion, one would expect to observe both a pressure and a distance dependence in the intensity of collisionally relaxed peak as indicated by equation 10. This implies that here we observe a concentration effect (by means of the nozzle backpressure), perhaps indicative of relaxation induced by dissociation of, or perturbation by a weakly bound complex. The backpressure of the carrier gas does not appreciably influence the intermolecular collision rates over the applicable pressure range (figure 2). For experiments in which the nozzle pressure was systematically varied, a pressure dependent Stern-Volmer relationship (increased fluorescence relaxation rate with increasing nozzle backpressure) was not produced, even though such an effect, dependent upon P_0 should be observed via equation 4.4.10. Apparently the predominant influence of increasing the backpressure of the carrier gas is to cool the intramolecular temperatures.

In contrast to the fact that we do not observe a distance dependent change in the intensity of the collisionally relaxed peak (figure 8), we have documented a laser to nozzle distance dependent influence on the fluorescence decay rate when nitrogen is used as a carrier gas. These results, obtained for λ_{ex}=3439.6 A° and λ_{det}=3577.5 A° are presented in figure 9, and corresponding results obtained with helium as the carrier gas are shown for comparison in figure 10. From the Stern-Volmer plot,

and using the calculated translational temperature for the specified expansion conditions (equation 4.4.4), a collision cross section of 82 $A^{\circ 2}$ was estimated. This value is similar to that obtained for biacetyl in a helium free jet expansion (7) using similar experimental conditions. It is surprising to find that biacetyl which exhibits efficient collision induced spin-orbit coupling has a collision cross section similar to that of anthracene. The measurement of a relatively large collision cross section for the nitrogen-anthracene interaction would at first appear to contradict the conclusion that hard sphere collisions are insignificant in causing relaxation in the free jet expansion. However, a possible explanation for these results would be the formation of a vdW complex. The bound species could efficiently redistribute energy by means of V → T, V → V, or V → V+T transfer, subsequent to excitation (16). However, the effects of bound species should not depend upon the distance from the nozzle, therefore the collisional effects observed in figure 9 are probably the result of intermolecular collisions prior to the freezin zone. For typical experimental conditions, X = 5 mm (X/D = 33). In comparison, the first data point in figure 9 represents a laser to nozzle distance of 1.0 mm (X/D = 6.8). As a final point with regard to the experimental results which reflect the influence of intramolecular collisions, there is evidence for excited state rotational relaxation obtained from comparison of rotational profiles subsequent to absorption and emission (refer to figure 5 in section 4.5). An explanation may be that the rotational broadening observed in the energy resolved fluorescence spectra are also collisionally induced.

In view of the experimental results presented in this section we are inclined to invoke the presence of a weakly bound or weakly interacting nitrogen-anthracene complex as an explanation for our findings. Although

calculations based upon the gas dynamics of free jet expansions indicate that intermolecular collisions should not occur in the region of the isentropic core, and despite the fact that evidence for collisional relaxation of anthracene in expansions of helium and neon was not observed, several lines of experimental evidence indicate that intermolecular interactions take place in the nitrogen expansion. A consistent interpretation of the results regarding collisional processes in the free jet expansion of anthracene would include the presence of a weakly bound nitrogen-anthracene complex. Since the amplitude of the relaxed transition at 3611.8 A° for λ_{ex}=3439.6 A° becomes saturated at high nitrogen backpressures (figure 5) it seems that at pressures above 100 psi most of the anthracene molecules in the expansion are associated with nitrogen complexes. The fact that a selective decrease in specific vibrational modes, complementing the increase of intensity for the relaxed transition at 3611.8 A°, implies that the nitrogen-anthracene interaction is probably mediated through the bath manifold or at least the internal energy distribution created by the laser excitation becomes redistributed among many intramolecular degrees of freedom by means of perturbation within the complex.

The formation of quasi-resonant and vdW complexes is favored by low internal temperatures, size of the molecules (well depth), and by the number of internal degrees of freedom for the collision partner (5,17). At the low translational temperatures produced by a supersonic expansion it is possible for collision partners to become trapped within the intermolecular centrifugal barrier. Impact with the repulsive wall redistributes the attractive energy among the exit translational channels, and among the intramolecular vibrations and rotations. In the case where the

number of the internal degrees of freedom is very large, as is the case for large polyatomic molecules, the energy will become redistributed such as to prevent the rapid dissociation of the complex. Subsequent excitation will dissociate the quasi-resonant complex which in turn will lead to further vibrational relaxation as energy is absorbed in the kinetic exit channel. This mechanism has been discussed in terms of the apparently large cross sections which exhibit weak inverse temperature dependence as observed for vibrational relaxation of I_2 in nitrogen expansions (5). Analogous efficiencies for collisionally induced vibrational relaxation are also indicated for dissociation of long lived vdW complexes (17). In terms of the quasi-resonant complex model (18), the pressure dependence for vibrational relaxation (figure 4) would reflect the number of weak complexes which are formed in the expansion. The absence of measurable fluorescence risetimes, supports the contention of a weak attractive barrier, and commensurate rapid dissociation following excitation. Predissociation lifetimes for vdW complexes have been determined to be on the order of a few hundred picoseconds (19,20).

Quantum beats are observed with all carrier gases used (helium, neon, and nitrogen) and become more prominent when nitrogen is used despite the fact that nitrogen-anthracene expansions exhibit the greatest propensity to form weak complexes. This behavior is explained by the greater degree of vibrational cooling realized in the nitrogen free jet expansion (refer to section 4.5 for a discussion of the vibrational temperature). We conclude that the phenomenon of quantum beats in anthracene is not directly related to consequences of intermolecular collisions or to complex formation, however, and as is discussed in greater detail in section 4.8, these processes may contribute to the intramolecular energy

and phase redistribution. It is likely that the interaction of anthracene and nitrogen in the complex is mediated through the large density of states which exist at intermediate excess energies and does not appear to be related to specific vibrational interactions. The relevance of the foregoing discussion on collisional processes in the free jet expansion, to the dynamics of intramolecular relaxation and redistribution will be discussed in detail with respect to quantum interference effects in anthracene.

REFERENCES

1. a) J. Tusa, M. Sulkes and S.A. Rice, J. Chem. Phys., **70,** 3136 (1979), b) G. ter Horst and J. Kommandeur, J. Chem. Phys., **76,** 137 (1982), c) T.D. Russel, B.M. Dekoven, J.A. Blazy and D.H. Levy, J. Chem. Phys., **72,** 3001 (1980).

2. R.A. Coveleskie, D.A. Colson and C.S. Parmenter, J. Chem. Phys., **72,** 5774 (1980).

3. D.H. Levy, Adv. Chem. Phys., **47,** 323 (1981).

4. J.P. Toennies, W. Welz and G. Wolf, J. Chem. Phys., **71,** 614 (1979).

5. G.M. McClelland, K.L. Saenger, J.J. Valentini and D.R. Herschbach, J. Phys. Chem., **83,** 947 (1979).

6. P.R. Berman, J.M Levy and R.G. Brewer, Phys. Rev. A, **11,** 1668 (1975).

7. W. Henke, H.L. Selzle, T.R. Hays, S.H. Lin and E.W. Schlag, Chem. Phys. Lett., **77,** 448 (1981).

8. D.M. Lubman, C.T. Rettner and R.N. Zare, J. Phys. Chem., **86,** 1129 (1982).

9. H. Ashkenas and F.S. Sherman, in *Rarefied Gas Dynamics*, 4^{th} Symposium, V.2, ed. J.H. de Leeuw, Academic Press, New York, 1966, p. 84.

10. P.M. Felker, W.R. Lambert and A.H. Zewail, unpublished results.

11. W.R. Lambert, unpublished results.

12. A. Kantrowitz and J. Grey, Rev. Sci. Instr., **22,** 328 (1977).

13. R.E. Smalley, L. Wharton and D.H. Levy, Acc. Chem. Res., **10,** 139 (1977).

14. A. Zewail, W. Lambert, P. Felker, J. Perry and W. Warren, J. Phys. Chem., **86,** 1184 (1982), and W. Lambert, P.M. Felker and A. Zewail, unpublished results.

15. A. Tramer, in *Radiationless Transitions*, ed. E.C. Lim, Academic Press, New York, 1981, p. 337.

16. J.A. Beswick and J. Jortner, J. Chem. Phys., **74,** 6725 (1981), and references therein.

17. G. Ewing, Chem. Phys., **29,** 253 (1978).

18. R.W. Zwansig, J. Chem. Phys., **32,** 1173 (1960); and H.J. Loesch and D.R. Hershbach, J. Chem. Phys., **57,** 2038 (1972).

19. K.E. Johnson, W. Sharfin and D.H. Levy, J. Chem. Phys., **76,** 5295 (1982).

20. M.P. Casassa, F.G. Celli and K.C. Janda, J. Chem. Phys., **76,** 5295 (1982).

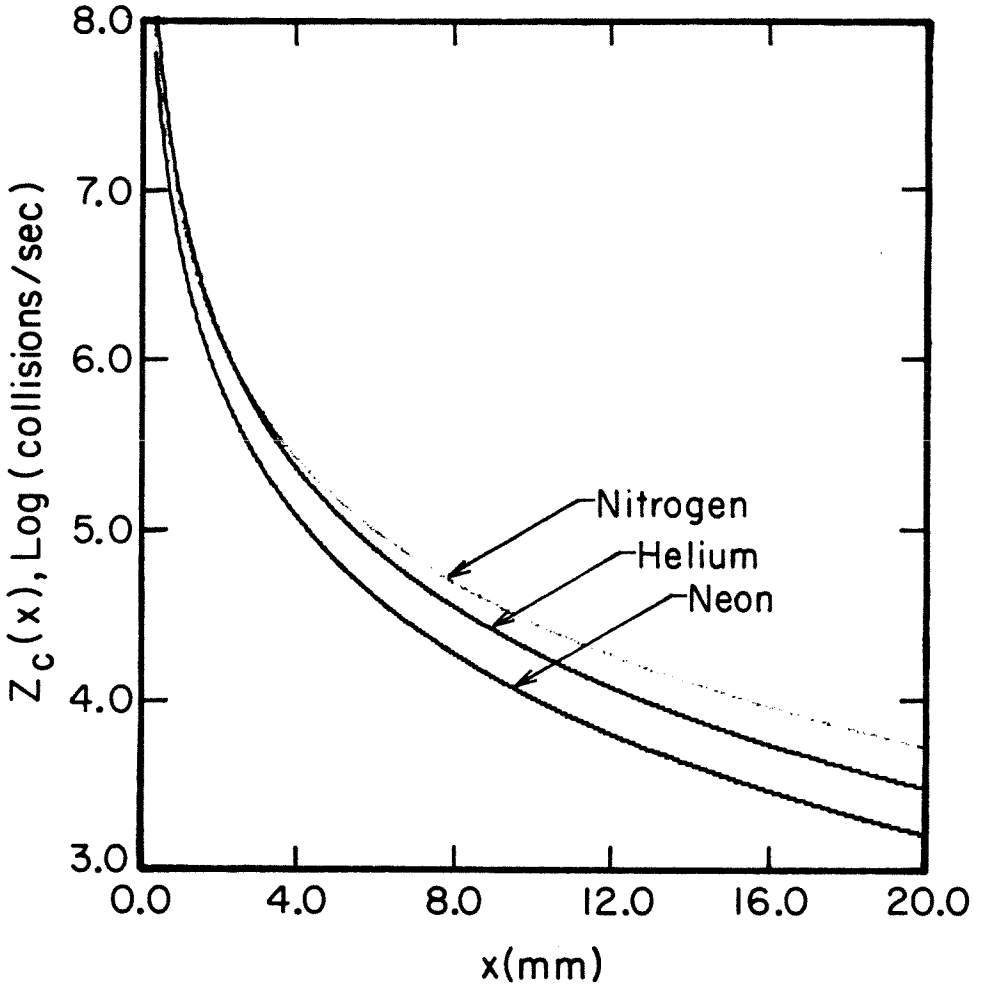

Figure 1.
The influence of the carrier gas on the intermolecular collision rate, $z_c(x)$. The collision rate, calculated from equation 4.4.10 is plotted as a function of distance from the nozzle, for nitrogen, neon, and helium. Rotational cross sections were taken from reference 5, being 43 $A^{\circ 2}$, 25 $A^{\circ 2}$, and 21 $A^{\circ 2}$ for nitrogen, neon, and helium, respectively. Standard expansion conditions were used: T_0=450 °K, D=150 microns, P=45 psi.

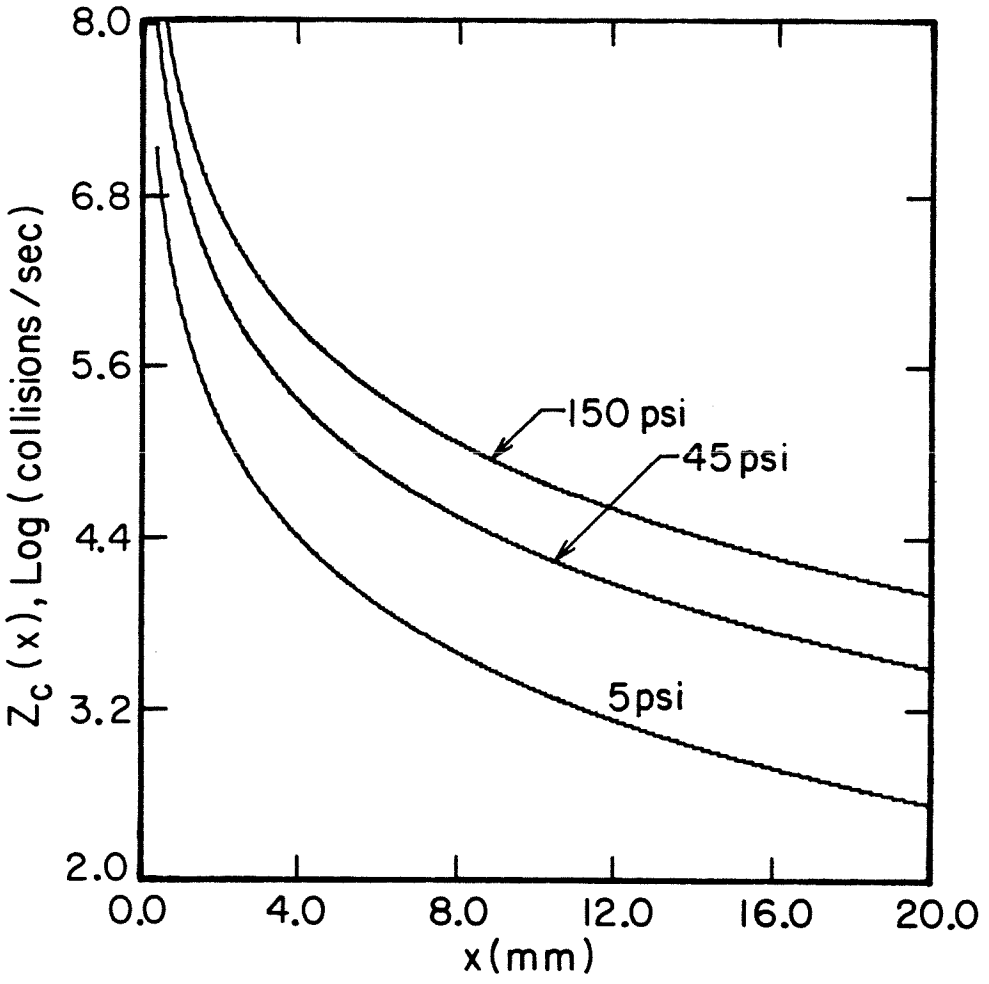

Figure 2.
The influence of the helium backpressure on the intermolecular collison rate, $z_c(x)$. The number of collisions per second for 150 psi, 45 psi, and 5 psi of helium pressure is presented as a function of distance from the nozzle. A collisional cross section appropriate for rotational energy transfer (5) was used. The expansion conditions are the same as those indicated for figure 1.

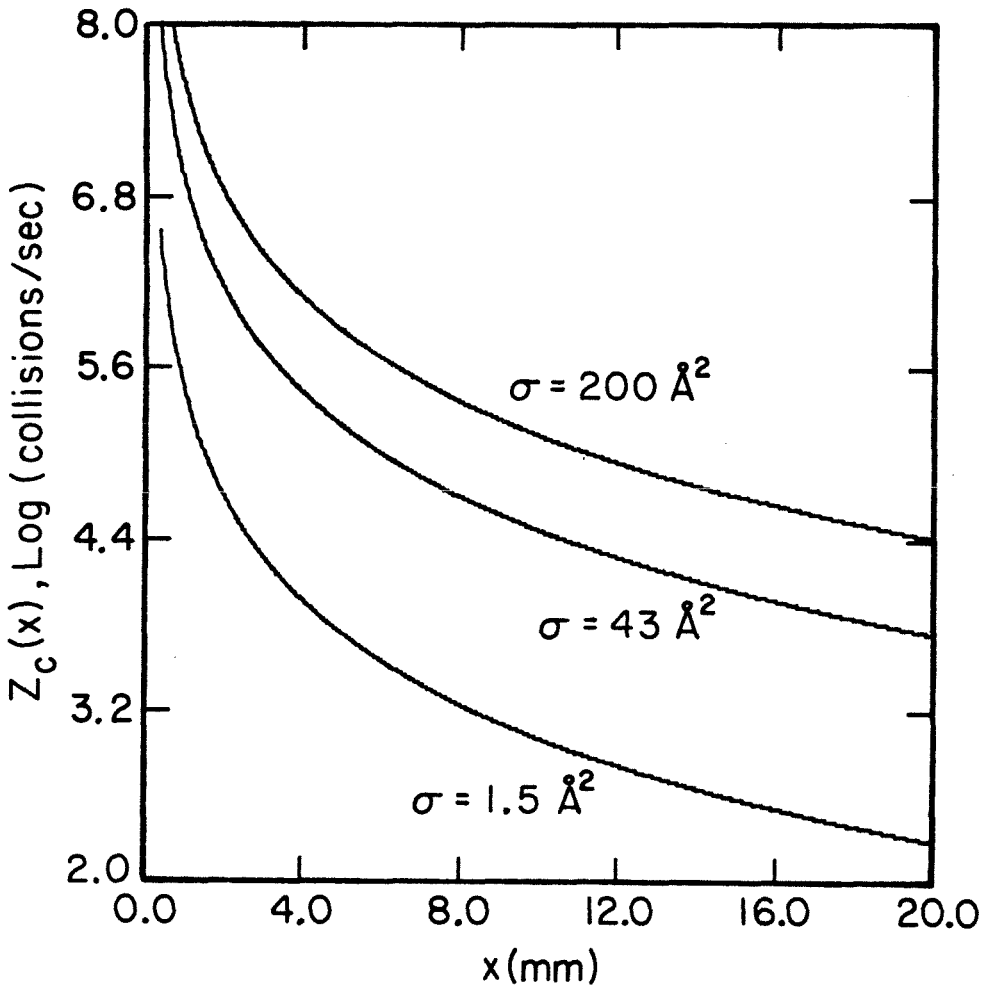

Figure 3.

The influence of the collisional cross section on the intermolecular collision rate in a free jet expansion. The collision rate is presented as a function of distance from the nozzle for different assumed values for the collisional cross section. The cross section was varied over two orders of magnitude, selecting values appropriate (5) for vibrational relaxation (1.5 A°^{2}), rotational relaxation (43 A°^{2}) and orbiting resonance interactions (200 A°^{2}). Standard expansion conditions were assumed and are presented in figure 1.

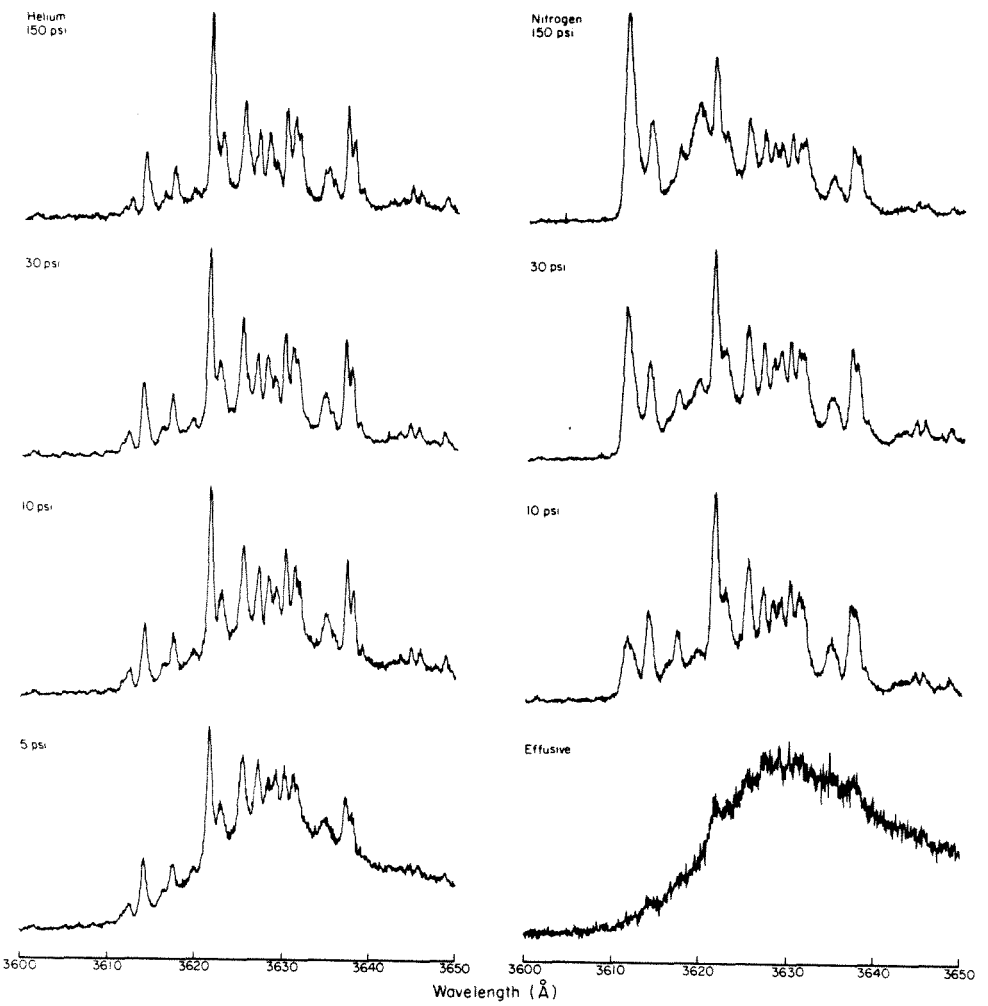

Figure 4.

The effect of the carrier gas and backpressure on the energy resolved fluorescence spectra of anthracene for 3439.6 A° (S_1+1380 cm^{-1}) excitation. Whereas the helium spectra only exhibit a pressure dependent reduction in the spectral congestion due to the decrease in the intramolecular rotational and vibrational temperature, the spectra taken with nitrogen show a pressure dependent increase in the intensity of the transition at 3611.8 A°. Standard experimental conditions were in effect: D = 150 micron, T_0 = 450 °K, X(laser to nozzle distance) = 6 mm. The effects of cooling are demonstrated by comparison with the effusive beam spectrum.

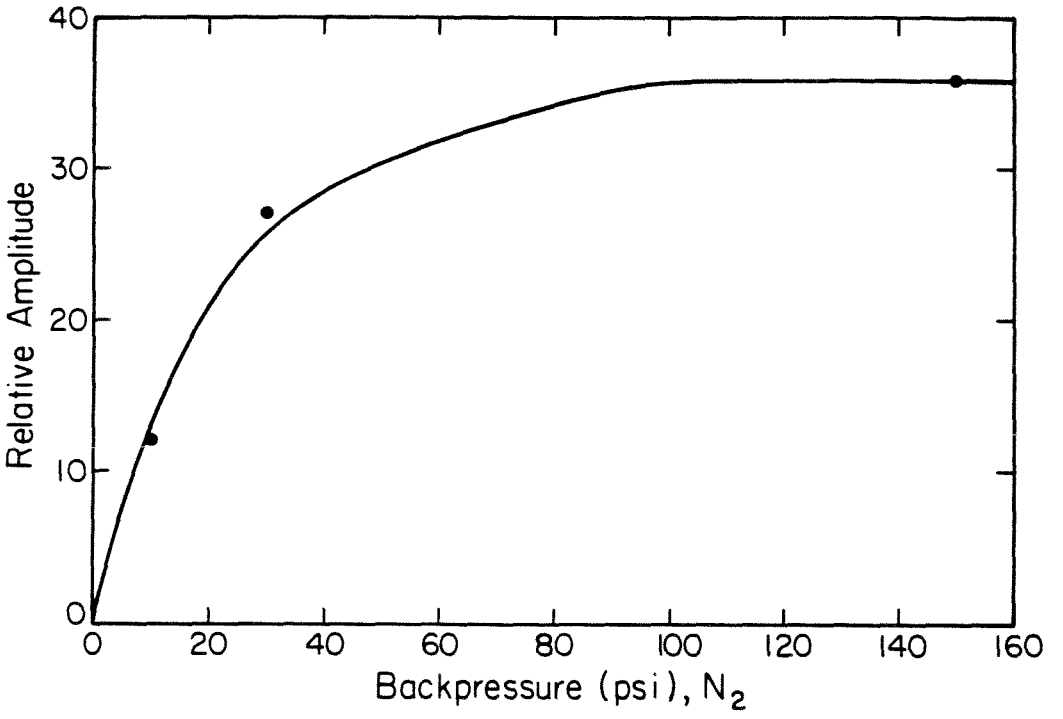

Figure 5.

The relative amplitude of the collisionally relaxed transition at 3611.8 A° with reference to figure 4 is presented as a function of the nitrogen backpressure. The experimental conditions are the same as those indicated for figure 4.

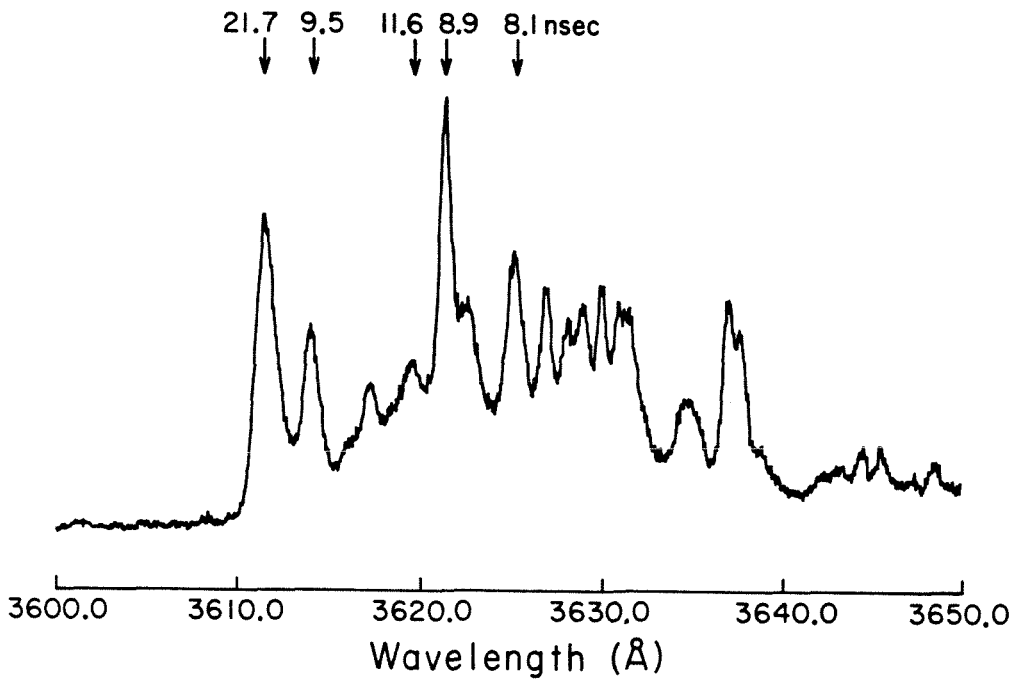

Figure 6.

The fluorescence lifetime of transitions in the region of the 1-1 transition (S_0+1380 cm^{-1} - S_1+1380 cm^{-1}) of anthracene for 3439.6 A° (S_1+1380 cm^{-1}) excitation. The collisionally relaxed transition appearing at 3611.8 A° is distinguished by the relatively long lifetime of 21.7 ± 0.3 nsec. The nitrogen backpressure used was 45 psi. The experimental conditions were otherwise the same as those indicated for figure 4.

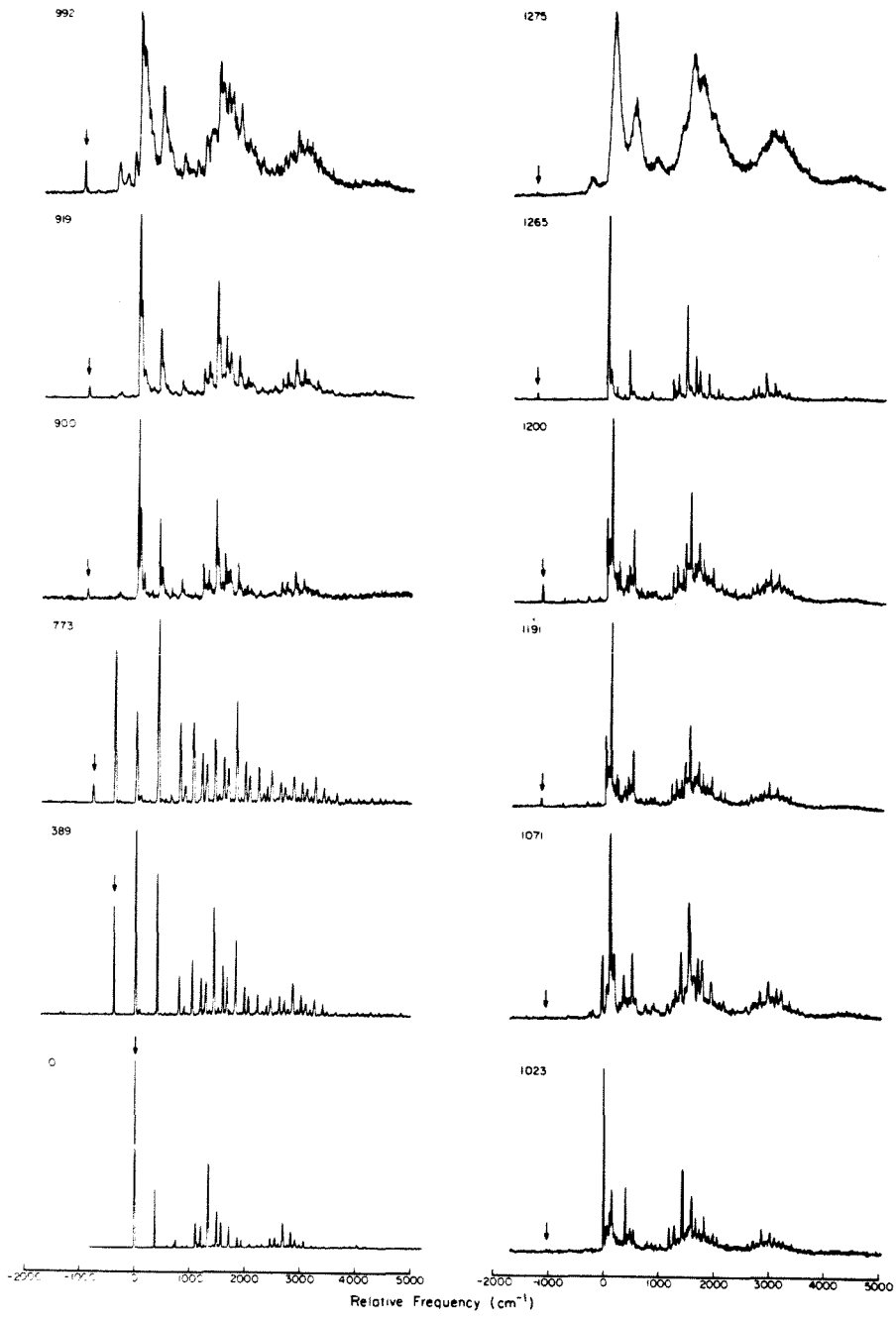

Figure 7.

Energy resolved fluorescence spectra of anthracene for different excitation wavelengths. The corresponding excess energies above the S_1, $^1B_{2u}$+ origin are indicated for each spectra. The relative excitation frequency for each spectrum is indicated by an arrow. In the context of the discussion presented in this section, the spectrum representing the region between 900 and 1200 cm^{-1} show evidence for collisional relaxation as indicated by transitions at 0 cm^{-1} (relative frequency). The experimental conditions are: D= 150 microns, T_0=450 °K, 45 psi nitrogen backpressure, X = 5 mm, monochromator resolution = 0.25 A°).

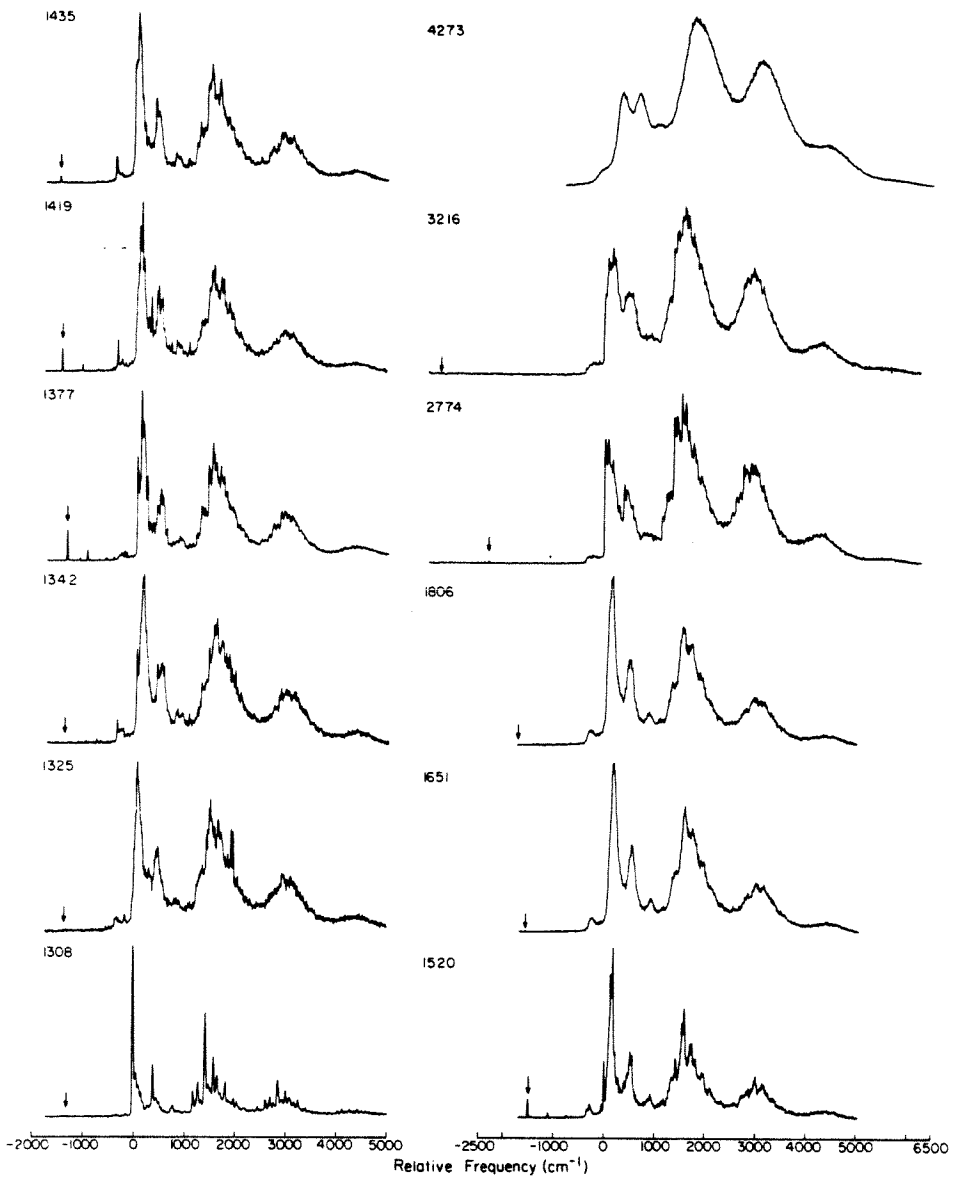

Figure 7, continued,

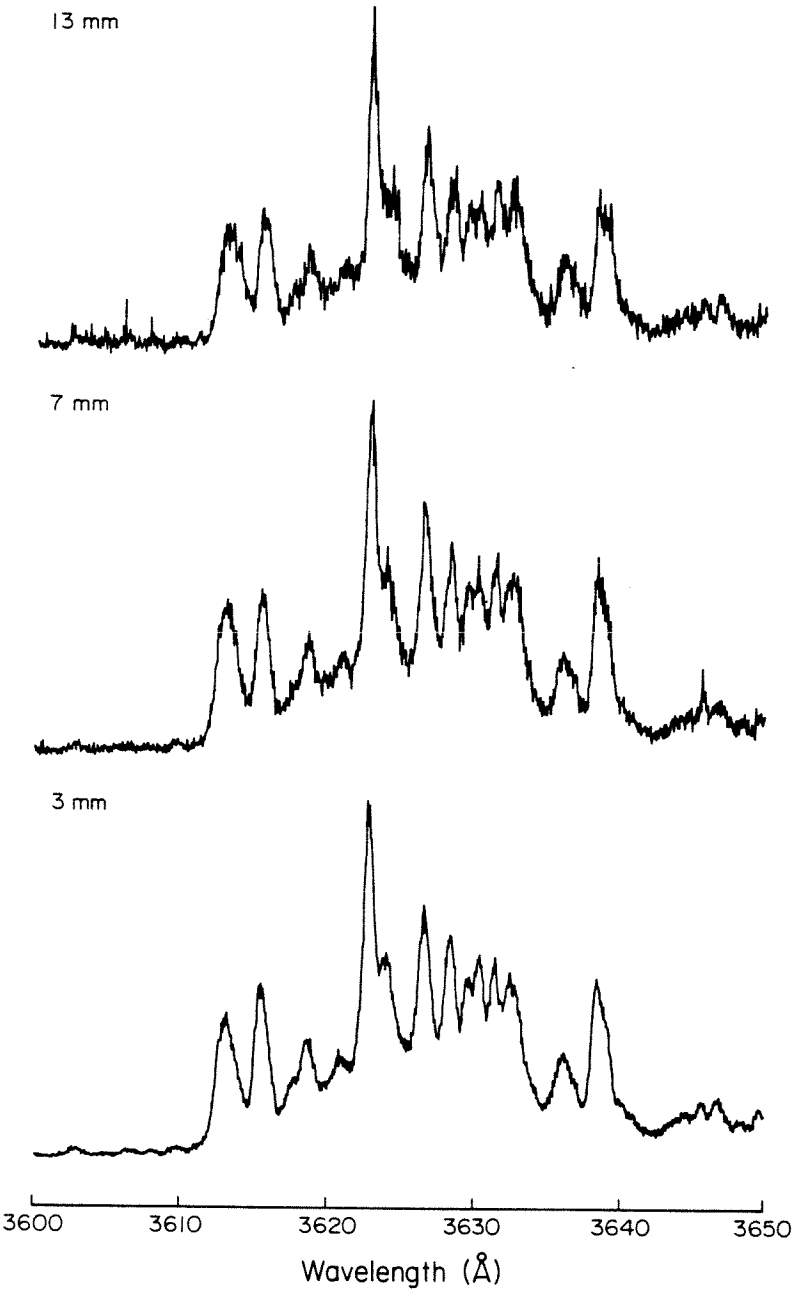

Figure 8.

A portion of the energy resolved fluorescence spectrum of anthracene in the region of the 0-0 transition is shown for different laser to nozzle distances from 3 mm to 13 mm. The relative intensities are shown to be independent of the distance between the laser and the nozzle. The excitation wavelength is 3449.6 A° (S_1 + 1380 cm^{-1}) and the nitrogen backpressure is 40 psi. All other experimental conditions are the same as those given for figure 4.

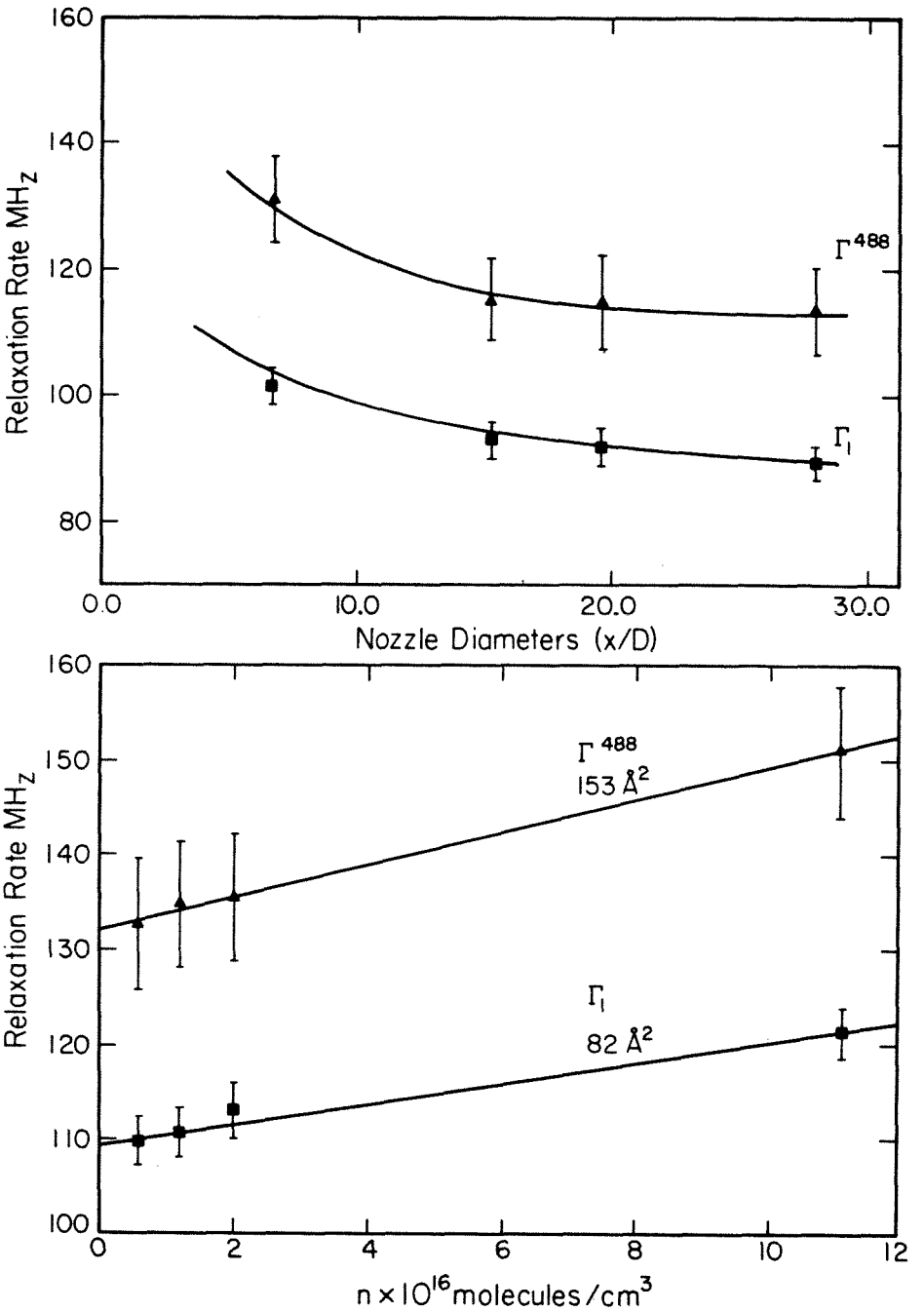

Figure 9.

The dependence of relaxation rates on the distance of the laser from the nozzle using nitrogen as the carrier gas. The experimental conditions were: D = 150 microns, T_0 = 450 °K, P = 45 psi. A laser to nozzle distance (X/D) of 10 corresponds to 1.5 mm. Normally, experiments were performed at laser to nozzle distances of 5 mm, corresponding to X/D = 33. Part a) shows the fluorescence decay rate, Γ_1, and the total dephasing rate, Γ, as a function of the laser to nozzle distance. Part b) shows the Stern-Volmer plot of the corresponding data. The collisional and dephasing crosssections are calculated to be 82 A°^{2} and 153 A°^{2}, respectively. Measurements of the relaxation rates and calculation of the Stern-Volmer relationship are discussed in section 4.9.

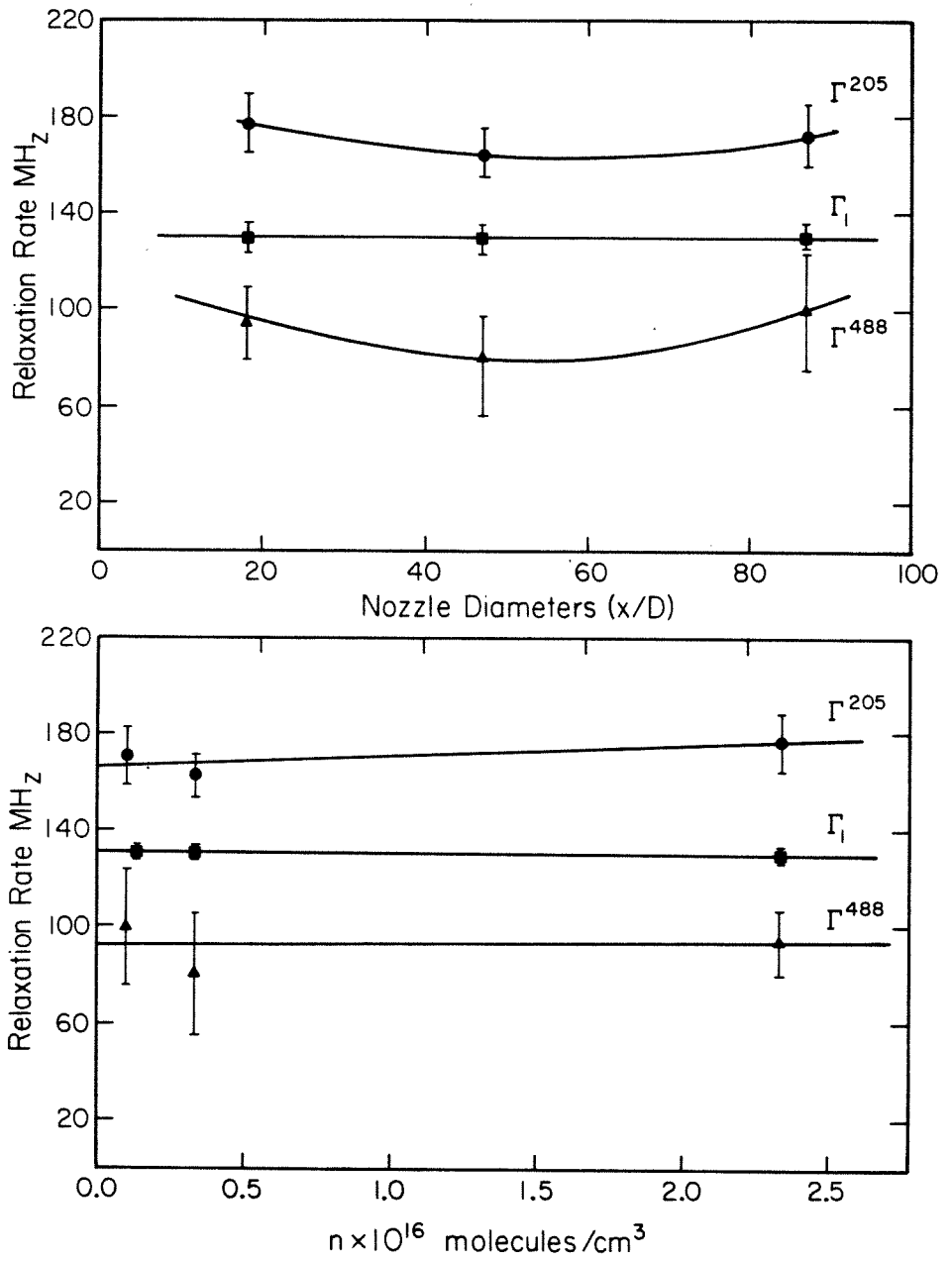

Figure 10.

The characteristic relaxation rates of anthracene in a helium expansion as a function of the laser to nozzle distance. Γ_{488} and Γ_{205} designate the total dephasing rates for the 488 MHz and the 205 MHz Fourier component of the quantum beat pattern. The excitation wavelength was 3439.6 A° (S_1 + 1380 cm^{-1}) and the detection wavelength was 3577.5 A°. The experimental conditions are the same as those indicated in figure 10. The Stern-Volmer relationship presented in Part *a*) indicates the absence of intermolecular collisions in the helium expansion. Details regarding the measurement of the relaxation rates and the determination of the Stern-Volmer relationship can be found in sections 4.7 and 4.9.

§4.5 *FLUORESCENCE EXCITATION SPECTRA OF ANTHRACENE : VIBRATIONAL ANALYSIS, VIBRATIONAL TEMPERATURE, AND COMPLEX FORMATION*

Analysis of fluorescence excitation spectra obtained in the region of the S_1 origin enables the determination of the vibrational temperature by means of analysis of vibrational hotband amplitudes. In addition, spectral features associated with various van der Waals (vdW) complexes generally appear to the low energy side of the origin. In the study of intramolecular energy and phase redistribution in isolated large molecules the generation of vdW complexes is undesireable from the standpoint of reproducing the spectral congestion which free jet expansion techniques are employed to effectively eliminate. Characterization of vdW species and their pressure and carrier gas dependence provides information regarding the molecular composition of the expansion. This knowledge enables the design of the experimental conditions which generate free jet expansions in which molecules are effectively isolated while simultaneously providing the mechansism for efficient cooling of the rotational and vibrational intramolecular degrees of freedom. On the other hand, a substantial field of research has evolved around the study of vdW complexes; the nature of weak intermolecular interactions (1) and solvation processes (2).

The efficiency of vibrational cooling and the characteristics of vdW complex formation of anthracene in a free jet expansion are presented in figures 1 and 2. A dramatic difference in the spectral features associated with helium and nitrogen expansions is observed. Whereas the helium-anthracene expansion is characterized by essentially pressure independent sharp spectral features to both higher and lower energy of the

origin, the nitrogen-anthracene expansion shows broad structureless features which broaden with increasing pressures, extending 300 cm^{-1} to the lower energy side of the origin at a backpressure of 55 psi. The pressure dependence of the nitrogen-anthracene expansion is presented in detail in figure 2. In contrast to the helium and nitrogen expansions, for similar experimental conditions the argon-anthracene free jet is dominated by vdW complex formation (3). The spectra shown in figure 1 can also be compared to the effusive beam spectrum (figure 3) which is dominated by spectral congestion originating from hotband transitions. The maximum amplitude of the effusive beam spectrum is one sixth that of the spectra which are shown in figure 1. This attests to the dramatic increase in the fluorescence yield which results as a consequence of the reduction in the non-radiative decay pathways upon rotational and vibrational cooling in free jet expansions. In addition, as ground state population becomes concentrated at lower quantum numbers, overlap with the laser bandwidth is increased.

Table 1 presents the vibrational analysis of the fluorescence excitation spectrum of anthracene expanded in helium. Based upon our assignments for the ground and excited state vibrational frequencies (section 3) the transitions which appear at -159 cm^{-1} and -172 cm^{-1} are assigned as hotbands corresponding to the transitions S_0+307 cm^{-1} ← S_1+230 cm^{-1} and S_0+395 cm^{-1} ← S_1+230 cm^{-1}, respectively. Similar assignments for these transitions have also been made by Hays et al. (4). The amplitudes of the hotband transitions reflect a vibrational temperature of 150 °K. The relatively high vibrational temperature is consistent with the general observation that helium is relatively inefficient at vibrationally cooling large molecules in free jet expansions (5). The high vibrational tem-

perature is in part the consequence of the high temperature of the nozzle source, 450 °C. The inefficiency of vibrational cooling with helium at these relatively low backpressures is exemplified by the absence of a pressure dependent reduction in the intensity of the hotband transitions. The remaining transitions in the helium-anthracene spectra, although exhibiting some narrowing as the result of increasing backpressure, do not show an overall change in the relative amplitudes. Assignment of the transitions appearing between -100 cm^{-1} and + 60 cm^{-1} as hotbands (other than the origin) would reflect unreasonably high vibrational temperatures. We therefore attribute these transitions to helium-anthracene vdW complexes.

Sharp spectral features attributed to vdW complexes have also been observed by Hays et al. (4) using argon as a carrier gas. The discrete nature of the vdW transitions implies that the complexes are composed of a small numuber of specifically bound helium atoms. Unfortunately, the absence of pressure dependent amplitudes prevents association of the transitions with specific vdW species through an $I \alpha P^{2n}$ dependence. The inability of increasing backpressure to support vdW complexes formation can in part be explained by the fact that vibrational cooling is incomplete. As the backpressure of helium is increased, further collisions of the carrier gas with anthracene will be ineffective in reducing the intramolecular temperature, thereby preventing further helium condensation. On the other hand, it is apparently unique to realize such a high degree of vdW complex formation in view of the low helium backpressures employed. Similar features associated with vdW complexes are typically observed in expansions of the heavier carrier gases, N_2, Ar, Xe and Kr (2). The use of helium expansions is generally promoted in order to minimize

the undesirable effects of carrier gas condensation (6,7). The inability of the helium dimer to support a bound state (8) prevents the nucleation of supercooled helium dimers. As a consequence, higher helium backpressures can generally be maintained in the absence of vdW complex formation, thereby enabling lower rotational and vibrational temperatures to be achieved. However, as a consequence of the low cooling cross section (9), relatively high stagnation pressures on the order of 10 → 100 atm are typically employed to achieve adequate cooling. In this context, free jet expansions of phthalocyanine produced at high values of PD = 200 torr-cm (100 atm, 25 micron diameter pinhole, T_0= 450 °C) are free of vdW complexes (10). The explanation submitted by Fitch et al. (10), that the low molecular density at the freezing in distance which is extended as the stagnation temperature is increased prevents helium vdW complex formation, appears to be insufficient in light of our results, for despite similar experimental conditions, substantial helium-anthracene complex formation is apparent in our free jet. Another interesting, although not unprecedented (11) observation is the appearance of transitions associated with complex formation to the blue of the origin. This result implies that the helium atoms are bound less strongly in the excited state of the complex than in the ground state. It is also possible that this structure is due to progressions of anthracene dimers (12).

In this discussion of the sharp features appearing in the region of the S_1 origin found in the helium-anthracene free jet expansion, the existence of dimers or 'mild excimers' (12) should not be ignored. Dimer formation has been observed in the expansion of dimethyl-tetrazine (DMT) in helium (12). The DMT dimer origin appears approximately 500 cm^{-1} to the red of the origin, however, transitions attributed to progres-

sions built on the dimer $6a_0^1$ ring-mode appear 40 cm^{-1} on either side of the S_1 origin of the uncomplexed DMT. Although we are unable to verify the existence of anthracene dimers in our helium expansion, since we did not search to lower energy, we have observed energy resolved fluorescence spectra indicative of anthracene dimers in argon expansions (13). Upon excitation to high excess energies (+2800 cm^{-1}), the energy resolved fluorescence spectrum reveals a broad shoulder to the red of the 2-2 origin (1400 cm^{-1} mode), similar to that obtained for anthracene dimers in solids (14,15). This feature exhibited a fluorescence lifetime of 33 nsec whereas the lifetime of the 2-2 origin was 6 nsec, characteristic of uncomplexed anthracene upon excitation to these excess energies. Again, definitive association of this feature as resulting from an anthracene dimer requires further studies on the spectroscopy of argon-anthracene expansions, particularly in the region of the S_1 origin.

In contrast to the helium-anthracene expansion, the nitrogen expansion is free of sharp spectral structure (figure 1). The comparison is directly made in figure 1, and the pressure dependence of the nitrogen-anthracene complexes is shown in figure 2. The spectra are characterized by broad structure appearing to the red of the S_1 origin and extending at higher pressures to -300 cm^{-1} (figure 2, 55 psi). The integrated area of the broad structure increases linearly with the backpressure of the carrier gas in contrast to the reduction in amplitude observed for the origin transition (figure 4b). The fact that the pressure dependence does not scale as P^{2n} prevents association of the structure with specific nitrogen complexes. Several sharp features also appear (Table 2), the most prominent being -41 cm^{-1} to the red of the origin. The intensity of this transition increases with increasing nozzle pressure up to 30 psi and then

decreases as the backpressure is further increased suggesting that this feature is associated with a low coordination complex.

Low frequency vibrations are also observed in the energy resolved fluorescence spectra (figure 5). Upon laser excitation to the S_0-40 cm^{-1} transition, the energy resolved fluorescence is identical to that of anthracene with the exception that progressions of a 30 cm^{-1} vibration are built upon each fundamental. Similar, although more complicated structure is seen in the energy resolved fluorescence upon excitation to the broad spectral features. Figure 5a shows the progressions arising from excitation to S_0-63 cm^{-1}.

The combination of broad and sharp pressure dependent spectral features to the red of the S_1 origin have been observed in argon-anthracene free jet expansions (4). The spectra are interpreted in terms of two types of complexes: 1) vdW molecules involving specifically oriented and vibrationally coupled complexes consisting of at most a few carrier gas atoms/molecules which are generally observed to some extent in free jet expansions of large molecules (5,11,16) and which are manifest as sharp spectral features, and 2) complexes involving a number of carrier gas atoms/molecules which reflect a non-specific cage interaction. Hays et al. (4) have discussed the increase in the radiative rate for the red-shifted transitions and attribute these findings to the increase in the nonradiative pathways available to the complexes relative to the uncomplexed anthracene molecule. Although we have not performed lifetime measurements on the nitrogen-anthracene complexes, in support of their findings we have noted a decrease in the fluorescence yield for the $S_0 \leftarrow S_1$ transition commensurate with the increase in the extent of complex formation (compare figures 1c and 1d). As the nitrogen backpres-

sure is increased, the intensity of the $S_0 \leftarrow S_1$ transition for the uncomplexed anthracene decreases, as a consequence of complex formation. Similarly, the total fluorescence yield for all transitions in this region decreases (figure 4), reflecting the lower fluorescence yield of the complexed species. Another similarity to the argon-anthracene complex (4) is the appearance of up to three distinct broad shoulders which appear at 100 cm^{-1} intervals to the low energy side of the origin. An interpretation of the broad spectral features in terms of nitrogen solvation of anthracene is, however, preliminary.

The differences in the dominant types of complexes produced in the free jet expansion of anthracene appear to be related in part to the extent of vibrational cooling produced by the carrier gas. Whereas, the vibrational temperature of anthracene in a helium expansion (PD=34 torr- -cm) is 150 °K, the corresponding vibrational temperature for the nitrogen expansion is < 50 °K at much lower nitrogen backpressures (PD=3.4 torr-cm). At higher nitrogen backpressures an estimate for the vibrational temperature cannot be accomplished due to the disappearance of any transitions which can be attributed to vibrational hotbands. The efficiency of vibrational cooling by heavier carrier gases is well documented (2,5,9), and is supported by our results. Relative cross sections for vibrational relaxation for the different carrier gases used in this study have been determined and the efficiencies discussed by McClelland et al. (9). The fact a that σ_{vib} for nitrogen is approximately 13 times greater than that for neon or helium has been attributed to the propensity of a diatomic to efficiently lose excess vibrational energy through vibrational predissociation of vdW complexes (17).

Although the investigation of vdW complexes is a major field of study

in and of itself, it has not been our goal to understand the processes involving complex formation and potentially solvent interactions in great detail. Our motivation in these studies has been to quantify the degree of vibrational cooling and to determine the extent to which anthracene complexes with the carrier gas are produced in our free jet expansion, and which as a consequence, would interfere with our ablility to investigate the intramolecular dynamics of uncomplexed anthracene. Since the dynamics of the cooling process for specific molecules in free jet expansions is understood only qualitatively and depends on a number of disparate factors, including the expansion conditions, the design of the jet apparatus and especially the specific diluent molecule, the characterization of free jet expansions is an essential step in the design and interpretation of free jet studies. The interpretation of the fluorescence excitation spectra provides a means for accomplishing this. As a consequence of our interest in the investigation of energy and phase redistribution in large molecules, we are interested in producing isolated molecules with well defined rotational and vibrational temperatures. In addition, we desire that any interference which might arise as a consequence of complex formation be minimized. The influence of these parameters upon intramolecular energy and phase dynamics is emphasized in our discussion of the quantum interference effects in anthracene.

REFERENCES

1. D.H. Levy, Adv. Chem. Phys., **47,** 323 (1981).

2. A. Amirav, U. Even and J. Jortner, J. Chem. Phys., **75,** 2489 (1981).

3. W.R. Lambert, P.M. Felker and A.H. Zewail, unpublished results.

4. T.R. Hays, W. Henke, H.L. Selzle and E.W. Schlag, Chem. Phys. Lett., **77,** 19 (1981).

5. A. Amirav, U. Even and J. Jortner, Chem. Phys., **51,** 31 (1980).

6. D.H. Levy, L. Wharton and R.E. Smalley, in *Chemical and Biochemical Applications of Lasers*, V.2, Academic Press, New York, 1977, p. 1.

7. D.H. Levy, L. Wharton and R.E. Smalley, Accounts Chem. Res., **64,** 134 (1977).

8. A.L.J. Burgmans, J.M. Farrar and Y.T. Lee, J. Chem. Phys., **64,** 1345 (1976).

9. G.M. McClelland, K.L. Saenger, J.J. Valentini and D.R. Herschbach, J. Phys. Chem., **83,** 947 (1979).

10. P.S.H. Fitch, C.A. Haynam and D.H. Levy, J. Chem. Phys., **73,** 1064 (1980).

11. S.M. Beck, M.G. Liverman, D.L. Monts and R.E. Smalley, J. Chem. Phys., **70,** 232 (1979).

12. D.V. Brumbaugh, C.A. Haynam and D.H. Levy, J. Chem. Phys., **73,** 5380 (1980).

13. W. Lambert, P. Felker and A.H. Zewail, unpublished results.

14. E.A. Chandross, J. Ferguson and E.G. McRae, J. Phys. Chem., **45,** 3546 (1966).

15. E.A. Chandross and J. Ferguson, J. Chem. Phys., **45,** 2554 (1966).

16. R.E. Smalley, L. Wharton, D.H. Levy and D.W. Chandler, J. Chem. Phys., **68,** 2487 (1978).

17. J.A. Beswick and J. Jortner, J. Chem. Phys., **74,** 6725 (1981).

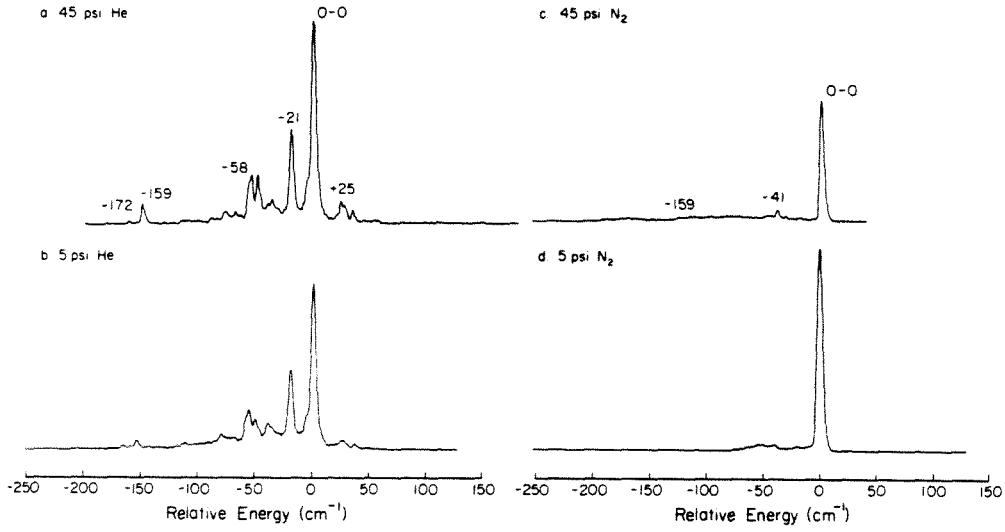

Figure 1.

Fluorescence excitation spectra of the S_1 $^1B_{2u}$+ origin of anthracene. The 0-0 origin is at 27687 cm^{-1}. Spectra were obtained for helium and nitrogen expansions at 45 and 5 psi backpressure, as indicated. The experimental conditions were: T_{10}=450 °K, D=150 microns, X=5 mm. The spectral resolution is 2.0 cm^{-1}.

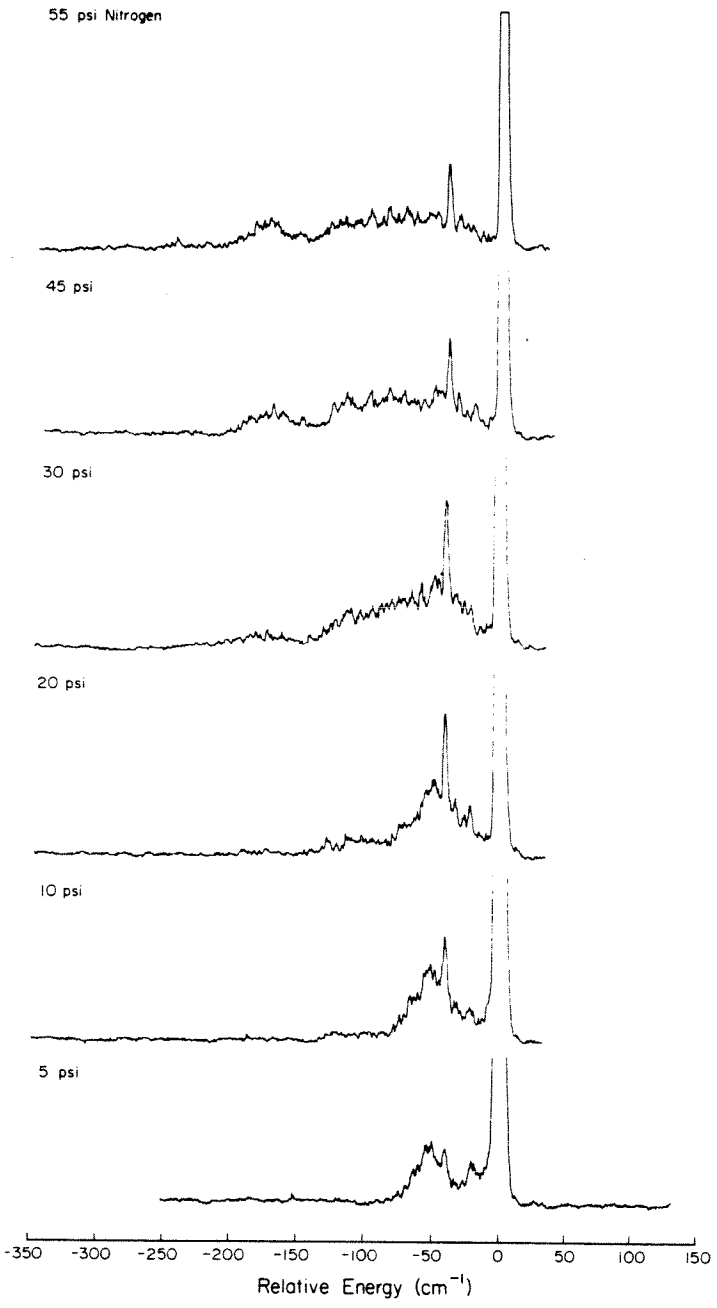

Figure 2.
The influence of the nitrogen backpressure on the fluorescence excitation spectra of anthracene to the low energy side of the S_1 origin. The experimental conditions are the same as those indicated for figure 1.

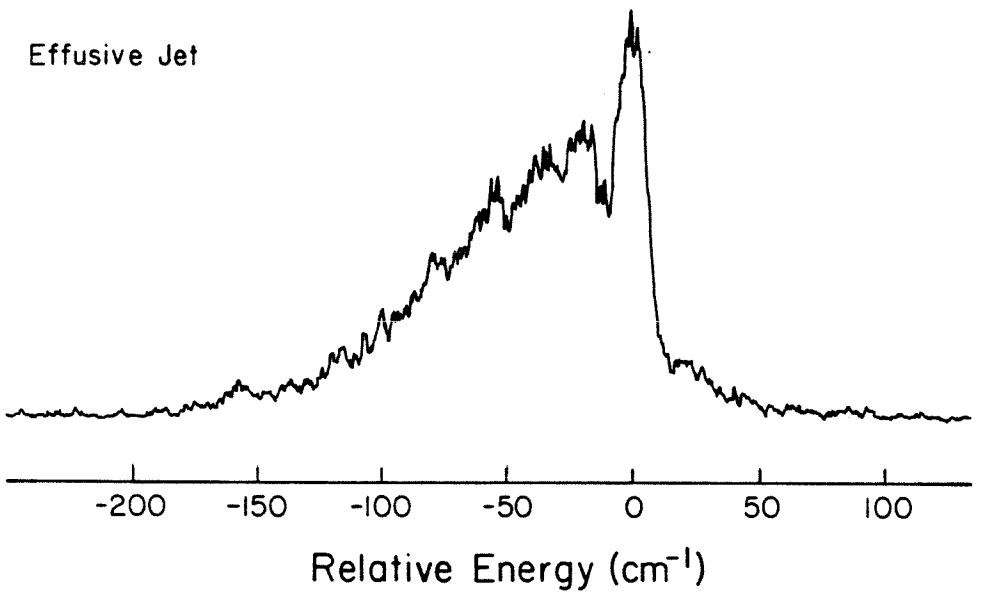

Figure 3.
The fluorescence excitation spectrum for an effusive beam of anthracene. All conditions were the same as for figure 1 with the exception that there was no backpressure. A rotational temperature of ~200 °K is calculated from the hotband contour.

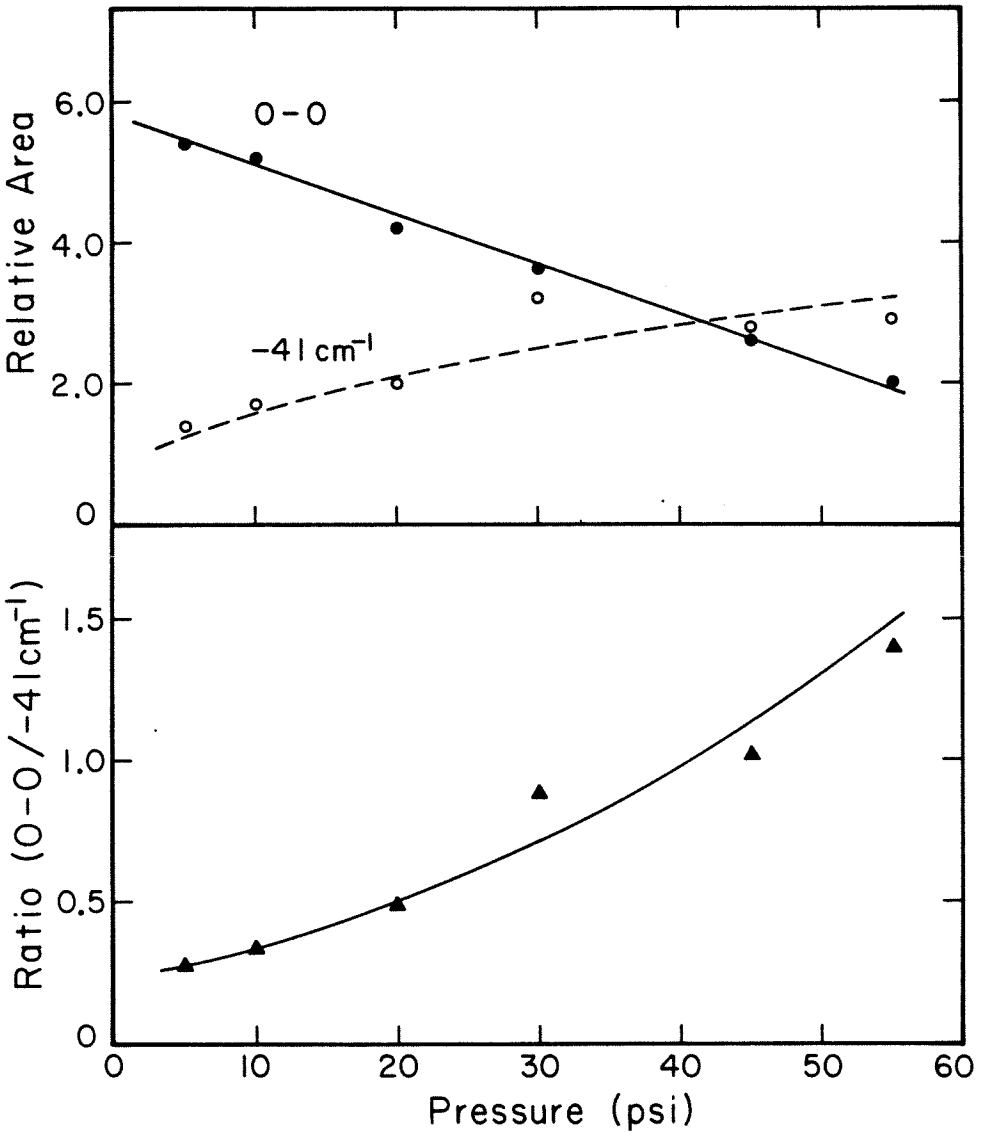

Figure 4.
The relative magnitude of the -41 cm^{-1} and the 0-0 transition with respect to the nitrogen backpressure. The magnitudes were determined from the areas of the respective peaks of the spectra presented in figure 2. In part b, the ratio of the two transitions is presented.

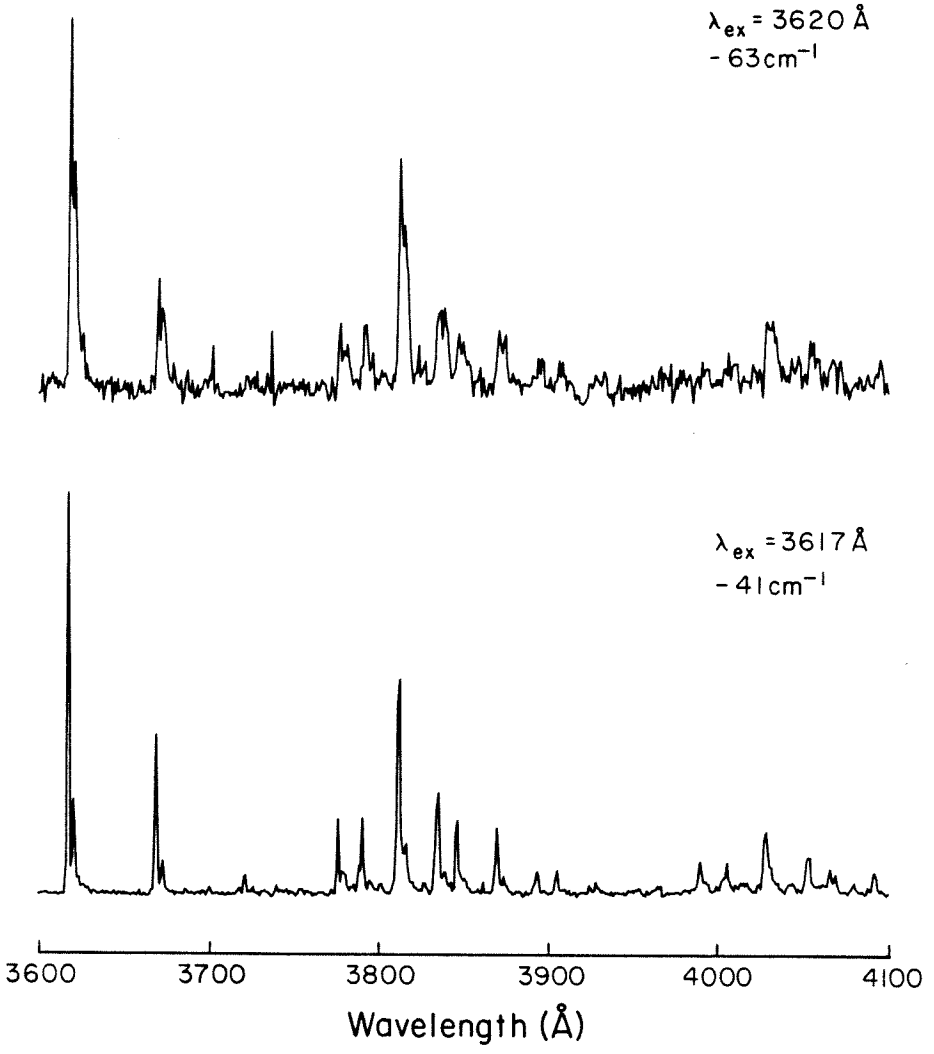

Figure 5.
The energy resolved fluorescence spectra of anthracene in a nitrogen expansion for excitation to S_1-40 cm^{-1} and S_1-63 cm^{-1}. A progression with a fundamental frequency of ~30 cm^{-1} is built upon each major transition. The experimental conditions are the same as those indicated in figure 1c.

Table 1. Vibrational analysis of the fluorescence excitation spectrum of anthracene expanded in helium in the region of the S_1 origin.[a]

Wavelength, A°[b]	$\Delta\upsilon$[c]	Intensity[d]	Assignment[e]
3602.4	56	2	--
3605.1	35	7	--
3606.5	25	11	--
3609.7	0	100	0-0 origin
3612.4	-21	46	--
3614.7	-38	12	--
3616.6	-52	24	--
3617.3	-58	24	--
3619.3	-74	6	--
3620.6	-84	6	--
3622.1	-95	4	--
3630.6	-159	10	$(S_0+387)-(S_1+230)$
3632.3	-172	2	$(S_0+395)-(S_1+230)$

a. The analysis refers specifically to the spectrum which is shown in figure 1.

b. Absolute wavelength accuracy, ±0.5 A°.

c. Accuracy, ±4 cm^{-1}.

d. Relative intensities were obtained from the respective amplitudes of the transitions.

e. The unassigned transitions are discussed in the text.

Table 2. Vibrational analysis for the fluorescence excitation spectrum of anthracene expanded in nitrogen for the region of the S_1 origin.[a]

Wavelength, A°[b]	$\Delta\upsilon$[c]
3609.8	0
3611.5	-13
3612.3	-20
3614.3	-34
3615.2	-41
3616.5	-52
3621.4	-88
3624.6	-113
3633.2	-178

a. The analysis refers to the dominate features appearing for the spectra presented in figure 1c.

b. Absolute wavelength accuracy, ±0.5 A°.

c. Accuracy, ±4 cm^{-1}.

§4.6 *ROTATIONAL TEMPERATURE: PRESSURE EFFECTS, CARRIER GAS EFFECTS, FLUORESCENCE EXCITATION AND EMISSION ROTATIONAL PROFILES.*

Consideration of rotational temperature is generally not explicitly required when discussing intramolecular energy dynamics of large molecules at high excess energies due to the necessarily large density of states. In this interpretation, specific rotational interactions are not expected to appear. At lower excess vibrational energies,however, and especially in molecular systems which exhibit substantial spin orbit coupling, the consequences of specific rotational J and K interactions on the radiative rate have been observed (1,2,3) and discussed in recent reviews (4,5). Recently, studies on singlet-triplet mixing in large molecules has been extended to include quantum beat spectroscopy (6,7). Nevertheless, our observation of quantum beats in anthracene and the subsequent investigation into the nature of the eigenstates which are responsible for the interference effect prompt consideration of the rotational contribution to this phenomena. Furthermore, as will be discussed in detail later, the pattern and modulation depth of the quantum beats in anthracene are found to be dependent upon the backpressure and the nature of the carrier gas. It is possible to attribute the influence of the carrier gas to three factors: collisional effects, vibrational temperature and/or rotational temperature. In order to assess the extent to which the intramolecular rotational temperatures are associated wtih the manifestation of quantum beats in anthracene, a systematic study of rotational temperature was undertaken.

The rotational cooling of small (8) and large molecules in supersonic free jet expansions has been shown to be very efficient and to closely

parallel the terminal translational temperature. For large molecules cooled in free jet expansions under conditions similar to those used in these experiments rotational temperatures of less than 0.5 °K have been documented and verified by comparison with calculated spectra (9). Determination of the translational temperature, therefore, can provide an estimate for the rotational temperature of anthracene. The terminal translational temperature is related to the temperature of the source, T_0, and the terminal Mach number by (7,10,11);

$$T_{trans} = T_0 t[1 + \tfrac{1}{2}(\gamma - 1)M_{at}^2]^{-1} \qquad (4.6.1)$$

where $\gamma = \frac{C_p}{C_v}$ is the specific heat capacity ratio and the terminal Mach number is defined by;

$$M_{at} = F(\gamma)\left\{\frac{K_{n0}}{\varepsilon}\right\}^{\frac{-(\gamma-1)}{\gamma}} \qquad (4.6.2)$$

The Knudsen number, K_{n0}, is the ratio of the mean free path to the nozzle diameter at the nozzle orifice, and ε designates the maximum fractional change in the mean random velocity per collision (assumed to be equivalent to unity). $F(\gamma)$ is an empirically derived constant which depends upon the specific heat ratios (9) (the pertinent values for monoatomic ($\gamma=\frac{5}{3}$) and diatomic ($\gamma=\frac{7}{5}$) carrier gases are 2.03 and 2.48, respectively). The Knudsen number can be defined in terms of the nozzle conditions;

$$K_{n0} = \frac{R\ T_0}{P_0\ D\ Q} \qquad (4.6.3)$$

where T_0 is the nozzle temperature, P_0, is the backpressure of the carrier gas, D is the diameter of the nozzle orifice, and Q is the hard sphere collision cross section for the interaction of the carrier gas with the diluent.

For our puposes, values for the collisional cross sections were obtained from those tabulated by McClelland et al. (8) which originally were estimated from Lennard-Jones potentials. The efficacy of this method for estimating terminal translational temperatures of binary gas mixtures has been discussed by Quah et al. (12,13).

The extent to which the rotational temperature of the seed molecules follows the translational temperature is determined by the effectiveness of the collisional cross section for rotational cooling. McClelland et al. (8) have shown that this approximation is valid for rotational cooling of I_2 in various gas expansions. Those studies have established that the terminal translational temperature varies as helium < nitrogen < neon < argon. The rotational cooling efficiency of the heavy monoatomic gases has been attributed to the velocity slip effect (14,15,16). During the expansion process, collisions of the light carrier gas will impart an acceleration to the heavier seed molecule. Hence, the local translational temperature will be considerably higher than the translational temperature of the bulk diluent gas. The velocity mismatch between the carrier and seed gases is proportional to the relative masses. Rotational relaxation being an efficient process throughout the expansion, the effective rotational temperature will follow the local translational temperature. However, the influence of the velocity slip effect is expected to be minimized at higher backing pressures and therefore should not significantly influence the flow dynamics of our expansion, especially when nitrogen is used as the carrier gas.

Calculated values for the terminal translational temperature for standard experimental conditions (T_0=450 °K, D=150 microns) are presented in figures 1 and 2 as a function of the carrier gas and the noz-

zle backpressure. The correspondence between the predicted and observed behavior is found to be much better for the heavier gases, neon and nitrogen (6,17), and therefore we expect the calculated values for the terminal translational temperature to be indicative of the internal rotational temperature of the diluent. The relative inefficiency of lighter gases at effecting vibrational and rotational cooling has been attributed to the velocity slip effect (14). At higher backpressures, however, the velocity slip effect will be reduced (8). Experimental estimates for the rotational temperature of anthracene were obtained from analysis of fluorescence excitation and energy resolved fluorescence spectra.

The low resolution rotational structure of the S_1 origin is shown in figures 3 and 4. The fluorescence excitation spectra reflect a 0.05 A° (0.4 cm^{-1}) resolution. The trends in the rotational temperature implied by these spectra are in qualitative agreement with the calculated values. Specifically, rotational cooling is more efficient in helium as compared with nitrogen (indicating the high pressure regime), and the rotational temperature decreases with increasing backpressure of the carrier gas. A characteristic feature of these spectra is the appearance of a shoulder appearing 0.18 A° (1.4 cm^{-1}) to the lower energy side of the main transition. It is possible that the shoulder is due to hotbands, vdW complex formation, or isotopic impurities. The fact that the shoulder appears when either helium or nitrogen is used as a carrier gas argues against vdW complex formation as being responsible. Considering the small differences in energy between the ground and excited state vibrational frequencies (section 3), particularly for the 230 cm^{-1}, 385 cm^{-1} and 395 cm^{-1} transitions, it is possible that hotband transitions are involved. The most likely explanation for the additional peak, however, is that it

reflects the origin of the mono C_{13}-anthracene isotope. Mono C_{13} substituted species should account for approximately 14 % of the anthracene molecules. The effect of C_{13} substitution would be to shift of the 0-0 transition to lower energy, consistent with that for the observed shoulder.

An estimation for the experimentally determined rotational temperature was made by comparing the fluorescence excitation spectra to calculated rotational contours. Due to the small rotational constants and therefore high J numbers involved, it was necessary to use expressions for the rotational energies and the dipole matrix elements appropriate for a prolate symmetric top (18,19,20) (since the asymmetry parameter for anthracene is κ=-0.911, this affords a reasonable approximation). The ground state rotational constants were determined from the equilibrium atom configuration (21) to be A=2.155 × 10^9 Hz, B=0.4537 × 10^9 Hz, and C=0.3748 × 10^9 Hz. Because of the low resolution of our spectra, an attempt was not made to directly fit the rotational lineshape. Estimates for the excited state rotational constants were made by comparison with results for naphthalene (22,23) where the excited state constants were found to be approximately 2 % less than the respective ground state rotational constants (empirically, minor changes in the excited state rotational constants had little influence on the calculated rotational lineshapes). Nuclear spin statistics (24) were not taken into account since the statistical weights for the different symmetry species are nearly equivalent (a,.89:b_1,.83: b_2,.83:b_3,1.0) and the differences in the energies of the lowest energy level of each symmetry species are on the order of only a few gigahertz, well below the limiting resolution of our spectra. Rotational contours were calculated for the perpendicular type B, out-of-plane transition allowing for ΔJ=0, ±1 and ΔK = ±1 selection rules.

Rotational profiles for emission were generated in a similar fashion beginning with the excited state rotational population. As a final step in the computation of rotational contours for comparison with the experimentally obtained spectra, the calculated rotational state distribution was convoluted with a function commensurate with the limiting instrumental resolution (a Gaussian function for comparison with absorption spectra reflecting the laser bandwidth, or a rectangular slit function for comparison with the resolved fluorescence spectra).

The rotational temperatures estimated from contour analysis for the spectra shown in figures 3 and 4 are approximatedly 1.0 0.5 °K for the spectra obtained using helium as a carrier gas and 2.0 ± 0.5 °K when nitrogen was used as a carrier gas. These values are in good agreement with the calculations for the terminal translational temperature (figures 1 and 2). Unfortunately, the marginal spectral resolution prevents a more accurate experimental determination of the rotational temperature. We have also noted a pressure dependent change in the rotational profiles. The linewidths (FWHM) of the S_1 origin decrease by 20 % and 10 % for helium and nitrogen, respectively, as the backpressure is increased from 15 to 45 psi. This reflects a change in the rotational temperature of approximately 0.5 °K.

Rotational contours of the energy resolved fluorescence upon excitation to the S_1 origin and to S_1+1380 cm^{-1} were also examined. The emission profiles reflect the transfer of the ground state rotational population into the excited singlet state manifold, and subsequent direct relaxation into the ground state. In the absence of nonradiative processes occuring in the excited state, the thermal rotational distribution observed in the emission should directly reflect transitions consistent with rigorous ΔJ =

0,±1 and $\Delta K = \pm 1$ selection rules for rotational transitions. Comparison of the experimental rotational contours for the absorption and emission spectra of the S_1 origin are shown in figure 5. Dramatic broadening of the rotational contour is observed in the emission spectrum. Although this is in part due to the lower resolution of the emission spectrum (0.25 A°, 2 cm^{-1}), the profile is consistent with a rotational temperature of 15.0 ± 2.0 °K. An increased broadening due to a change in J of ± 1 upon emission is insufficient to account for such large change in the rotational state distribution as confirmed by comparison with computer generated spectra. The broadening is only slightly dependent on the nature of the carrier gas (figure 6), and independent of the backpressure (not shown). Similar experiments were also performed for excitation to S_1 + 1380 cm^{-1} (figure 7). The rotational profiles of the resonance fluorescence ($\lambda_{ex} = \lambda_{det}$) are nearly identical to those obtained for excitation to lower energy and show similar carrier gas and pressure effects. Slight, but demonstrable broadening does occur, however, at higher (150 psi) carrier gas backpressures (figure 8). This was discussed in section 4.4 with respect to collision induced relaxation in the free jet expansion.

Based on comparison of the rotational profiles in absorption and emission it appears that it is insufficient to consider only the direct J,K dependent absorption and emission processes with regard to the rotational state distribution. Neither the asymmetry, nor, the ~10 cm^{-1} linewidth (FWHM) characteristic of an energy level population with a relatively high rotational temperature is capable of being modeled using this approach. The implication of our results is that there exists mechanisms for excited state rotational relaxation which tend to thermalize the rotational energy distribution and which are relatively independent of the ini-

tial ground state rotational distribution, and also of the density of states. It is difficult to arrive at an explanation in terms of strictly intramolecular energy redistribution among rotational states. The broad rotational distribution which appears in the fluorescence is likely to be explained as the result of weak intermolecular collisional processes in the free jet expansion. This line of argument is supported by the increase in broadening observed at higher carrier gas pressures as evidenced in figure 8. The resolved fluorescence for these transitions does not exhibit a buildup prior to the exponential decay, as would result from hard sphere collisions (25,26). The broadening may be a consequence of perturbation by vdW complexes (section 4.4).

In this discussion it has been shown that the experimentally determined rotational temperatures qualitatively agree with the calculated terminal translational temperatures. Although insufficient instrumental resolution has compromised the ability to acquire direct, quantitative measurements of the rotational temperature as a function of carrier gas and backing pressure, the general pressure dependent trends associated with the calculated terminal translational temperature should be valid and will therefore be used to correlate internal rotational temperatures with pressure and carrier gas dependent changes of the quantum beat spectra. It should be pointed out here that the beat frequencies correspond to interaction between states separated by 205 MHz and 488 MHz, whereas the rotational moments of inertia in anthracene are; I_A=215 MHz, I_B= 454 MHz and I_C=375 MHz. The eigenstates which are responsible for the quantum beats therefore cannot be related to rotational energy level structure in a "straightforward" manner. The extent to which the interference is a manifestation of rotational states will be

addressed in a subsequent section.

REFERENCES

1. W.E. Howard and E.W. Schlag, J. Chem. Phys., **68,** 2679 (1978).

2. G. ter Horst, D.W. Pratt and J. Kommandeur, J. Chem. Phys., **74,** 3616 (1981).

3. G. ter Horst, and J. Kommandeur, J. Chem. Phys., **76,** 137 (1982).

4. W.E. Howard and E.W. Schlag, in *Radiationless Transitions*, ed. S.H. Lin, Academic Press, New York, 1980, p. 81.

5. F.A. Novak, S.A. Rice, M.D. Morse and K.F. Freed, in *Radiationless Transitions*, ed. S.H. Lin, Academic Press, New York, 1980, p. 135.

6. P.M. Felker, W.R. Lambert and A.H. Zewail, Chem. Phys. Lett., **89,** 309 (1982).

7. B.J. Van der Meer, H. Th. Jonkman, G.M. ter Jorst and J. Kommandeur, J. Chem. Phys., **76,** 2099 (1982).

8. G.M. McClelland, K.L. Saenger, J.J. Valentini, and D.R. Herschbach, J. Phys. Chem., **83,** 947 (1979).

9. For example, a) S.M. Beck, D.E. Powers, J.B. Hopkins, and R.E. Smalley, J. Chem. Phys., **73,** 2019 (1980); b) S.M. Beck, M.G. Liverman, D.L. Monts and R.E. Smalley, J. Chem. Phys., **70,** 232 (1979); c) M. Gurnick, J. Chaiken, T. Benson and J.D. McDonald, J. Chem. Phys., **74,** 99 (1981).

10. J.B. Anderson and J.B. Fenn, Phys. Fluids, **8,** 780 (1964).

11. H. Ashkenas and F.S. Sherman, *Rarefied Gas Dynamics*, 11th Symposium, V.2, ed. J.H. de Leeuw, Academic Press, New York, 1966, p. 84.

12. C.G. Quah, Chem. Phys. Lett., **63,** 141 (1979).

13. C.G.M. Quah and J.B. Fenn, *Rarefied Gas Dynamics*, 11th Symposium, V.2, Commissariat A L'Energie Atomique, Paris, 1979, p. 885.

14. R.A. Larsen, S.K. Neoh and D.R. Herschbach, Rev. Sci. Instr., **45,** 1511 (1974).

15. R. Campargue and J.P. Breton, Entropie, **42,** 18 (1971).

16. N. Abauf, J.B. Fenn and D.R. Miller, Rarefied Gas Dynamics, **5,** 1317 (1967).

17. D. Coe, F. Robbe, L. Talbot and R. Cattolica, Rarefied Gas Dynamics, **11,** 800 (1979).

18. C.H. Townes and A.L. Schawlow, *Microwave Spectroscopy*, Dover Publications, New York, 1955.

19. D.R. Lide, Jr., J. Chem. Phys., **20,** 1761 (1952).

20. H.C. Allen, Jr., and P.C. Cross, *Molecular Vib- Rotors*, Wiley and Sons, New York, 1963.

21. B.N. Cyvin and S.J. Cyvin, J. Phys. Chem., **73,** 1430 (1969).

22. K.K. Innes, J.E. Parkin and D.K. Ervin, J. Mol. Spectrosc., **16,** 406 (1965).

23. A.J. McHugh and I.G. Ross, Spectrochim. Acta, **24,** 441 (1970).

24. E.B. Wilson, Jr., J. Chem. Phys., **3,** 276 (1935).

25. A. Zewail, W. Lambert, P. Felker, J. Perry and W. Warren, J. Phys. Chem., **86,** 1184 (1982).

26. M. Sulkes, J. Tusa and S.A. Rice, J. Chem. Phys., **72,** 5733 (1980).

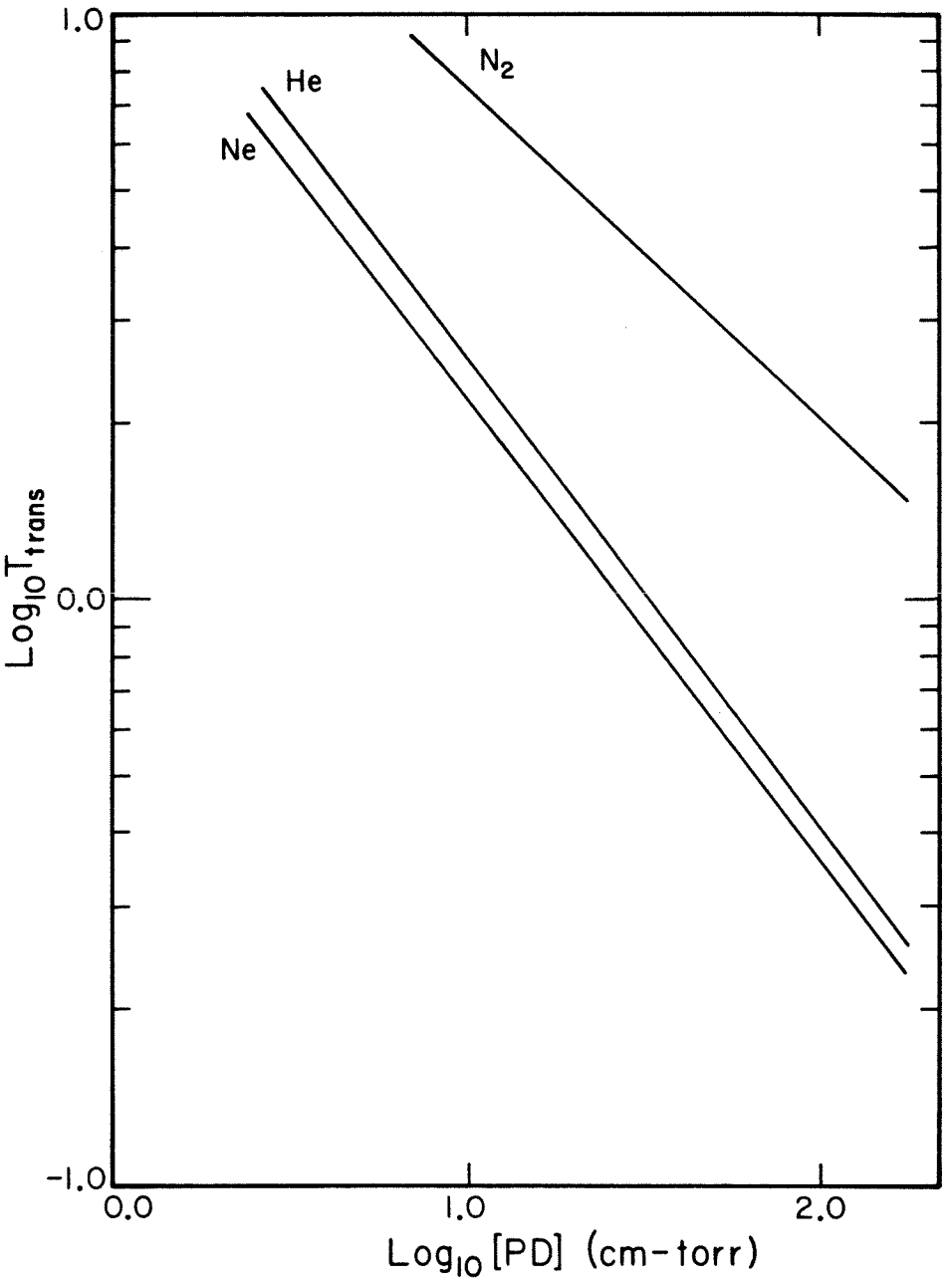

Figure 1.
The terminal translational temperature calculated using equation (1) in the text is presented with respect to the carrier gas pressure. The fixed pinhole diameter was 150 microns. The nozzle temperature was 450 °K.

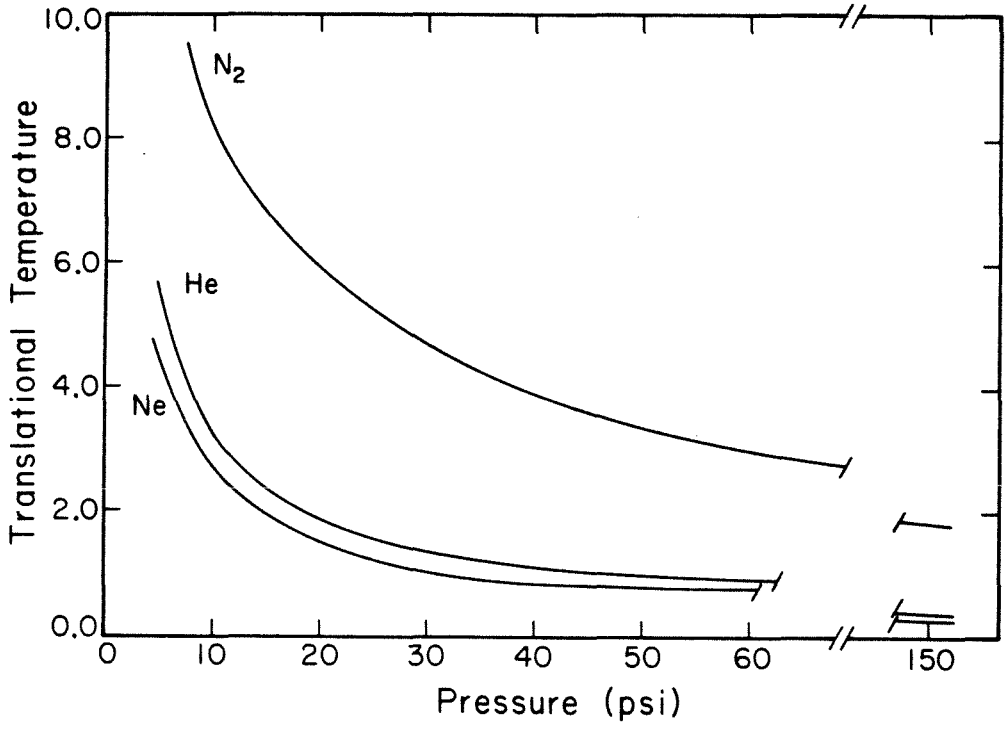

Figure 2.
Calculated values for the terminal translational temperatures for nitrogen, helium, and neon expansions. The values are the same as those presented in figure 1 except the abscissa is given directly in units of pressure for clarity.

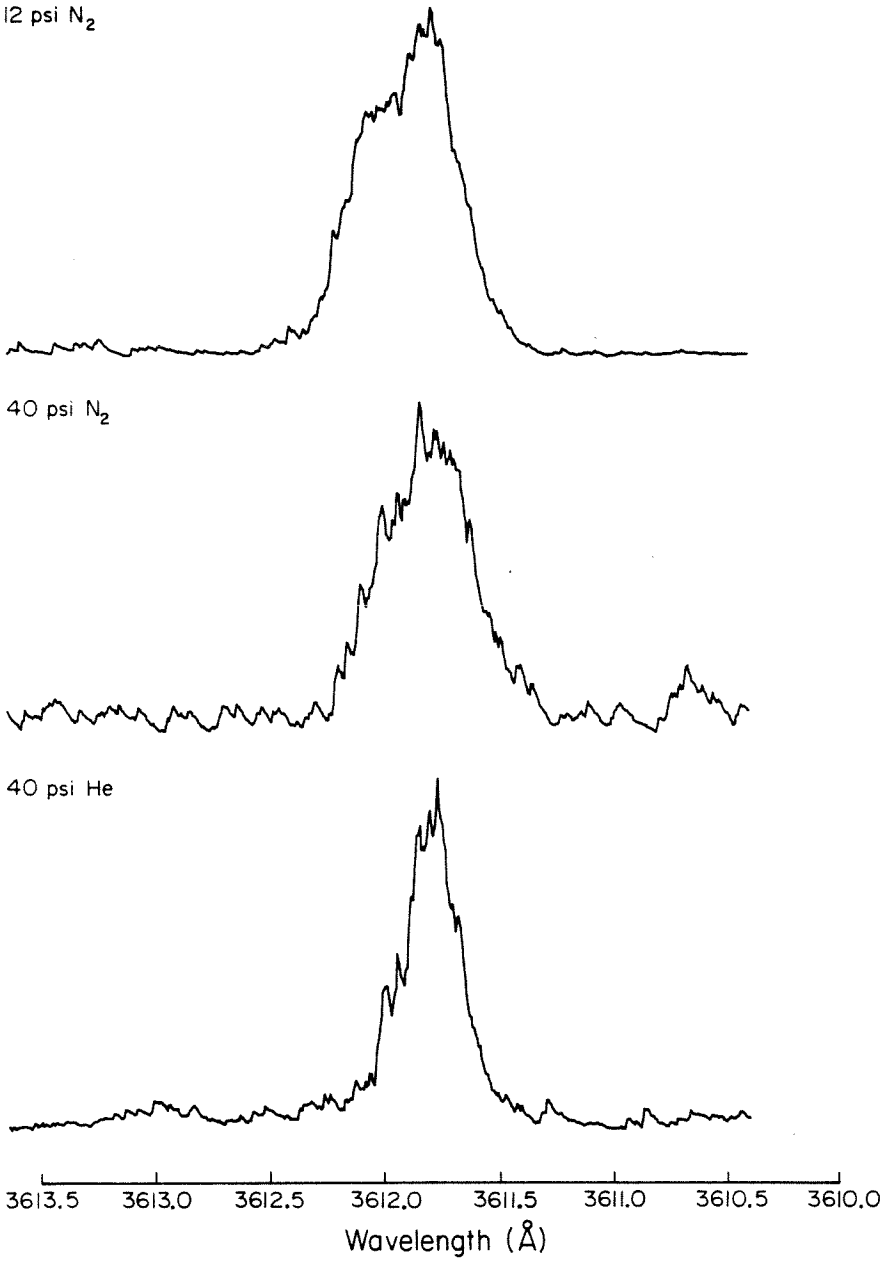

Figure 3.

Fluorescence excitation spectra of the S_1, $^1B_{2u}$+ origin of anthracene. The nitrogen laser resolution was 0.05 A° and the nozzle temperature was 340 °K. A shoulder to the low energy side of the main transition is particularly evident in the 12 psi nitrogen expansion.

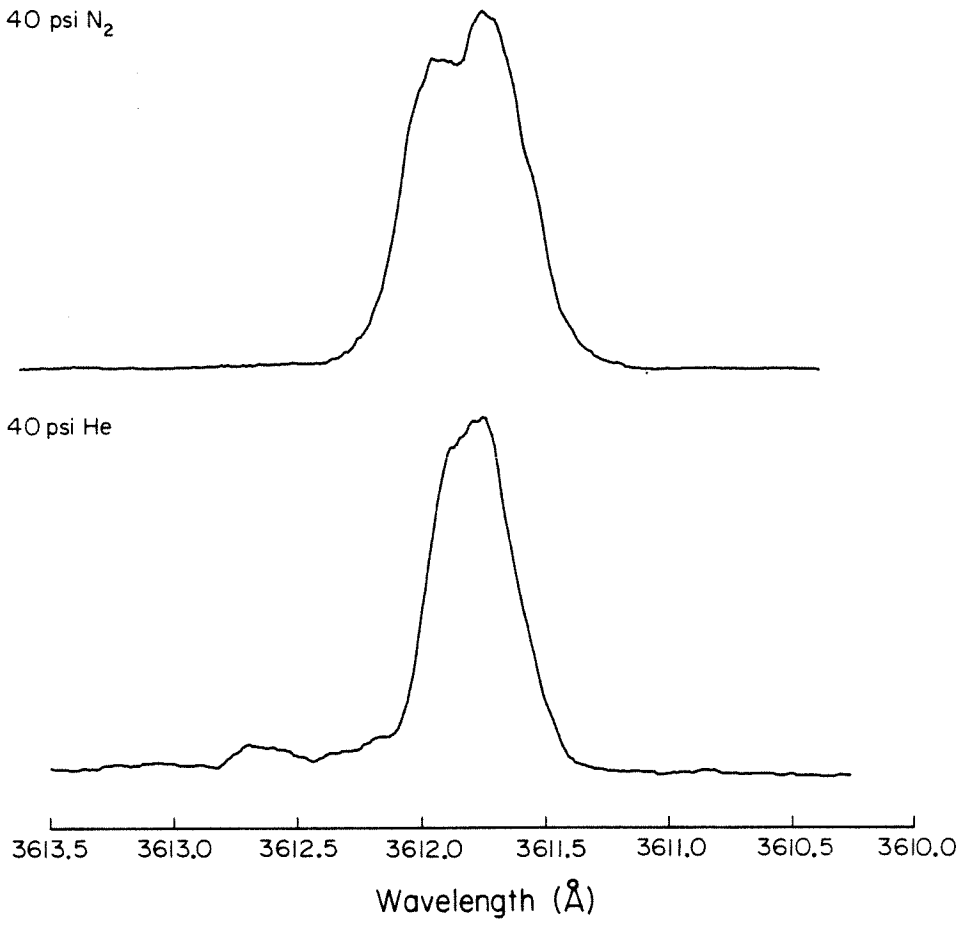

Figure 4.
Fluorescence excitation spectra of the S_1 origin of anthracene for a nozzle temperature of 450 °K. The spectral resolution was 0.05 A°.

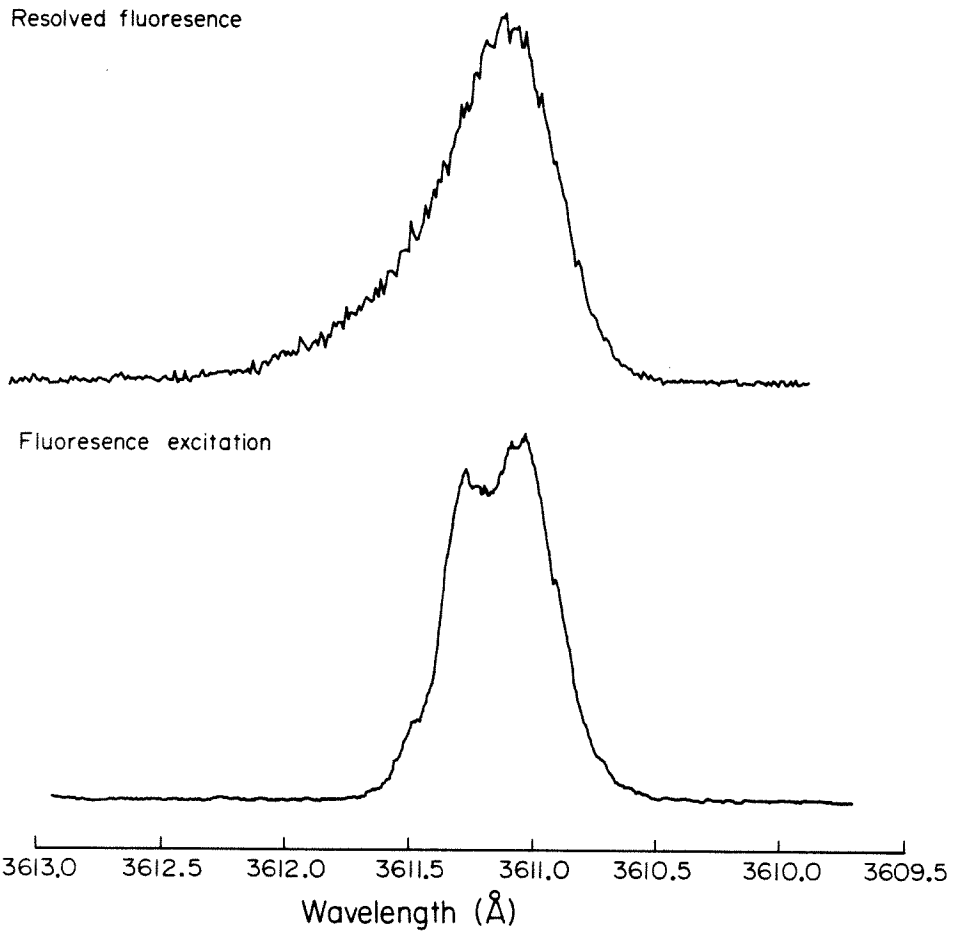

Figure 5.

Comparison of the resolved emission and the fluorescence excitation spectra for the S_1 origin of anthracene. The nozzle temperature was 450 °K and the nitrogen backpressure was 45 psi. The resolved fluorescence spectrum was obtained for excitation to 3611.8 A° with a laser bandwidth of 0.5 A° and a detection resolution of 0.25 A°. The resolution of the fluorescence excitation spectrum was 0.05 A°. Note the broadened rotational profile exhibited by the transition subsequent to emission.

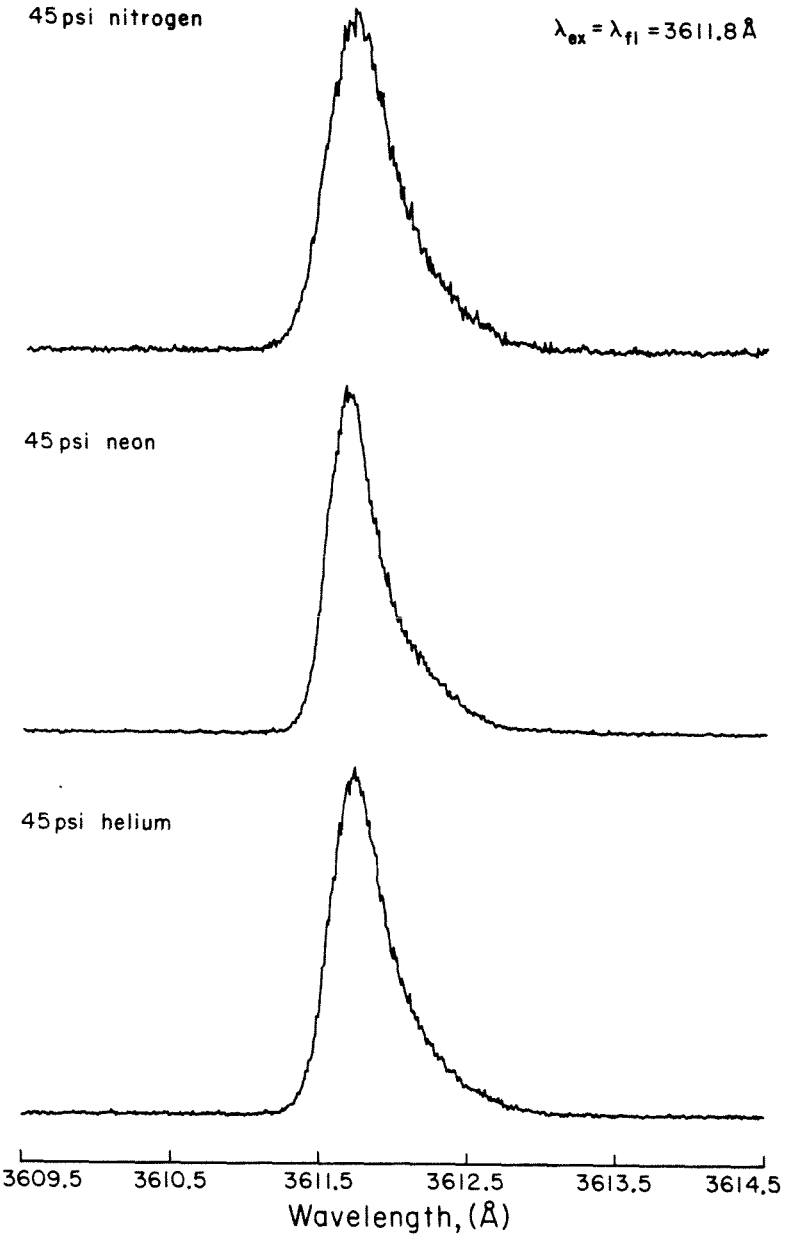

Figure 6.

Comparison of the energy resolved fluorescence spectra of anthracene for different carrier gases. Emission was detected with a resolution of 0.25 A° for excitation to 3611.8 A° with a bandwidth of 0.5 A°. The experimental conditions were: T_0=450 °K and D=150 microns. A slight broadening of the rotational contour is exhibited in the nitrogen expansion. There was no change in the observed profiles when the pressure was changed from 5 to 150 psi for a given carrier gas.

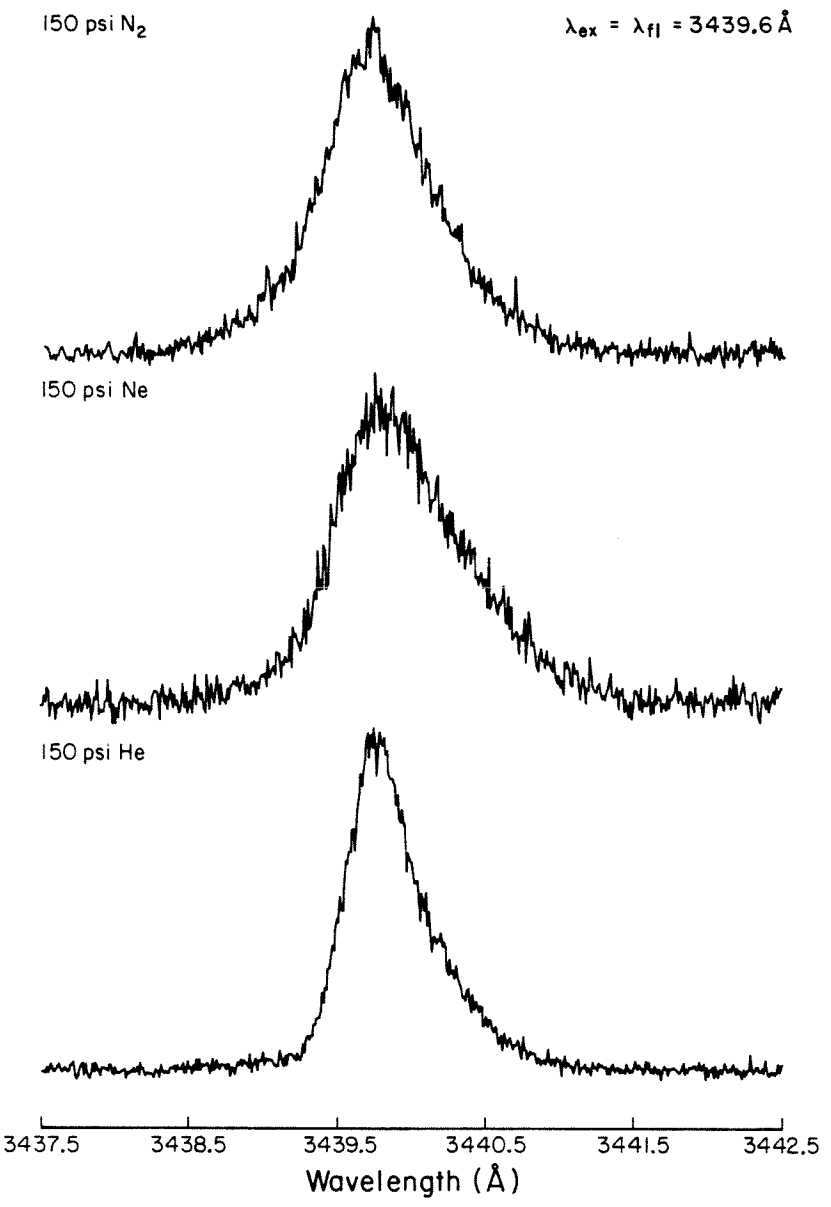

Figure 7.
The rotational contour of the $S_1 + 1380$ cm^{-1} (3439.5 A°) transition of anthracene. The energy resolved fluorescence spectra show similar structure with the exception of slight broadening for the nitrogen expansion.

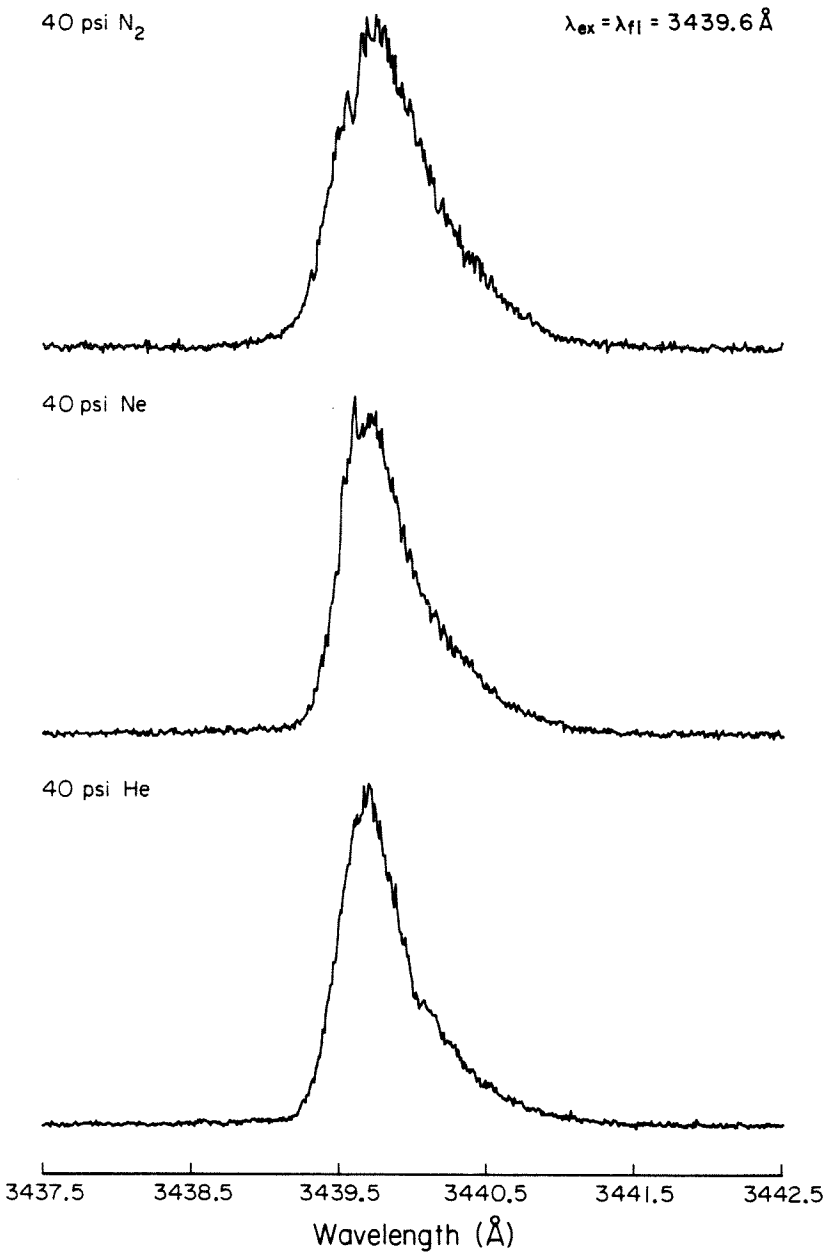

Figure 8.
The rotational contour of the 3439.6 A° transition obtained for the energy resolved fluorescence at high carrier gas pressures. Considerable broadening is exhibited when 150 psi backpressures are used, especially for the heavier gases, nitrogen and neon, The nozzle temperature was 450 °K and the pinhole diameter was 150 microns.

§4.7 *QUANTUM BEATS AND VIBRATIONAL REDISTRIBUTION IN LARGE MOLECULES*

§4.7.1 *Introduction*

Our observation of quantum beats in anthracene and trans-stilbene is the first example of quantum interference effects associated with intramolecular vibrational redistribution. The distinguishing feature of this result is that coherence between specific quasi-discreet energy levels can be detected despite the fact that interaction with a dense manifold of states dominates the intramolecular dynamics of the molecular system. The mathematical formalism for the treatment of an optically prepared system interacting with the radiation field and the bath subsystem, specifically with reference to quantum beats, is presented in a number of recent papers (1-10). The description of the quantum mechanical system will serve as the context for a discussion of the spectral and temporal properties of the molecular fluorescence. Here we present the general principles which underly the current concepts which formulate a basis from which to interpret the experimental observables manifested in the time and evergy resolved fluorescence of large polyatomic molecules. Specifically, a three level model which enables analysis of the quantum beats (10) is reviewed, and the extension to more rigorous theoretical treatments is discussed. In order to realize the full potential from the analysis of the quantum beats, and the extent to which quantum beats can be used as a probe to understand intramolecular energy and phase dynamics in large molecules, particularly with respect to the damping rate which can provide information regarding both elastic and inelastic dephasing rates, the inclusion of subsystem interactions in a complete

treatment is essential.

§4.7.2 *Simple Model*

In order to give a simple picture of the quantum beats, the dynamics of a three level system (figure 1) can be developed in terms of the energy basis set. Upon coherent excitation, the excited state can be represented by a linear combination of the two states (1);

$$|\Psi(0)> \; = \; a_1|\Phi(0)_1> + a_2|\Phi(0)_2> \tag{4.7.1}$$

The states $|\Phi(0)_i>$ evolve in time according to,

$$|\Phi(t)_i> \; = \; exp[-(\frac{i}{h})\, E_i \; t \;]\; |\Phi(0)_i> \tag{4.7.2}$$

If the decay of the states is described phenomenologically by the term $exp(-\frac{1}{2}\Gamma_i \; t \;)$, then the temporal development of the superposition state is given by;

$$\begin{aligned} |\Phi(t)> = a_1 \, exp[-(\tfrac{i}{h})\, E_1 - \tfrac{1}{2}\Gamma_1 \, t \;]\; |\Psi(0)_1> \\ + \, a_2 \, exp[-(\tfrac{i}{h})E_2 - \tfrac{1}{2}\Gamma_2 \, t \;]\; |\Psi(0)_2> \end{aligned} \tag{4.7.3}$$

The expression for the intensity of the light emitted at time t, obtained from the probability amplitude for the electric dipole emission is;

$$\begin{aligned} I(t) \; &\approx \; |<0|\, er \; |\Psi(t)>|^2 \\ &= \; a_1<0|\, er' \; |\Phi(t)_1> + a_2<0|\, er'' \; |\Phi(o)_2> \end{aligned} \tag{4.7.4}$$

where e is the polarization vector of the emitted photons and r is the dipole operator. Denoting $<0|er\,|\Phi_i(0)>$ by A_i and $\frac{1}{2}(\Gamma_1 + \Gamma_2)$ by Γ:

$$\begin{aligned} I(t) \; &\approx \; |a_1A_1|^2 \, exp(-\Gamma t) + |a_2A_2|^2 + exp(-\Gamma t) \\ &+ \; a_1a_2{}^*A_1A_2{}^* exp[-(\tfrac{i}{h})(E_1 + E_2)t \; - \Gamma t \\ &+ \; a_1a_2{}^*A_1A_2{}^* exp[+(\tfrac{i}{h})(E_1 + E_2)t \; - \Gamma t \end{aligned} \tag{4.7.5}$$

The emission intensity therefore varies periodically with frequency $\frac{1}{h}(E_1 + E_2)$ provided that dipole matrix elements exist which radiatively couple the coherently prepared excited states to a common ground state. The damping rate for an isolated system is determined by the radiative decay rate. It can be seen that a requisite condition for the interference terms not to vanish is that $\omega_{1,2} > \frac{\Gamma}{2}$, i.e. that the linewidths of the states be less than the energy separation between the states. Equation 4.7.5 can be generalized in terms of the density matix by defining the density operator immediately after excitation by $\rho(0) = |\Psi(0)><\Psi(0)|$. Using $|\Phi_1>$ and $|\Phi_2>$ of definite energy as basis elements of the excited state, the density matrix in the energy representation is given by $<\Phi_i|\ \rho(0)\ |\Phi_j> = \rho_{ij} = a_i a_j^*$.

This development is adequate for describing the dynamics of isolated atomic systems (12) and serves to exemplify some important points regarding quantum beats. Quantum beats of single atomic or molecular systems measured by photon counting experiments can arise only from excited states (12). The interference term in equation 4.7.5 reflects the indistinguishability of the transition process for the two states. Whereas the coherent laser excitation can prepare a superposition of the two excited states, the intrinsically incoherent spontaneous emission process is unable to produce a coherent ground state population. In principle, it is possible to distinguish between the emission frequencies to the ground state levels by spectrally resolving the spontaneous emission. If the resolution is such that the fluorescence component of only a single superposition state is detected, quantum beats would not be observed.

The observation of quantum interference effects in the spontaneous emission also establishes the intramolecular origin (12). Should the

quantum beats arise from a collective molecular ensemble, their experimental observation would be compromised by the finite spatial excitation region, and in our case by the low molecular density in the free jet expansion ($\sim 10^{11}$ molecules/cm^3), and the residual Doppler width of the expansion (~200 MHz perpendicular and ~20 MHz axial). These properties of the free jet expansion would prevent the simultaneous coherent excitation of two molecules. Doppler effects will not influence the quantum beat pattern originating from superposition states since the velocity induced shift is a common factor for both states. Furthermore, the method of detection used in our experiments, photon counting, determines that we are observing the probability amplitude of a single emitted photon for 'each' laser excitation pulse. If a standard square law detector (photomultiplier tube) were used, an interference term originating from two photons of different energies simultaneously impinging on the cathode could be produced. Single photon counting techniques prevent this from occurring.

A requisite condition for the creation of an excited state superposition is that the coherence width of the excitation source must be larger than the energy separation between the two zero order levels. If the excitation bandwidth is large compared to the energy separation between the states, one cannot ascertain whether both states are optically active or whether the interference arises from the coupling of a state which uniquely carries oscillator strength from the ground state, with a non-optically active state. The latter situation is exemplified by the observation of quantum beats in aza-aromatics (13) and α-dicaronyls (14) where the superposition states are of mixed singlet-triplet origin.

§4.7.3 *Discussion of Current Treatments of Vibrational Relaxation*

The interpretation of the molecular dynamics depends upon the basis set used to describe the system. In the context of a zero order level or normal mode description the ground state is coupled to a single or many zero order levels which in turn are nonradiatively coupled to other sets of states which may or may not exhibit oscillator strength to the vibronic ground state levels. The primary states which carry oscillator strength from the ground state are characterized by a linewidth due to the effective Born-Oppenheimer terms and by certain level spacings. The effective Hamiltonian is determined by matrix elements appropriate for the interaction among the coupled levels (i.e. anharmonic, spin-orbit). The coupling may be to vibronic levels of the same electronic manifold or to vibronic levels of other lower lying electronic states through the breakdown of the Born-Oppenheimer approximation, or through spin-orbit mechanisms. This treatment implicitly contains the idea of sequential coupling between intramolecular subsystems. Partial diagonalization of the molecular Hamiltonian leads to exact molecular eigenstates which are linear combinations of the wavefunctions determined by the zero order Hamiltonian and the interaction terms. An absorption band corresponds to excitation of a zero order state oscillator strength spread over many molecular eigenstates. The width of the excitation bandwidth with respect to the spread of the eigenstates determined by the coupling coefficients is important in determining the dynamics of the system (15,16). If the excitation bandwidth is less than the spread of the zero order oscillator strength which spans the molecular eigenstates of the system, then it is in principle possible to observe deviations from exponential relaxation. The possibility of generating interference effects

is implicit in both the zero order and the molecular eigenstates pictures (2).

The extension to a treatment which is more appropriate for more realistically describing the dynamics of molecular systems (for example references 1 and 2) begins by designating the excited molecular state at $t = 0$ in terms of a well defined set of molecular eigenstates with definite phase relationships; $|\Psi(0)> = \sum_{s}^{\delta\omega} C_s \; |s>$, where the summation is over the states encompassed within the coherence width of the laser excitation pulse and C_s determines the optical accessibility of the specific states within the laser bandwidth. For $t > 0$, the excited state of the molecule evolves according to;

$$\exp^{-i(\omega_s - i\frac{\Gamma}{2})t} \tag{4.7.6}$$

where, for the moment, the damping is due entirely to radiative decay to the ground state manifold, $|g>$. The total rate of photon emission to the ground state with average frequency $\bar{\omega}_g$ is given by (1);

$$P(t) \; = \; |a(\bar{\omega}_g)|^2 <g \; |\mu\rho(t)\mu| g> \tag{4.7.7}$$

where $\rho(t) = |\Psi_e(t)><\Psi_e(t)|$ and in terms of the molecular eigenstates basis;

$$P(t) \; = \; \sum_{gg'}^{\delta\omega} \gamma_{ss'g} \, C_s \, C_{s'}^{*} exp\left[-i(\omega_{ss'} - \frac{i}{2}(\Gamma_s + \Gamma_s'))\right] t \tag{4.7.8}$$

where the summation is over the frequency spanned by the coherence width of the laser, and $\gamma_{ss'g}$ is the coherent radiative damping matrix, ($\gamma_{ss'g} \alpha <g \; |\mu| s><s' |\mu| g> \; C_g^2$). The diagonal terms represent the experimental radiative decay rates for each state $|s>$ while the nondiagonal terms produce interferences in the fluorescence.

It is important to understand the physics implied by equation 4.7.8, since the formula is sufficient to describe the general experimentally observed spectral features of polyatomic molecules. With reference to figure 2, the absorption spectrum determined by $|C_s|^2$ is defined as a set of Lorentzian profiles of width, Γ_n , which may contain many eigenstates, $|s_i>$. If the excited states are prepared by pulse excitation from $|g>$ then the phase relationships among the C_s are such that the interference among the $|s>$ states will lead to nonradiative decay with rate constant Γ_n. Γ_n is in turn proportional to the number of eigenstates contained within each Lorentzian defining the absorption profile by $\Gamma_n \alpha 2\pi V^2\rho$, where ρ is the density of states and V^2 is the average coupling matrix element between the states. The excited states are radiatively coupled to one, or several ground states $|g>$ as determined by the dipole matrix elements implicit in $\gamma_{ss'g}$. The radiative decay to a specific $|g>$ state may contain both exponential and oscillatory components depending upon the width of $|C_s|^2$ compared to ω_s, the difference in frequency between two states $|s>$ which are radiatively coupled to a common $|g>$ state. The ability to experimentally observe interference effects depends upon having two sets of eigenstates which are distinguished by separate absorption Lorentzians, radiatively coupled to a common ground state. In order to observe quantum beats for a specific detection frequency, $\delta\omega_g$, the contribution of the interfering terms must not be obscured by single exponential terms. This treatment adequately explains to a first approximation the quantum beats observed in large moleucles.

Upon excitation to low excess energies in dicarbonyls (14,17) and aza-aromatics (13), interference effects are observed in the total fluorescence. This indicates that a small number of molecular eigenstates are

excited at $t = 0$, such that the oscillatory components do not destructively interfere to produce an apparent exponential fluorescence decay. On the other hand, the corresponding situation with anthracene, when excited to moderate excess energies, is complicated by the simultaneous excitation of a large number of eigenstates with overlapping Lorentzian distributions. In this case the observation of quantum beats depends upon resolving the specific decay channels, $\delta\omega_g$, since the oscillatory behavior is for the most part obscured by the large number of interfering components as indicated by equation 4.7.8.

Although equation 4.7.8 provides a framework for understanding relaxation and redistribution processes in large polyatomic molecules, the structure of $|s>$ and the contributions to the decay rate are generally not known. It is therefore useful to present a different mathematical framework from which an experimental quantum beat pattern can be analyzed and the structure of the excited state manifold and the radiative and nonradiative relaxation rates can be discussed. This can be accomplished in terms of the Liouville equation. The equation of motion for a multilevel system can be written using the density matrix method (1,8,10) by;

$$\dot{\rho}(t) = -i\,\hat{L}\hat{\rho}(t) - \hat{\Gamma}\hat{\rho}(t) \qquad (4.7.9)$$

where $\hat{L} = \hat{L}_0 + \hat{L}'$ is the Liouville operator. $\hat{L}_0$ is responsible for the initial preparation of the system, in our case through the optical dipole matrix element between the ground and excited states, and which is turned off at $t = 0$. $\hat{L}'$ is the interaction Liouville operator which induces coupling between the $|s>$ states (and is proportional to the coefficients C_i in equation 4.7.8). $\hat{\Gamma}$ is the damping operator which refects relaxation due to both elastic and inelastic processes. Although the contributions to $\hat{\Gamma}$ will be

subsequently discussed in section 4.9, for the present purposes the damping operator will be considered to include only elastic terms. For a three level system where a is the ground state and n and m are the states which are responsible for quantum beats, the time dependence of state m, for example is given by (10);

$$\frac{\rho_{nn}(t)}{\rho_{nn}(0)} = \exp\left(-t\frac{\Gamma}{\Lambda^2}\right)\left\{(\omega^2 + 2\hbar^{-2}|H'|^2) + 2\hbar^{-2}|H'|^2\cos\Lambda t\right\} \qquad 4.7.10$$

where $\Lambda^2 = \omega^2 + 4\hbar^2|H'|^2$, $\Gamma = \frac{1}{2}(\Gamma_1 + \Gamma_2)$, and where it has been assumed that the decay rates of the two excited states are equal. The second term in equation 4.7.10 describes a damped oscillatory behavior. The physical parameters of the time resolved fluorescence decay can be evaluated most easily by taking the Fourier spectrum of the decay curve, hence, applying Fourier transformation to equation 4.7.10 gives;

$$I = 2\frac{\Gamma}{\Lambda^2}\left[\omega^2 + \frac{2|H'|^2}{\hbar^2}\right] + \frac{|H'|^2}{\hbar^2}\left[\frac{1}{(\omega - \Lambda) + \Gamma^2} + \frac{1}{(\omega + \Lambda) + \Gamma^2}\right] \qquad (4.7.11)$$

The Fourier spectrum consists of a half-Lorentzian term at zero frequency with a width determined by Γ and a full Lorentzian centered at the beat frequency, Λ with a width characterized by the total dephasing rate, Γ. When the fluorescence from many coupled states is accepted by the detector, the signal will be proportional to $\sum_i \frac{\rho_{ii}(t)}{\rho_{ii}(0)}$ and the Fourier transform will exhibit several components. Equation 4.7.11 therefore provides a convenient means of analyzing a complicated quantum beat pattern.

It is important to note that in the previous description both the exponential and oscillatory terms are decaying at the same rate. This

result is the consequence of the original assumption that pure dephasing was not considered in the decay rate such that $\Gamma = \frac{1}{2}(\Gamma_1 + \Gamma_2)$, where Γ_i is the decay rate of the diagonal elements of the density matrix. Γ_i includes both radiative and nonradiative components of the population relaxation. With the addition of a pure dephasing components, Γ_d, the total dephasing rate is given by (8) $\Gamma = \frac{1}{2}(\Gamma_1 + \Gamma_2) + \Gamma_d$. The physical origin of pure dephasing can be described in terms of the loss of phase coherence among the interacting eigenstates due to statistical fluctuations in the environment to which the system is coupled (i.e. off diagonal density matrix elements). Although pure dephasing is well recognized as being a consequence of intermolecular interactions (i.e. phonons, collisions), it is of considerable interest and controversy as to whether pure dephasing relaxation, mediated by means of the intramolecular bath states, can occur in an isolated molecule (18).

Whereas classification of T_1 and T_2 type relaxation processes is well established in the field of magnetic resonance (19), in terms of the multilevel dynamics of large polyatomic molecules the distinction is not as well defined (18,20). The ambiguity lies in the formulation of the theoretical framework for the dynamical processes (the partitioning of the system Hamiltonian) which in turn depends upon the available experimental information on any particular system. The master equation approach lends itself to the description of an isolated molecular subsystem consisting of a vibrational subsystem interacting with a thermal reservoir (18,20). Regardless of the basis set used to describe the molecular system, from an experimental viewpoint, the separation of population relaxation and pure dephasing terms resides in the ability to independently measure the population relaxation (T_1) and the total relaxation rates

(homogeneous linewidth). Several experimetnal techniques which have been applied to the investigation of dephasing phenomena include; coherent transient experiments (21), overtone spectroscopy (22,23) and nonlinear time resolved (i.e. Raman) spectroscopy (24). In the context of the master equation treatment, pure dephasing relaxation is equivalent to the experimentally determined absorption lineshape while the fluorescence decay rate is proportional to population relaxation (18). The success of the aforementioned experiments in establishing total dephasing rates has relied upon the ability to eliminate inhomogeneous contributions to the lineshape.

The quantum beats are directly related to the homogeneous lineshape through the Fourier transformation of the damped oscillatory component of the fluorescence (equations 4.7.10 and 4.7.11) and thereby a direct measurement of the total dephasing rate is obtained . Quantum beats reflect the phase coherent properties of the system. On the other hand, the population relaxation rate is determined from the fluorescence decay rate. This is true if pure dephasing is defined in terms of elastic interactions. The population relaxation rate is determined from the decay of the molecular system in the absence of quantum beats. With reference to equation 4.710, the two relaxation rates are responsible for damping the first and second terms as follows;

$$\frac{\rho_{ii}(t)}{\rho_{ii}(0)} = exp\left(\frac{-t\Gamma_{fl}}{\Lambda^2}\right)\left\{\omega^2 + 2h^{-2}\,|H'|^2\right\} + exp\left(-t\frac{\Gamma}{\Lambda^2}\right)\left\{\frac{2|H'|^2}{h^2}\cos\Lambda t\right\} \qquad (4.7.12)$$

where Γ_{fl} is the energy population (T_1^{-1}) relaxation rate. Γ_{fl} includes both radiative and nonradiative processes. The nonradiative dynamics can be of intramolecular and/or intermolecular origin. Aside from the

eigenstates responsible for the quantum beats, additional states which exhibit exponential decays may also be simultaneously detected. For a complicated level structure, as exists for a large polyatomic molecule, especially at higher excess energies, the number of eigenstates which contribute to the single exponential terms is difficult to determine. This is in contrast to the aza-aromatic and bicarbonyl molecules which have so far been investigated where it is reasonable to expect that all combinations of eigenstates exhibit an oscillatory decay.

The treatment of the molecular dynamics previously discussed is by definition appropriate for a closed, few level system, where the damping is due entirely to radiative decay, and hence more suitable for application to the case where excitation is to low excess vibrational energy and where the eigenstates of the system are well defined. This is particularly true in the recent quantum beat experiments (13,14,25) where the eigenstates are of mixed singlet-triplet character. The small number of optically active singlet states at low excess energy allows selective vibronic excitation to be achieved and hence a tractable number of interference terms are produced.

This approach, however, is inadequate to completely describe the dynamics of a large polyatomic molecule for the reason that additional quantum mechanical subsystems interact with the initially optically prepared system. Although many theoretical discussions have been presented (1-9), exact solutions would have little relevance to the situation considered herein, due to the fact that a definition of the subsystems, the damping matrices and the mutual interactions are to a large extent problematic. The purpose here is to present a context in which to discuss the experimental observables. In particular one would like to

explain, 1) the broad (unresolved) and sharp features which appear in the resolved fluorescence, 2) the relationship of radiative decay rates to the cooling conditions of the free jet expansion, and, 3) how the quantum beats are influenced by the excitation, detection and free jet expansion conditions. As seen from the Fourier transform of the quantum beat pattern, equation 4.7.11, the linewidth is proportional to the total dephasing rate. If one is able to understand the contribution of subsystem coupling to the total dephasing rate then one is in a position to use the quantum beat damping rate as a probe of the internal dynamics of the molecular system.

Again, the starting point is the Liouville equation (equation 4.7.9), however, the distinction is now made between the subset of modes which are optically accessible, and the background modes. The optically accessible modes are those whose corresponding potential surfaces are similar in both the ground and the excited states, and correspond to transitions in the molecular absorption spectrum. These subsystems can have both intramolecular and intermolecular origins. For example, the formation of complexes in the free jet expansion can contribute additional subsystems (26). $\hat{L}_0$ and $\hat{L}'$ are effective Liouville operators for optically accessible modes and are responsible for generating coherent oscillatory dynamics within the system. The modes of a particular subsystem are either inelastic or elastic as defined by the coupling mechanisms, $\hat{L}'$, with the optically prepared state. Coupling of inelastic modes is responsible for intramoleuclar energy redistribution and gives rise to longitudinal, or T_1 relaxation, while the elastic or bath modes induce loss of phase coherence, a manifestation of transverse, T_2, relaxation. The damping matrix elements are defined in terms of dissipative or longitudinal relaxation

rates, Γ_i, and the total dephasing rate, T_2, which reflects both the dissipative and pure dephasing components such that, $\Gamma = \Gamma_{ij} + \frac{1}{2}(\Gamma_i + \Gamma_j)$.

A coupling scheme appropriate for a discussion of IVR in anthracene is presented in figure 3. The following discussion is based upon the approach developed by Rhodes (1) which is sufficiently general to incorporate the potential for observing interference effects in the resolved emission at high densities of rotational and vibrational states. In the two resonance system shown in figure 3, $|a>$ is the ground state and $|b>$ is the optically accessible state. States $|b>$ and $|c>$ are distinguished by the properties of the corresponding emission. The relaxation constant γ_b is associated with resonance and unrelaxed fluorescence to states of the $|a>$ manifold, and γ_c indicates relaxed emission to lower energy states other than $|a>$. The $|c>$ states are quasi-degenerate with the $|b>$ states and experience little change in the electronic potential surface upon excitation and hence the transition can be characterized by a change in the vibrational or rotational quantum number (2). The large number of $|c>$ states which exist at high excess vibrational energies result in the apparent broadening of the fluorescence associated with the transitions. Both γ_b and γ_c incorporate nonradiative decay. The terms, V_{ab} and V_{bc} represent radiative coupling between states $|a>$ and $|b>$, and, a nonradiative interaction between states $|a>$ and $|b>$, respectively. Terms can also be included to designate elastic coupling with background modes, and are equivalent to interactions which induce pure dephasing. This scheme implies a sequential coupling between the radiatively prepared states and the background modes, and therefore indicates a potential for observing a risetime in γ_c associated with the magnitude of V_{bc}. Evidence for this behavior has not been observed experimentally except perhaps in

the O_2 fluorescence quenching experiments of Coveleskie et al. (27) and the time resolved measurements by Tramer et al. (28) on p-difluorobenzene, presumably as a consequence of the process modulated by V_{bc} being more rapid than the experimentally observable time scales used. With the exception of these experiments there was no evidence of temporal evolution of specific vibronic levels. Extensive studies by Smalley et al. (29) on alkyl benzenes failed to reveal evidence of spectral evolution on a nanosecond time scale. Recent experiments in this laboratory (30) have indicated a picosecond buildup in the fluorescence associated with exciplex formation of anthracene- $(CH_2)_3$-N,N-dimethylaniline. The extent to which this reflects the sequential transfer of vibrational energy from the chromophore to vibrations of the alkyl chain is currently under investigation. Therefore, in large polyatomic molecules it is generally true that $\gamma_c \gg \gamma_b$ when considering intramolecular vibrational redistribution and electronic relaxation. This is especially true if $|c>$ is nonradiatively coupled to many levels, as would be the case where the density of $|c>$ states is very large such that the linewidths of the eigenstates overlap, in which case $\Gamma_c \propto 2\pi V_{bc}\rho_c$, or when the $|c>$ subsystem is perturbed by an external subsystem such as a weakly bound complex or an intermolecular collision.

The overall dynamics of the system can be realized by considering the relative rates for the various processes denoted in figure 3 (1). Quantum beats are exhibited when the coupling between states $|b>$ and $|c>$ is strong. As a result, the excitation spectrum consists of two distinct transitions to states originating from the diagonalization of $|b>$ and $|c>$. Upon coherent preparation, interference terms will be evident in the fluorescence. If the linewidth of the states overlap, quantum beats will

not be observed. Within the bandwidth of the laser, the possibility exists that many eigenstates with various degrees of coupling, will be prepared. These states will give rise to the relaxed and unrelaxed exponential fluorescence decay components, and possibly give rise to additional oscillatory terms.

§4.7.5 *Conclusion*

For large molecules in the gas phase, even at low excess vibrational energies, the level structure is congested due to ground state thermal population. The successful solution to this problem in recent years has been the application of laser spectroscopy to supersonic free jet expansions where internal rotational and vibrational temperatures on the order of 0.5 °K and 50 °K are typically achieved. The near isolated molecule conditions of the expansion also reduce, if not eliminate, intermolecular interactions. At low excess vibrational energies, single vibronic level excitation has enabled the observation of quantum beats in a number of molecular systems (13,14,25). However, at higher excess energies, the oscillatory behavior vanishes, presumably as a result of the increasing number of optically prepared and also bath (in these cases, triplet) states. At intermediate excess energies (~1500 cm^{-1} above the S_1 origin) in the first excited singlet state, the enormous number of vibrational, rotational and bath states would seem to prohibit the resolution of interference phenomena. This conclusion, however, is based upon an intuitive judgment which presumes equivalent coupling strengths and dipole matrix elements. When the mean spacing between the effective molecular eigenstates is appreciably smaller than the radiative width then the statistical limit will be encountered and the manifestations of selective coupling will be averaged. Quantum beats will be observed

provided that the level spacing ($\Delta\omega$) is comparable to or smaller than the radiative width, Γ (Wigner-Weisskopf limit). Quantum beats are therefore an indication of quasidiscrete level structure and have recently been discussed in this context (30).

The detection of quantum beats requires the excitation by a laser pulse which is equal to or less in duration than the periods of the resolvable beat components. Furthermore, the coherence width of the excitation pulse must be comparable to or greater than the energy level spacing between the interfering states. The observation of quantum beats in a large molecule such as anthracene at intermediate excess vibrational energies (implying a large density of $|c>$ states) would therefore require a fortuitous combination of intrastate coupling strengths and emission dipole matrix elements. With regard to the detection conditions, the observation of quantum beats in the fluorescence requires a judicious choice of the frequency domain to be selected for observation. In large polyatomic molecules such as anthracene, the large number of bath states, implying a large number of subsequently destructively interfering oscillatory terms, would then prevent the observation of quantum beats in the broad (unresolved) relaxed emission component, γ_c. On the other hand, the presence of discrete emission indicates specific dipole matrix elements associated with unrelaxed fluorescence, thereby favoring the appearance of quantum beats in this spectral region.

The observation of quantum beats in anthracene and trans-stilbene at $\sim$1400 cm^{-1} of excess vibrational energy indicates that there is distinct radiative and presumably vibronic properties of specific eigenstates in the presence of unspecified relaxation pathways. In the terminology of radiationless transition theory, this establishes the intermediate level

structure. In anthracene, quantum beats are observed despite a vibrational density of states of 100 states/cm^{-1} and an excitation bandwidth (~1 A°) which spans a large number of rotational states. The presentation of our experimental results on anthracene and trans-stilbene, and a discussion of quantum beats in intermediate level structures are presented in the following sections.

REFERENCES

1. W. Rhodes, J. Chem. Phys., **75,** 2657 (1982).

2. K.F. Freed and A. Nitzan, J. Chem. Phys., **73,** 4765 (1980).

3. R. Haberkorn, H.L. Selzle, W. Dietz, S.H. Lin and E.W. Schlag, Chem. Phys., **52,** 363 (1980).

4. K. Lendi, Chem. Phys., **46,** 179 (1980).

5. P. Grigolini and A. Lami, Chem. Phys., **30,** 61 (1978).

6. A. Villaeys and G. Klein, Chem. Phys. Lett.; **90,** 85 (1982).

7. A. Villaeys and K.F. Freed, Chem. Phys., **13,** 271 (1976).

8. S.H. Lin and H. Eyring, Proc. Natl. Acad. Sci. USA, **74,** 3623 (1977).

9. H. Kono, Y. Fujimura and S.H. Lin, J. Chem. Phys., **75,** 2569 (1981).

10. R. Haberkorn, H.L. Selzle, W. Deitz, S.H. Lin and E.W. Schlag, Chem. Phys., **52,** 363 (1980).

11. M. Sargent, M.O. Scully and W.E. Lamb, Jr., *Laser Physics*, Addison-Wesley, Reading, Mass., 1974.

12. S. Haroche in *High Resolution Laser Spectroscopy*, ed. K. Shimoda, Springer Verlag, New York, 1976, p. 253.

13. P.M. Felker, W.R. Lambert and A.H. Zewail, Chem. Phys. Lett., **89,** 309 (1982).

14. J. Chaiken, M. Gurnick and J.D. McDonald, J. Chem. Phys., **74,** 117 (1981).

15. W. Rhodes, Chem. Phys., **31,** 335 (1978).

16. C.A. Langhoff, Chem. Phys., **20,** 357 (1977).

17. J. Chaiken, M. Gurnick and J.D. McDonald, J. Chem. Phys., **74,** 117 (1981).

18. S.H. Lin in *Radiationless Transitions*, Academic Press, New York, 1980.

19. A. Abragam, *The Principles of Nuclear Magnetism*, Oxford University Press, London, 1961.

20. S. Mukamel, Chem. Phys., **31,** 327 (1978).

21. T.E. Orlowski and A.H. Zewail, J. Chem. Phys., **70,** 1390 (1979), and A.H. Zewail, Acc. Chem. Res., **13,** 360 (1980) and references therein.

22. J.W. Perry and A.H. Zewail, J. Chem. Phys., **70,** 582 (1979), R.L. Swofford, M.E. Long and A.C. Albrecht, J. Chem. Phys., **65,** 179 (1977).

23. K.V. Reddy, D.F. Heller and M.J. Berry, J. Chem. Phys., **76,** 2814 (1982).

24. A. Laubereau, S.F. Fischer, K. Spanner and W. Kaiser, Chem. Phys., **31,** 335 (1978).

25. W. Henke, H.L. Selzle, T.R. Hays, S.H. Lin and E.W. Schlag, Chem. Phys. Lett., **77,** 448 (1981).

26. J.A. Beswick and J. Jortner, J. Chem. Phys., **74,** 6725 (1981), and references therein.

27. R.A. Coveleskie, D.A. Dolson and C.S. Parmenter, J. Chem. Phys., **72,** 5774 (1980).

28. N. Halberstadt and A. Tramer, J. Chem. Phys., **73,** 6343 (1980).

29. J.B. Hopkins, D.E. Powers and R.E. Smalley, J. Chem. Phys., **72,** 5039 (1980), 5049 (1980).

30. P.M. Felker, J.A. Syage, W.R. Lambert and A.H. Zewail, in press, Chem. Phys. Lett..

31. R.C. Sharp, E. Yablonovitch and N. Bloembergen, J. Chem. Phys., **76,** 2147 (1982).

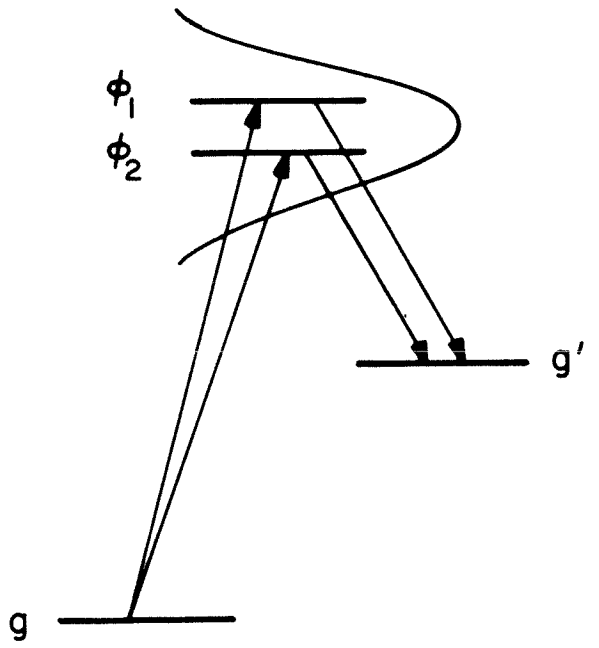

Figure 1.
Schematic diagram of a three level system. The excited states, Φ_1 and Φ_2, are coherently prepared within the excitation bandwidth, and are radiatively coupled to a common ground state level, g'. The coherent superposition and common radiative properties indicate the basic requirements for the generation of interference effects in the resolved fluorescence (equation 4.7.5).

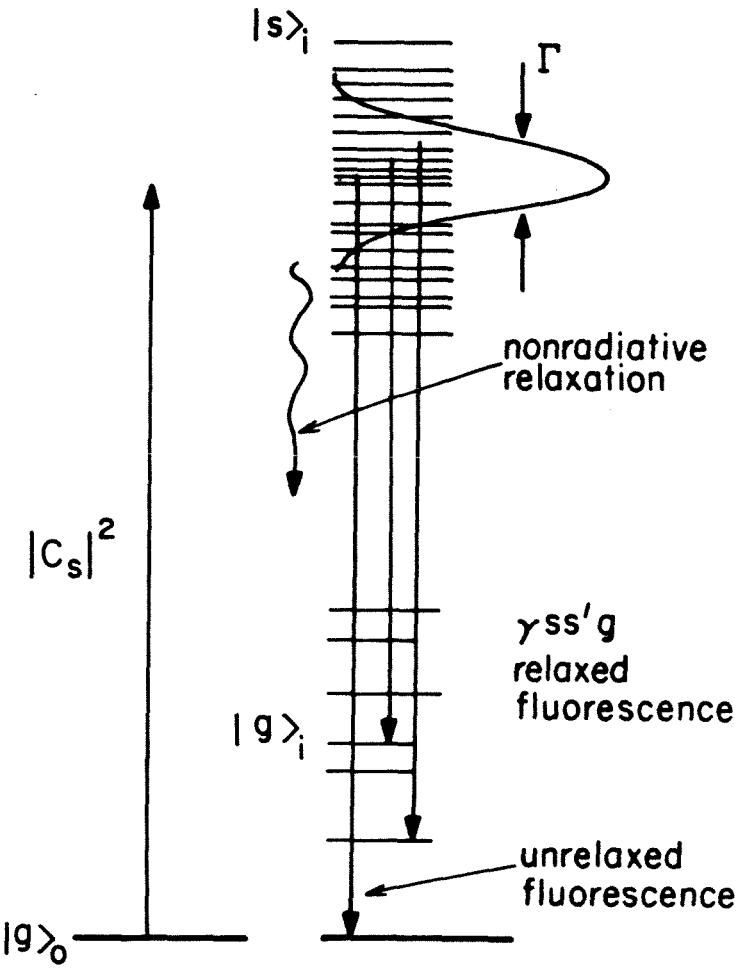

Figure 2.

A schematic diagram of the generalized level structure and relaxation pathways in a large polyatomic molecule. Within the laser bandwidth a number of molecular eigenstates, $|s\rangle_i$, are initially prepared depending upon the optical dipole matrix elements, $|C_s|^2$ with the ground state level(s), $|g\rangle_0$. The linewidths of the individual eigenstates are determined by the total dephasing rate, Γ. The excited states can decay by nonradiative and radiative mechanisms. The latter is divided into two components, the unrelaxed and the relaxed fluorescence. The excited states associated with the relaxed fluorescence are radiatively coupled to vibronic levels built upon the 0-1 transition (resonance), whereas the states identified with the relaxed fluorescence component are radiatively coupled to other levels, $|g\rangle_i$.

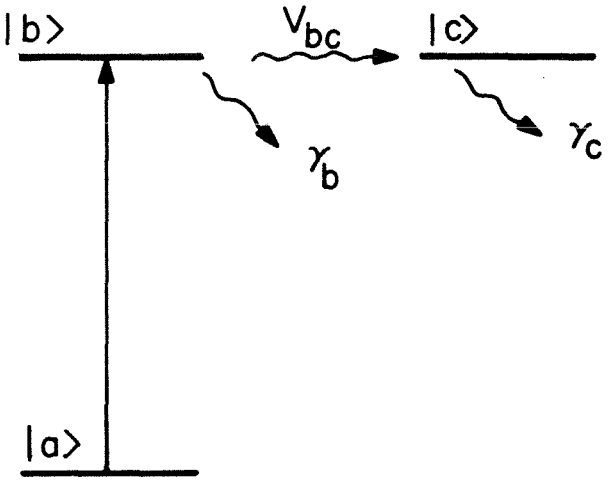

Figure 3.
An illustration of the level structure and coupling mechanisms in a large polyatomic molecule. The general features are the same as indicated in figure 2 except that the coupling, V_{bc} , between the optically accessible states, $|b>$, and the bath manifold of states, $|c>$ is explicitly included. γ_b and γ_c represent both nonradiative and radiative relaxation channels which may be distinct. In addition, however not included, the coupling between the states $|a>$ and $|b>$, and between states $|b>$ and $|c>$ may be modulated by elastic (dephasing) perturbations.

§4.8 *VIBRATIONAL RELAXATION: EXCESS ENERGY DEPENDENCE OF TIME AND FREQUENCY RESOLVED FLUORESCENCE*

§4.8.1 *Introduction*

An understanding of intramolecular vibrational relaxation (IVR) and redistribution is central to the concepts of energy and phase dynamics in large polyatomic molecules. The primary question which one would like to address is the extent to which, for an isolated molecular system, the vibrational relaxation and redistribution dynamics can be considered as progressing from that of an isolated quantum mechanical system characterized by discrete energy level structure and modulated by well defined coupling mechanisms, to that of a statistical system interacting with a large effective thermal resevoir. That a basis exists for describing the molecular level structure in terms of a progression from a sparse vibrational manifold to a quasicontinuum characterized by a high density of states with increasing excess energy within an electronic manifold has been well documented (1). The ability to quantitatively approach this problem in large molecules resides in the degree to which the molecular energy level structure can be determined, and in the measurement of the specific intrastate coupling rates and mechanisms which are active in inducing energy and phase relaxation and redistribution. Implied in the latter is the knowledge of the molecular interaction with the radiation field which is essential in determining the initial distribution of excited vibronic states. The development of free jet expansion techniques has enabled the production of nearly isolated molecules with reduced internal rotational and vibrational temperatures. Combined with the techniques of laser spectroscopy, the dynamics of large polyatomic molecules

can therefore be studied in the absence of spectral congestion resulting from the ground state thermal distribution, and in an environment where intermolecular interactions have been substantially reduced. Whereas absorption spectroscopy primarily provides information regarding the optical accessibility of the molecular eigenstates, frequency and time resolved spectroscopy reflect the consequences of intramolecular dynamics. To this end, the examination of the excess energy dependence of the resolved fluorescence and the associated relaxation rates is a productive endeavor and has been extensively applied to the study of intramolecular vibrational energy relaxation in large polyatomic molecules cooled in free jet expansions (1).

The energy level structure of the first excited singlet manifold of large molecules as determined by fluorescence excitation spectroscopy is characterized by three regimes. At low excess vibrational energies, $E_v \approx$ 0-1000 cm^{-1}, the level structure is sparse and exhibits well defined vibronic transitions. At intermediate excess energies, $E_v \approx$ 1000-3000 cm^{-1}, a broad background gradually develops, to the point where at high excess energies, $E_v \approx 2000\ cm^{-1}$, the broad features dominate the spectral structure and discrete transitions are no longer observed. The excess energy dependent broadening reflects both spectral congestion which originates from the large number of combination bands which exist at higher excess energies, and from increased anharmonic mixing which is induced by the high density of states. These trends appear to reflect general properties of all large polyatomic molecules (1,2,3). The importance of the density of non-optically active states in contributing to the observed broadening is exemplified by the work of Smalley et al. (4) on alkylbenzenes where the energy for the onset of spectral broadening is

reduced with increasing length of the alkyl chain. As careful studies in our laboratory have shown, however (5,6), it is not entirely straightforward to distinguish between sequence congestion and the effects of non-radiative coupling in fluorescence excitation experiments. It is clear, nevertheless, that as the excitation energy is increased, the ability to selectively excite single vibronic energy levels is considerably compromised. The region at which a transition is made from a 'quasi-discrete' energy level structure to that of a statistical distribution has been termed the onset of the quasicontinuum, and is important with regard to defining the distribution of molecular eigenstates which can be prepared by laser excitation. The congested level structure in the quasicontinuum corresponds to overlapping resonances and prevents selective excitation of individual molecular eigenstates. As will be discussed in detail later, it is in this intermediate excess energy region that one expects to observe evidence for selective and competetive intramolecular dynamic processes.

The manifestations of intrastate mixing are more prominent in energy resolved emission spectra. As is the case for fluorescence excitation (absorption) spectra, the energy resolved emission demonstrates a transition where, upon excitation to low excess vibrational energies, the emission exhibits only discrete transitions, to a region at high excitation energies where the energy resolved emission is broad and structureless. The excess energy region intermediate between these two extremes reflects various contributions of sharp and unresolved spectral features which are strongly dependent upon the vibronic state which is optically prepared, and serves, as in the absorption spectra, as evidence for the onset of the vibrational quasicontinuum. The importance of distinguishing

between unrelaxed and relaxed fluorescence is due to the nature of the excited states which are involved in the fluorescence. Whereas the unrelaxed fluorescence originates from the initially prepared set of eigenstates, the relaxed fluorescence is interpreted as arising from bath state transitions. Since the transfer of population from the initially prepared set of eigenstates to the bath manifold is implied, the appearance of relaxed fluorescence is therefore indicative of intramolecular vibrational relaxation. The bath modes are populated through coupling (i.e. anharmonic) with the optically prepared singlet states. A point should be made here regarding the basis used to interpret the IVR processes. In the zero order picture one considers a set of energy levels which are diagonalized with respect to the radiation field. Subsequent to excitation, energy and phase become redistributed according to the intrastate coupling. From the standpoint of the molecular eigenstates basis, the molecular states are diagonalized with respect to all intrastate coupling. The system is therefore initially prepared in a nonstationary state which is a linear superposition of a number of molecular eigenstates. In this case, IVR is a consequence of the loss of phase coherence among the molecular eigenstates. In the intermediate excess energy region, the ratio of the intensity of the unrelaxed and relaxed fluorescence is a measure of the amount of relative bath mode character. Considerable effort has been expended to establish the nature of intramolecular vibrational redistribution from comparison of the intensities of the unrelaxed and relaxed fluorescence features in gated time resolved experiments (4). Conclusions from these studies reveal that vibrational redistribution is an apparently fast process on the observation time scale (< 1 nsec), based upon the failure to observe a temporal development of the resolved

fluorescence features, and non-exponential decays.

The behavior of the radiative decay rates as a function of excess vibrational energy of excitation complements the dependence exhibited by the spectral features. The general trend is for the radiative decay rate to increase with increasing excess vibrational energy. This trend parallels the energy dependence of the nonradiative decay rates and the reduction in the fluorescence quantum yield with increasing excess energies (7). In the intermediate excess energy region the decay rates are observed to be dependent upon the mode of excitation. It has also been shown (8) that the unrelaxed fluorescence exhibits a faster decay rate than that for the relaxed component.

Previous investigations initiated by other laboratories into the nature of IVR in large molecules cooled in free jet expansions have been performed using nitrogen and YAG pumped dye lasers where, despite the high resolution (0.3 cm^{-1}, or with an internal etalon, 0.03 cm^{-1}) the minimum pulse width is 5 nsec, thereby restricting the observation of temporal development to nanosecond time scales. Recent evidence obtained by Tramer et al. (8) has suggested that IVR proceeds on a sub-nanosecond time scale. By comparing the radiative decay rates and the time resolved fluorescence spectra of p-difluorobenzene, the investigators were able to establish a redistribution time of approximately 300 psec. Upon excitation to the intermediate excess energy region ($\delta\nu$ =2200 cm^{-1}), the sharp spectral features which are superimposed upon a broad continuous background exhibit a quasi-biexponential decay. The fast component (0.3 ± 0.1 nsec) is interpreted as the direct consequence of energy transfer between the optically accessible states and the background modes. This result therefore suggests the value of investigating

the picosecond dynamics of relaxation in large molecules. If the IVR rate is on the order of several hundred picoseconds in vapor experiments, the extension to free jet expansions, where the combined aspects of reduced spectral congestion, implying the possibility of selective vibronic excitation, and the near collision free environment, would tend to favor reducing the total relaxation rate, and thus increase the probability of experimentally observing the manifestations of IVR. However, despite the potential for studying IVR in large molecules which Tramer et al.'s (8) work implies, the conclusions are in contradiction to earlier work performed by, for example Parmenter et al. (9). Using collision induced quenching to depopulate bath modes, these investigators established a redistribution time for p-difluorobenzene on the order of 10 psec.

It is well known from radiationless transition theory, (10) and is indeed a test of current concepts regarding intramolecular dynamics, that the observation of selective mode coupling would most likely be manifest in the intermediate excess energy region. This regime, as discussed above, and as based upon experimental evidence, is expected to exhibit selective relaxation for favorable excitation and detection conditions. In terms of sequential coupling between optically prepared and bath modes, it is anticipated that upon single vibronic level excitation there would be temporal evolution of the spectral structure in the emission, and also non-exponential fluorescence decays characterized by a buildup, indicative of $| b > \rightarrow | c >$ energy transfer. Furthermore, one would anticipate that these processes would be highly dependent upon the nature of the vibronic mode excited and the structure of the bath manifold at that particular energy. Although evidence for selective coupling in this region exists, as implied by the presence of both unrelaxed

and relaxed emission features appearing in the resolved fluorescence, estimates for the time scale of the vibrational redistribution processes are, at present, controversial.

The combination of picosecond laser excitation and supersonic fee jet techniques has enabled us to extend these studies to the subnanosecond time regime. Most importantly however, the use of nearly transform limited picosecond pulses (< 15 psec) enables the coherent preparation of a well defined set of eigenstates (2 cm^{-1}). In order to eliminate extraneous contributions due to complicated mixing between electronic states, such as is the case for naphthalene where the oscillator strength is achieved through the mixing of the $^1B_{3u}$ S_1 and $^1B_{2u}$ S_2 states, and which by creating additional relaxation pathways, might tend to obscure any mode selective coupling, anthracene was chosen for our investigations. The comparatively simple electronic and vibrational energy level structure of anthracene is comprehensively discussed in section 3.

§4.8.2 *Results and Discussion*

The fluorescence excitation spectrum for the $S_1 \rightarrow S_0$ is characterized by a region at low excess energies of well separated vibronic transitions and a region of combined unresolved and sharp spectral features beginning around 1200 cm^{-1} (see figure 3.3). In figure 1, the region around 1400 cm^{-1} of excess vibrational energy is shown. The spectroscopic assignments for the vibronic transitions can be found in section 3. The onset for the broad structure associated with the quasicontinuum found for anthracene is similar to that for other large aromatics under

effectively similar experimental conditions, being between 1000 → 2000 cm^{-1} for pentacene (3c), and tertacene (3a), and 4000 cm^{-1} for naphthalene (2a). At 1200 cm^{-1}, the density of vibrational states built upon the first excited singlet is approximately ρ = 100 states/cm^{-1}. Since efficient coupling between the system and bath manifolds is indicated by $\gamma\rho >> 1$ where γ corresponds to the radiative decay width ($\gamma \approx 10^8$ Hz for anthracene at ν_{ex} = 1200 cm^{-1}), the density of vibrational states is apparently insufficient to induce intrastate coupling at these excess energies. The large amount of vibrational structure which appears at ν_{ex} = 1400 cm^{-1} and particularly the sidebands associated with the strong resonances indicates a substantial degree of vibronic coupling. The distribution of the oscillator stength in this region indicates that any excitation would prepare a complicated distribution of zero order levels and furthermore would have the most potential for exhibiting differential intramolecular dynamics.

The manifestations of intramolecular vibrational energy redistribution are much more apparent in the energy resolved fluorescence spectra. These spectra are presented in figure 2 as a function of excess excitation energy in the first $^1B_{2u}$+ electronic state of anthracene. The final spectrum, at $\delta\nu_{ex}$ = 4273 cm^{-1} is equivalent to excitation of the fourth harmonic of the prominent 1400 cm^{-1} ring breathing mode. This series of spectra demonstrates the energy dependent broadening of the transitions associated with the degree of coupling among the zero order levels in both the ground and excited state manifolds. The spectra are consistent with studies whereby the energy resolved fluorescence can be characterized by three distinct spectral regions: sparse, intermediate, and quasicontinuum.

Sparse level structure in the resolved fluorescence appears upon excitation below 800 cm^{-1}. For excitation to the electronic origin ($\delta\nu_{ex}$ = 0 cm^{-1}) the resolved fluorescence is dominated by the $S_1(0) \rightarrow S_0(0)$ transition as is appropriate for small configurational changes between the S_0 and S_1 potential surfaces of anthracene. Excitation to the 389 cm^{-1}, a_g fundamental and the first overtone ($\delta\nu_{ex}$ = 773 cm^{-1}) produced fluorescence features which originate from selective excitation of well defined, nearly harmonic, vibronic levels in the S_1 manifold of a large molecule. The features correspond to the transitions $S_1(\nu_i'') \rightarrow S_0(\nu_i' + \bar{\nu}')$. Only unrelaxed emission occurs in this low excess energy region. The apparent broadening observed at $\delta\nu_{ex}$ = 773 cm^{-1} is the result of insufficient spectral resolution.

In the region between 900 cm^{-1} and 1600 cm^{-1} both relaxed (broad) and unrelaxed (sharp) emission is observed. The ratio of the intensity of the relaxed compared to the unrelaxed fluorescence is a measure of the bath mode character and is seen to be dependent upon the mode excited. A dramatic example of the influence of small changes in the excitation wavelength on the resolved emission spectra in this excess energy region is presented in figure 4. This combination of spectral features is characteristic of intermediate level structure. The progressions associated with relaxed fluorescence are built upon the 1-1 transition (0.0 cm^{-1} relative frequency) indicating that the molecular eigenstate does not change vibrational quantum number during the transition (11). Several other important features to note are: 1) the dramatic change in the degree of unrelaxed fluorescence ($\delta\nu_{exc}$ = 919 cm^{-1}, 992 cm^{-1}, 1191 cm^{-1}, 1200 cm^{-1}, 1377 cm^{-1} and 1419 cm^{-1}), 2) the appearance and steady increase with excess energy of a shoulder which appears approximately 200 cm^{-1} to the

blue of the 1-1 transition, and 3) the observation of splitting for various transitions ($\delta\nu_{exc}$ = 900 cm^{-1}, 1200 cm^{-1}, 1377 cm^{-1}, 1419 cm^{-1}, 1520 cm^{-1}). The splittings have also been observed by Jortner et al.(3a) who discuss their appearance in terms of nuclear molecular eigenstates. Effectively, the anharmonic intrastate coupling between zero order states in the S_0 and S_1 electronic manifolds independently cause a splitting in the molecular eigenstates within the two manifolds. Anharmonic coupling strengths are on the order of a few wavenumbers for aromatic vibrational modes. Excitation of a single molecular eigenstate of the electronic manifold will subsequently result in emission to both molecular eigenstates in the S_0 manifold, thereby resulting in the splitting of the vibronic transition. The degree of splitting provides a measure for the energetic span of the mixed zero order levels. The energy difference between split transitions which we observe in anthracene are of similar magnitude to those observed by Jortner et al. (3a) for tetracene, being on the order of 50 cm^{-1}. Intuitively, this seems to imply an extremely large degree of intrastate coupling.

We have confirmed (section 4.4) that some of the sharp features observed in the emission spectra originate from collisionally induced vibrational relaxation to the vibrationless level of S_1. The nitrogen expansion reflects a certain degree of weak complex formation and the manifestation of the perturbation on anthracene is also found to be mode selective appearing as a transition at 0.0 cm^{-1} relative frequency (0-0 transition). The formation of nitrogen-anthracene complexes does not influence the intensities of the spectral features associated with the relaxed fluorescence as confirmed by comparison with spectra obtained for helium and neon expansions. The mode selective dependence of the

resolved fluorescence features cannot be directly attributed to common properties of the state which is initially excited. For example, the collisional features are independent of the symmetry, relative oscillator strength, or whether the mode is a fundamental or combination band.

The increase in spectral broadening and general trends exhibited in anthracene fluorescence as a function of excess excitation energy are paralleled by the spectral shift of the 1-1 peak relative to the position of the 0-0 transition (figure 3). In the region between 900 cm^{-1} and 1600 cm^{-1} the red shift for the 1-1 transition exhibits considerable state selective deviation while the trend is relatively constant at both higher and lower excess excitation energies. The red shift is attributed to relative differences in the mixing amplitudes for coupling between the optically accessible states and the bath modes in the ground and excited state manifolds (3a,11). The trend in the red shift is very similar to that observed for the excess energy dependence of the radiative decay rate (figure 7).

Increasing the excitation energy 1600 cm^{-1} above S_1 and to higher energies results in broad energy resolved emission spectra. At the highest excess energies ($\delta\nu_{exc}$ = 4273 cm^{-1}), the fluorescence is similar to that observed for thermal gas phase experiments. In this region the density of bath or $|\ c\ >$ states is very large and the mixing with the optically prepared states is complete, being equivalent to the statistical limit.

The extent to which the density of the bath states affect the energy for the onset of the quasicontinuum in anthracene can be assessed by observing the influence of isotopic substitution. Deuterium substitution will lead to a decrease in the vibrational frequencies of the C-H modes and therefore should increase the excess energy dependence of the non-

radiative decay rate. An analogous approach has been implemented by Smalley et al. (4) towards the study of IVR in alkyl benzenes whereby the density of bath states in modified by increasing the length of the alkyl chain. In this regard, the d_2- and d_{10}-anthracene isotopes were studied. The energy dependence of the resolved fluorescence is presented in figures 5 and 6, respectively, and show trends similar to those of h_{10}-anthracene. This is not a surprising result when one considers that the vibrational structure does not significantly change upon deuteration (refer to the spectra for excitation to the S_1 origin, 0 cm^{-1}, and section 3), and hence there is little alteration in the density of states arising from the vibrational structure. An additional noteworthy feature is the excellent example of state splitting observed in the d_2-anthracene spectrum for $\delta\nu_{exc}$ = 840 cm^{-1}.

Several attempts were made to observe spectral evolution of the emission using a time gate centered on the first 100 psec of the time resolved decay. We were unable to observe a mode selective change in the amplitudes of the spectral features for any transition excited, particularly in the intermediate excess energy region. This implies that the intramolecular vibrational redistribution rate is faster than 100 psec, and that the features which we observe in the resolved fluorescence originate from an equilibrated distribution of molecular eigenstates. This is in contrast to the 300 psec redistribution time determined for p-difluorobenzene by Tramer et al. (8).

The excess energy dependent decay rates for h_{10}-anthracene and the deuterated derivatives are presented in figure 7. For all excitation energies the time resolved fluorescence exhibited single exponential decays. The lifetime for 0-0 excitation ($\delta\nu_{exc}$ = 0 cm^{-1}) of h_{10}-anthracene in the

free jet expansion was 23.5 ± 0.3 nsec as compared to the gas phase room temperature value of 5.6 nsec (13). This value obtained by us is in agreement with that obtained by Schlag et al. (14) who determined a radiative lifetime for the 0-0 transition of 24.9 nsec.

For both h_{10}- and 9,d_1-anthracene, the fluorescence decay rate increases steadily with increasing excitation energy until, at 2000 cm^{-1} of excess vibrational energy, corresponding to the onset of the quasicontinuum as determined from the energy resolved fluorescence spectra (figure 2), there is no further change in the radiative rate. The fluorescence lifetime in this region is 5.5 ± 0.5 nsec and is equivalent to the value measured for thermal samples (13). Since the density of states (vibrational states built upon S_1) is on the order of 100 states/cm^{-1} at ν_{exc} = 2000 cm^{-1} it is unlikely that the constancy of the decay rate at higher excess energies is due to the thermalization of the bath modes. It is also unlikely that interaction with a second singlet state is responsible for the leveling of the decay rate with increasing excess energy, since the S_2 $^1B_{3u}$- state origin is located 3131 cm^{-1} above the S_1 state (15), and well above where the threshold is reached. The relatively constant values for the fluorescence decay rates over large excess energy regions has also been observed in anthracene vapors (13,16). It is possible that at high excess energies, the fluorescence decay rate is determined by selective intrastate anharmonic mixing among specific vibrational states as opposed to being mediated by nonspecific mixing of bath states.

The fluorescence decay rates for 9,10- and d_{10}-anthracene show an initial decrease in the region of sparse level structure (ν_{exc} < 900 cm^{-1}) and subsequently follow a behavior similar to h_{10}- anthracene above ν_{exc} = 1000 cm^{-1}, achieving a minimum lifetime of 5.5 ± 0.5 nsec. The initial

reduction in the fluorescence decay rates with increasing excess energy for d_{10}- and 9,10 d_2-anthracene as compared to the decay rate of the origin can be explained by invoking the presence of a nearby triplet origin. At these low excess energies (ν_{exc} < 1000 cm^{-1}), the excited state vibrational level structure is sparse and therefore relaxation is determined primarily by coupling with lower energy electronic state manifolds.

Whereas the first triplet $^3B_{3u}$+ state of anthracene is located approximately 11,700 cm^{-1} below the S_1, $^1B_{2u}$+ state (17), four triplet origins are estimated to lie in the region of the S_1, $^1B_{2u}$+ singlet (12,18). The first $^3B_{3u}$+ and second $^3B_{2u}$+ states are located approximately 560 cm^{-1} and 970 cm^{-1} below S_1, respectively. The first $^3B_{1g}$+ state origin has been measured to be located about 500 cm^{-1} below the $^1B_{2u}$+ state (19) while the calculated energy of the $^3B_{3u}$- origin is approximately 2300 cm^{-1} above the S_1 origin (18). Although studies of liquid anthracene solutions indicate that intersystem crossing from lower vibronic levels of the S_1 $^1B_{2u}$+ state occurs predominantly to the first $^3B_{1g}$+ state (16,20), the symmetry of the $^3B_{3u}$- state is appropriate for direct spin orbit coupling with the singlet $^1B_{2u}$+ state (21). Based upon experimental evidence which locates the $^3B_{3u}$- state approximately 1300 cm^{-1} above the $^1B_{2u}$+ state as indicated by dramatic changes in the fluorescence decay rates of anthracene vapors (16), it is probable that at energies slightly above the singlet origin, intersystem crossing to the $^3B_{3u}$- state becomes an important pathway for electonic relaxation. Although the gradual excess energy dependent increase in the radiative rate for h_{10}- and d_1-anthracene is in contrast to the location of nearby triplet origins and therefore may reflect the consequences of the increased density of states originating from the $^3B_{1g}$+ manifold, the relaxation rates for 9,10 d_2- and d_{10}- sub-

stituted anthracenes appear to be qualitatively consistent with a proximity mediated intersystem crossing. At 1100 cm^{-1} of excess vibrational energy, the fluorescence decay rate for the d_{10}- and 9,10 d_2- derivatives are 0.6 MHz compared to 2.2 MHz and 1.9 Mhz for the respective relaxation rates of the 0-0 transitions (figure 7). A similar retardation in the electronic relaxation rate has been observed by Jortner et al. (3a) for tetracene. The retardation of the decay rate can be the consequence of a number of factors, and a definite conclusion is difficult to achieve because of insufficient knowledge regarding the relative degree of singlet and triplet mediated relaxation, and also the relative contribution of nonradiative and radiative pathways to the total fluorescence rate.

The reduction in the fluorescence decay rate at ν_{exc} = 1000 cm^{-1} may be the result of increased triplet character of the molecular eigenstates influenced by the proximity of a nearby triplet origin. At small values of the energy gap, a decrease in the nuclear Franck-Condon factors is expected. An additional interpretation resides in the fact that the inducing modes for spin orbit coupling will be out-of-plane bending modes (21) and it is these modes which are modified to a greater extent by position dependent deuterium isotope substitution (22). Deuterium substitution will lead to a reduction in the C-H out-of-plane bending amplitude and thus will reduce the nonradiative transition rate. As a final point, it is interesting to note that the excess excitation energy at which the minimum decay rate is observed corresponds to the transition between sparse and intermediate level structure as interpreted from the energy resolved fluorescence spectra (figure 5).

A qualitative determination of the composition of the molecular eigenstates which compose the excited state manifold can be made by

monitoring the dependence of the fluorescence decay rate on the detection wavelength for a fixed excitation energy. The fluorescence decay rate for spectral features of the energy resolved fluorescence will reflect the Franck-Condon factors for the specific transitions and the nonradiative decay rate. The dependence of the fluorescence relaxation rate upon the detection energy is presented in figure 8. The comparative decay rates exhibit similar trends with regard to the composition of the molecular eigenstates as is observed in the energy and time resolved fluorescence spectra. Whereas at low ($\nu_{0,0} - \nu_{det}$ = 0 cm^{-1}) and high ($\nu_{0,0} - \nu_{det} \approx$ 4500 cm^{-1}) excitation energies, the fluorescence decay rates are relatively independent of the detection frequency, the corresponding behavior is very erratic in the region of intermediate level structure. The substituted anthracenes show similar trends. In figure 9, the decay rates for λ_{exc} = 3132 A° (ν_{ex} = 4243 cm^{-1}) as a function of the detection energy for h_{10}- and d_{10}-anthracene are compared. The mode dependence in this region can imply the presence of excited state nonradiative pathways associated with specific radiative decay channels. As previously discussed, it is not unreasonable to expect manifestations of differential intrastate coupling to become apparent at intermediate excess energies (i.e. for excitation ~2900 cm^{-1}). On the other hand, the large change in the decay rates for ~350 cm-1 excitation is probably accounted for by differences in the Franck-Condon factors associated with specific transitons, since the effective density of states in this excess energy region is probably insufficient to induce non-selective coupling.

REFERENCES

1. See for example, A. Zewail, W. Lambert, P. Felker, J. Perry and W. Warren, J. Phys. Chem., **86,** 1735 (1982); C.S. Parmenter, J. Phys., Chem., **86,** 1735 (1982), and references therein.

2. a) S.M. Beck, D.E. Powers, J.B. Hopkins and R.E. Smalley, J. Chem. Phys., **73,** 2019 (1980); b) S.M. Beck, J.B. Hopkins, D.E. Powers and R.E. Smalley, J. Chem. Phys., **74,** 43 (1981); c) J.B. Hopkins, D.E. Powers, and R.E. Smalley, J. Chem. Phys., **72,** 5039 (1980); d) J.B. Hopkins, D.E. Powers, S. Mukamel and R.E. Smalley, J. Chem. Phys., **72,** 5049 (1980).

3. a) A. Amirav, U. Even and J. Jortner, J. Chem. Phys., **75,** 3770 (1981); b) A. Amirav, U. Even and J. Jortner, Chem. Phys. Lett., **72,** 12 (1980); c) A. Amirav, U. Even and J. Jortner, Opt. Commun., **32,** 266 (1980).

4. J.B. Hopkins, D.E. Powers and R.E. Smalley, J. Chem. Phys., **73,** 683 (1980), and references therein.

5. W.R. Lambert, J. Perry and A.H. Zewail, to be published.

6. J.A. Syage, P.M. Felker, W.R. Lambert and A.H. Zewail, to be published.

7. C.-S. Huang, J.C. Hsieh and E.C. Lim, Chem. Phys., **28,** *30 (1974).*

8. N. Halberstadt and A. Tramer, J. Chem. Phys., **73,** 6343 (1980).

9. R.A. Coveleskie, D.A. Dolson and C.S. Parmenter, J. Chem. Phys., **72,** 5774 (1980).

10. For example see, K.F. Freed in *Radiationless Processes in Condensed Phases*, ed. F.K. Fong, Springer Verlag, New York, 1976, p. 24; J. Jortner and S. Mukamel in *The World of Quantum Chemistry*, ed. R. Daudel and B. Pullman, Reidel Pub., Boston, 1974, p. 145.

11. K.F. Freed and A. Nitzan, J. Chem. Phys., **73,** 4765 (1980).

12. Y.H. Meger, R. Astier and J.M. Leclercq, J. Chem. Phys., **56,** 801 (1972).

13. C-S. Huang, J.C. Hsieh and E.C. Lim, Chem. Phys. Lett., **28,** 130 (1974).

14. T.R. Hays, W. Henke, H.L. Selzle and E.W. Schlag, Chem. Phys. Lett., **77,** 19 (1981).

15. W.R. Lambert, P.M. Felker and A.H. Zewail, to be published.

16. U. Laor, J.C. Hsieh and P.K. Ludwig, Chem. Phys. Lett., **22,** 150 (1973).

17. S.F. Mason and R.D. Peacock, Chem. Phys. Lett., **21,** 406 (1973).

18. R. Parsier, J. Chem. Phys., **24,** 250 (1956).

19. R.E. Kellogg, J. Chem. Phys., **44,** 411 (1966).

20. A. Kearwell and F. Wilkinson, J. Chim. Phys. Physiochim. Biol., # 125 (1970).

21. B.R. Henry and W. Siebrand, J. Chem. Phys., **54,** 1072 (1971).

22. B.R. Henry and J.L. Charlton, J. Am. Chem. Soc., **95,** 2782 (1973).

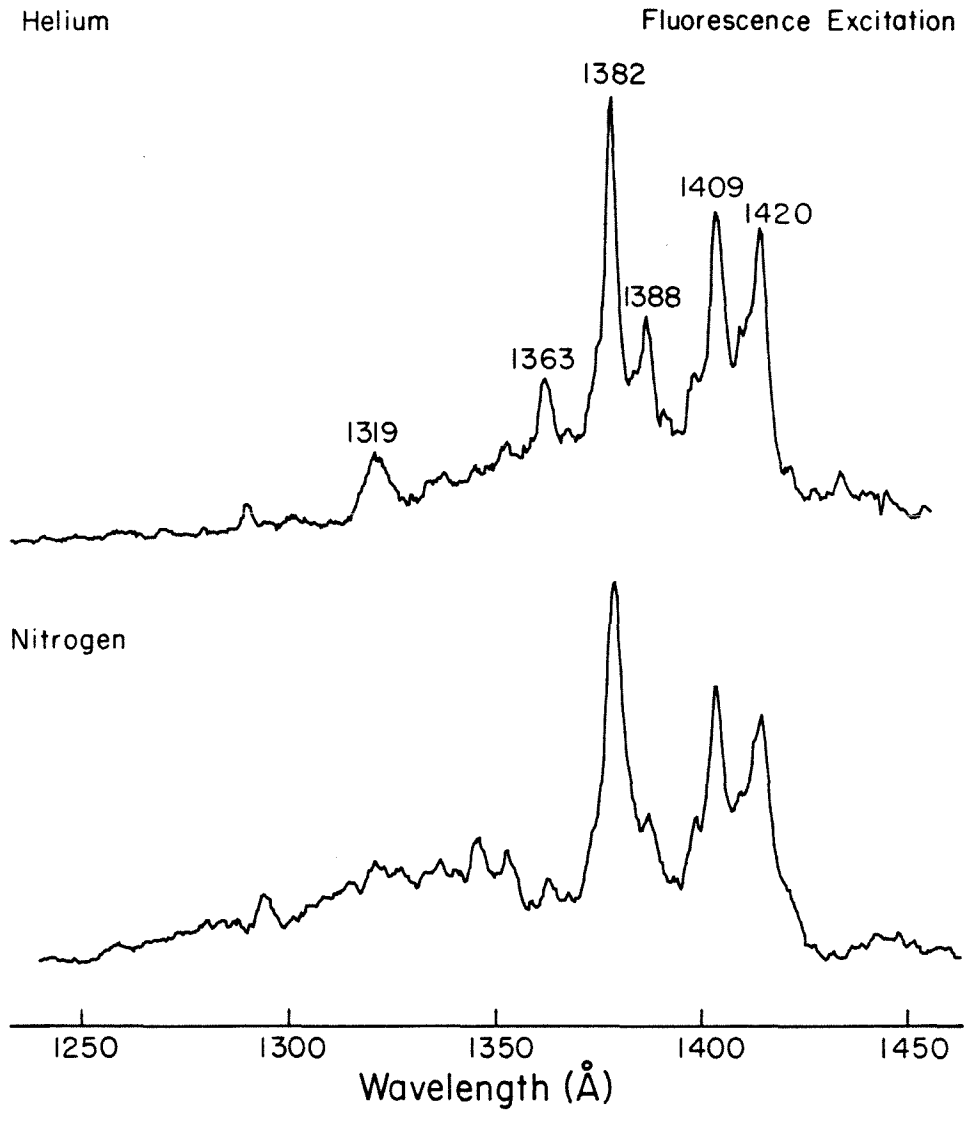

Figure 1.

Fluorescence excitation of anthracene in free jet expansions of helium and nitrogen ~1400 cm^{-1} above the S_1 origin. The resolution of the UV doubled, nitrogen pumped dye laser was 0.05 A°. The experimental conditions were, T_0 = 450 °K, P=45 psi, D=150 micron, and X=5 mm. Specific features of the fluorescence excitation spectra are further discussed in sections 3 (vibrational assignments) and 4.5 (vibrational temperature and vdW complex formation). The amplitudes have not been normalized to the laser power.

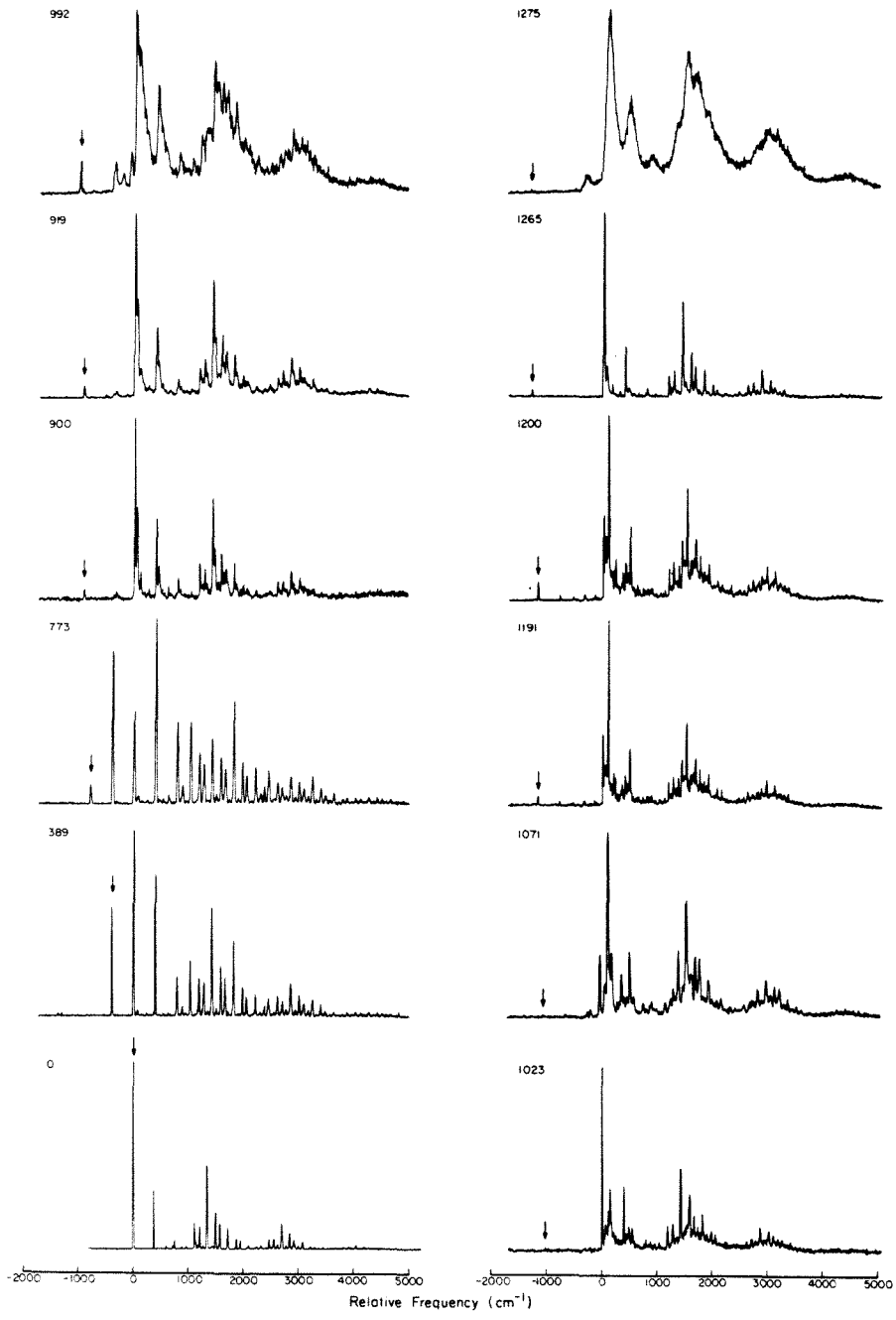

Figure 2.

Energy resolved fluorescence spectra for different excitation energy above the S_1 $^1B_{1u}$ singlet origin and the relative frequency with respect to the origin (3611.8 A°) is shown for each spectrum. The evolution from discreet to statistical level structure is exemplified. In the intermediate excess energy region (900 cm^{-1} - 1520 cm^{-1}) both relaxed and unrelaxed spectral components are observed, the relative contributions of which are dependent upon the specific optically prepared vibronic level. The following expansion conditions were used: T_0=450 °K, P=45 psi nitrogen, D=150 microns, X=5 mm.

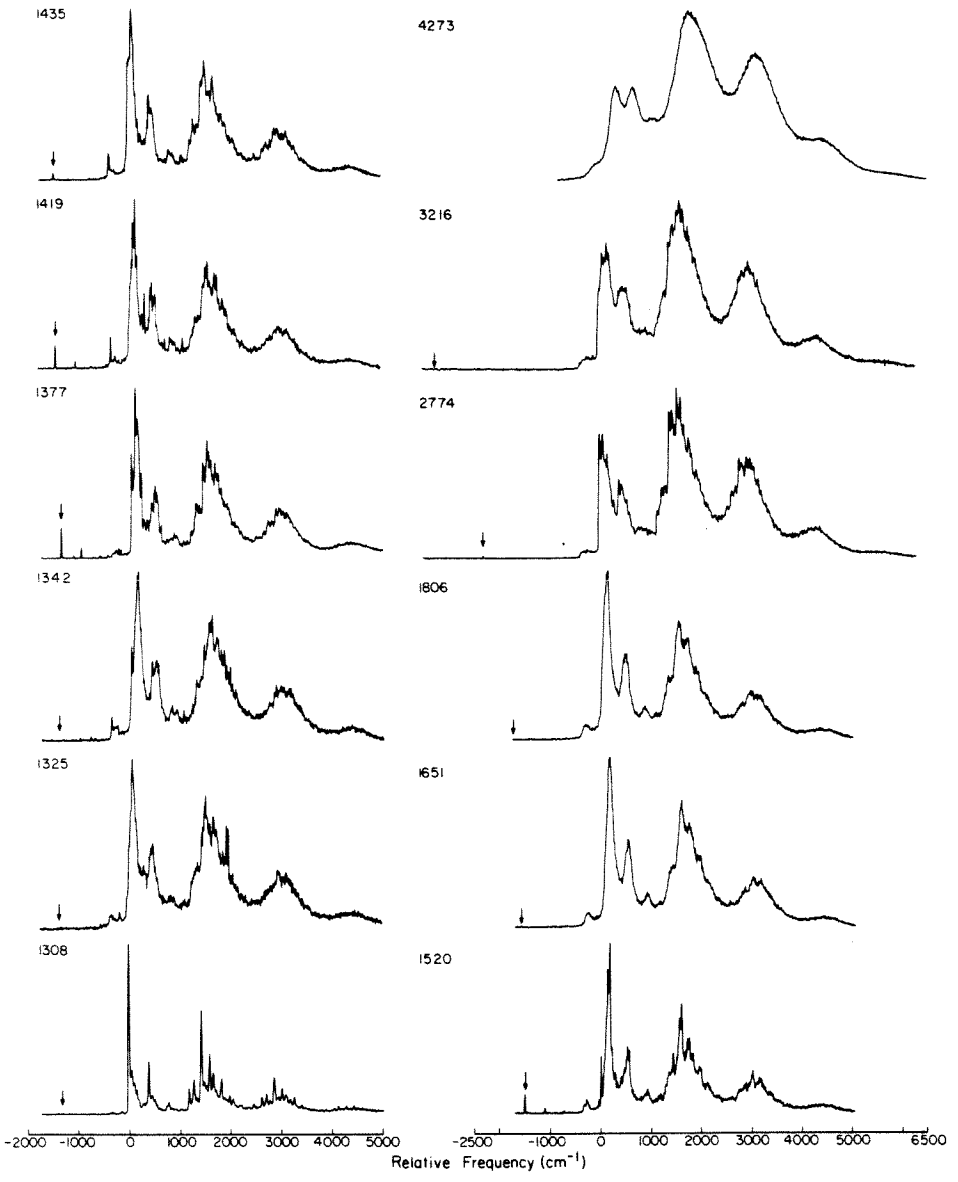

Figure 2, continued,

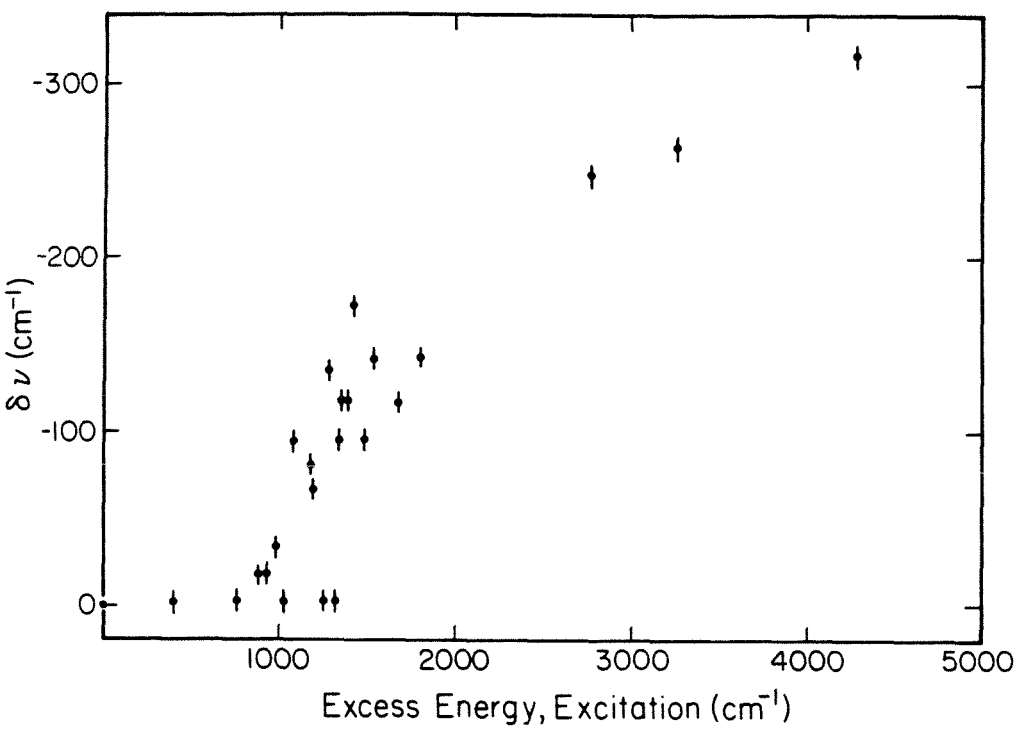

Figure 3.
The excess energy dependent red shift of the (1-1) transitions. The relative energy of the (1,1) transiton (peak exhibiting the largest amplitude) was determined from the spectra presented in figure 2. In the region between 900 cm^{-1} and 2000 cm^{-1}, the magnitude of the shift is observed to be erratic, corresponding to properties of intermediate level structure.

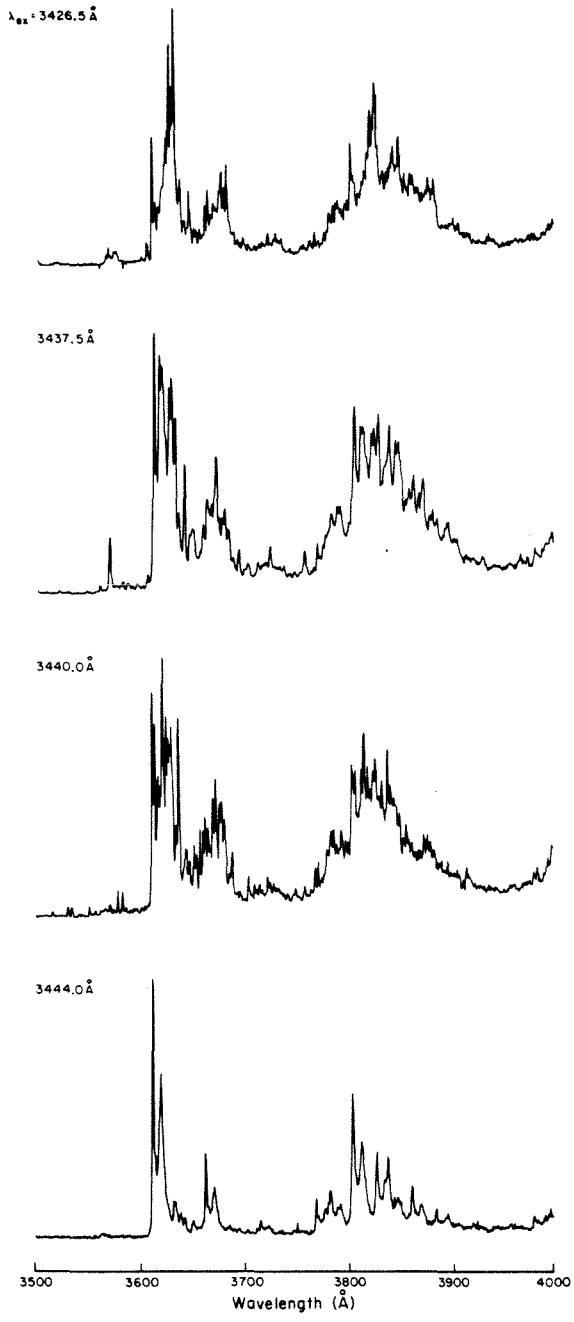

Figure 4.

An example of the dramatic dependence of the energy resolved fluorescence upon the optically prepared vibronic level. The excitation wavelengths are indicated in the figure and correspond to excess energies of approximately 1400 cm^{-1}. The large density of partially resolved spectral structure suggests that the apparent broadening is the consequence of congestion arising from the large number of optically allowed vibronic transitions.

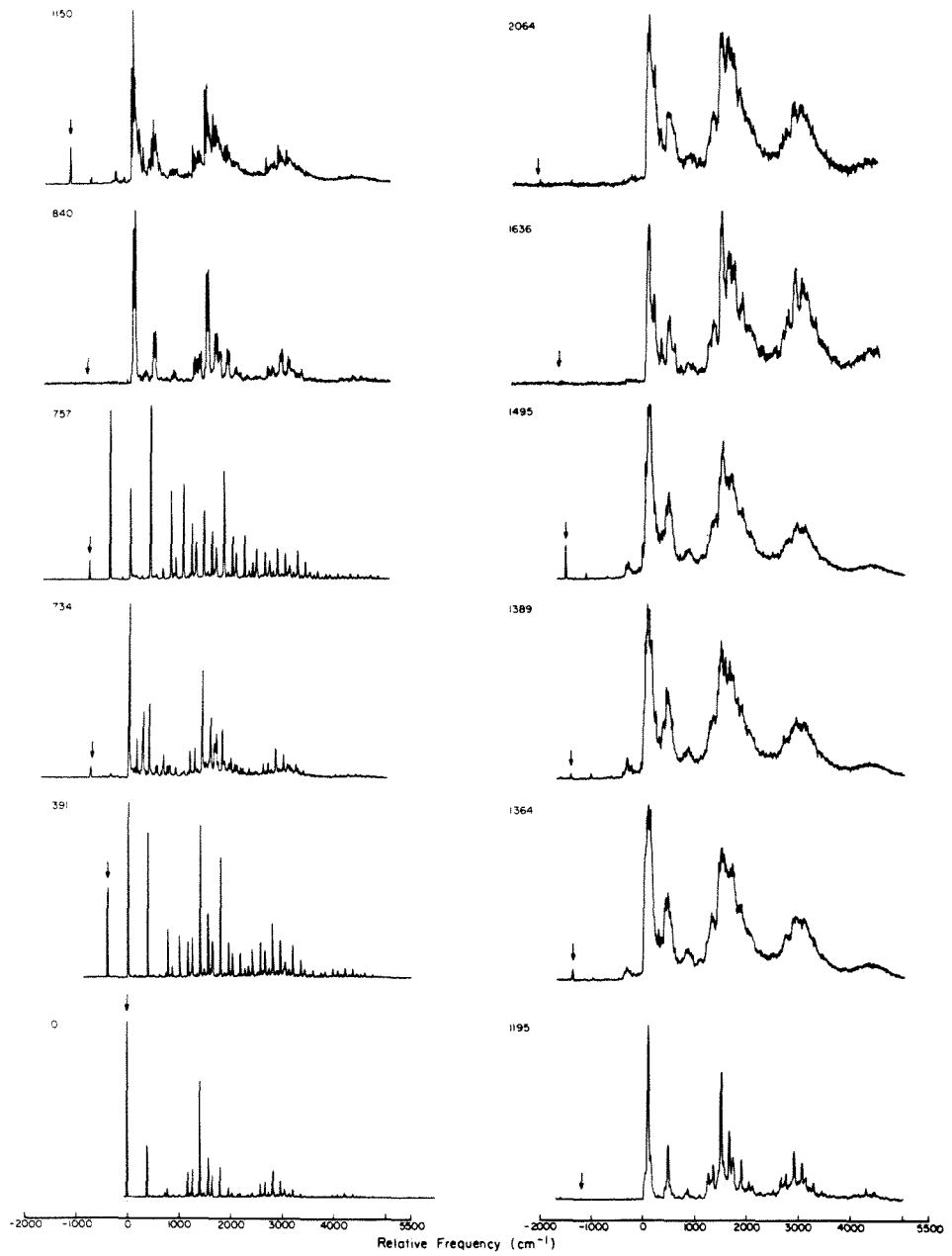

Figure 5.
Energy resolved fluorescence spectra for d_2-anthracene. The excess excitation energy above the S_1 origin and the relative frequency are indicated in the figure. The experimental conditions are the same as those given for figure 2.

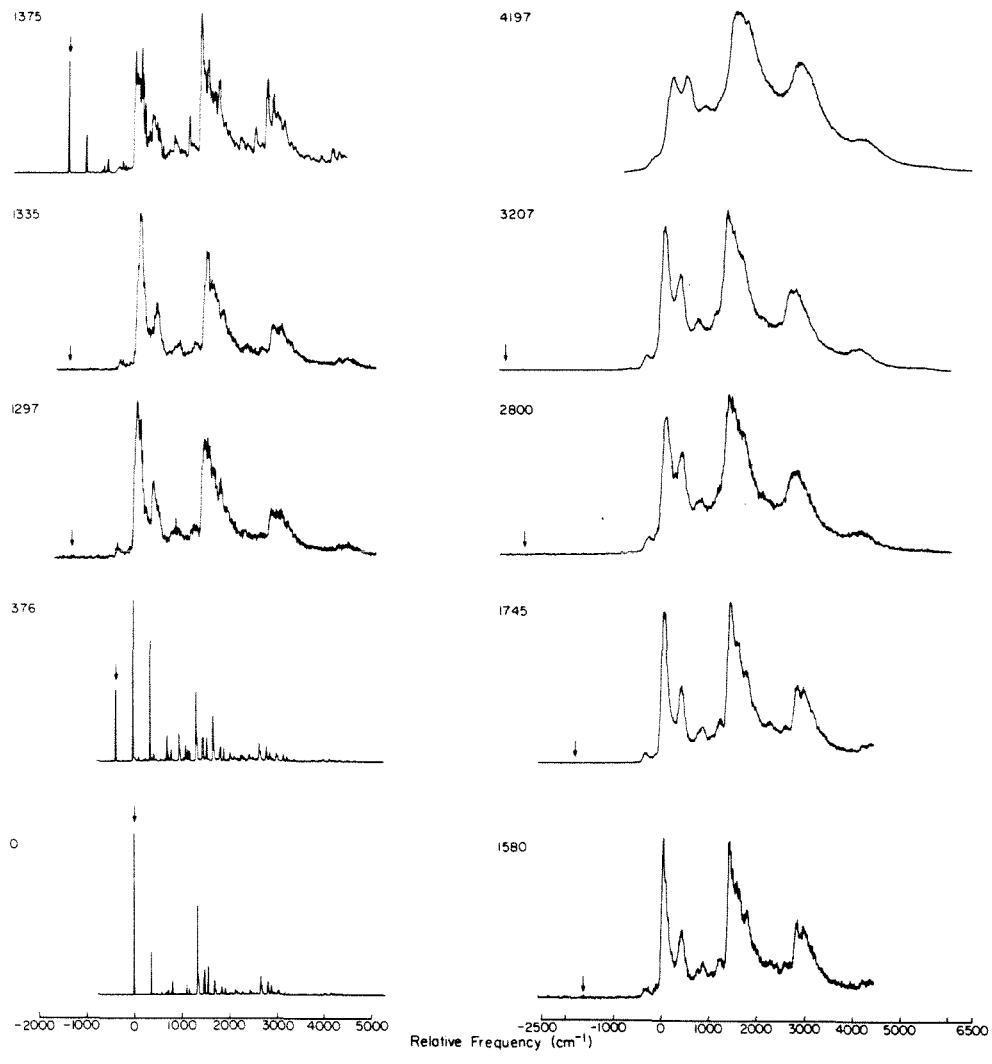

Figure 6.

Comparison of the energy resolved fluorescence spectra of anthracene for different carrier gases. Emission was detected with a resolution of 0.25 A° for excitation to 3611.8 A° with a bandwidth of 0.5 A°. The experimental conditions were: T_0=450 °K and D=150 microns. A slight broadening of the rotational contour is exhibited in the nitrogen expansion. There was no change in the observed profiles when the pressure was changed from 5 to 150 psi for a given carrier gas.

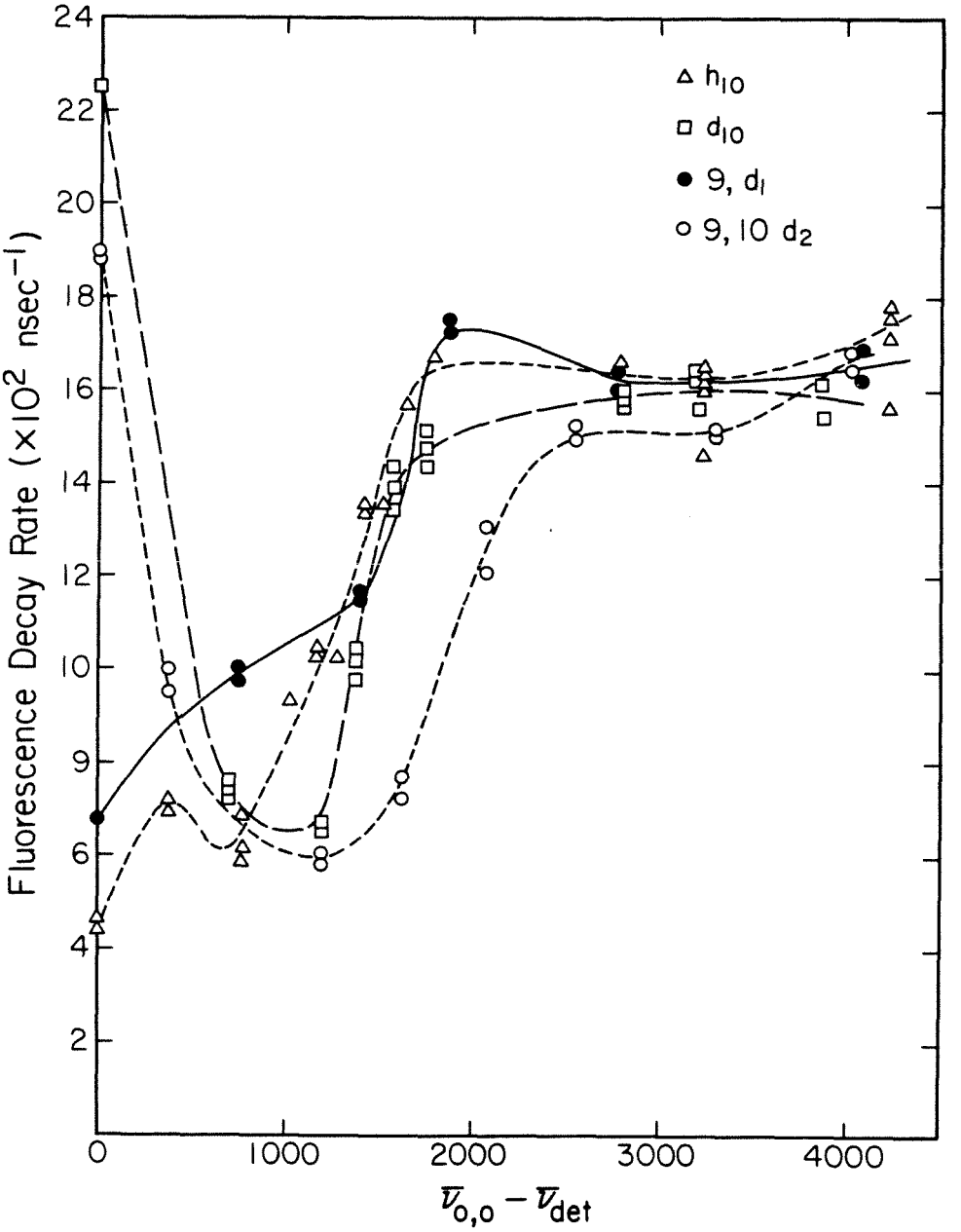

Figure 7.

Fluorescence decay rates for h_{10}-, 9,d_1-, 9,10 d_2- and d_{10}- anthracene as a function of the excess vibrational energy above the S_1 origin. Multiple points at a given excess vibrational energy correspond to measurements made for different transitions in the particular energy resolved fluorescence spectrum. The differences are therefore real and should not be interpreted as an indication of experimental error. The lifetimes of the S_1 origins are: h_{10}-, 23.5 ± 0.3 nsec; d_1- 14.8 ± 0.4 nsec; d_2-, 5.1 ± 0.4 nsec; d_{10}- 4.4 ± 0.2 nsec.

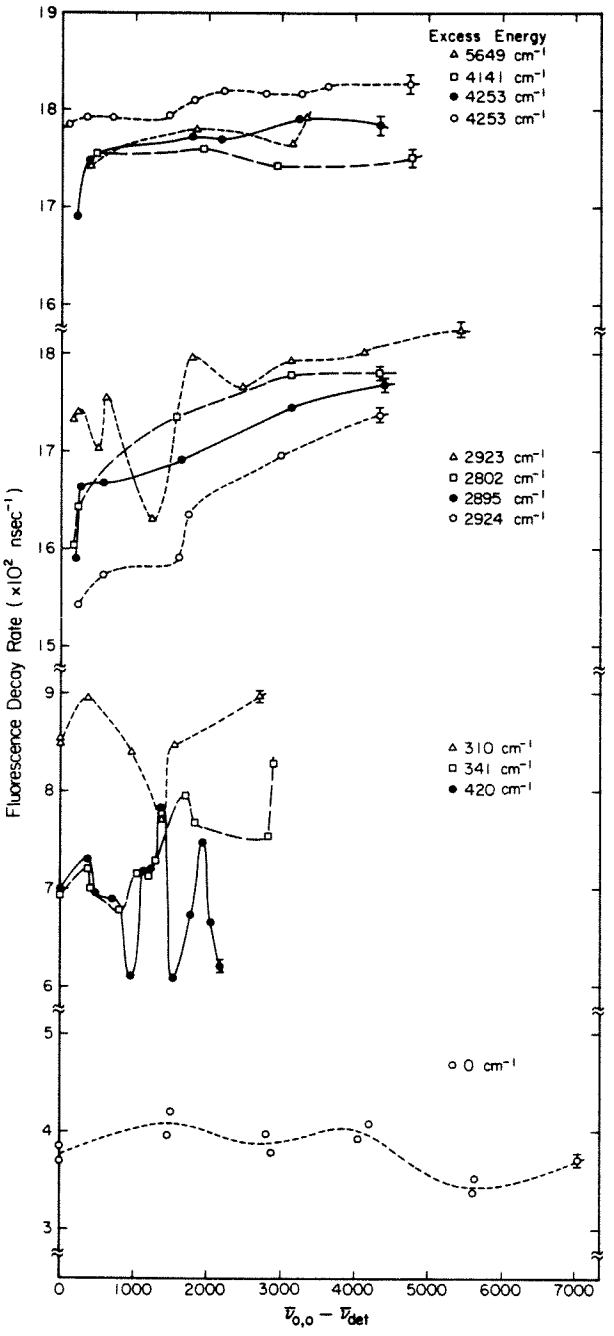

Figure 8.

Fluorescence relaxation rates of h_{10}-anthracene. The excitation energy relative to the S_1 $^1B_{2u}$ origin is indicated in the figure. For each excitation energy, the relaxation rate was measured for different transitions appearing in the energy resolved fluorescence spectrum. The relative energy above the 3611.8 A°, 0-0 transition is indicated along the abcissa. Differences in the decay rates which appear for identical excitation energies are attributed to slight changes in the expansion conditions. The experimental conditions were: T_0=450 °K, P=45 psi nitrogen, D=150 microns, X=5 mm.

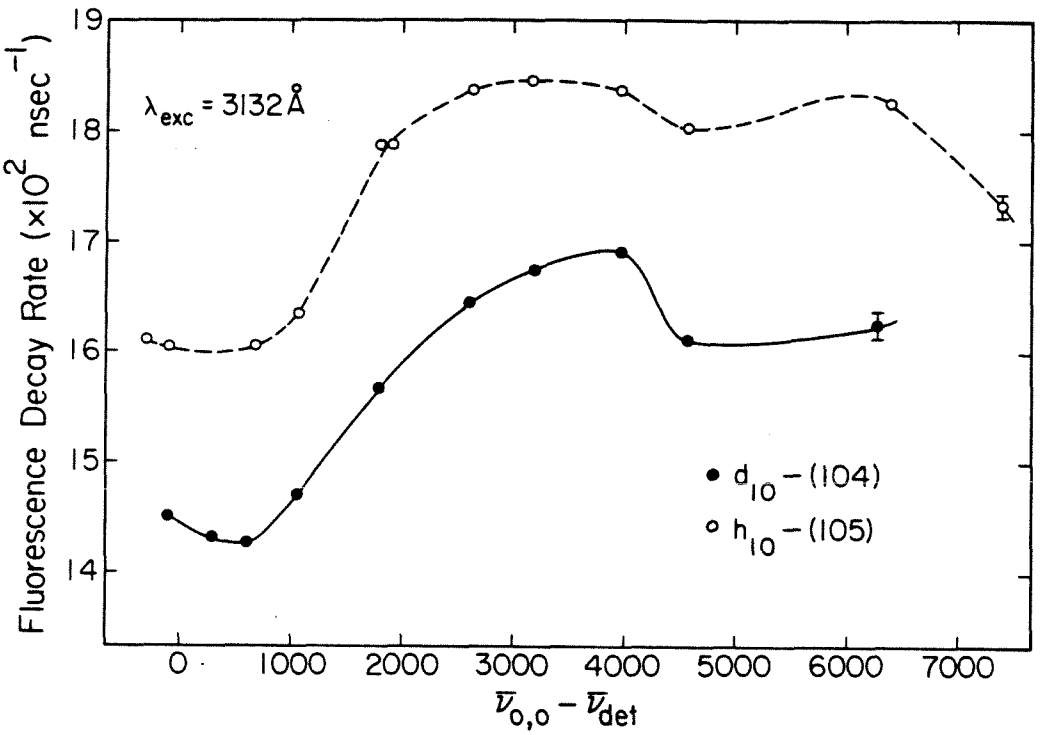

Figure 9.
The excess energy dependence of the fluorescence decay rates for h_{10}- and d_{10}-anthracene for excitation to 3132 A° (S_1+4241 cm^{-1}). The two isotopic species are seen to exhibit similar trends at this high excitation energy.

§4.9 *QUANTUM BEATS IN ANTHRACENE*

§4.9.1 *Energy Dependence of Quantum Beats*

The observation of quantum beats in the time resolved anthracene emission, as exemplified in figure 1 is by no means ubiquitous, and depends upon very specific excitation and detection conditions. Aside from the requisite temporal properties of the laser pulse and detection electronics (coherence width, pulse duration, system response time) which establish the observable beat freqencies, the spectral conditions for which quantum beats in anthracene were detected are well defined. Quantum beats were observed only upon excitation to 3439.6 ± 0.25 A° corresponding to 1380 ± 3 cm^{-1} above the S_1 $^1B_{2u}$ origin. The 1380 cm^{-1} mode is assigned as a b_{3g} C-C-H bending vibration (section 3). An example of the quantum beats observed in the energy resolved fluorescence of anthracene is presented in figure 1. The beat frequency indicates a separation between the interfering states of 488 ± 10 MHz (0.0162 ± 0.0003) cm^{-1}). For excitation to this excess energy, both the fluorescence excitation (figure 2) and the energy resolved fluorescence (figure 4) spectra are characterized by sharp and unresolved emission features commensurate with intermediate level structure. The sharp fluorescence excitation features appearing in the region around 1400 cm^{-1} of excess vibrational energy can be assigned to various fundamental and combination bands (section 3). In this region, the weakly optically allowed b_{1u}, b_{2u} and b_{3u} vibrations have considerable intensity thereby indicating the influence of vibronic coupling in this spectral region. The extent to which the broad absorption feature is associated with spectral congestion is difficult to access considering the low resolution (0.5 A°) with which the

spectra were acquired.

The underlying vibrational structure is more easily revealed in the energy resolved fluorescence upon excitation to the S_1 origin (figure 3). The broadening observed when nitrogen is used as the carrier gas (figure 3b) is attributed to rotational congestion and perhaps weak collisional relaxation (for a discussion refer to section 4.4). For excitation to low excess energies the energy resolved fluorescence is characterized by discrete transitions to ground state vibrations. Whereas there is little difference between the vibrational frequencies for the ground and excited state as is expected for aromatic molecules where there exists only a slight difference between the two potential surfaces, the Franck-Condon factors are substantially different. In the absorption spectrum, the 1382 cm^{-1} b_{3g} vibration was stronger than the a_g fundamental at 1409 cm^{-1} and the (395+1022) cm^{-1} combination band at 1420 cm^{-1}. The situation is reversed in the energy resolved fluorescence spectrum. Furthermore, several transitions appear in the fluorescence spectra, which were only observed in the absorption spectra as sidebands. Again many of these transitions are associated with b_{1u}, b_{2u} and b_{3u} fundamentals or various combination bands (section 3).

The energy resolved fluorescence spectrum of anthracene for excitation to 3439.6 A° shows characteristics of both relaxed and unrelaxed fluorescence. Transitions associated with the unrelaxed fluorescence component are built upon the (1,0) transition (0 cm^{-1}) and appear with frequencies characteristic of ground state vibrations. The transitions of the relaxed fluorescence component are built upon transitions appearing in the region of the (1,1) origin at 1400 cm^{-1}. In addition to these features, the anthracene spectrum obtained in a nitrogen expansion exhi-

bits collisionally relaxed transitions built upon the (0,0) S_1 origin. The first such transition appears at (27689.3 + 1382.6) cm^{-1} 3439.7 A° and the progressions of the 390 cm^{-1} and 1400 cm^{-1} vibrations are readily distinguished upon comparison with the spectrum obtained for a helium expansion. Collisionally relaxed transitions are not observed in the corresponding fluorescence excitation spectra (figure 2). The region around 1500 cm^{-1} in figure 4a is complicated and reveals interesting properties as the result of vibronic coupling. The normally weak fundamentals of b_{2u} and b_{1u} symmetry (b_{2u}, 1402 cm^{-1}, b_{1u} 1427 cm^{-1}, b_{2u} 1459 cm^{-1} and b_{2u} 1534 cm^{-1}) reflect a large intensity and show strong progressions of the 237 cm^{-1} and 388 cm^{-1} vibrations. This is especially true for the dominant 1459 cm^{-1} b_{2u} mode. The combination bands of the 390 cm^{-1} vibration which appear at 1503 cm^{-1}, 1512 cm^{-1} and 1527 cm^{-1} also exhibit anomalously large intensities compared to analogous transitions for excitation to the S_1 origin. An explanation (1) for the multiple origins of the relaxed fluorescence component which appear upon excitation to intermediate excess energies would be to consider the redistribution of low energy (< 100 cm^{-1}) vibrational quanta to produce a new wavefunction, $|e,n_a,0> \rightarrow |e,n_a',n_b'>$. The new wavefunction no longer contains a quanta of the initially optically prepared vibrational mode, and is radiatively coupled directly to the corresponding vibronic ground state level, $|e,n_a',n_b'> \rightarrow |g,n_a',n_b'>$. For the specific case of anthracene, the loss of a vibrational quanta with energy less than 100 cm^{-1} does not correspond to a known vibration. The lowest frequency in-plane mode is at 237 cm^{-1} (2) and the lowest frequency out-of-plane mode appears at 106 cm^{-1} (3). Higher resolution of the energy resolved fluorescence spectra obtained for excitation to transitions in the region around 1400 cm^{-1} of excess

vibrational energy should provide interesting results regarding mode specific vibronic coupling in anthracene.

Energy resolved fluorescence spectra for S_1+1380 cm^{-1} excitation are presented in figure 4 and the transition frequencies and assignments are presented in table 1. With reference to table 1, the assignments for the ground state vibrations associated with quantum beats are : *a*) 0 cm^{-1} resonance fluorescence; *b*) 390 cm^{-1}, a_g fundamental; *c*) 1125 cm^{-1}, b_{2u} fundamental; d) 1518 cm^{-1}, (1125+390) cm^{-1} combination band; e) 1910 cm^{-1}, (1125+2×390) cm^{-1} combination band; and f) 2292 cm^{-1}, (1125+3×390) cm^{-1} combination band. These assignments reflect the fact that quantum beats are only associated with the unrelaxed fluorescence component. The unrelaxed fluorescence is built upon the (0,1) transition and is interspersed with relaxed features above ~1380 cm^{-1}. The richness of the energy resolved fluorescence spectra for S_1+1380 cm^{-1} excitation would indicate that any apparent broadening would be a consequence of spectral congestion and unresolved structure. In addition, the spectrum obtained with nitrogen as a carrier gas exhibits collisionally relaxed features, in particular at 1383 cm^{-1}. The nature of the collisional relaxation is discussed in section 4.4. The assignments for the unrelaxed fluorescence features are also indicated in table 1. The 390 cm^{-1} and 1125 cm^{-1} vibrations are described by CC-CCC (breathing-quinoidal), and CC-CCH (quinoidal) motions, respectively (2). Quinoidal motion indicates relative compression and extension of adjacent C-C bonds. The similar motional characteristics of the two vibrations provide a strong coupling mechanism and thus helps to explain the persistence of the (1125+n×390) cm^{-1} progression. These vibrations are unique in anthracence in that they are the only low energy modes (below 1550 cm^{-1}) which exhibit

predominantly quinoidal motion (2). This unique vibrational character, since it would tend to inhibit anharmonic coupling with other vibrations, undoubtedly contributes to the fact that quantum beats at these energies are predominantly associated with fluorescence for the (1125+n×390) cm^{-1} progression. In addition, the dipole matrix elements for unique vibrational symmetries would tend to be well defined with respect to that for other molecular vibrations.

In view of the spectral congestion, the assignment of the 1125 cm^{-1} transition as a b_{2u} fundamental might seem ambiguous. Several transitions can appear in this region including the b_{3g} 1112 cm^{-1}, b_{2u} 1125 cm^{-1}, and b_{1u} 1138 cm^{-1} fundamentals and the (390+745) cm^{-1} a_g combination band. The assignment of the 1125 cm^{-1} transition was based upon the following criteria: 1) the observed ground state vibrational frequencies are in excellent agreement with those determined from force field calculations (section 3), 2) the intensity of the 1125 cm^{-1} transition is larger than can be explained on the basis of an a_g (390+745) cm^{-1} combination band, 3) weak transitions approximately 10 cm^{-1} to either side of the 1125 cm^{-1} peak are consistent with the vibrational frequencies for the b_{3g} 1112 cm^{-1} and b_{1u} 1138 cm^{-1} fundamentals, and, 4) although the large oscillator stength implied by the amplitude of the 1125 cm^{-1} transition is unusual for a b_{2u} fundamental, it is preceded by the appearance of the b_{1u}, 239 cm^{-1} transition. One would anticipate that the 239 cm^{-1} and 1125 cm^{-1} modes are related, if not by symmetry, perhaps by similar vibrational motions.

A distinctive feature of the energy resolved fluorescence spectrum for S_1+1380 cm^{-1} excitation is the appearance of a transition at 236.8 ± 3.0 cm^{-1}. This transition was not observed for any other excitation energy

(see figure 2, section 4.8) although it is observed in the fluorescence excitation spectrum (see figure 3, section 3.3). The 237 cm^{-1} mode has been designated on the basis of force field calculations to be a b_{1u} fundamental (2). This b_{1u} mode is the lowest frequency planar vibration in anthracene. This vibration involves both C-C and C-C-C angular bending deformations characterized as an in-phase bending motion of the molecule along the long molecular axis. The frequency of this particular b_{1u} vibration exhibits a substantial dependence upon the molecular length (2), being 360, 239, 163, and 119 cm^{-1} for naphthalene to pentacene, respectively. This behavior can be understood by analogy with the bending vibrations of elastic rods where, since the vibration corresponding to this b_{1u} mode does not possess an axial mode, the frequency decreases as the length of the vibrating body increases (4). For this type of vibration one does not expect large anharmonicity due to H-H repulsive forces, since, in this case these forces are produced from symmetric terms in the potential function. Nevertheless, it is reasonable to presume that a substantial b_{1u} excited state vibrational character is generated from anharmonic coupling with the strongly optically allowed a_g 1380 cm^{-1} fundamental. Before considering the association of the b_{1u} 237 cm^{-1} vibration with quantum beats, it is important to discuss the energies in the resolved fluorescence at which quantum beats are observed.

The energies (relative to S_0) at which quantum beats were observed in the resolved fluorescence for excitation to S_1+1380 cm^{-1} are indicated in figure 4. Recall that oscillatory terms in the fluorescence originate from well defined coherently prepared eigenstates in the excited state manifold which radiate to a common ground state. The characteristics of the energy resolved fluorescence spectrum therefore reflect the projec-

tion, by means of the radiative dipole matrix elements, of the excited molecular eigenstates to the ground state manifold. Quantum beats are observed for the resonance fluorescence, and discrete spectral features appearing at 387, 1125, 1515, 1908, and 2292 cm^{-1}. Higher resolution energy resolved fluorescence spectra for these transitions as well as examples of the time resolved decays are presented in figure 5.

An essential aspect of these experiments which enabled the observation of quantum beats was the resolution of the fluorescence. Within the detection bandwidth, a group of eigenstates could be selected which are radiatively coupled to the coherently prepared set of eigenstates in the S_1 manifold. In this manner, radiation originating from interfering states could be selected and distinguished from the non-interfering eigenstates. The distinction between interfering (producing quantum interference effects) and non-interfering eigenstates is to be considered a working definition in terms of our experimental conditions. It is certainly plausible that quantum interference exists between several, if not all eigenstates, thereby engendering quantum beats at many emission energies. However, the temporal properties of the laser pulse and the detection system, and the limited spectral resolution establish practical limitations. The 250 psec response of our photon counting system determines the maximum observable beat frequency. The destructive interference of multiple oscillatory terms on the time scale of the experiment will lead to an effective single exponential fluorescence decay. Therefore, in order to reduce this incoherent contribution, spectral resolution is indicated and can only be successful if primarily the oscillatory fluorescence component can be selected. In view of the small number of transitions which exhibit quantum beats in anthracene (figure 4), one would not expect to

observe quantum beats in the total fluorescence, as is indeed the case. As a final point, a largely semantic controversy (1,5,6) exists in the literature regarding the degree of resolution required to observe quantum beats in large molecules. Our experiments clearly exemplify that resolution, as used here, is a relative concept. It is of course necessary to employ a detection bandwidth which is greater than the energy separation between the, nominally, two interfering eigenstates. However, depending upon the number of eigenstates prepared and the dipole matrix elements which define the fluorescence, one must to some degree discriminate non-oscillatory components (on the experimental time scale). Whereas in the experiments performed on the aza-aromatics and dicarbonyls where relatively few eigenstates are prepared such that quantum beats can be observed in the total fluorescence (7), in our case, the large number of eigenstates prepared in anthracene prohibits the observation of quantum beats in the spectrally integrated emission.

The contribution of non-oscillatory emission components wtihin the detection bandwidth is indicated by the beat modulation depth for the various transitions. The quantum beat patterns shown in figure 5 vary with respect to the relative magnitude of the oscillatory component. This result is interpreted as being due to the relative contributions of non-oscillatory fluorescence components. In order to distinguish quantum beats for the transitions embedded within the spectrally congested region of the relaxed fluorescence, (1515 cm^{-1}, 1908 cm^{-1} and 2292 cm^{-1}) it was necessary to reduce the detection bandwidth to 0.25 A° as compared to 1.0 A° for the other transitions. The beat frequencies for all transitions were identical within experimental error. The common beat frequency suggests that the same set of eigenstates is responsible for the

quantum interference effects and supports the contention that the interference effects arise from excited state energy splittings.

In order to assess the importance of vibrational structure on the appearance of quantum beats in anthracene, the deuterated species, 9 d_1-; 9,10 d_2- and d_{10}- anthracene were investigated. Quantum beats were not observed for d_{10}- and 9,10 d_2-anthracene despite the near identity of the vibrational frequencies to those of h_{10}-anthracene (section 3). Although we conclude that beats were not observed for d_1- anthracene, an important observation should be noted. During a single experimental run, quantum beats were observed in the total integrated fluorescence of d_1-anthracene for excitation to transitions appearing in the hotband region to the red of the S_1 origin and the S_1+390 cm^{-1} fundamental. The beat frequency was approximately 895 MHz. Although the quantum beats observed for d_1-anthracene were reproducible during that particular experimental run, the phenomena could not be reproduced on subsequent days. Since the beats appeared for excitation to a vibrational hotband or a nitrogen-d_1-anthracene complex, we attribute our failure to reproduce the results as a consequence of the sensitivity to free jet cooling conditions.

Despite the overall similarity of the energy resolved fluorescence for d_{10}- and h_{10}-anthracene upon excitation to S_1+1380 cm^{-1} (figure 6), neither quantum beats nor the 237 cm^{-1} vibration were observed for d_{10}-anthracene. Complete deuteration significantly alters the vibrational frequencies of anthracene (see section 3) such that one would not expect to observe the same vibrational coincidences. For example, upon deuteration the 239 cm^{-1} and 394 cm^{-1} modes have freqencies of 222 cm^{-1} and 380 cm^{-1}. Although the association of the 237 cm^{-1} vibration with the

appearance of quantum beats is at present circumstantial, it does suggest the presence of specific vibrational or vibronic interactions. Although it it possible to envision laser excitation to a number of vibrational states exhibiting unique symmetries and couplings, and which gain substantial oscillator strength through anharmonic interaction with the optically allowed 1380 cm^{-1} b_{3g} vibration, the explanation appears to be more subtle than the generation of combination bands from in-plane fundamentals. Furthermore, no out-of-plane vibrations have been observed at 239 cm^{-1} (3) nor could an out-of-plane vibration be expected to exhibit optical activity.

The determination of the nature of the vibronic states which are excited within the laser bandwidth at S_1+1310 cm^{-1} will require high resolution spectroscopy. Schlag et al. (8) have performed two photon spectroscopy on benzene in which spectral features on the order of 80 MHz have been resolved at excess energies of 1343 cm^{-1}. Application of similar techniques to anthracene free jet expansion should provide valuable information regarding the excited state level structure. In light of our results, one could expect to observe the effects of subtle anharmonic interactions.

REFERENCES

1. K.F. Freed and A. Nitzan, J. Chem. Phys., **73,** 4765 (1980).

2. K. Ohno, J. Mol. Spectrosc. **77,** 329 (1979).

3. G. Neerland, B.N. Cyvin, J. Brunvoll, S.J. Cyvin and P. Klaeboe, Z. Naturforsch., **35a,** 1390 (1980).

4. I.G. Main, *Vibrations and Waves in Physics*, Cambridge Univ. Press, New York, 1978.

5. W. Rhodes, J. Chem. Phys., **86,** 2657 (1982).

6. K. Lendi, Chem. Phys., **46,** 179 (1980).

7. For example, P.M. Felker, W.R. Lambert and A.H. Zewail, Chem. Phys. Lett., **89,** 309 (1982); J. Chaiken, M. Gurnick and J.D. McDonald, J. Chem. Phys., **74,** 106 (1981).

8. E. Riedle, H.J. Neusser and E.W. Schlag, J. Chem. Phys., **75,** 4231 (1981).

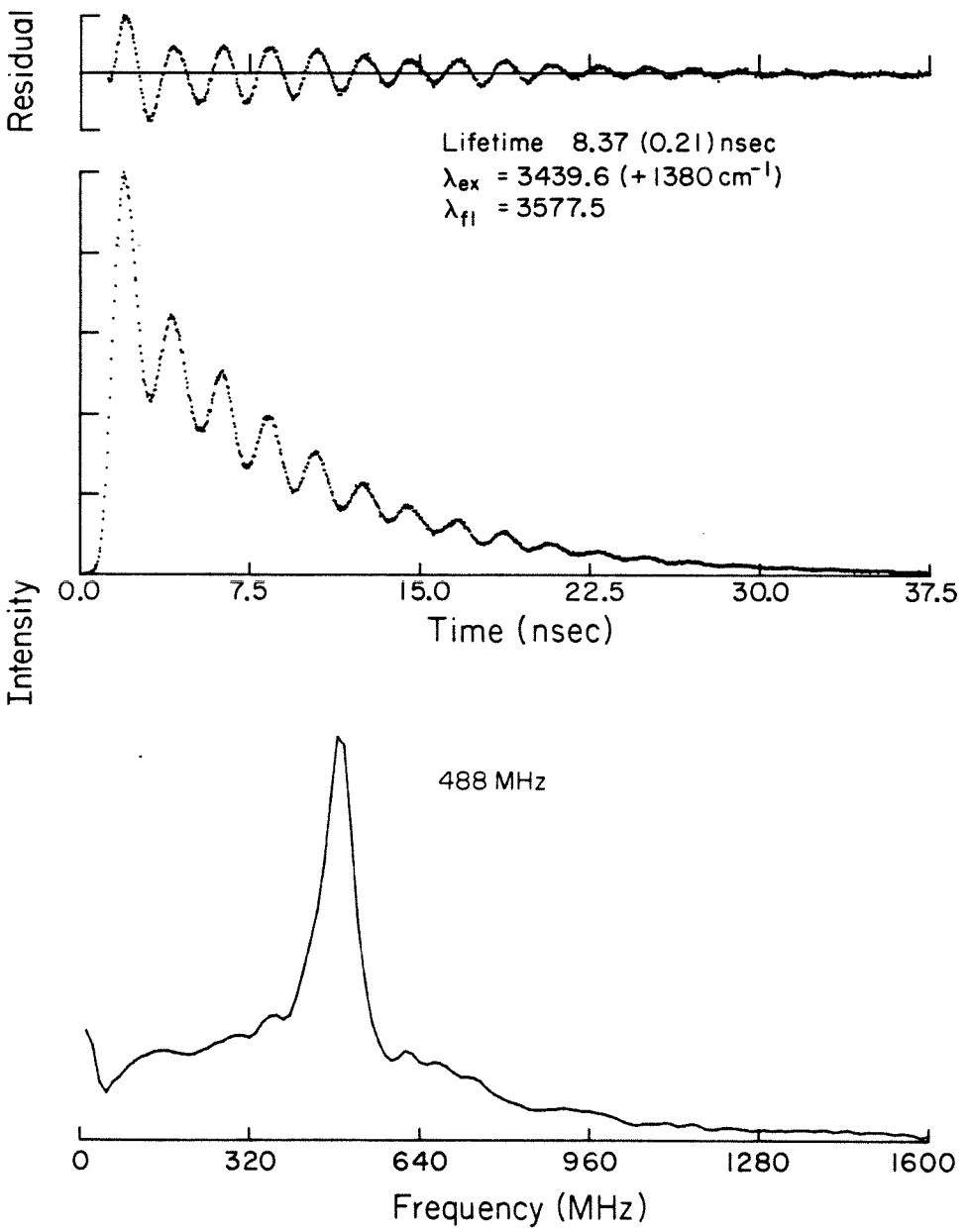

Figure 1.

Quantum beats in anthracene. The modulated fluorescence decay was obtained for λ_{ex}=3439.6 ± 0.3 A° (S_1+1380 cm^{-1}) and λ_{det}=3577.5 A°. The fluorescence lifetime obtained from the best fit to a single exponential is 8.4 nsec. The beat frequency is 488 ± 10 MHz. The excitation bandwidth was 0.5 A. The laser coherence width was 3 cm^{-1}. The residual obtained by subtracting the best single exponential fit from the modulated decay is presented along with the Fourier transform of the residual. The FWHM of the Lorentzian fit to the Fourier transform peak is 71 MHz. The expansion conditions were: T_0=450 °K, D=150 microns and X=5 mm.

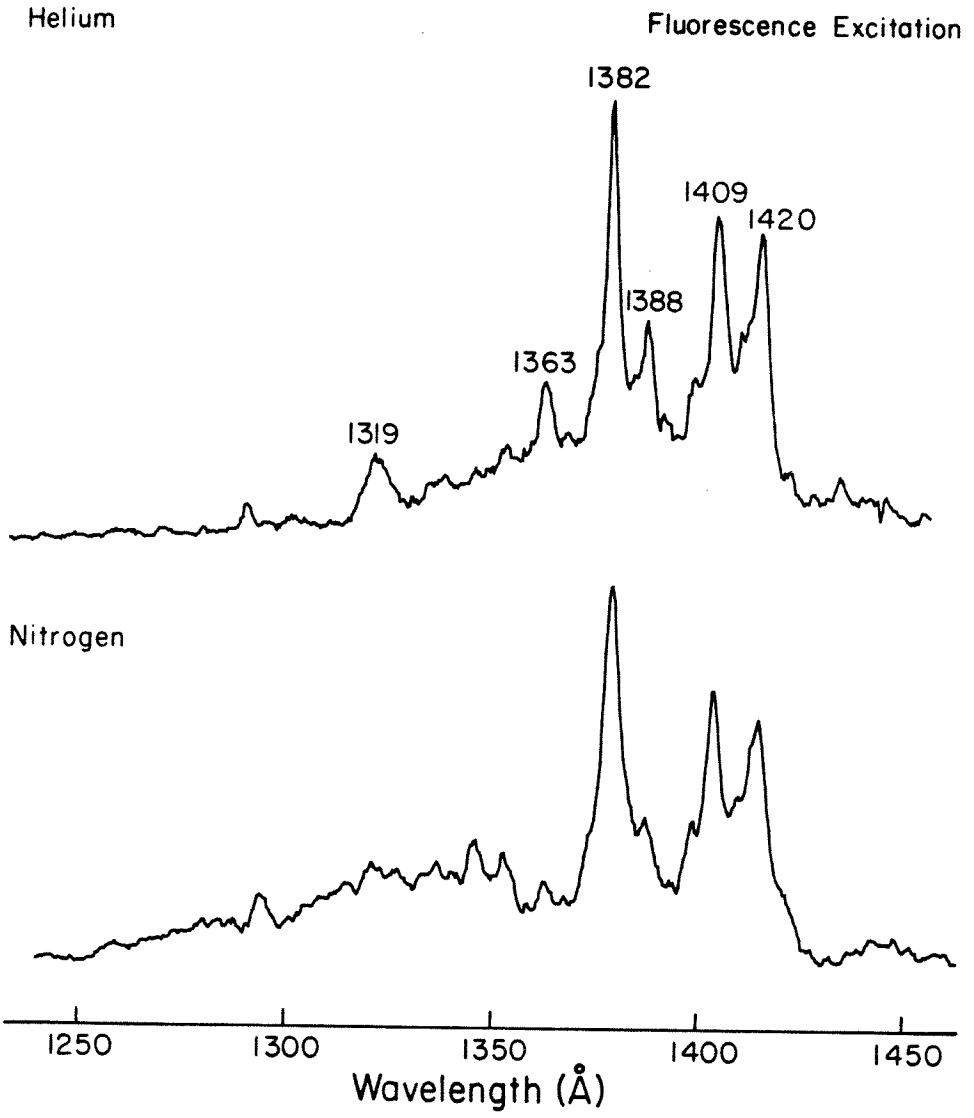

Figure 2.
The fluorescence excitation spectra of anthracene in the region of $S_1 + 1380\ cm^{-1}$. Spectra are presented for helium and nitrogen expansions and show the complicated level structure and unresolved background. The resolution was $0.3\ cm^{-1}$.

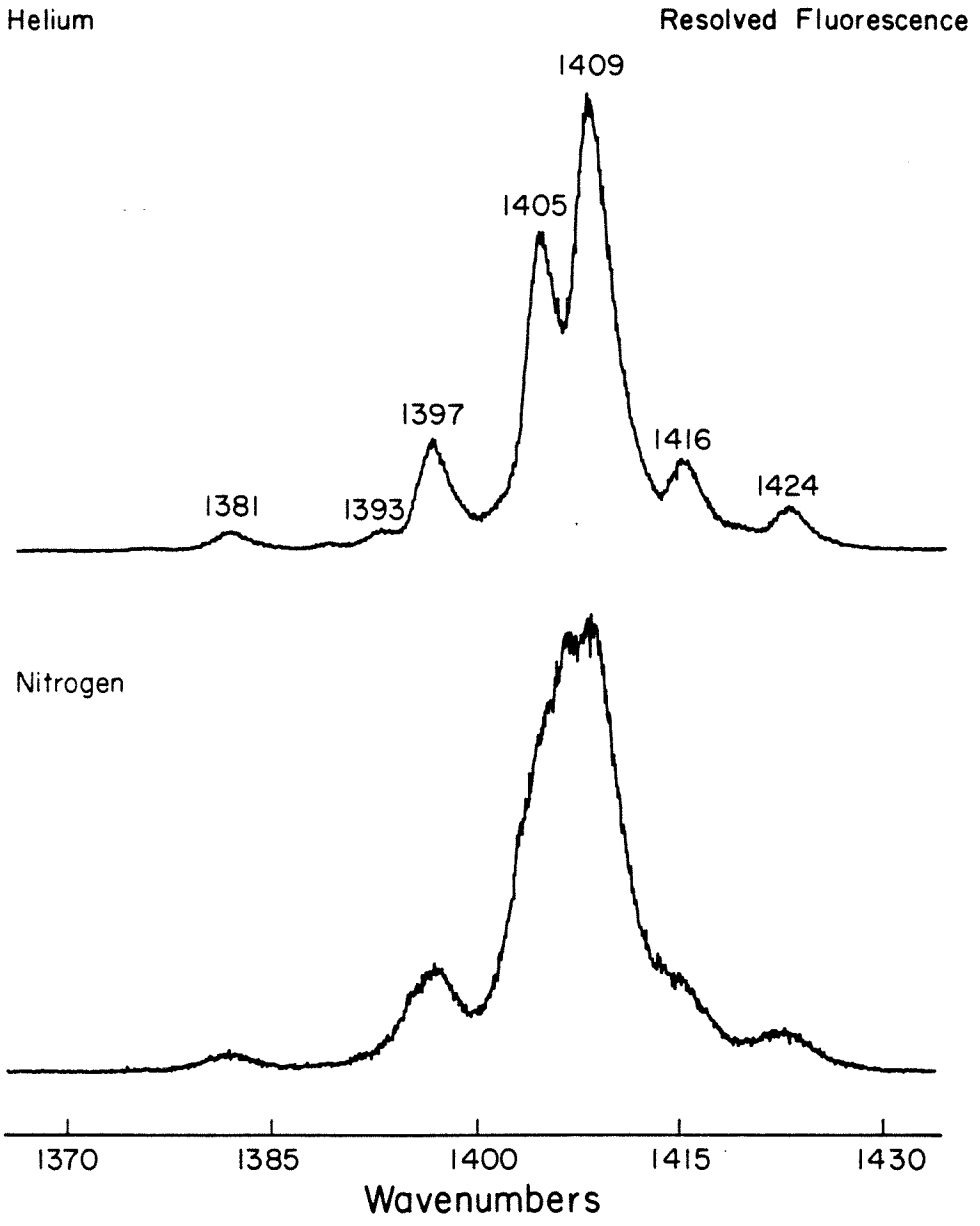

Figure 3

A portion of the energy resolved fluorescence spectra of anthracene for excitation to the S_1 origin. The 0.3 A° resolution spectra in the region of the 1400 cm^{-1} transition shows the large number of vibronic levels which exhibit far different Franck-Condon factors than appear in the fluorescence excitation spectra shown in figure 2. The 1380 cm^{-1} transition is expanded in the insert. The spectrum obtained for a nitrogen expansion exhibits either rotational or collisional broadening.

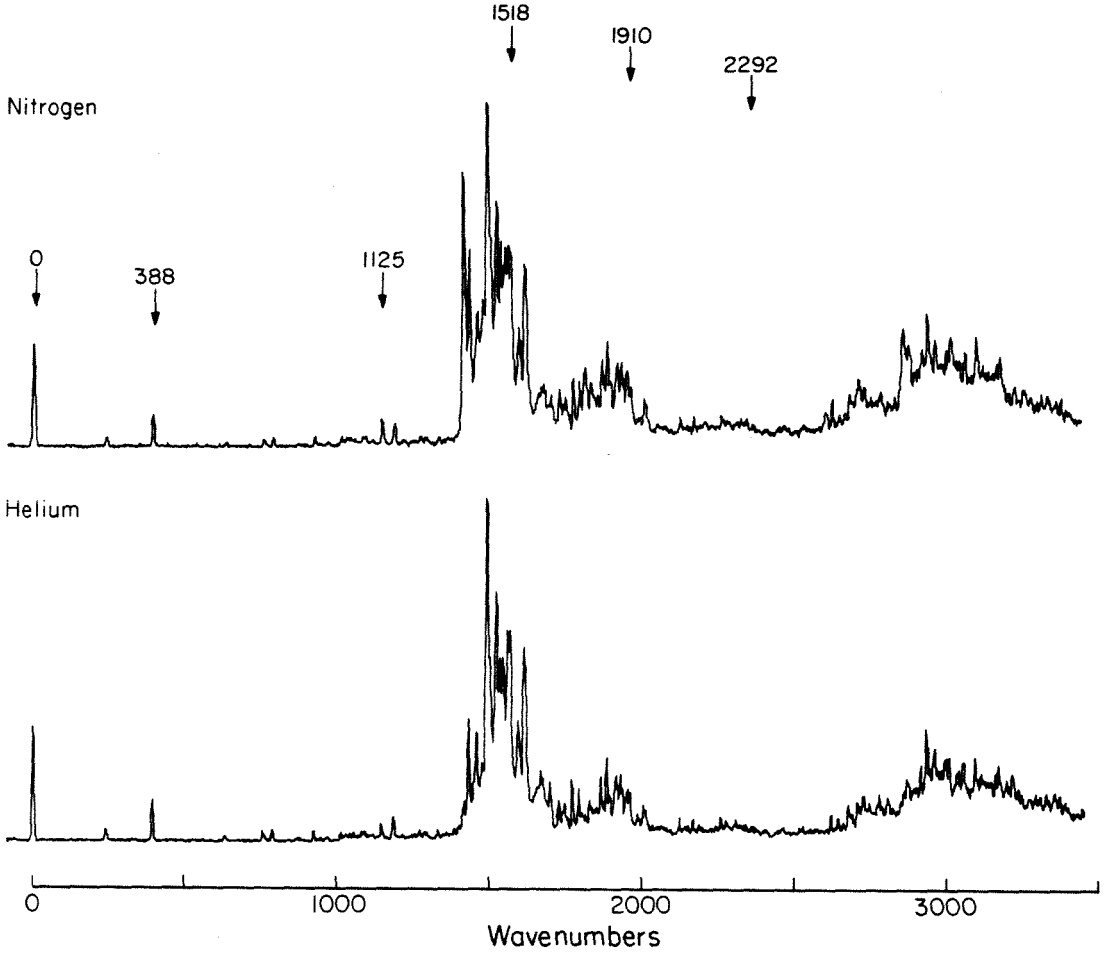

Figure 4.

The energy resolved fluorescence spectrum of anthracene for λ_{ex}=3439.6 A° (S_1+1380 cm^{-1}). The transitions for which quantum beats were observed in the time resolved fluorescence are indicated by arrows. The spectral features associated with the unrelaxed and relaxed fluorescence components are discussed in the text. Collisionally relaxed transitions are observed for the spectra obtained for a nitrogen expansion. The resolution was 0.3 A°. The assignments for the transitions are tabulated in table 2. The expansion conditions were: $T_{0=}$450 °K, P_0= 45 psi nitrogen, D= 150 microns, X= 5 mm.

Figure 5.

The high resolution (0.3 A°) energy resolved fluorescence spectra of the transitions which exhibit quantum beats and the corresponding time resolved fluorescence decays. The transitions refer to those indicated in figure 4. The exact detection wavelength (0.5 A° bandwidth) is indicated by an arrow. The residuals of the time resolved spectra are normalized by the reciprocal of the number of counts so as to accentuate the oscillatory behavior. The experimental conditions are the same as those indicated for figure 4.

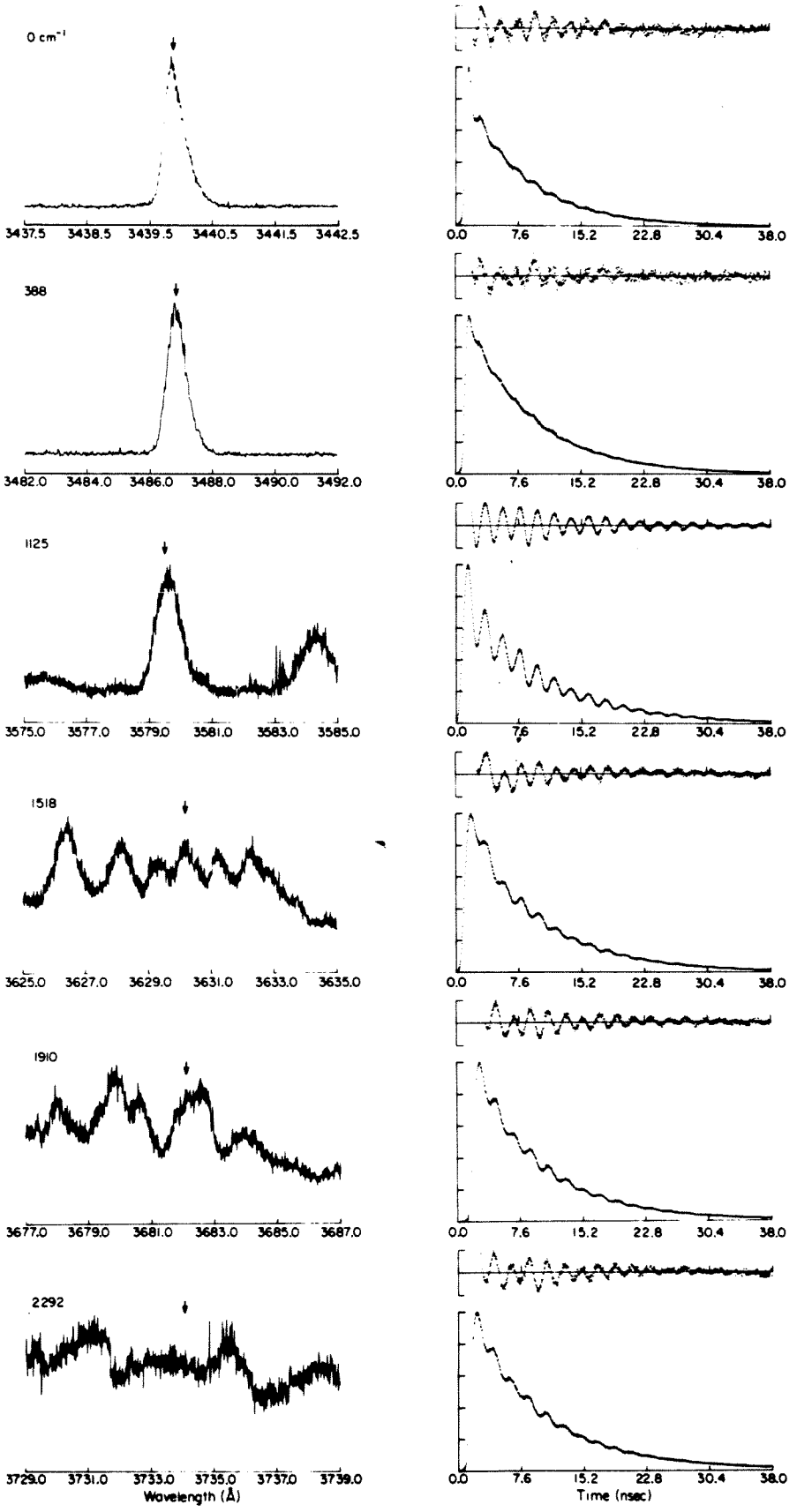
0 cm⁻¹
3437.5 3438.5 3439.5 3440.5 3441.5 3442.5
388
3482.0 3484.0 3486.0 3488.0 3490.0 3492.0
1125
3575.0 3577.0 3579.0 3581.0 3583.0 3585.0
1518
3625.0 3627.0 3629.0 3631.0 3633.0 3635.0
1910
3677.0 3679.0 3681.0 3683.0 3685.0 3687.0
2292
3729.0 3731.0 3733.0 3735.0 3737.0 3739.0
Wavelength (Å)
0.0 7.6 15.2 22.8 30.4 38.0
Time (nsec)

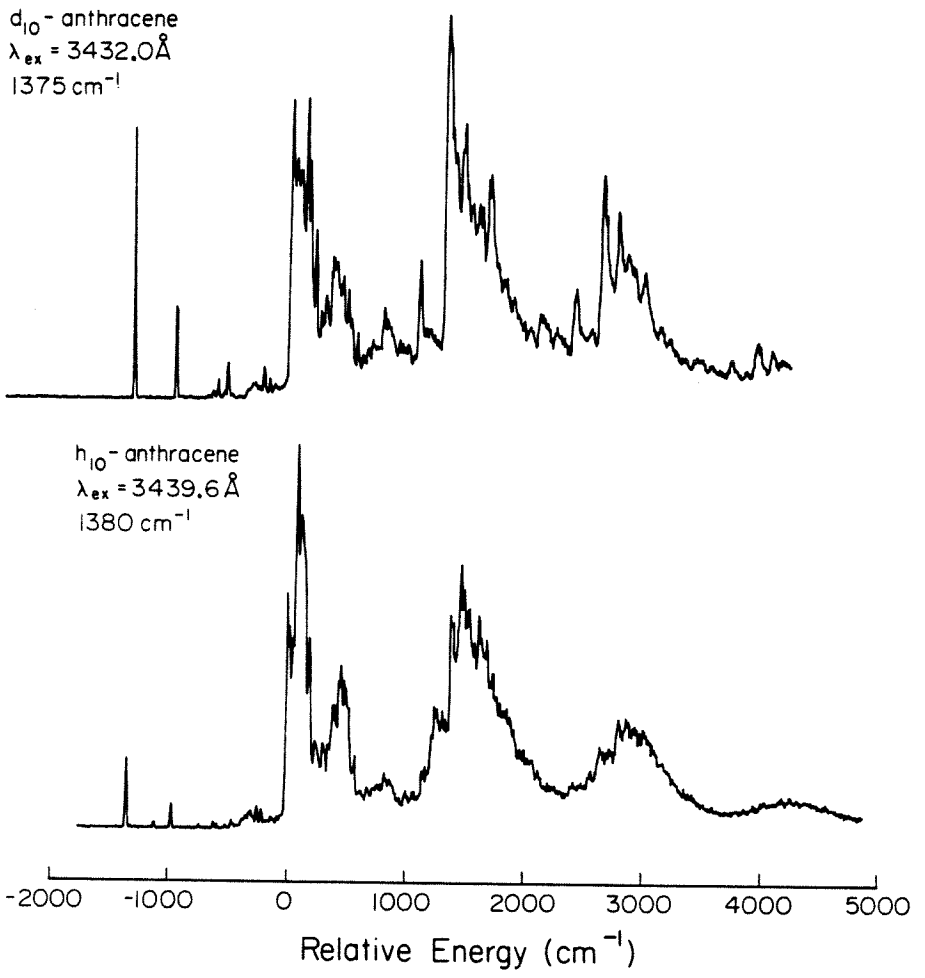

Figure 6.
The energy resolved fluorescence of h_{10}- and d_{10}- anthracene for λ_{ex}=3439.6 A° (ν_{ex}=1380 cm^{-1}) λ_{ex}=3432.0 A° (ν_{ex}=1375 cm^{-1}), respectively. Both spectra are very similar except for the absence of the 237 cm^{-1} transition in the d_{10}-anthracene spectrum. Quantum beats were not observed in d_{10}-anthracene.

Table 1. Vibrational frequencies and assignments of the energy resolved fluorescence for λ_{ex} = 3439.7 A°.

Energy, cm^{-1}	Intensity	Assignment[a]
0	31	0,1 origin
237	5	b_{1u} 239
390	11	a_g 394
604	2	b_{2u} 532
624	3	--
699	2	--
745	4	a_g
775	4	(2×390)
855	3	a_u
875	3	b_{3u}
909	5	b_{3g} 909
922	3	--
950	3	b_{3u}
996	5	a_g 1006
1011	4	b_{2u} 1000
1023	4	(390+624)
1035	4	--
1066	4	--
1125	10	b_{2u} 1125
1162	8	a_g 1165
1194	4	b_{3g} 1184
1248	5	b_{3g} 1275
1261	5	--
1305	5	b_{1u} 1309

1383	80	b_{3g} 1184, 0-0
1402	58	a_g 1403
1428	41	b_{1u} 1447
1446	44	--
1459	100	b_{2u} 1461
1489	72	(2×745)
1502	60	(390+1112)
1518	59	(390+1125)
1526	59	(390+1136)
1533	57	b_{1u} 1532
1562	36	a_g 1557
1580	54	b_{3g} 1575
1635	17	(237+1402)
1641	20	--
1665	14	(237+1427)
1695	22	(237+1459)
1714	18	--
1736	26	--
1760	26	--
1772	33	0-0+390
1796	25	--
1816	22	(2×909)
1830	37	--
1846	41	(390+1459)
1857	28	--
1878	33	(2×745+390)
1891	33	(390+1518)

1910	24	(2×390+1125)
1942	25	(390+1525)
1942	12	(2×390+1162)
1949	10	(390+1561)
1955	12	--
1966	16	(390+1580)
1990	10	(2×996)
2006	8	--
2019	8	--
2021	8	--
2030	8	--
2054	10	--
2064	10	--
2081	10	(624+1459)
2103	8	--
2112	10	--
2124	10	--
2144	8	(624+1518)
2161	9	0-0 + 2×390
2182	8	--
2188	8	--
2197	8	(745+1459)
2213	11	--
2231	10	--
2240	9	(2×390+1459)
2247	9	(2×1125)
2263	9	(745+1518)

2274	10	--
2281	10	(3x390+1112)
2292	10	(3x390+1125)
2305	10	(390+1919)
2312	8	(2x390+1533)
2326	8	(2x1162)
2333	8	--
2351	7	(2x390+1578)
2358	7	(1162+1194)

a. Assignments are made in comparison with the calulated values of reference 2.

§4.9.2 Influence of Excitation and Detection Conditions

In an effort to understand the origin of quantum beats and their relationship to intramolecular dynamics we have focused on the study of the 1125 cm^{-1} transition (λ_{ex}=3439.6 ± 0.3 A°, λ_{det}=3578.0 ± 0.3 A°), which exhibited the largest beat modulation depth. The energy resolved fluorescence in the region of the 1125 cm^{-1} transition is shown in figures 7 and 8. The dominant structure in this region of the spectra can be assigned to in-plane vibrations of a_g, b_{3g}, b_{1u}, b_{2u}, and b_{3u} symmetry and combinations thereof (see table 1). Although appearing in a relatively congested area, the 1125 cm^{-1} transition is well resolved with respect to neighboring transitions. At higher resolution (figure 8), the 1125 cm^{-1} peak is observed to be comprised of two asymmetric vibronic transitions which are separated by 0.3 A° (2.3 cm^{-1}). The asymmetry is also observed in the energy resolved emission for the resonance fluorescence (λ_{ex} = λ_{det}= 3439.5 A) and is attributed to rotational structure (see section 4.6). The double peak, however, is not a general feature of transitions in the resolved fluorescence spectra. Possible assignments for the lower frequency transition include; 1) b_{3u}, 1112 cm^{-1} fundamental; 2) b_{1u}, 1138 cm^{-1} fundamental, or 3) a_g, (745+390) cm^{-1} combination band.

Although the modulation depth of the quantum beats changed with the detection wavelength, there was no effect upon the overall beat pattern (figure 9). The quantum beats appeared to be associated more strongly with the higher frequency transition (λ_{det}=3577.8 A°). The dependence of the spectral features and the quantum beat parameters upon the excitation wavelength are presented in figures 10 and 11, respectively. The laser excitation wavelength (0.3 A° bandwidth) was varied from 3439.0 A° to 3440.0 A°. Other than an apparent increase in the amplitude

of the collisionally relaxed transition at 3611.8 A°, the vibronic structure of the energy resolved fluorescence did not significantly change. Quantum beats are not observed for 3439.1 A° and 3439.4 A° excitation. Judging from the signal to noise ratio, the optimal wavelength for exciting the vibronic transition associated with quantum beats is 3439.65 A°. This excitation wavelength also corresponds to that for which the maximum beat modulation depth is observed (figure 11). Both the modulation depth and the total dephasing rate attain maximum values at 3439.65 A° excitation, whereas the fluorescence decay rate remains relatively constant.

The laser bandwidth and pulse duration determine the distribution of eigenstates initially prepared. The coherence width of the laser pulse, determined from autocorrelation measurements, in particular, established the energy region which is coherently excited. In the extreme limits such that the laser bandwidth or coherence width are narrower than the energy difference between the interfering eigenstates, quantum beats will not be observed. In order to achieve resolution of the interfering eigenstates in anthracene, the pulse bandwidth or coherence width would need to be less than 500 MHz (0.017 cm^{-1}). The influence of the picosecond laser pulse characteristics on the quantum beats in anthracene is shown in figures 12, 13, and 14. The spectral bandwidth and temporal pulse width was systematically changed by insertion of tuning elements (wedge, 2 or 3 plate birefringent filter, fine tuning etalon, and solid etalon) into the picosecond dye laser cavity. In this manner the bandwidth was varied from 2.36 A° to 0.24 A°, and conversely, the pulse coherence width changed from 24.3 cm^{-1} to 3.2 cm^{-1}. The temporal characteristics of the picosecond laser pulse was determined for the fundamental frequency. When the solid etalon was placed within the laser

cavity, multiple pulsing ensued. The entire pulse envelope for these conditions was within the system response time and therefore did not interfere with the ability to acquire temporal data. Although difficult to measure, apparently the coherence time was still sufficient for in-phase preparation of the eigenstates, as quantum beats were still observed. In all cases, it is probable that substructure of the picosecond pulse determines the actual coherence properties of the laser excitation (1,2). Variation of the laser pulse characteristics (bandwidth and pulse duration) over the experimentally accessible range did not have a dramatic effect on the quantum beats (figures 13 and 14). This is understandable considering the laser bandwidth and coherence width were always much greater than the energy separation between the interfering eigenstates. However, to the extent that within the excitation and detection bandwidth many molecular eigenstates are initially prepared, the dynamics of non-interfering states will be monitored. This is demonstrated in figure 15 where the relative amplitudes of features associated with the relaxed fluorescence component are observed to depend upon the laser bandwidth. A particularly strong excitation bandwidth dependence is observed for the collisionally relaxed transition which appears at 3611.8 ± 0.25 A°. We have previously interpreted the 'collisionally' relaxed emission to be a consequence of the interaction of a weak nitrogen-anthracene complex. The large amplitude at 3611.8 ± 0.25 A° for a 2.68 A° bandwidth excitation could therefore be explained on the basis that the broad bandwidth pulse excites transitions which are associated specifically with the nitrogen-anthracene complex and which are apparently distinct (with reference to 0.41 A° bandwidth excitation) from the bare anthracene molecule. The differential contribution of the optically prepared eigen-

states is also observed in the fluorescence decay rate. The fluorescence decay rate is observed to decrease with the reduction of the laser bandwidth. Since the total dephasing rate, as determined from the damping of the oscillatory contribution, does not exhibit a corresponding change, a change in the decay rates for the non-oscillatory eigenstates is implied. Within the laser bandwidth, molecular eigenstates which exhibit different decay rates can be prepared and subsequently become manifest in the average decay rate. This is also implied by the change in the observed decay rates (up tp 20%) as a function of the detection wavelength for a fixed excitation energy (as will be discussed in detail later). Clearly, the observation of quantum beats in anthracene is favored by the use of excitation and detection conditions which select only the interfering eigenstates.

REFERENCES

1. D.P. Millar and A.H. Zewail, submitted Chem. Phys.,

2. S.L. Shapiro, R.R. Cavanagh, and J.C. Stephenson, Opt. Lett., **6,** 470 (1981).

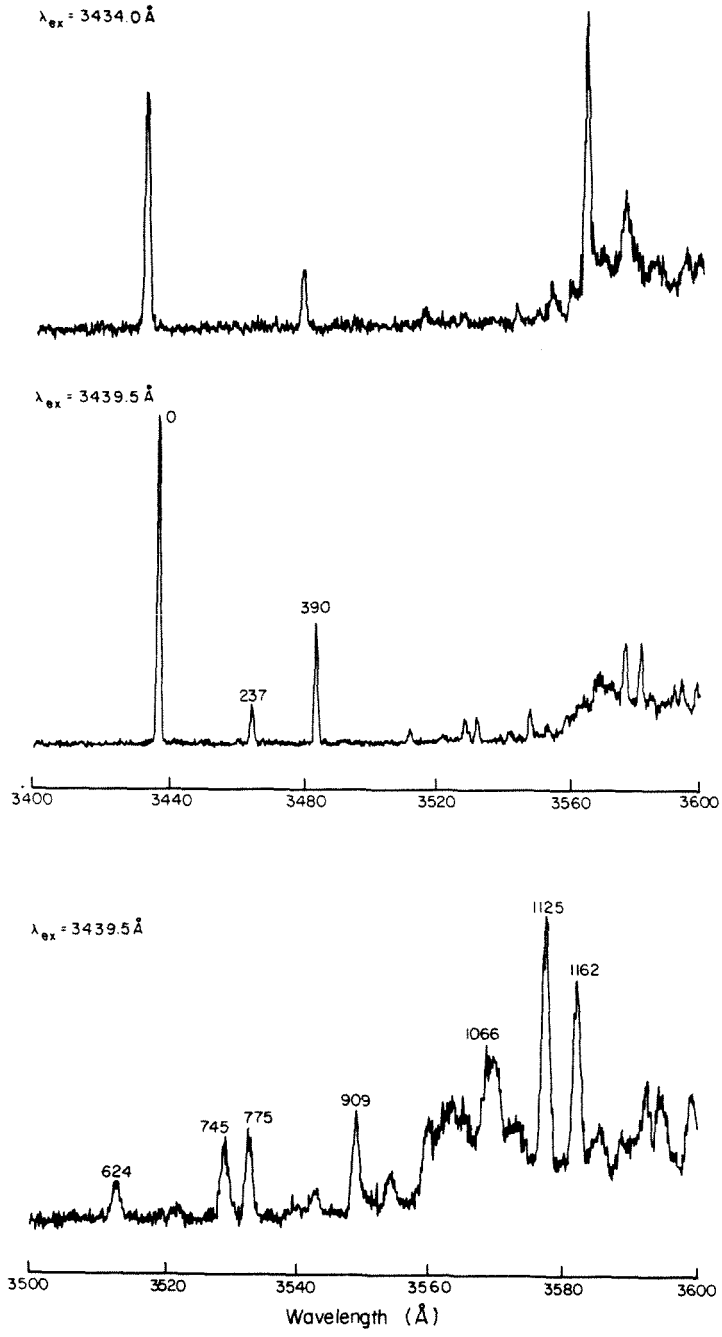

Figure 7.

The energy resolved fluorescence of anthracene in the region of the unrelaxed fluorescence. The excitation wavelength is indicated in the figure and the resolution was 0.3 A°. The spectrum for λ_{ex}=3434.0 A° is included for comparison. The region around the 1125 cm^{-1} (3577.5 A°) transition for which the most deeply modulated beat pattern was observed, is shown in the lower spectrum. Frequencies and assignments for these transitions are presented in table 1.

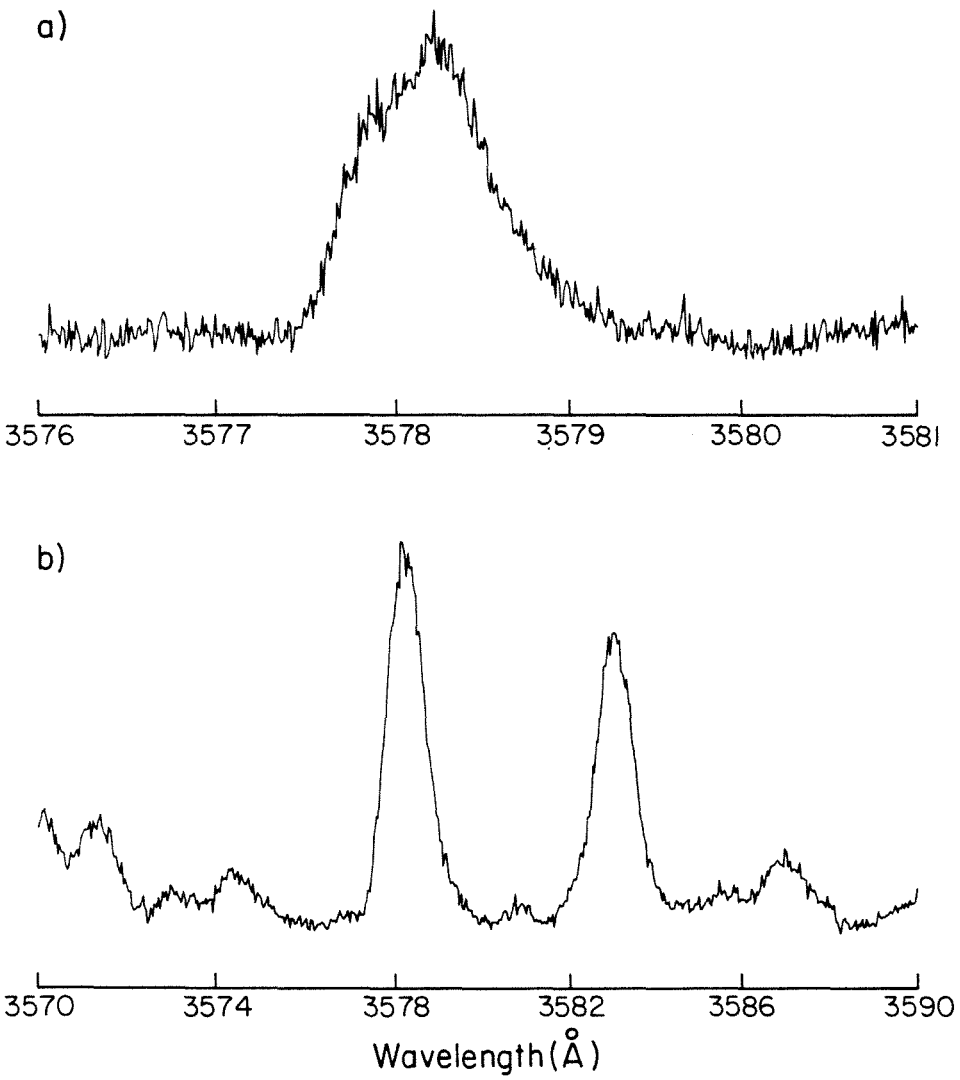

Figure 8.
The high resolution (0.25 A°) spectrum of the 1125 cm^{-1} transition showing the 0.3 A° splitting of the transition.

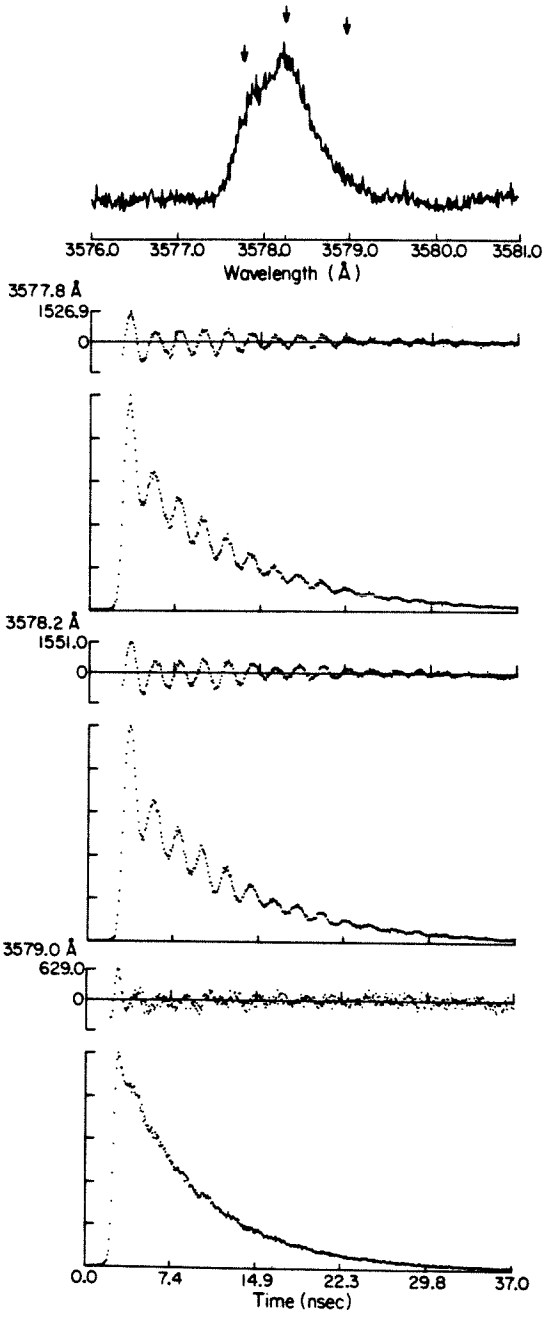

Figure 9.
The influence of the detection wavelength (0.25 A° resolution) on the quantum beat pattern. The detection wavelengths corresponding to the time resolved spectra are indicated by arrows.

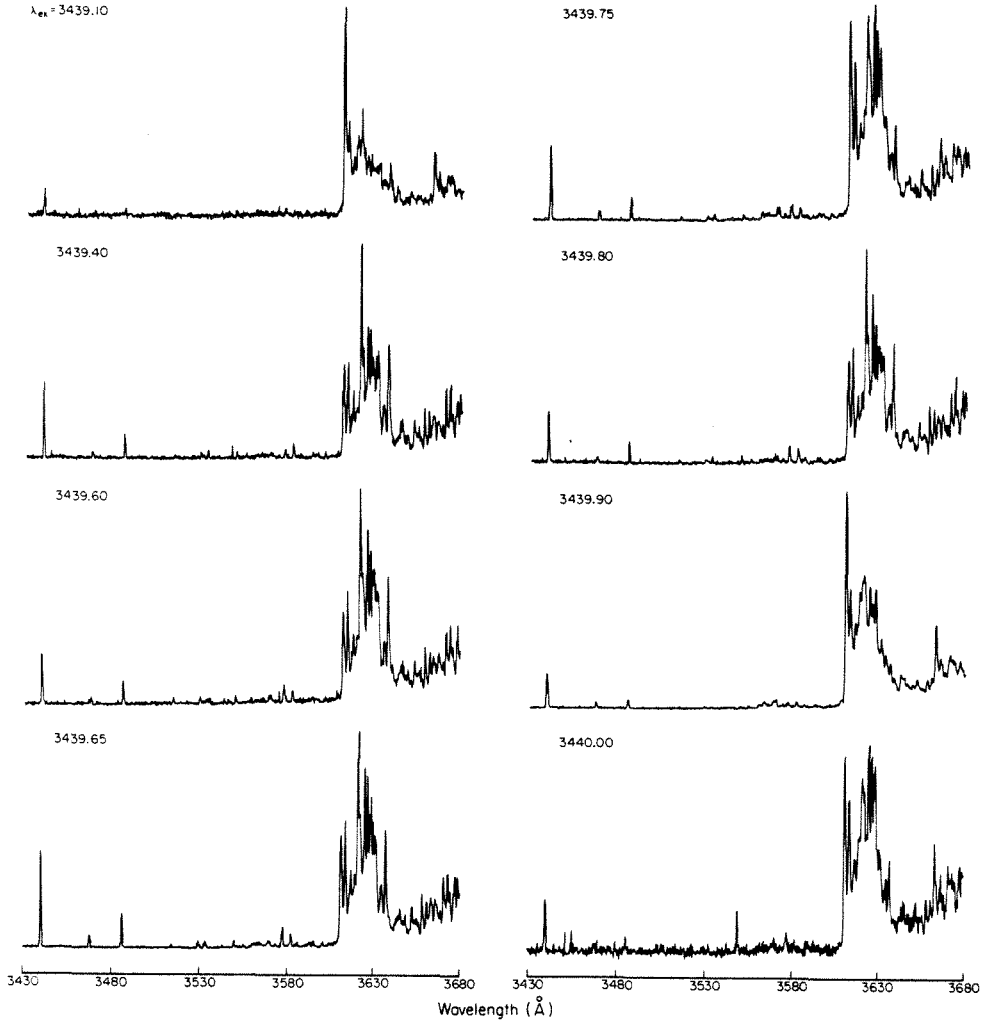

Figure 10.

The influence of the excitation wavelength on the energy resolved fluorescence. The excitation wavelength (0.5 A° bandwidth) was varied from 3439.1 to 3440.0 A°. A dramatic difference in the vibrational structure is not observed. The vibronic transition is centered at 3439.65 A°. The expansion conditions were: T_0=450 °K, P_0= 45 psi nitrogen, D=150 microns, X=5 mm.

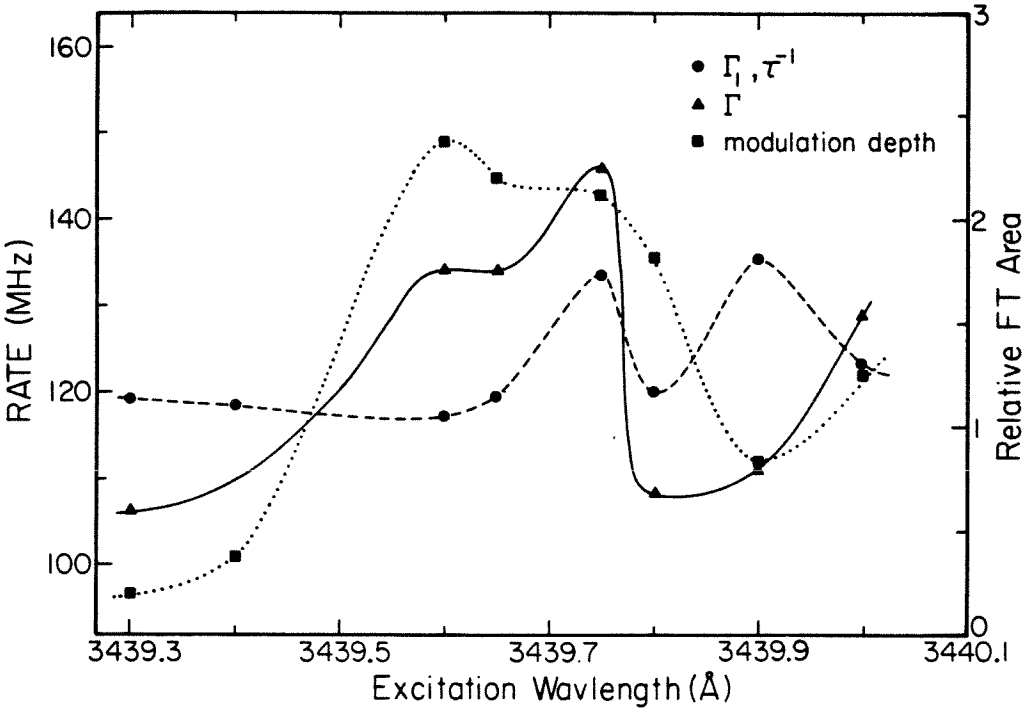

Figure 11.
The influence of the excitation wavelength (0.5 A° bandwidth) on the fluorescence lifetime, total dephasing rate, and the beat modulation depth. The detection wavelength was 3577.5 A°. The maximum beat modulation depth appears at 3439.65 A°. The energy resolved fluorescence for the indicated excitation wavelengths are presented in figure 10.

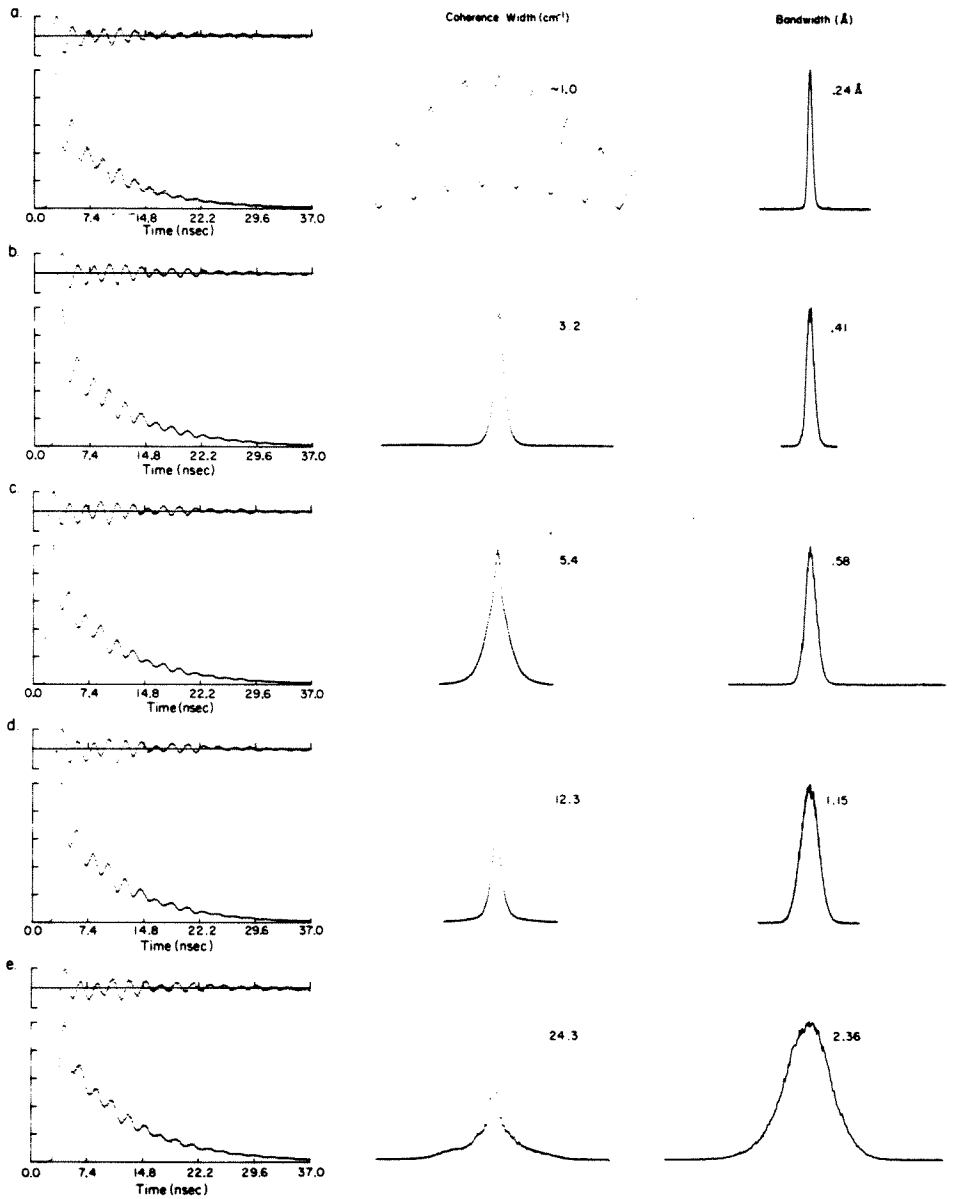

Figure 12.
The influence of the laser bandwidth and coherence width on the quantum beats for the 1125 cm^{-1} transition. The picosecond pulse characteristics were modified by the insertion of intracavity tuning elements: *a*) 3 plate birefringent filter (BRF), fine tuning etalon(FTE) and solid etalon; *b*) 3 plate BRF, FTE; *c*) 2 plate BRF; *d*) 3 plate BRF; *e*) wedge. The temporal pulse characteristics were determined using autocorrelation techniques and the laser bandwidth in the ultraviolet was measured directly with a monochromator.

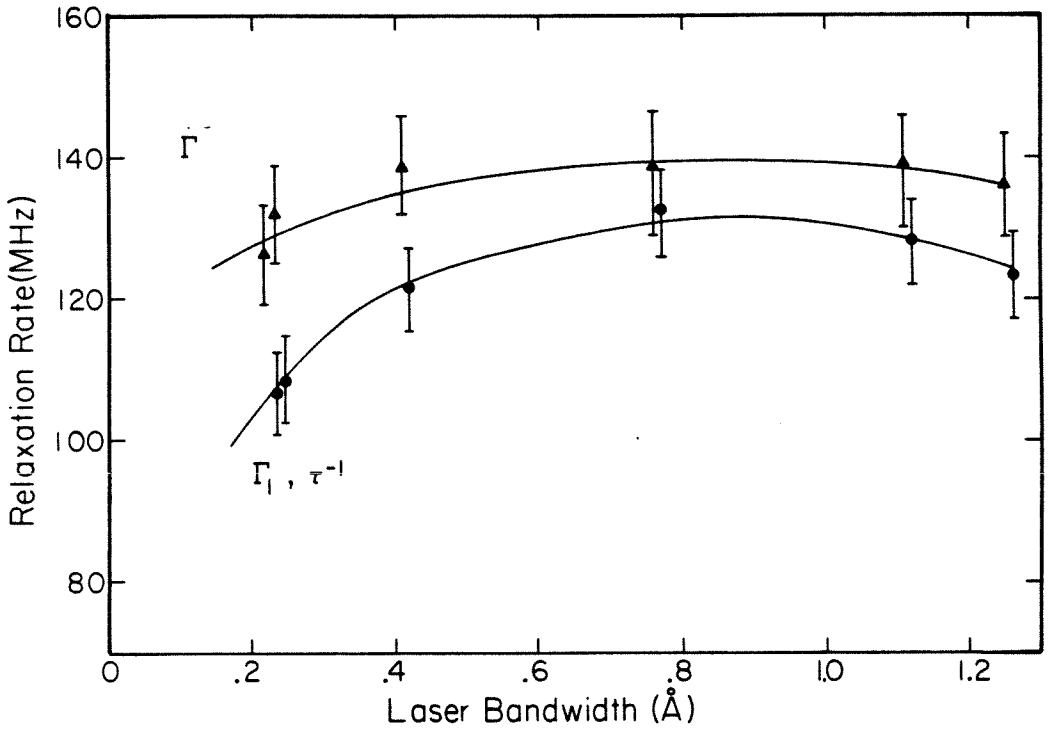

Figure 13.

The effect of the laser bandwidth on the fluorescence decay rate and the total dephasing rate (Lorentzian linewidth (FWHM) of the Fourier transform peak). The excitation wavelength was 3439.6 (S_1+1380 cm^{-1}) and the detection wavelength was 3577.5 A°. A wider excitation bandwidth corresponds to the preparation of a greater number of molecular eigenstates. The values refer to the analysis of the spectra presented in figure 12.

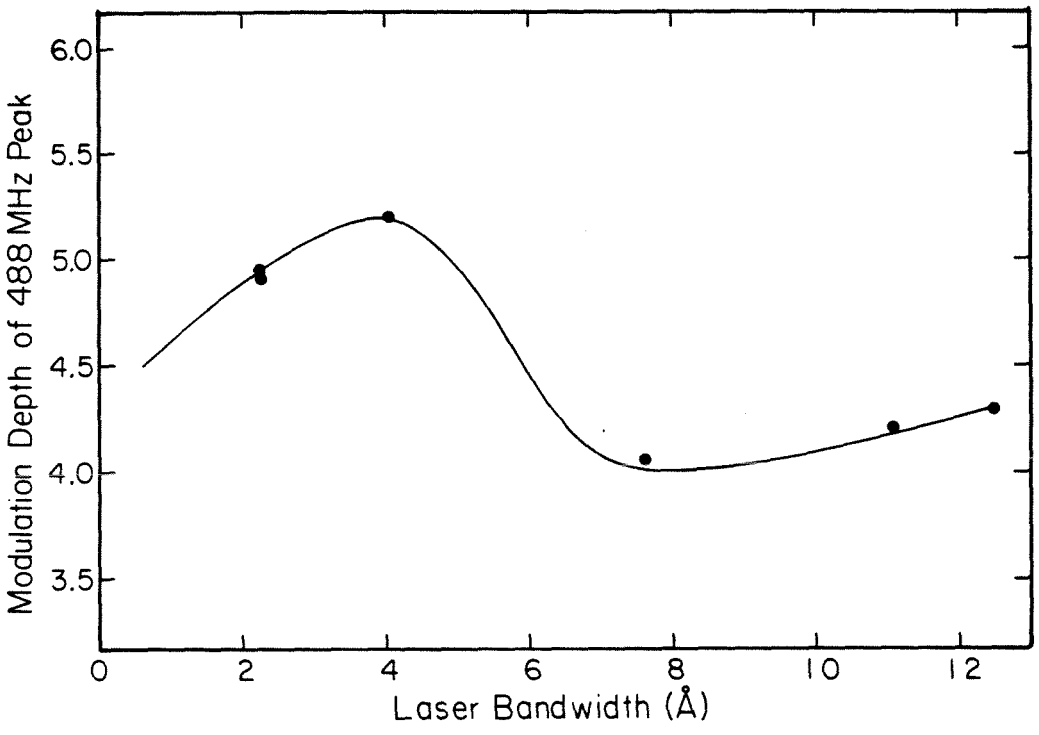

Figure 14.
The effect of the laser excitation bandwidth on the beat modulation depth. The modulation depth corresponds to the area of the Fourier transform peak. The values refer to analysis of the spectra presented in figure 12.

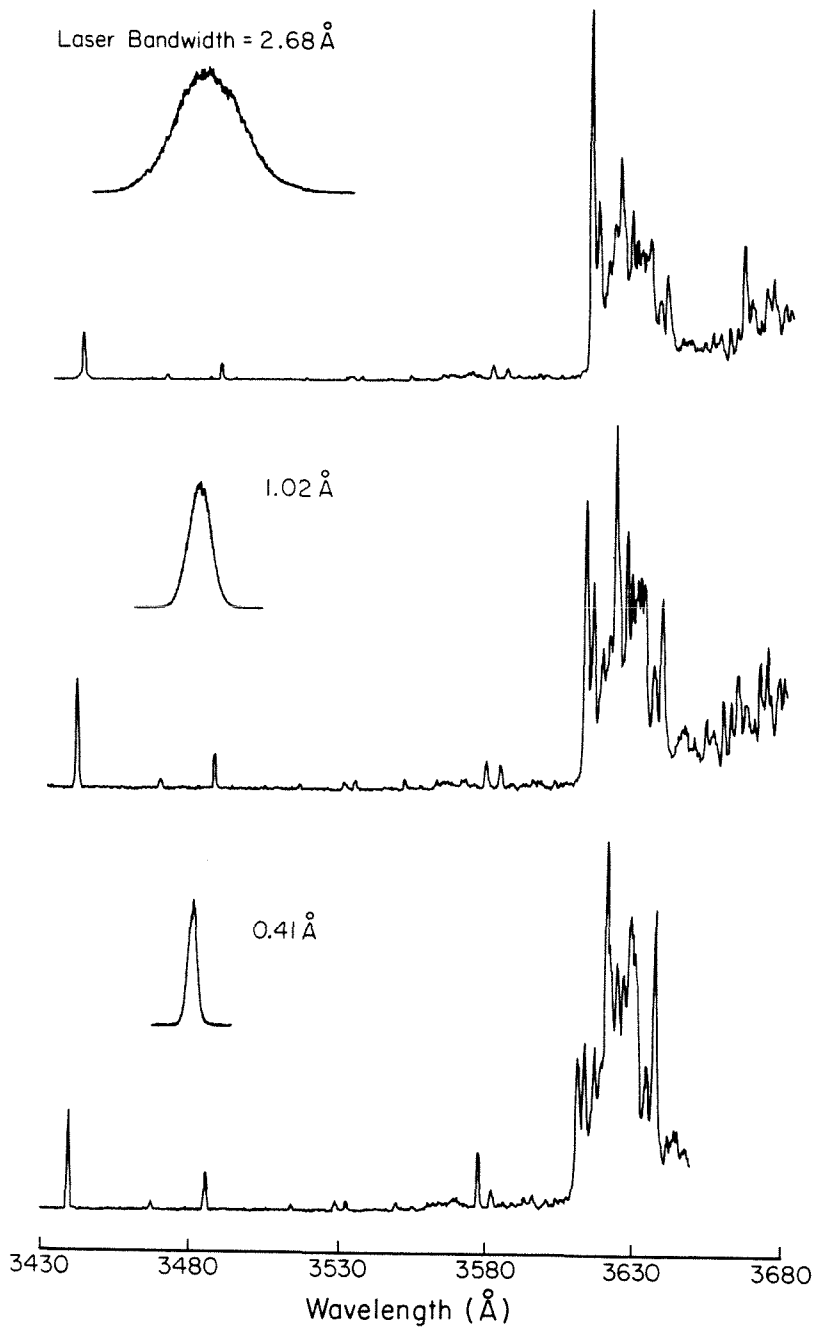

Figure 15.
The influence of the laser bandwidth on the energy resolved fluorescence spectra for λ_{ex} = 3439.6 A°. The collisionally relaxed transition appears at 3611.8 A°.

§4.9.3 Influence of Intermolecular Collisions

As previously discussed (section 4.4), the appearance of quantum beats in the energy resolved fluorescence of anthracene is not compromised by the formation of weakly bound complexes in the free jet expansion. Whereas helium and neon expansions of anthracene are free of spectral features which would indicate complex formation, in nitrogen expansions, broad absorption bands are observed to the red of the S_0-S_1 origin and collisionally relaxed transitions are observed in the energy resolved fluorescence. The conclusion that nitrogen-anthracene complexes are produced is in part based upon the failure to rationalize hard sphere collisions from both a theoretical and experimental standpoint. Quantum beats are observed in nitrogen-anthracene expansions despite evidence of collisional relaxation. Collisional relaxation is therefore likely to be mediated by the large number of bath states and not by eigenstates associated with the unrelaxed fluorescence component. The influence of intermolecular collisions on the dephasing and population relaxation is determined by analyzing the time resolved fluorescence as a function of the laser-to-nozzle distance. Apparently, the main influence of increasing the carrier gas backpressure is on the intramolecular rotational and vibrational temperature as will be discussed later in this section. In figure 16, quantum beat spectra and the respective Fourier transforms are presented for laser to nozzle distances from 1 mm to 20 mm (X/D = 6 → 120). When nitrogen was used as the carrier gas, the beat frequency remained constant at 485 ± 10 MHz. The influence of the distance of the laser from the nozzle on the fluorescence and the total dephasing decay rates is shown in figure 17. Both decay rates increase with the onset of collisions. Using calculated values for the molecular density in the free

jet expansion as a function of distance from the nozzle, an estimate for the collisional cross section can be obtained. Using the formulae for the number density and relative beam velocity (1);

$$n = n_0 \left\{ 1 + \tfrac{1}{2} (\gamma - 1) M_{eff}^2 \right\}^{\frac{-1}{\gamma-1}} \qquad (4.9.1)$$

and,

$$V = V_0 \left\{ 1 + \tfrac{1}{2} (\gamma - 1) M_{eff}^2 \right\}^{-\frac{1}{2}} \qquad (4.9.2)$$

where,

$$M_{eff} = 3.65 \left(\frac{X}{D} - 0.4\right)^{0.4} - 0.82 \left(\frac{X}{D} - 0.4\right)^{-0.4} \qquad (4.9.3)$$

(appropriate for a diatomic gas, $\gamma = 7/5$) and, $V_0 = (3 R \frac{T_0}{m})^{\frac{1}{2}}$, where, T_0 = 150 °C, a Stern-Volmer plot can be produced (figure 17). Analysis yields an estimate for the collisional cross section of 82 $A^{\circ 2}$ and a dephasing cross section of 153 $A^{\circ 2}$. These values are of the same order of magnitude as those reported by Henke et al. (2) for helium-biacetyl collisions in a free jet expansion. The dependence of the distance from the laser to the nozzle upon the nitrogen-anthracene interaction should be compared to the absence of an effect on the relaxation rates observed for helium-anthracene expansions (figure 18). From the zero pressure intercepts, values for the isolated anthracene Γ_1, Γ, and Γ_d relaxation rates can be obtained (using the definition of the characteristic relaxation rates loosely to be, the fluorescence decay rate, the homogeneous linewidth of the transition , and the total dephasing rate). For anthracene in nitrogen, the characteristic relaxation rates are found to be: Γ_1 = 109.9 ± 0.1 MHz ($\propto$ 9.10 nsec), Γ = 132.3 ± 0.4 MHz ($\propto$ 7.56 nsec) and Γ_d = 22.4 ± 0.5 MHz

($\propto$ 44.6 nsec). It should be reaffirmed that the population relaxation which, as measured, may very well contain predominant contributions from states not associated with the interference terms, but which are nevertheless excited and detected within the experimental bandwidths. The difference in the zero pressure limits for Γ_1 and Γ may be due to a number of factors including; 1) errors in the Fourier transform, 2) intermolecular interactions, 3) intramolecular dephasing, or 4) the inappropriateness of the decay rates for describing the relaxation of multilevel systems. It should be emphasized that a laser to nozzle distance of 6.5 nozzle diameters corresponds to laser excitation prior to the freezin distance. At this distance, intermolecular collisions are expected to determine the relaxation. Experiments are typically performed at a laser to nozzle distance of 33 nozzle diameters (5 mm). Comparison of the zero pressure intercepts obtained in nitrogen and helium expansions reveal a substantial discrepancy (note the different scales used for the Stern-Volmer plots). The query which this presents will serve as an introduction to the discussion of the influence of the carrier gas and backpressure on the intramolecular dynamics of anthracene. Suffice it to conclude that, to the extent that the damping rate of the quantum beats reflects collisional relaxation, quantum interference effects can be used to obtain information regarding intermolecular interactions in free jet expansions.

REFERENCES

1. D.M. Lubman, C.T. Rettner and R.N. Zare, J. Phys. Chem., **86,** 1129 (1982).

2. W. Henke, H.L. Selzle, T.R. Hays, S.H. Lin and E.W. Schlag, Chem. Phys. Lett., **77,** 448 (1981).

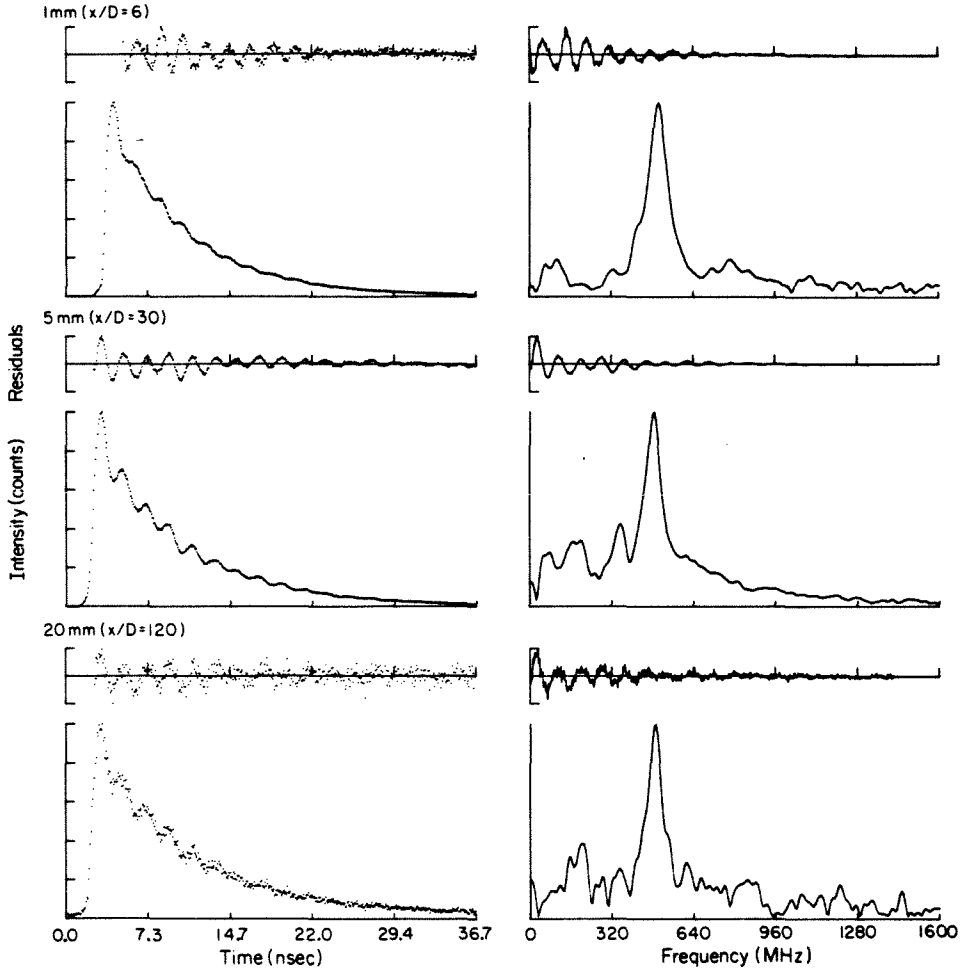

Figure 16.
The influence of the intermolecular collisional rate, proportional to the laser to nozzle distance, on the quantum beats. Standard expansion conditions were used. The excitation and detection wavelengths were 3439.6 A° and 3577.5 A°, respectively.

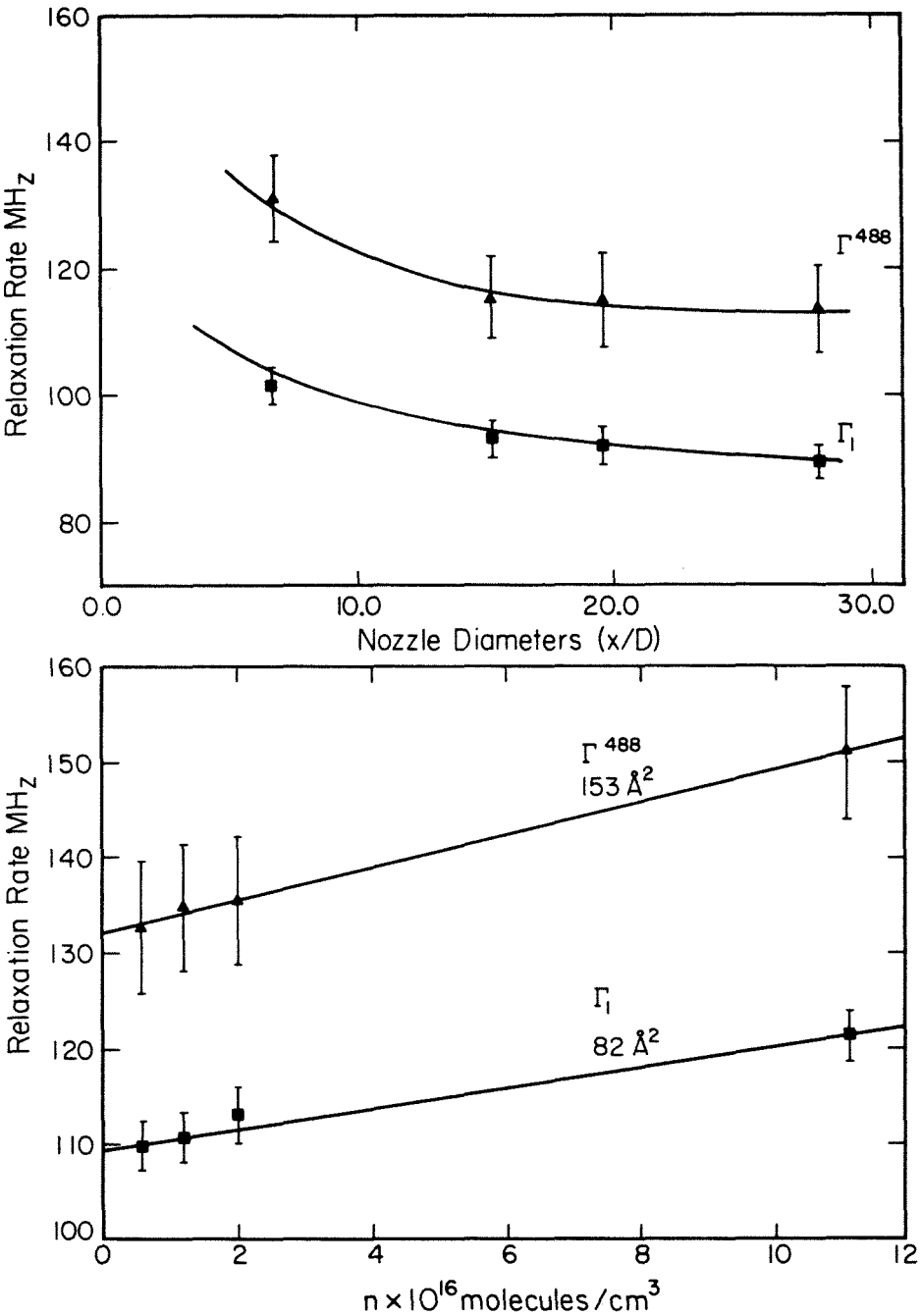

Figure 17.
The influence of the intermolecular collision rate on the fluorescence decay rate and the total dephasing rate for anthracene in a nitrogen expansion. The data are also presented in terms of a Stern-Volmer relationship in order to obtain destructive cross sections. The calculation is described in the text.

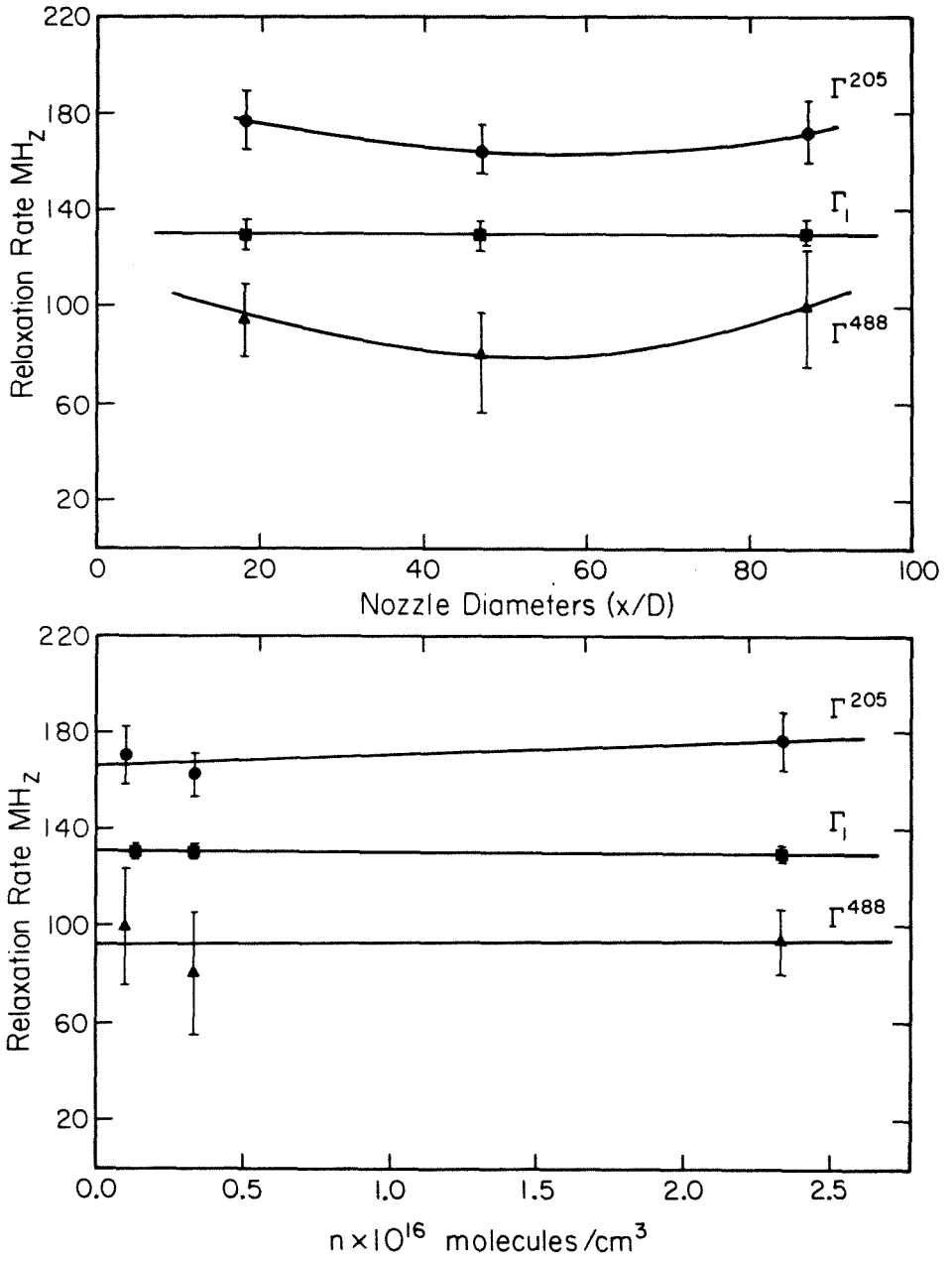

Figure 18.
The influence of the intermolecular collision rate on the relaxation rates of anthracene.

§4.9.4 Characteristic Relaxation Rates

The principal motivation for using different carrier gases and nozzle backpressures in experiments employing jet expansion techniques is to achieve conditions which efficiently cool the internal degrees of freedom of the seed molecules while minimizing the formation of intermolecular complexes. The appropriate selection of expansion conditions is in part determined by limitations imposed by the specific vacuum system, and also by the thermodynamics responsible for the transfer of intramolecular vibrational and rotational energy to translational motion in the expanding gas. Despite the careful work performed by McClelland et al. (1) on the thermodynamics of iodine free jet expansions, the extension of their results to the cooling of large polyatomic molecules is not straight forward, although general trends are consistent. Rotational cooling, being very efficient, approximately follows the translational temperature of the expansion and depends upon the nature of the carrier gas such that helium > neon > nitrogen in order of decreasing rotational cooling efficiency. The reciprocal trend is found for vibrational cooling. The efficiency of both rotational and vibrational cooling is found to be logarithmically dependent upon the backing pressure of the carrier gas. Limitations are in turn imposed by the ability of the carrier gas to form complexes with the seed molecules. Since helium is less likely to foster complex formation due to the instability of bimolecular complexes, it is more widely used as a carrier gas, although for small throughput vacuum systems, low pressure argon expansions have been shown to be effective. The appropriate choice of carrier gas and backing pressures used to efficiently cool any specific molecular system is therefore at present largely an empirical process.

Since quantum beats are a manifestation of high resolution spectral structure (by means of the energy difference between the states responsible for a specific beat frequency) and of intramolecular dynamics (through measurement of the homogeneous lineshape of molecular eigenstates obtained from the Fourier transform of the oscillatory component), the quantum beat pattern can be expected to reflect the intramolecular temperature. The vibrational and rotational temperatures of anthracene in our free jet expansion have been discussed in sections 4.5 and 4.6, respectively. Other than estimates for the rotational and vibrational temperatures of 1 °K and 50 °K, with a backpressure of 45 psi helium, and corresponding temperatures of 5 °K and < 50 °K for nitrogen expansions, the limited spectral resolution prevents an accurate and systematic measurement of internal anthracene temperatures. The following discussion is therefore of necessity qualititative with regard to association of the changes of the quantum beat parameters with intramolecular temperatures. In light of the present understanding of the thermodynamics of polyatomic molecules in free jet expansions, the relationship between internal temperature and quantum interference effects is problematic in the sense that investigating the interrelationship is one of the objectives of this study.

In our previous communication (2), we reported that the modulation depth of the oscillatory fluorescence component depended upon the carrier gas which was used according to the order, helium < neon < nitrogen. These experiments were performed with a single plate birefringent filter in the laser cavity, producing an excitation bandwidth and coherence width of approximately 2.0 A° and 20 cm^{-1}, respectively. For these excitation conditions, the characteristics of the quantum beat pattern

were insensitive to the nature or backpressure of the carrier gas. However, when the laser bandwidth was reduced to 0.5 A°, upon incorporation of appropriate tuning elements into the laser cavity (i.e. three plate birefringent filter), dramatic effects were observed in the quantum beat pattern which were dependent upon the expansion conditions.

Other than the appearance of a collisionally relaxed transition at 3611.8 A° when nitrogen was used as a carrier gas, a carrier gas or pressure dependent influence upon the energy resolved fluorescence spectra for 3439.6 ± 0.25 A° (S_1+1380 cm^{-1}) excitation was not observed (figure 19). The dramatic influence upon the temporal properties of the quantum beats, however, is shown in figure 20. Whereas the beat pattern in a nitrogen expansion is independent of the backpressure, the oscillatory component exhibits a pressure dependent evolution in helium and neon expansions. These effects are more easily revealed in the corresponding Fourier transforms of the quantum beats shown in figure 21. The beat pattern is comprised of, nominally, two components at 488 ± 10 MHz, and 205 ± 10 MHz. There are possibly two other components at 359 ± 10 MHz and at 50 ± 10 MHz. When helium is used as the carrier gas, the quantum beat pattern demonstrates a complete evolution from the 488 MHz component at 5 psi backing pressure to the 205 MHz component at a back pressure of approximately 60 psi (figures 22 and 23). In order to obtain a quantitative estimate of the pressure dependent trends seen in the anthracene quantum beats for the different carrier gases studied, the normalized magnitude of the Fourier components (as determined from the areas of the frequency domain peaks) were determined, and are presented in figure 24. For neon and helium there is a reciprocal evolution of intensity from the 488 to 205 MHz frequency component. At

approximately 15 psi, the intensities of the two components are equivalent.

Studies of the pressure and carrier gas dependent effects upon the fluorescence excitation spectra in the region of the S_1 origin indicate that the vibrational temperature remains essentially unchanged for the conditions used in these experiments (see section 4.5). Although a vibrational hotband is observed in helium-anthracene expansions, the relative intensity does not change as a function of the backpressure, while the complete absence of hotbands in the nitrogen expansion indicates that the vibrational temperature is well below 50 °K. It is therefore unlikely that the pressure dependence of the Fourier components associated with the quantum beats are related to vibrational temperatures. There is evidence, however, that intramolecular rotational temperature is involved. Making the reasonable assumption that the rotational temperture parallels the translational temperature of the expansion (1), the calculated (refer to section 4.6 for details) rotational temperature can be plotted as a function of the carrier gas backpressure. In figure 25, the pressure dependence of the rotational/translational temperature for helium, neon, and nitrogen are presented. Although absolute temperatures may be in error, the general trends and relative magnitudes for the different gases should prevail. Even at the lowest backpressures used in these experiments, the rotational temperatures obtained for helium or neon expansions are only equivalent to those obtained for nitrogen at high backing pressures. This is consistent with the failure to observe a 205 MHz Fourier component in nitrogen expansions. The actual anthracene rotational temperature may be higher than calculated due to the consequences of complex formation. The results of collisional relaxation in nitrogen expan-

sions are especially evident at backpressures greater than 45 psi. The similar behavior reflected by the Fourier components for helium and neon expansions (figure 24) are paralleled by the pressure dependent rotational temperatures. In fact, the magnitude of the 205 MHz Fourier component is linear with rotational temperature, beginning abruptly at 3 °K (10 psi) (figure 26).

Additional evidence for the dependence of anthracene intramolecular dynamics on the rotational temperature is obtained from measurements of the fluorescence decay rates. In figure 27a, the fluorescence decay rate as a function of the carrier gas and backpressure is presented. The decay rates were obtained from the best single exponential fit to the decay for 3439.6 ± 0.25 A° excitation and 3577.5 A° detection. Whereas the decay rate is independent of the backpressure for nitrogen expansions, the decay rates increase at reduced helium and neon backpressures. Associating backpressure with the rotational temperature, the data can be presented according to figure 27b, where the fluorescence decay rate in a helium expansion is still seen to exhibit a nonlinear relationship with respect to the rotational temperature. It is expected that the principal consequence of the rotational temperature is to define an initial ground state distribution of rotational states. To a first approximation, optical excitation will populate an excited state rotational distribution in anthracene according to $\Delta J = \pm 1,0$ and $\Delta K = \pm 1$ selection rules appropriate for B type transitions of a nearly prolate top. An estimate for the number of rotational states populated for a given temperature was obtained by integrating the rotational envelope generated from band contour analysis for specific temperatures. In this way a more physically realistic model of rotational temperature dependent trends can be real-

ized. When the data of figure 27b are presented in this manner, as shown in figure 28, a linear relationship is obtained.

The results of figure 28 would imply a J and/or K dependence of the fluorescence decay rate. The effect of rotations on the nonradiative decay rate has been a subject of several recent studies. Whereas there appears to be little dependence of the nonradiative rate on the rotational states in formaldehyde (3) and naphthalene (4), K dependent effects have been observed in para-benzoquinone (5) and pyrazine (6). Whereas para-benzoquinone exhibits a decreasing decay rate with increasing J, the decay rate of the fast exponential component in pyrazine reflects a K^2 dependence. Our data suggest that similar to pyrazine, the nonradiative decay rate increases with higher rotational quantum numbers. An alternative, although related, explanation would be that at higher internal temperatures, a longer effective density of states would initially be prepared. The fluorescence decay rate is directly related to the rotational temperature through intramolecular inelastic collisional processes in the same way that the intermolecular collisions are accomodated. The fluorescence decay is composed of both radiative and non-radiative components, $\Gamma = \Gamma_1^{nr} + \Gamma_1^{r}$. As additional nonradiative decay channels become active, the fluorescence decay rate would increase proportional to the standard formula, $n = 2\pi^2 V^2 \rho$. With reference to figure 28, 'zero temperature' values for the population decay rates are found to depend upon the carrier gas, being 120.4 ± 0.8 MHz for nitrogen, 114 ± 1.8 MHz for neon, and 95.3 ± 5.5 MHz when helium is used as a carrier gas. These differences possibly reflect contributions from other nonradiative decay channels not associated with rotational dependent relaxation. These might include the effects of vibrational temperature or perturbation by

weak collisional complexes. Certainly for the case represented by nitrogen, where the influence of collisions are documented, (for example in the laser to nozzle distance experiments), collisionally induced redistribution can be expected to dominate any potential rotation specific relaxation.

As the final topic regarding the influence of the carrier gas and backpressure upon the quantum beats observed in anthracene, the measurements for the total dephasing rates will be presented and discussed. The total dephasing rate was determined from the linewidth of the frequency domain peak (homogeneous linewidth) obtained upon Fourier transformation of the oscillatory component of the fluorescence decay (refer to section 4.7). The total dephasing can be considered to contain contributions from both population relaxation and pure dephasing according to $\Gamma = \frac{1}{2}(\Gamma_1 + \Gamma_2) + \Gamma_d$ where Γ_i represents the population decay rate of the molecular eigenstates in the excited state manifold. It should be emphasized that this relationship among the relaxation rates should be considered operational since the applicability to multilevel systems is not completely established. Pure phase relaxation can originate from intermolecular collisions or potentially from interaction of the optically excited states with the bath manifold. The population decay rate is equivalent to the fluorescence decay rate. In figure 29, values for Γ_i and Γ are presented as a function of the nitrogen backpressure. The rates are independent of pressure, demonstrating that increasing the carrier gas pressure does not induce changes in the intermolecular collisional rate as is observed when the distance of the laser from the nozzle varied (figure 16). A pure dephasing rate of approximately 12 MHz can be calculated and can possibly be attributed to the persistence of weak collisional

relaxation in the nitrogen expansion.

The well behaved trends for the fluorescence decay and total dephasing rates observed in nitrogen expansions are in dramatic contrast to that observed for helium and neon. The temporal decay of anthracene fluorescence in expansions of helium and neon is complicated by the appearance of nominally two oscillatory components between 10 psi and 50 psi. Measurements of the characteristic relaxation rates in helium and neon expansions are presented in figures 30 and 31. The decay rates are observed to change dramatically but smoothly with increasing backpressure. The data represented by figures 29, 30 and 31 were obtained for identical experimental conditions. All spectra for a particular gas were obtained during the same experimental run. It is very interesting to note that the total dephasing rate is oftentimes less than the population relaxation rate, in apparent contradiction to the general formulation of relaxation rates summarized in the Bloch equation. Although the possibility exists that artifacts generated during the Fourier transformation of the residual are responsible for the unexpected values obtained for the total dephasing rates in helium and neon expansions, we see that the rates determined in the nitrogen expansion (figure 29) by similar methods are well behaved.

A posssible explanation for the discrepancy lies in the fact that, whereas the total dephasing rate is determined by the average homogeneous linewidth of the interfering eigenstates, the fluorescence decay rate as measured may contain contributions from many molecular eigenstates which are not associated with the oscillatory components. A consistent explanation for the observed results in figures 30 and 31 would then invoke a slower population decay rate for the interfering eigenstates

than that for other fluorescence components. An upper limit to the fluorescence decay rate of these states would therefore be equal to the total dephasing rate. That the interfering eigenstates would exhibit a slower relative fluorescence decay rate is not unreasonable if one considers that the eigenstates responsible for the quantum beats are effectively 'decoupled' from other nonradiative and nonradiative relaxation channels (particularly those associated with the relaxed fluorescence). Provided that this interpretation is correct, one might expect that nonradiative relaxation pathways are inactive for the interfering eigenstates. The difference in the total dephasing rates for the 205 MHz and 488 MHz components would indicate that different eigenstates are responsible for the Fourier components. The dramatic, although smooth variation in Γ throughout the pressure range studied would also indicate that subtle energy and phase relaxation and redistribution is modulated by the intramolecular rotational distribution.

REFERENCES

1. G.M. McClelland, K.C. Saenger, J.J. Valentini and D.R. Herschbach, J. Phys. Chem., **83,** 947 (1979).

2. W.R. Lambert, P.M. Felker, and A.H. Zewail, J. Chem. Phys., **75,** 5958 (1981).

3. J.C. Weisshaar and C.B. Moore, J. Chem. Phys., **70,** 5135 (1979).

4. U. Boesl, H.J. Neusser and E.W. Schlag, Chem. Phys. Lett., **31,** 1 (1975).

5. G. ter Horst and J. Kommandeur, J. Chem. Phys., **76,** 137 (1982).

6. G. ter Horst, D.W. Pratt and J. Kommandeur, J. Chem. Phys., **74,** 3616 (1981).

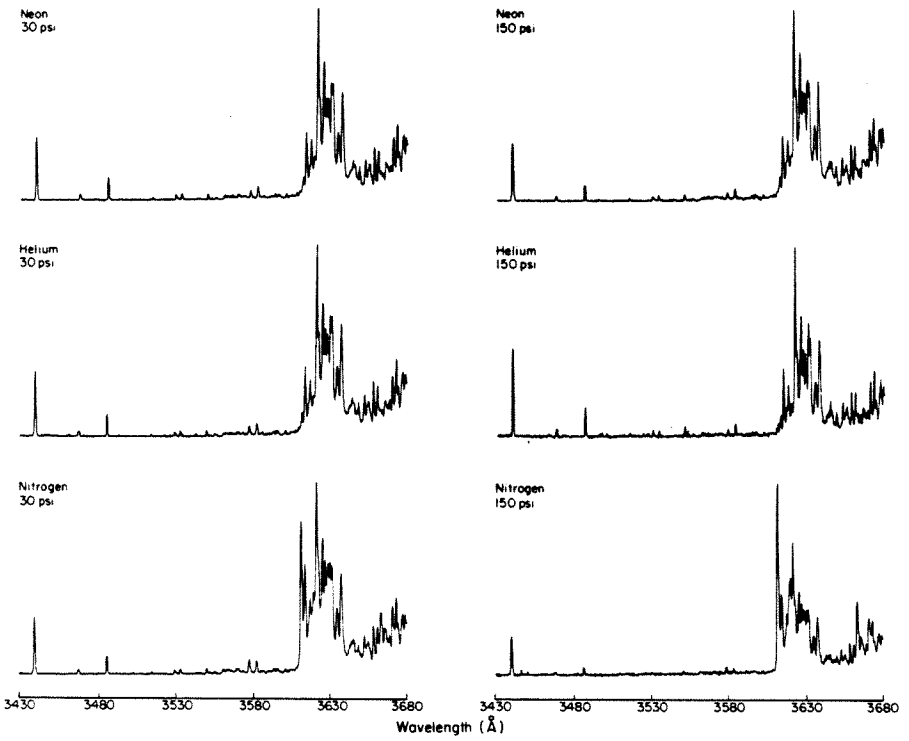

Figure 19.
The influence of the carrier gas and backpressure on the energy resolved fluorescence of anthracene for excitation to S_1 +1380 cm^{-1}. The spectra are very similar except for the collisionally relaxed component observed in nitrogen expansions. The resolution was 0.25 A°.

Figure 20.

Characteristic quantum beat patterns produced in helium, neon and nitrogen free jet expansions. The spectra were obtained for λ_{ex} = 3439.6 A° and λ_{det} = 3577.5 A°. The residuals are normalized to the number of counts so as to accentuate the modulation pattern. The expansion conditions were; T_0= 450 °K, D=150 microns, X= 5 mm.

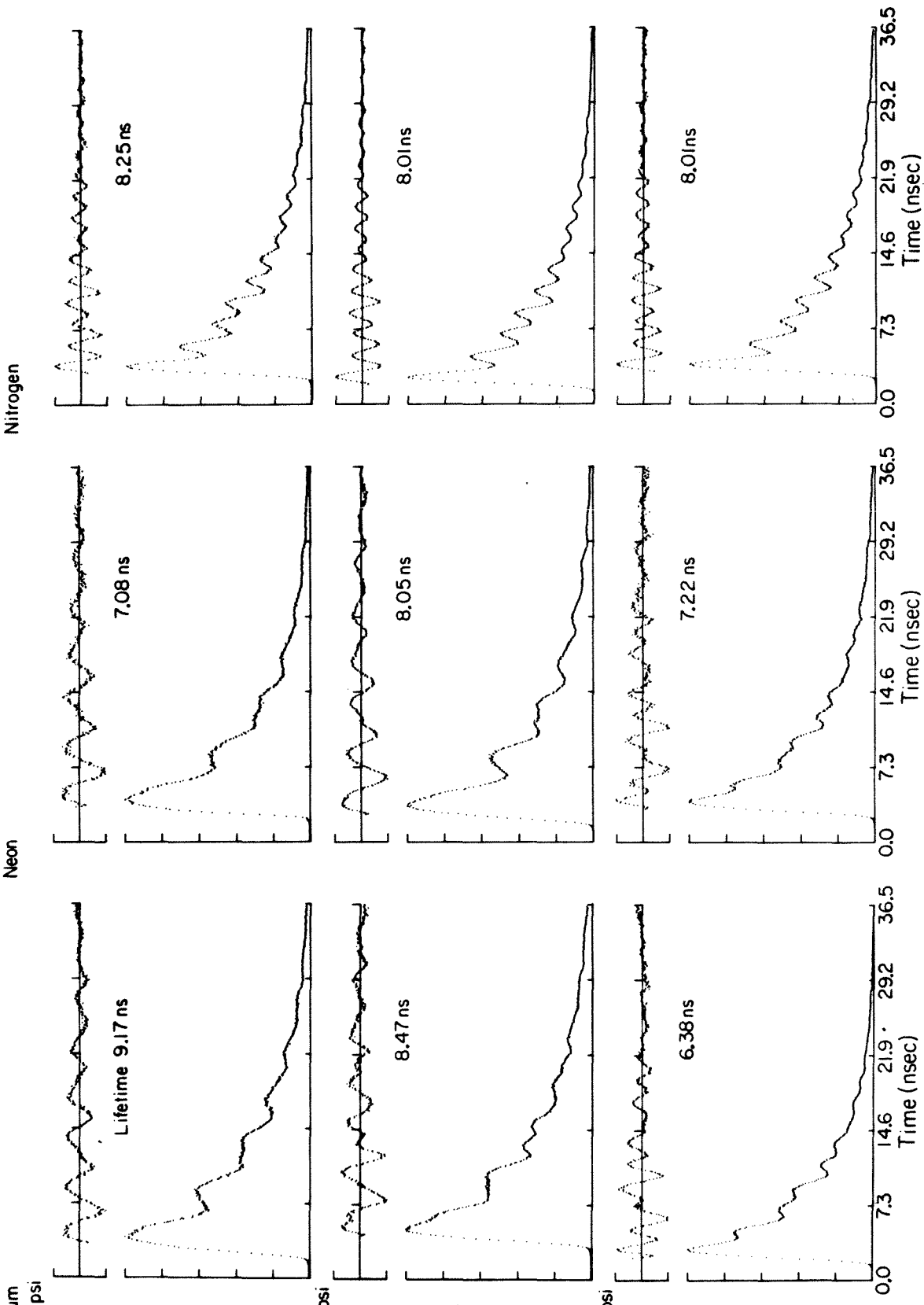
Helium
Neon
Nitrogen
150 psi
45 psi
10 psi
Residual
Intensity
Lifetime 9.17 ns
7.08 ns
8.25 ns
8.47 ns
8.05 ns
8.01 ns
6.38 ns
7.22 ns
8.01 ns
0.0
7.3
14.6
21.9
29.2
36.5
Time (nsec)

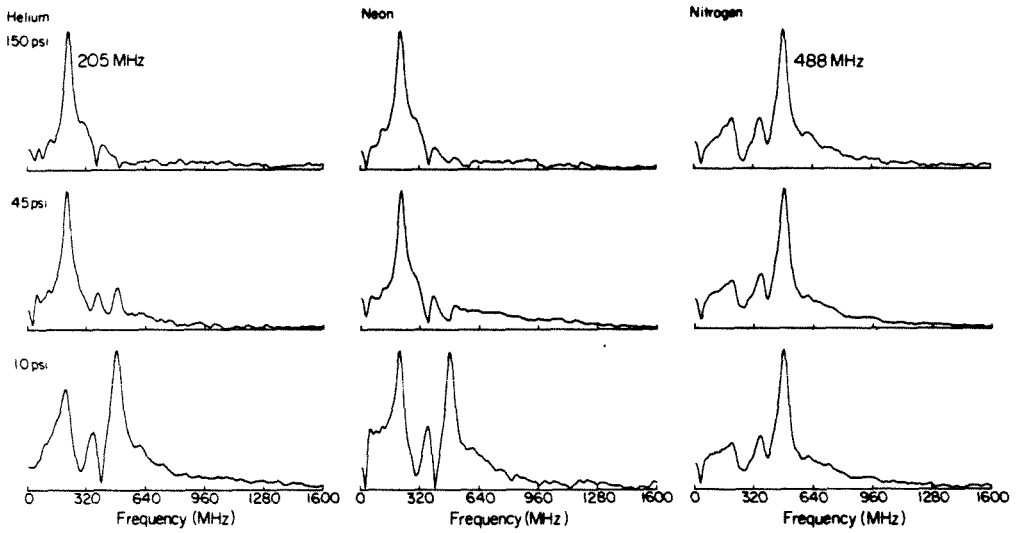

Figure 21.
The Fourier transforms of the quantum beats presented in figure 20. The peaks appear at 205 ± 10 MHz and 488 ± 10 MHz.

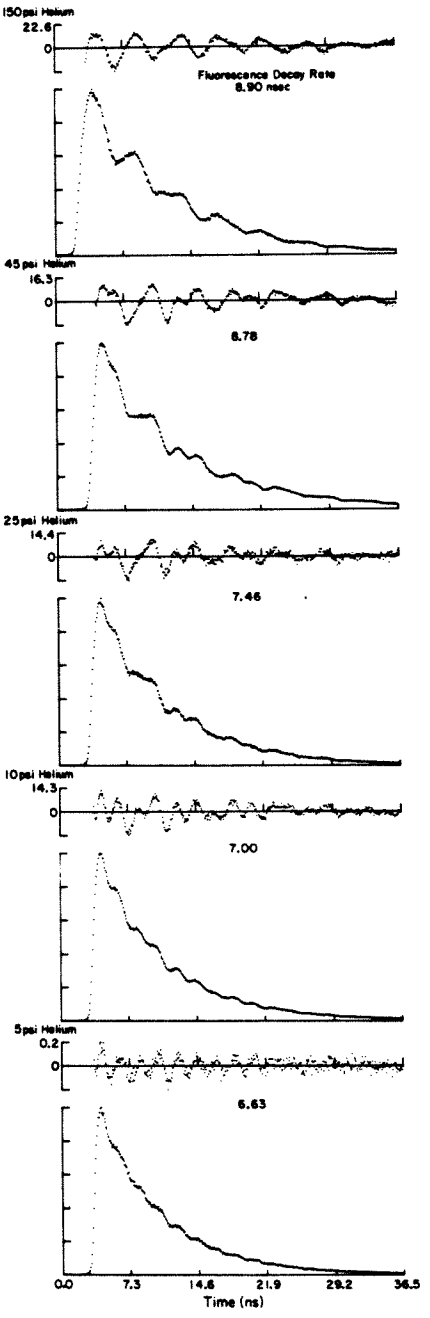

Figure 22.
The evolution of the 205 MHz and 488 MHz oscillatory component with increasing helium backpressure. The residuals have been normalized to the number of counts in order to emphasize the modulation pattern.

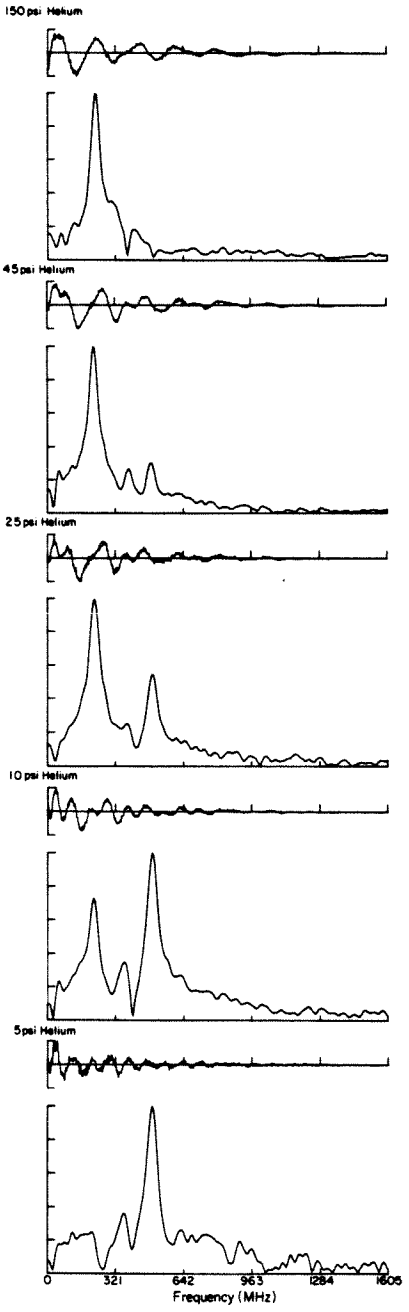

Figure 23.
The Fourier transform of the quantum beats presented in figure 22. The steady change from a 488 MHz component at a helium backpressure of 5 psi to a 205 MHz component at 150 psi is shown.

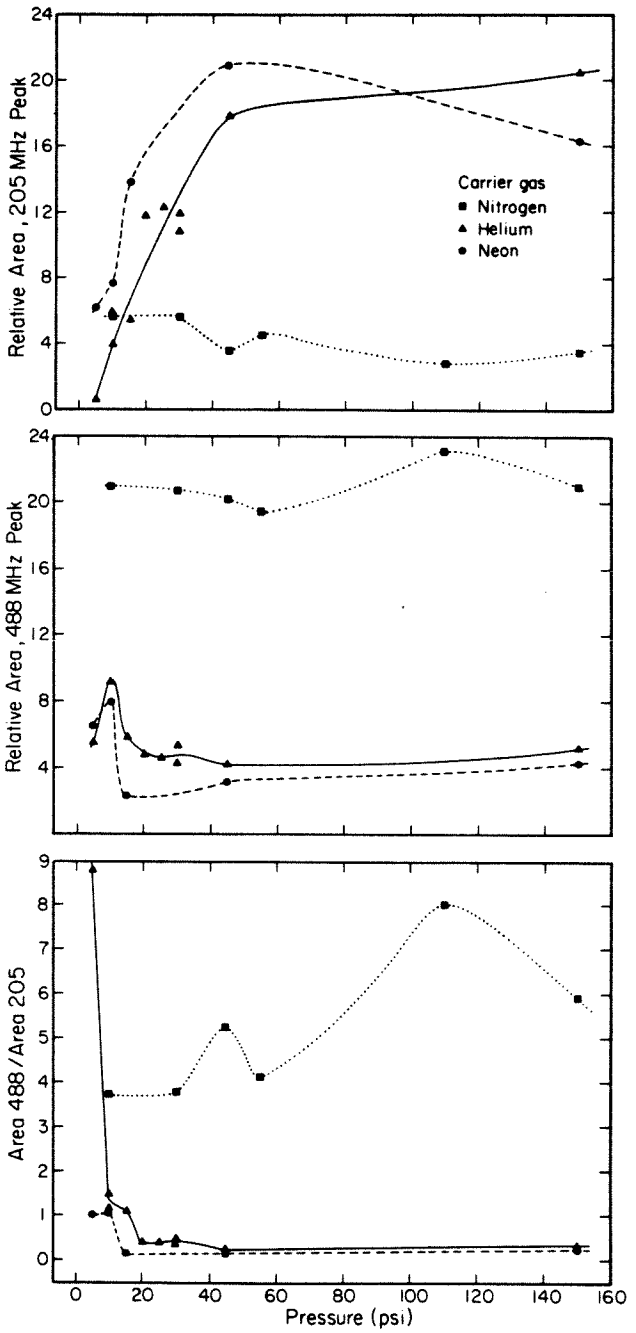

Figure 24.

Quantification of the amplitudes of the 205 MHz and 488 MHz Fourier components presented in figure 21: *a*) the influence of the carrier gas and backpressure upon the amplitude of the 205 MHz Fourier component, *b*) the influence of the carrier gas and backpressure upon the amplitude of the 488 MHz Fourier component, *c*) the ratio, 488 MHz/205 MHz, of the Fourier components. The amplitude of the Fourier component, determined from the integrated area of the respective peaks is proportional to the modulation depth of the quantum beats.

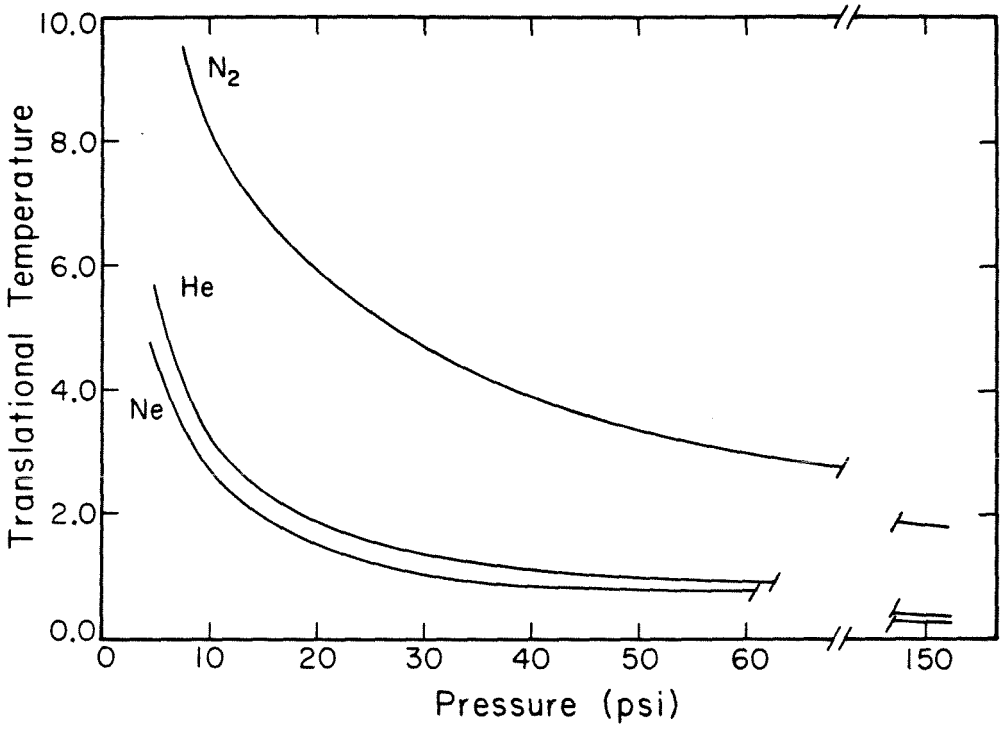

Figure 25.
The calculated terminal translational temperature plotted as a function of the carrier gas and backpressure. The translational temperature is proportional to the rotational temperature. Details of the calculation can be found in section 4.6.

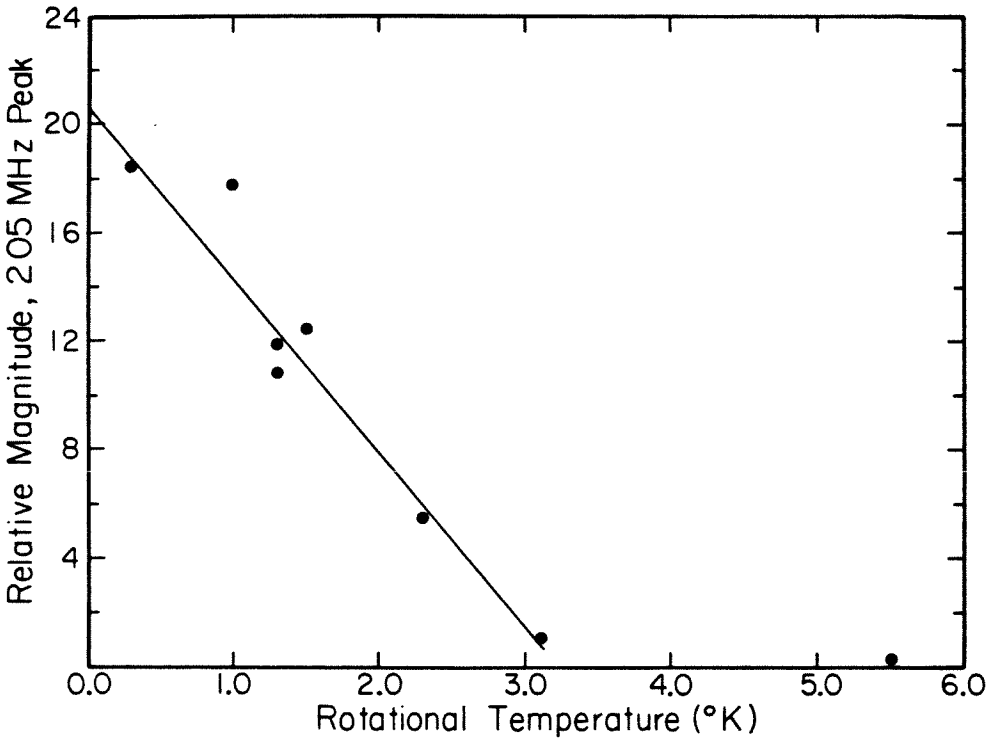

Figure 26.
The dependence of the magnitude of the 205 MHz Fourier component obtained from the transforms presented in figure 23, upon the calculated rotational temperature. The rotational temperature was assumed to be proportional to the terminal translational temperature which is in turn proportional to the backpressure of the carrier gas (figure 25).

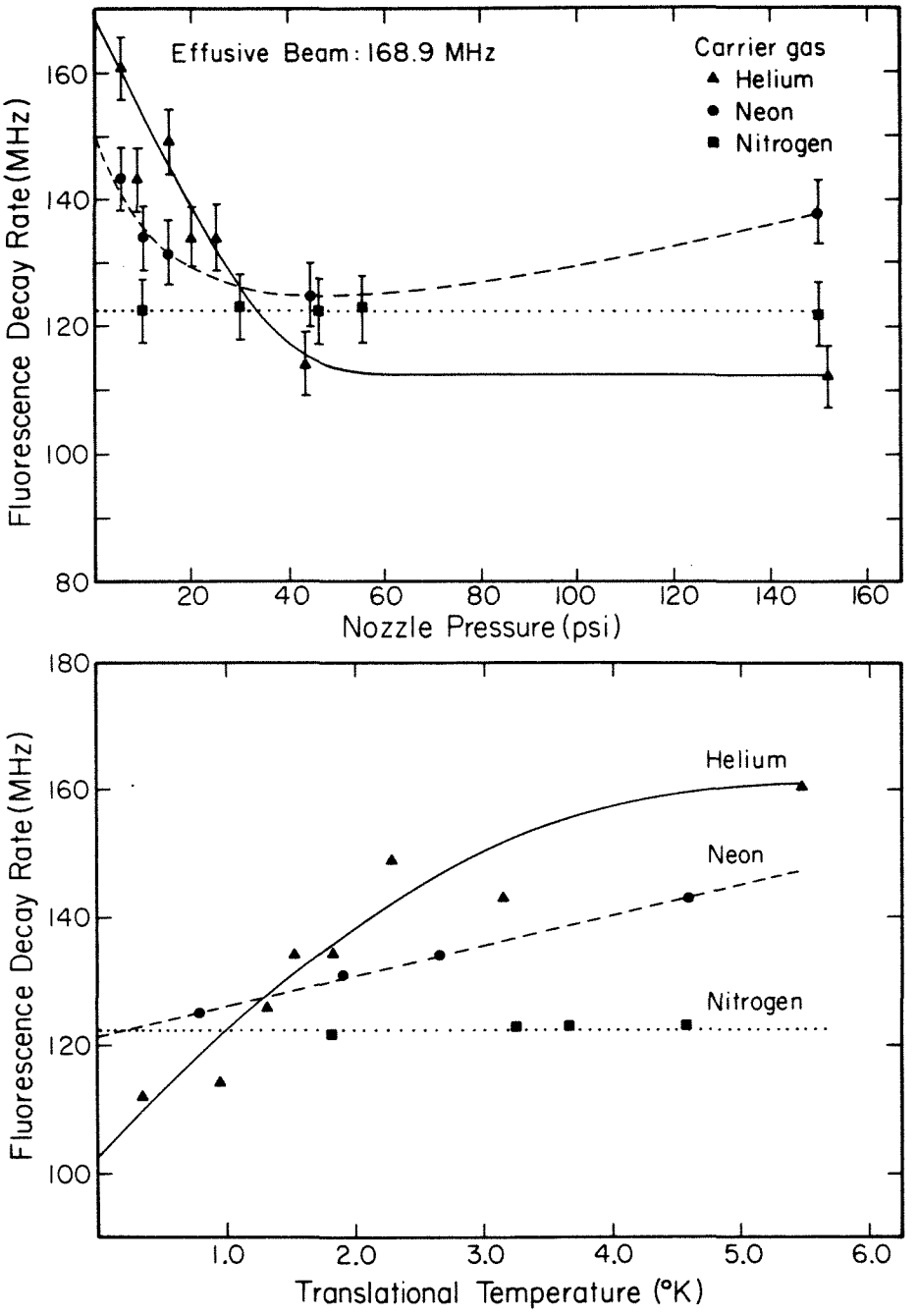

Figure 27.
The influence of the carrier gas and the nozzle backpressure on the fluorescence decay rate. In part b, the data are presented with respect to the terminal translational temperature which is directly proportional to the rotational temperature.

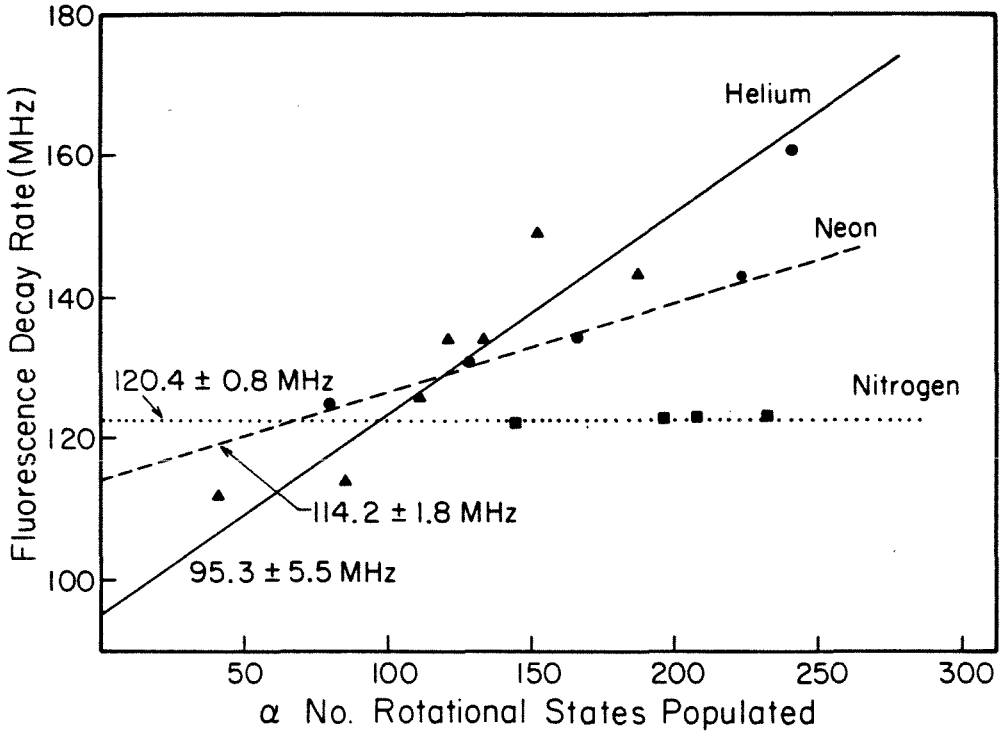

Figure 28.
The fluorescence decay rate as a function of the number of rotational states populated. Linear dependences are obtained for the decay rates of ahthracene in helium, neon and nitrogen expansions. The method used for estimating the number of rotational states populated is discussed in the text.

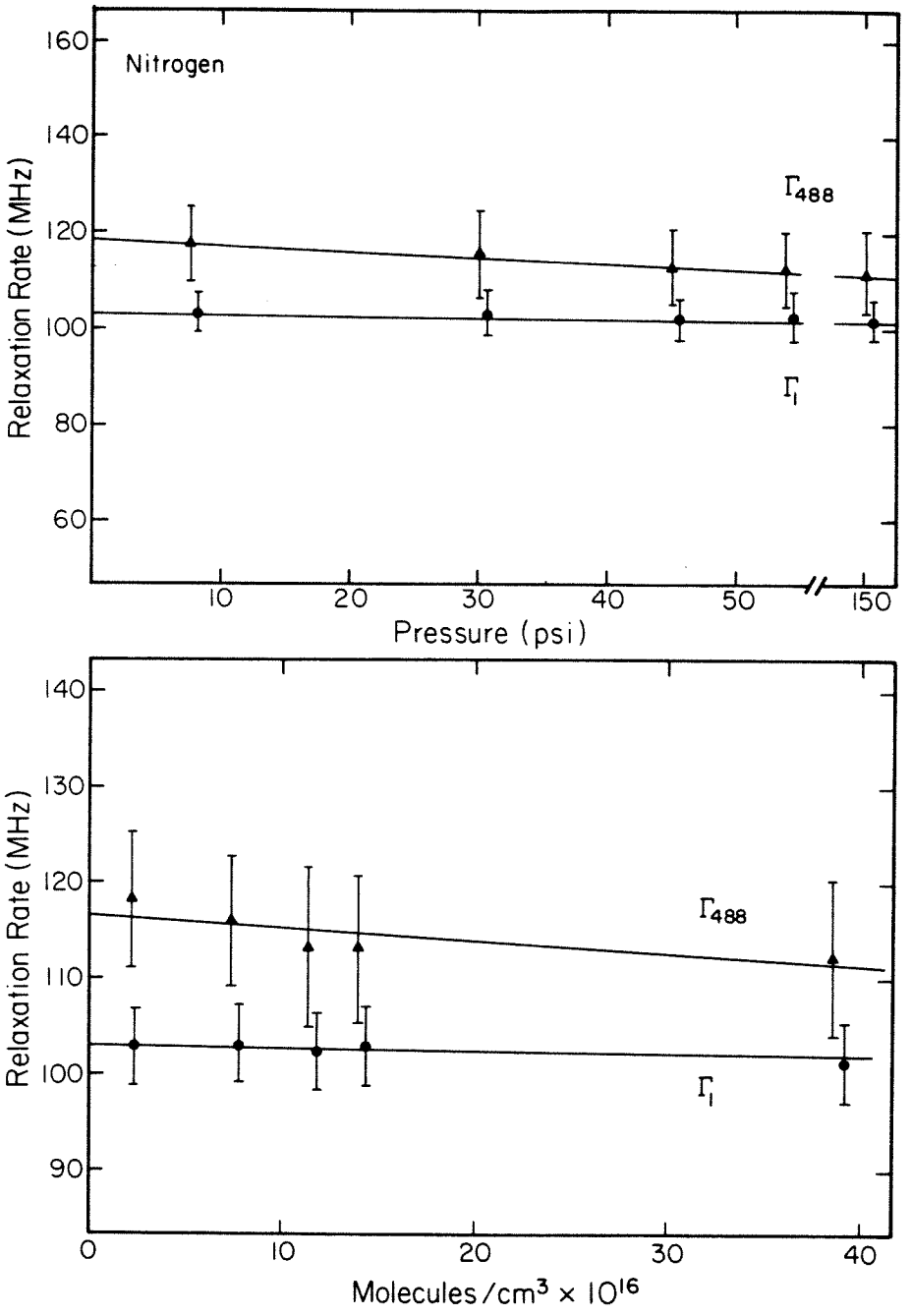

Figure 29.

The fluorescence relaxation rate, Γ_1, and the total dephasing rate, Γ, for anthracene in a nitrogen expansion. The fluorescence relaxation rate was determined from the exponential decay and the dephasing rate was determined from the FWHM of the Lorentzian fit to the Fourier peak and is proportional to the homogeneous linewidth. The relaxation rates do not show a dependence upon the nitrogen backpressure. In the lower section, the decay rates are presented in terms of a Stern-Volmer relationship. The 80% confidence limits are indicated.

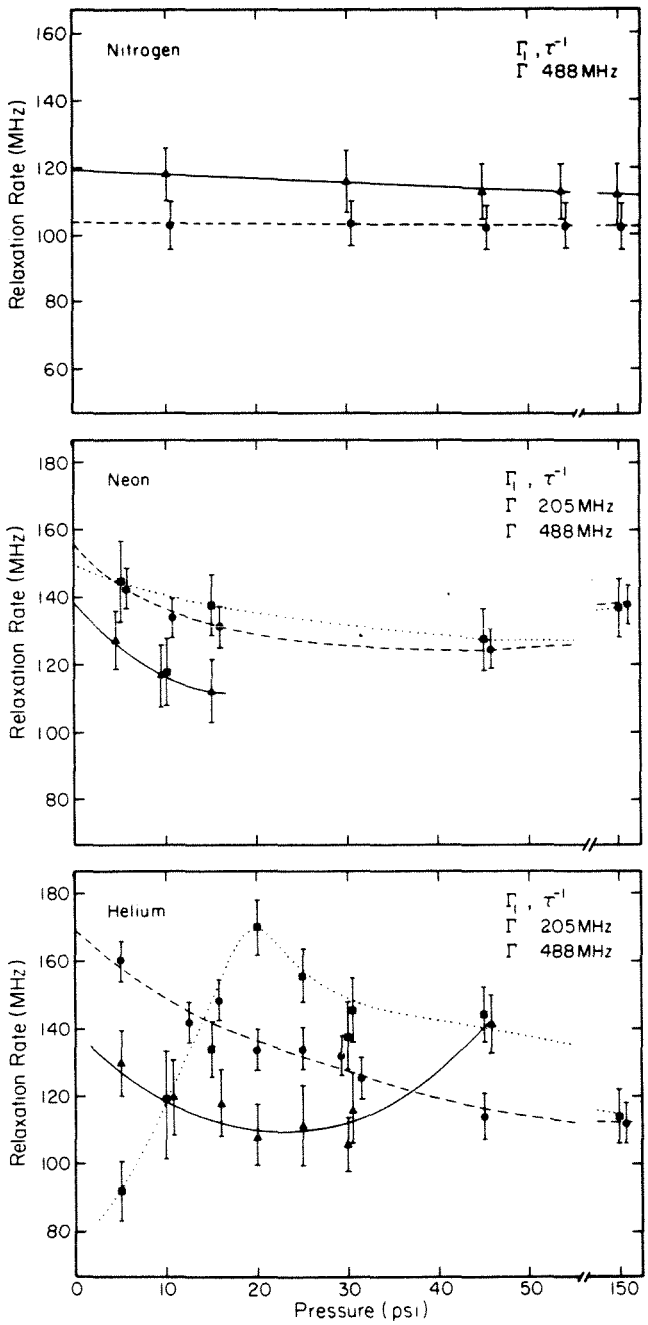

Figure 30.

The characteristic relaxation rates for anthracene in neon (part a) and helium (part b) free jet expansions. The fluorescence decay rate, Γ_1, and the total dephasing rates for the 205 MHz, Γ_{205}, and the 488 MHz, Γ_{488}, Fourier components are presented in terms of the carrier gas backpressure. The 80% confidence limits are indicated. The expansion conditions were: T_0=450 °K, D= 150 microns, X = 5 mm.

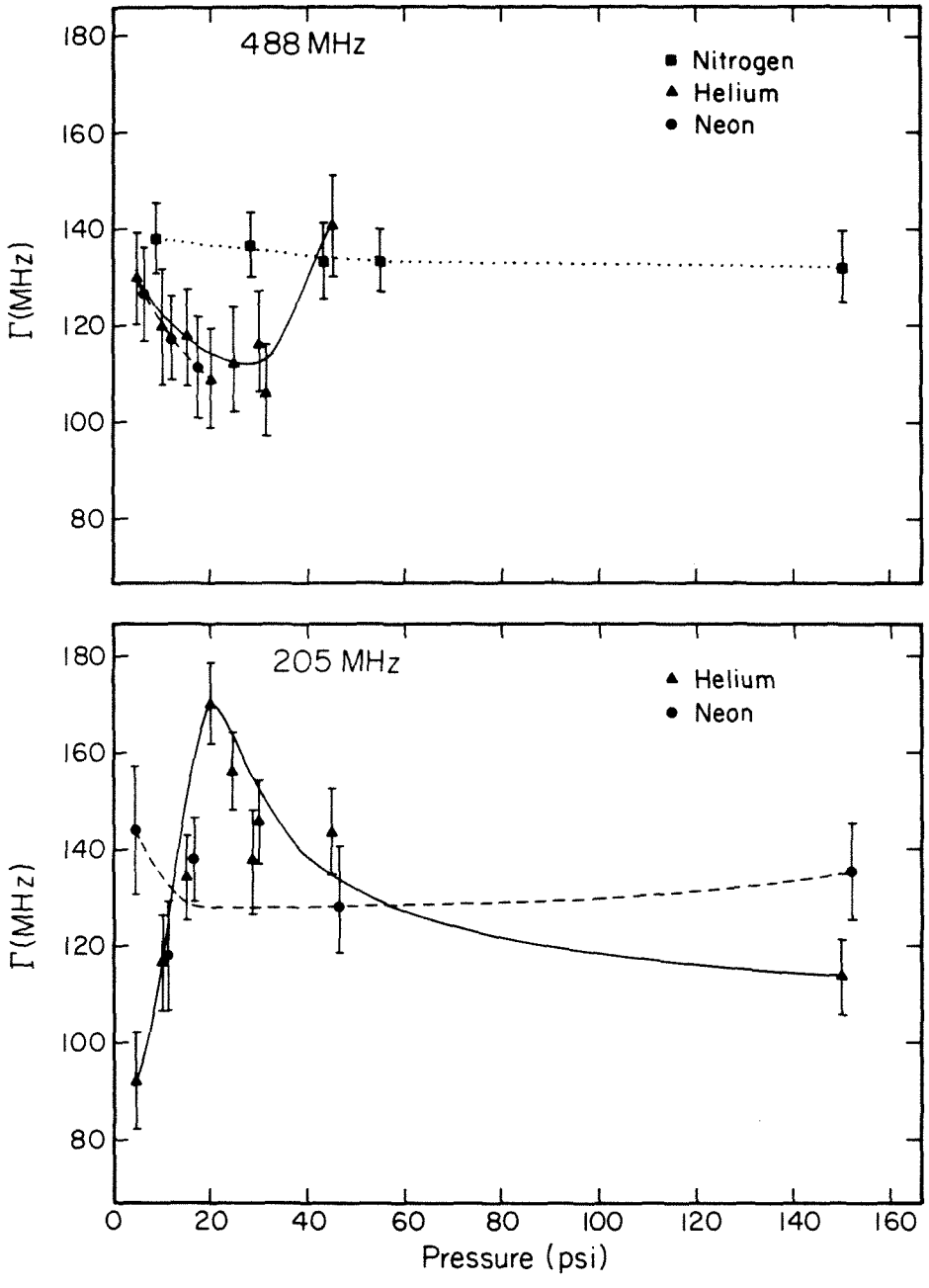

Figure 31.
The pressure dependence of the total dephasing rate for the 488 MHz Fourier component (part a) and the 205 MHz Fourier component (part b) for anthracene in helium, neon and nitrogen expansions. The experimental conditions are the same as those indicated in figure 30. The 80% confidence limits are indicated.

§4.10 APPLICATION OF EXTERNAL FIELDS

§4.10.1 Introduction

The application of external fields in optical steady state experiments using techniques such as level crossing, modulated pumping, and double resonance, has enabled high resolution spectroscopy of Doppler broadened transitions (1). Similar methods have been applied to the transient behavior of the fluorescence signal, where the influence of external fields is manifested in the modulation of quantum beats. Reviews by Haroche (2) and Dodd and Series (3) describe the general theory of and applications to which quantum beat spectroscopy on atomic and small molecules perturbed by external fields has been extended. Magnetic, electric, and radiofrequency fields have been used to modulate the excited state energy level structure in order to obtain information regarding, for example hyperfine structure, and Zeeman splittings.

Recently, following the observation of quantum beats in large molecules (4), the influence of the application of weak magnetic fields on quantum beat patterns observed in aza-aromatics (5) and dicarbonyls (6) has been reported. These experiments have been essential in determining the electronic origin of the interfering states. Due to the large spin orbit coupling in these molecules, the result of an externally applied magnetic field is to perturb the degree of mixing between the singlet and triplet states, primarily as the result of J and dependents shifts in the energies of the triplet states (5). Furthermore, there is evidence that external magnetic fields mix triplet states having different J values in these molecular systems (5), and magnetic field effects on radiationless transitions have been discussed in detail (7,8,9). In an effort to understand the

nature of the eigenstates which are responsible for the interference effects in anthracene, the influence of applied external magnetic, stark and RF fields on the quantum beat pattern was studied. To a first order approximation the anticipated effect of applied static magnetic and electric fields would be to shift the energies of the triplet and singlet states, respectively, and as a consequence, would potentially induce a change in the frequency or number of the characteristic interference component. With regard to the RF field, it is anticipated that if the coupling between/among the interfering eigenstates is the consequence of a direct dipole mechanism, the application of an RF field at the resonance frequency should result in an increased beat modulation depth.

§4.10.2 *Magnetic Field*

The application of a static magnetic field will result in shifts in the energy levels of a molecular system according to the angular momentum associated with the particular states. In the absence of internal orbital angular momentum, the spin-orbit interaction for a fixed magnetic field is proportional to $H \times S$ and will result in spin sublevel energy shifts in addition to the zero field splitting. The influence on the rotational energy levels is given by;

$$E = E_0 - \mu \cdot H - \tfrac{1}{2} H \cdot \chi \cdot H + \ldots\ldots \qquad (4.10.1)$$

where μ is the magnetic dipole moment and χ is the magnetic susceptibility. The effect of the first order Zeeman term is to lift the degeneracy of the m_j levels of a particular J state while the second order term mixes different j states, and for low magnetic fields, shifts the energies of the mixed states according to $| H |^2$. Furthermore, the orientation of the magnetic field with respect to the molecular symmetry axes will deter-

mine which states will become mixed. The application of a magnetic field to molecular systems which exhibit substantial spin-orbit coupling also has been observed to increase the nonradiative decay rate (7,9). This phenomenon has been explained in terms of symmetry modification of the molecular eigenstates and in particular that of the triplet sublevels (7,8), and in terms of second order coupling of orbital and angular momentum (10).

For molecular systems which exhibit quantum beats in the fluorescence decay, the magnetic field induced energy shifts are manifested by specific changes in the quantum beat pattern. In this regard, field dependent frequency shifts, splittings and amplitudes of the Fourier components of the quantum beat pattern have been observed for pyrazine (5). Polarization effects (orientation of the magnetic field with respect to the laser polarization axis and the detection polarization) were not observed in this system, presumably because of rotational reorientation of pyrazine in the free jet expansion on the time scale of the fluorescence decays. The initial importance of observing magnetic field effects on the quantum beats in pyrazine is confirmation of the mixed singlet-triplet character of the molecular eigenstates. With the exception of the work performed in our research group, quantum beats in large molecules have only been observed and studied for molecules which exhibit large spin orbit coupling (aza-aromatics and dicarbonyls), and hence, reflect the mixed singlet-triplet character of the eigenstates involved in the quantum interference. The success of these experiments has relied upon a discrete rotational energy level structure, and as a consequence, at high excess energies the quantum beat phenomenon disappears (11).

The study of magnetic field effects on the quantum beats in anthra-

cene was motivated by our interest in establishing the electronic origin of the eigenstates responsible for the interference. Radiationless transitions in large aromatic molecules are generally postulated as proceeding through interaction with the triplet manifold of states (12). The nonradiative relaxation channels possess a high degree of triplet character owing to the presence of four lower lying triplet origins, and therefore it is not unreasonable to expect magnetic field effects on the relaxation rates in anthracene.

The magnetic field was applied by means of a water cooled Helmholtz coil, calibrated using a gaussmeter (Bell model 610). The laser beam, propagating perpendicular to the magnetic field, crossed the free jet 8 mm from the pinhole. Fields up to 200 gauss could be applied before thermal instability became a problem. In pyrazine, and applied magnetic field of 200 Gauss is capable of producing a frequency shift of 20 MHz in the Fourier component associated with the quantum beats (5).

The application af a static magnetic field did not produce an observed change in any aspect of the energy or time resolved fluorescence of anthracene. There was no observed influence on the energy resolved fluorescence spectrum for 3439.5 A° (S_1 + 1380 cm^{-1}) or 3611.8 A° (S_1, 0-0) excitation. There was also no change in the fluorescence decay rate for excitation to the S1 origin (3611.8 A°) or in the characteristic relaxation rates or modulation depth of the quantum beats. The dependence of the applied magnetic field on the fluorescence relaxation rate and the total dephasing rate are shown in figure 1. Furthermore, the orientation of the magnetic field with respect to the laser or detection polarization did not have an influence on the energy or time resolved fluorescence. The interpretation of the absence of a magnetic field effect

on the quantum beats is complicated by the fact that the number of interacting states which are responsible for the quantum beats in anthracene is not known and is possibly large considering the high density of rotational and vibrational states at S_1+1380 cm^{-1}. This situation is in contrast to the aza-aromatics and dicarbonyl systems where a relatively small number of singlet vibronic and triplet states are coupled. Since there are four triplet states to lower energy than S_1+1380 cm^{-1}, ρ_T is very large and adjustments in the energy levels induced by the external field could have no observable effect on the quantum beats if a large number of states are coupled with the optically prepared state. The purpose here has not been to attempt to shift the triplet spin sublevels of T_4 into resonance (which would certainly not be possible with the small magnetic fields available). The direct mixing of triplet state sublevels with the singlet manifold should not be necessary in order to observe a magnetic field dependence on the quantum beats in anthracene. If the interaction of the eigenstates is similar to that for the singlet-triplet mixing of 'discrete' eigenstates, which is accomplished with magnetic fields of only a few gauss. From these experiments it can be concluded, that either the eigenstates responsible for the quantum beats in anthracene are not of mixed singlet-triplet character, or, that there is coupling between a large number of $|J,M>$ levels in both the singlet and triplet manifolds which in turn exhibit interference effects.

§4.10.3 *Stark Field*

By analogy with the description for the energy levels of a molecule perturbed by an applied magnetic field, the energies in an applied electric field are given by (13);

$$W = W_0 - D\cdot E - \tfrac{1}{2}E\cdot\alpha\cdot E - \ldots\ldots \qquad (4.10.2)$$

where $D_\alpha = -\left(\frac{\partial \omega}{\partial E_\alpha}\right)$ is the electric dipole moment and $\alpha_{\alpha\beta} = -\left(\frac{\partial^2 \omega}{\partial E_\alpha \partial E_\beta}\right)$ is the polarizability tensor. Since anthracene is non-polar in both the ground and S_1 $^1B_{2u}$ excited state (14,15), the first non-zero term in the field induced correction to the energy is determined by the polarizability tensor, which relates the difference in polarizability of the $^1A_{1g}$ ground state and $^1B_{2u}$ excited states. Contributions due to electric field induced mixing with other singlet states is expected to be negligible. The nearest singlet state of opposite parity (^1B_1g) is calculated (16) to be approximately 10,000 cm^{-1} to higher energy than the $^1B_{2u}$ state, far beyond the energy difference for which electric field induced mixing has been observed (15,16). In order for an applied electric field to influence the pattern of the quantum beats by means of energy level shifts it would be necessary for the, nominally, two interfering states to exhibit measurable different electric polarizabilities. Stark shifts of 5 to 45×10^{-3} cm^{-1} (0.15 to 1.35 GHz) have been observed for the 0-0 transition of the $^1B_{2u} \leftarrow {}^1B_{1g}$ transition of anthracene in naphthalene at cryogenic temperatures for an applied field of 10^{-5} volts/cm (15).

The Stark plates were mounted 1 cm apart such that the free jet and the laser beam could cross orthogonally and unhindered. The closest distance between the teflon mount for the Stark plates and the nozzle assemble was approximately 2 mm. Interference of the mount with the free jet expansion was not a problem as determined by the observation of typical quantum beat patterns. The Stark electrodes were made from quartz plates with dimensions of 30 mm × 10 mm × 1.5 mm. Since in this configuration fluorescence is collected through the Stark plates, it was essential to design the conductive electrode surface such as to have a maximum transmittance in the near UV. For this reason, a thin gold film

(50 A° thick) was deposited on the surface and the ends reinforced with contact pads (11,16). The plates were 50 % transmittive in the wavelength range of interest and a field of 4 KV/cm could be applied before arcing occurred.

The results of electric field application on the relaxation rates and modulation depth of the quantum beats is shown in figure 2. Based upon the low magnitude of the Stark shifts observed in the anthracene mixed crystal work of Hochstrasser et al. (15), the corresponding second order Stark shift for an applied field of 4KV/cm would be between 0.25 and 2.00 MHz, and well below the resolution with which differences in beat frequencies could be observed in our experiments. Furthermore, the absence of an electric field effect is not unexpected considering that the optically prepared singlet states are associated with only the $^1B_{2u} \leftarrow {}^1A_{1g}$ transition and hence exhibit similar polarizability tensors.

§4.10.4 Radiofrequency Field

When an oscillatory external field is applied to a coherently prepared superposition of states which are coupled by a dipole matrix element at a frequency commensurate with the reciprocal of the energy between the two states, population will be driven coherently between the two states. Unlike optical double resonance experiments where the optical excitation is incoherent and the application of an RF field subsequently creates a coherent superposition of states (20,21) which in turn is detected by observing modulation in the fluorescence decay, the result of an RF field interaction with a system prepared by a laser is determined by the optical transition properties of the eigenstates. The modulation depth of the quantum beats observed in the fluorescence will be determined by the relative difference in the optical dipole matrix elements. The larger the

difference between the radiative dipole moments of the states coupled by the RF field, the larger will be the modulation depth of the quantum beat signal. On the other hand, if the coupled states are prepared with nearly the same initial population, the effect of the RF field will be simply to drive the population between the coupled states and no change in the beat modulation depth would be expected. Therefore, application of an RF field to an optically and coherently prepared system will provide information regarding the presence of a magnetic dipole coupling matrix element between/among the excited hyperfine levels (1), and the relative optical dipole matrix elements for emission.

The RF coil with dimensions of 20 mm × 10 mm was mounted such that the free jet passed along the axis of the coil. The coil was tuned to 400 MHz with a tapped-parallel tuned circuit soldered onto the coil (22). The coil was center tapped with the opposite ends grounded to enable the laser to more easily pass through the coils. The Q of the circuit was 20, and was in part determined by the proximity of the coil to the metal nozzle assembly. The RF source and amplifier provided a peak field intensity of $\sim 10^{-3}$ Oersted. As anticipated, the application of an RF field did not change the quantum beat modulation depth or the fluorescence relaxation rates. As was the case for the application of the Stark field, this result is more than likely accounted for by the fact that the interfering eigenstates belong to the same electronic manifold and therefore dipole transitions coupling the states are forbidden.

§4.10.5 *Conclusion*

There is no obvious influence of external fields on the quantum beats in anthracene. Indeed, it is reasonably argued that even if intramolecular interactions which were influenced by external fields did exist, owing to

the large density of excited states (both optically and nonoptically active) the manifestation would be subtle at best. The most definite conclusion which can be reached with reference to these experiments concerns the absence of magnetic field effects. Regardless of the intramolecular coupling mechanisms, the reasons for the appearance of quantum beats in anthracene upon excitation to high excess energies is not as straightforward as is the situation with the aza-aromatics and dicarbonyls where mixed singlet-triplet states are definitely responsible for the interference effects.

REFERENCES

1. For example see A. Corney, *Atomic and Laser Spectroscopy*, Clarendon Press, Oxford, 1977: and C.H. Townes and A.L. Schawlow, *Microwave Spectoscopy*, Dover Publications, New York, 1975.

2. S. Haroche, Topics Appl. Phys., **13,** 256 (1976).

3. J.N. Dodd and G.W Series, *Progress in Atomic Spectroscopy*, ed. W. Hanle and H. Kleinpoppen, Plenum, London, 1977.

4. J. Chaiken, T. Benson, M. Gurnick and J.D. McDonald, Chem. Phys. Lett., **61,** 195 (1979).

5. P.M. Felker, W.R. Lambert and A.H. Zewail, Chem. Phys. Lett., **89,** 309 (1982).

6. W. Henke, H.L. Selzle, T.R. Hayes, S.H. Lin and E.W. Schlag, Chem. Phys. Lett., **77,** 448 (1981).

7. H.G. Kuttner, H.L. Selzle and E.W. Schlag, Israel J. Chem., **16,** 264 (1977).

8. P.R. Stannard, J. Chem. Phys., **68,** 3932 (1978).

9. C. Michel and C. Tric, Chem. Phys., **50,** 341 (1980).

10. W. Strek, Chem. Phys., **61,** 611 (1979).

11. J. Chaiken, M. Gurnick and J.D. McDonald, J. Chem. Phys., **74,** 106 (1981).

12. C.-S. Huang, J.C. Hsieh and E.C. Lim, Chem. Phys. Lett., **28,** 130 (1974).

13. W.H. Flygare, *Molecular Structure and Dynamics*, Prentice Hall, New Jersey, 1978.

14. J.W. Sidman, J. Chem. Phys., **25,** 115, 122 (1956).

15. R.M. Hochstrasser and C.M. Klimcak, Mol. Cryst. Liq. Cryst., **58,** 109 (1979).

16. Y.B. Malykhanov, Opt. Spectrosc., **43,** 254 (1977).

17, R.M. Hochstrasser, L.W. Johnson and H.P. Trommsdorf, Chem. Phys. Lett., **21,** 251 (1973).

18. *American Institute of Physics Handbook*, McGraw Hill, New York, 1972.

19. We would like to thank Dean Neikirk for his advice and the use of his vacuum deposition apparatus.

20. J.N. Dodd and G.W. Series, Proc. Chem. Soc., **263A,** 353 (1961).

21. J.N. Dodd, G.W. Series and M.J. Taylor, Proc. Chem. Soc., **273A,** 41 (1963).

22. H.L. Krauss, C.W. Bostian and F.H. Raab, *Solid State Radio Engineering*, Wiley, New York, 1980: and *Reference Data for Radio Engineers*, Sams and Co., New York, 1975.

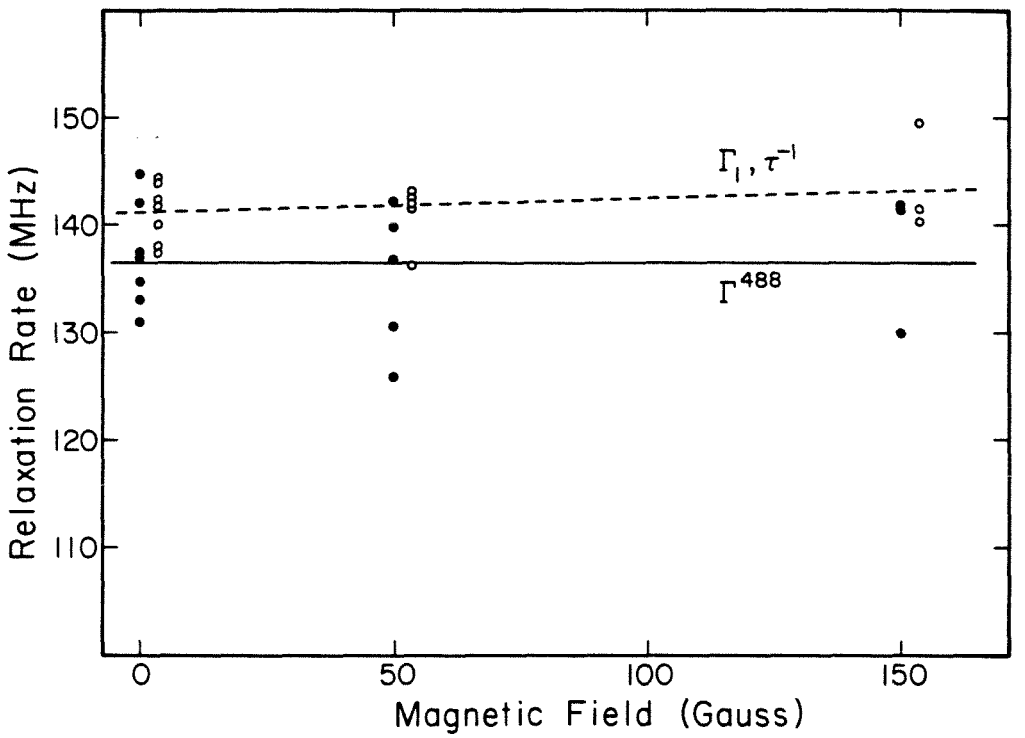

Figure 1.

Magnetic field dependence of the relaxation rates for 3439.6 A° (S_1 +1380 cm^{-1}) excitation. The relatively large difference in the relaxation rates for a given field strength is in part due to the fact that these experiments were performed on several different days and therefore reflects slight changes in the fee jet expansion conditions. The experimental conditions were as follows: 45 psi nitrogen, T_0 = 450 °K, D= 150 microns, X = 10 mm. The fluorescence and total dephasing relaxation rates are identical within the calculated uncertainty.

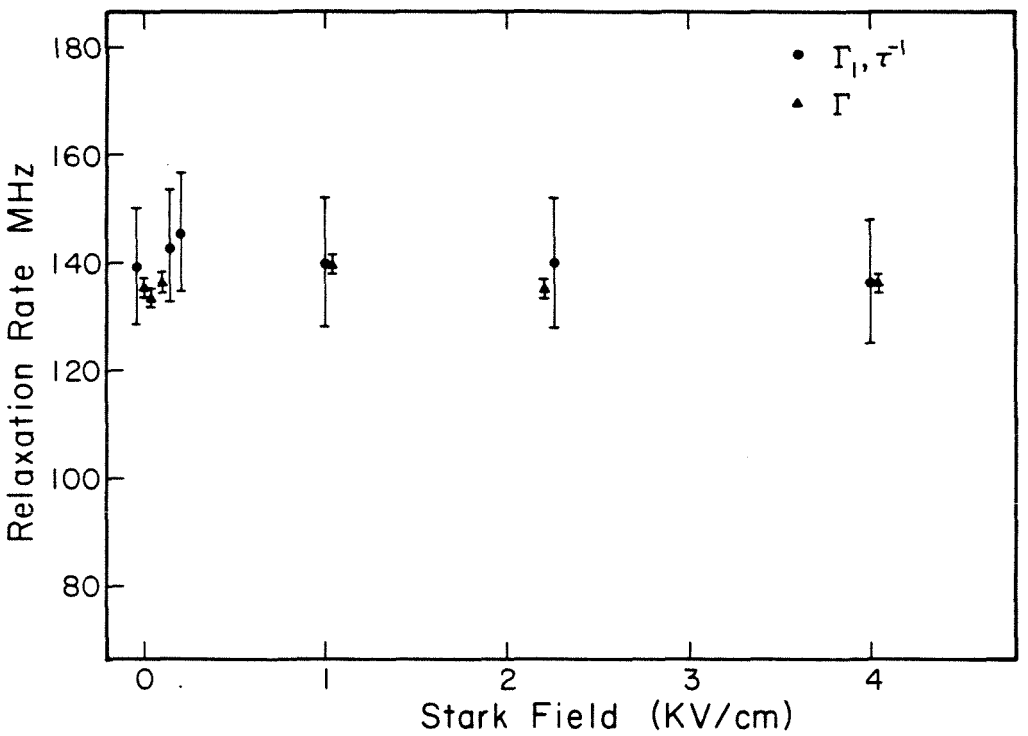

Figure 2.
Stark field dependence of the characteristic relaxation rates and modulation depth of the quantum beats. The parameters for excitation to 3429.6 A° (S_1 +1380 cm^{-1}) are independent of the electric field strength. The experimental conditions are the same as those indicated in figure 1.

§4.11 Conclusion

The combination of picosecond laser spectroscopy and free jet techniques has revealed new properties of the intramolecular dynamics of isolated large polyatomic molecules. Previously, the investigation of intramolecular dynamics in large molecules at high excess energies was primarily relegated to an indirect treatment afforded by the analysis of resolved fluorescence spectra while direct observation of temporal evolution was limited by the nanosecond pulse width of the laser excitation. Upon picosecond coherent preparation of a limited set of molecular eigenstates within the large density of vibronic levels, ~1380 cm^{-1} above the origin of the first excited singlet state of anthracene, we have documented the appearance of quantum interference effects in the energy resolved fluorescence decay. The damping rate of the oscillatory component is to a first approximation equivalent to the fluorescence decay rate, being approximately 130 MHz. An upper limit for the homogeneous linewidth of the eigenstates as inferred from the beat frequency is approximately 250 MHz. The observation of quantum beats establishes the quasi-discrete character of the level structrure in a large polyatomic molecule at this excess energy, and is a manifestation of selective vibronic interactions.

In as much as the expansion conditions influence the intramolecular dynamics, an understanding of the hydro- and thermodynamics of free jet expansions is essential. Our motivation has been to understand the dynamics of intramolecular energy and phase redistribution by means of radiative and especially nonradiative processes. At present, a rigorous understanding of free jet expansion dynamics for large molecules has not been developed. As a consequence, in this study we have been resigned to

balance the discussion of intramolecular dynamics while confronted with an imperfect knowledge of the influence of free jet dynamics. In order to take full advantage of and to realize the full extent of the quantitative information afforded by analysis of quantum interference effects in large molecules, a quantitative understanding of beam dynamics is imperative. To this purpose the rotational temperature, vibrational temperature, complex formation, and intermolecular collision processes of anthracene in a free jet expansion are discussed.

In an effort to understand the nature of the states responsible for the quantum interference effects, we have undertaken a number of studies including, chemical substitution, application of external fields, and modification of the free jet expansion conditions (internal temperatures). The most revealing information was obtained from vibrational analysis of the energy resolved fluorescence spectra and by the carrier gas and backpressure dependent changes in the Fourier components of the quantum beat pattern. The importance of the vibrational properties of the wavefunction are implied by the appearance of quantum beats for a unique excitation wavelength, the necessity to frequency resolve the fluorescence decay, and by the appearance of the 237 cm^{-1} vibration in the energy resolved fluorescence only for the excitation energy at which beats are observed. The nominal zero-order vibronic level which is coherently prepared by the ~10 psec laser pulse is a strongly optically allowed b_{3g} fundamental at 1380 cm^{-1} above the electronic origin of the first excited singlet state. The failure to observe a temporal evolution of the energy resolved fluorescence with a 100 psec window, or to document biexponential decays indicates that the populations which are monitored are established subsequent to intramoleuclar vibrational redistribution.

The appearance of a 237 cm^{-1} b_{2u} vibration in the energy resolved fluorescence as well as quantum beats on specific transitions, most notably on the a_g 387 cm^{-1} and 1125 b_{1u} cm^{-1} fundamentals and combinations thereof, imply specific interference among vibronic levels. The observation of quantum beats does not necessarily imply coupling between states since it is sufficient that two eigenstates be coherently prepared and be radiatively coupled to a common lower energy state in order to produce interference effects. Anharmonic coupling is invoked as a means to explain the common radiative properties of the eigenstates which are responsible for the quantum beats, and the acquisition of substantial oscillator strength by the generally inactive b_{1u} and b_{2u} vibrations.

The importance of the rotational level structure is suggested by the carrier gas and pressure effects on the Fourier components of the beat pattern. This phenomenon was especially evident for helium-anthracene expansions where a dominant component at 205 MHz became reduced simultaneously with the increase in a 488 MHz component as the backpressure was reduced from 150 to 5 psi. Changes in the expansion conditions influence the intermolecular collisional rates within the free jet, the intramolecular rotational and vibrational temperatures, and the formation of vdW complexes. Collisional effects and complex formation have been determined to be significant only to the extent that the internal temperatures are perturbed. Thus, the formation of weak complexes in the nitrogen-anthracene expansion ensures that the 488 MHz Fourier component persists at all backpressures. It is difficult to explain the multiple Fourier components seen in helium and neon expansions solely on the basis of vibrational temperature since the vibrational temperature

is measured to change very little over the pressure ranges studied. A more probable explanation resides in the influence of the rotational temperature. The impact of rotational temperature can arise from modification of the spectral overlap of rotational envelopes or from the contribution of different $|J,K>$ rotational populations. Therefore, in view of the present results, it seems appropriate to consider the quantum beats as arising from rotational properties of selective vibronic states.

In contrast to the isolated occurence of quantum interference phenomena in anthracene, in trans-stilbene, we also observe quantum beats in the fluorescence decay for a number of transitions appearing in the energy resolved fluorescence for excitatiton between 500 and 1200 cm^{-1} above the S_1 origin. These results are reported in the subsequent paper. Clearly, further experiments incorporating greater temporal and spectral resolution are indicated for understanding the nature of the eigenstates responsible for the interference effects. Aside from the aspects of quantum interference effects being a manifestation of high resolution spectroscopy and in as much as the damping rate of the oscillatory decay reflects the homogeneous properties of the molecular eigenstates, quantum beats can be used as a means for investigating the dynamics of inelastic and elastic, energy and phase relaxation and redistribution in large molecules.

5. *QUANTUM BEATS AND VIBRATIONAL REDISTRIBUTION IN TRANS- STILBENE*

Abstract

Quantum beats appear in the time and energy resolved fluorescence of trans-stilbene free jet expansions upon picosecond laser excitation to a number of transitions between 500 and 1200 cm^{-1} of excess vibrational energy above the first excited singlet state. The beat frequencies are consistently 734 MHz except for excitation to the 780 cm^{-1} vibration which exhibited a 1309 MHz component. The persistence of the beat frequency over this relatively wide excess energy range is discussed in terms of vibrational motion.

§5.1 *Introduction*

In recent years, quantum interference effects have been observed for a number of large molecules(1,2,3). The application of supersonic free jet expansion techniques has enabled the production of isolated molecules with thermally cooled ground state rotational and vibrational populations which has allowed a coherent preparation of a finite number of molecular eigenstates. In the majority of cases, represented by the studies on aza-aromatics and dicarbonyls, quantum beats are observed in the time resolved, spectrally integrated, fluorescence upon excitation to low excess energies (<1000 cm-1) above the first excited singlet state (2,3). For these molecules, the quantum interference phenomenon has been confirmed to arise as a consequence of the mixed singlet-triplet character of the molecular eigenstates (2). Recently, in this laboratory, by combining picosecond laser excitation and supersonic free jet techniques, quantum beats have been observed in the energy resolved fluorescence decay of anthracene (1,4). In contrast to the discrete level structure characteristic of the excess energies for which interference effects have been documented for the aza-aromatics and dicarbonyls, the level structure at 1380 cm-1 of excess vibrational energy in anthracene is complicated by the essentially statistical distribution of rotational and vibrational density of states. The predominant features of the energy resolved fluorescence reflect the consequences of intramolecular vibrational redistribution. The implications of this result are significant with regard to the concepts of intramolecular phase and energy redistribution and relaxation in large molecules. Not only does the documentation of interference effects establish the quasi-discrete nature of the molecular eigenstates at relatively large excess vibrational energies, but quantum interference

effects present a means of probing the specific mechanisms of vibronic coupling in large molecules. The interfering states are effectively projected out of all other states by means of similar emission matrix dipole elements. A complete understanding, however, of the vibronic character of the eigenstates responsible for the interference effects in anthracene is at present not established (4).

The photoisomerization of substituted ethylenes is a fundamental problem in chemistry (5) and in particular the photophysical processes associated with the trans-cis isomerization of stilbene is a subject of considerable current interest (6,7). Recent evidence locates the threshold for torsional rotation of the ethylenic bond at an excess energy approximately 1200 cm-1 above the first excited singlet, ^1B_u* state (7). In addition, the dynamics and spectroscopy of trans-stilbene reflect the high density of states existing at moderate excess energies as a consequence of several low frequency torsional modes associated with the twisting of the phenyl groups with respect to the ethylenic plane. In conjunction with our studies regarding the specific mechansim responsible for stilbene photoisomerization (7) we have observed quantum beats in the energy and time resolved fluorescence. In contrast to anthracene, where quantum interference effects were observed only for a single excitation wavelength (1,4), several transitions between 500 cm-1 and 1200 cm-1 exhibit oscillatory components in the resolved fluorescence. The widespread distribution of quantum beats observed in the energy resolved fluorescence of trans-stilbene suggests a common vibronic origin for the interfering eigenstates. Our present interpretation implicates the association of phenyl torsional modes with the interference phenomena observed in trans-stilbene.

§5.2 *Experimental*

The experimental apparatus consisting of a synchronously pumped cavity-dumped picosecond dye laser and a supersonic free jet apparatus was similar to that previously described (1). The laser bandwidth, obtained using an intracavity two plate birefringent filter and fine tuning etalon was measured to be 0.5 A° (coherence width, 3 cm^{-1}). Trans-stilbene (zone refined or scintillation grade, Kodak) heated to 80 °C was expanded through a 150 micron pinhole with a 35 psi back pressure of helium or neon. The distance from the laser excitation region to the nozzle was 5 mm. The fluorescence was collected with f/1 imaging optics and resolved with a microprocessor controlled scanning monochromator. Data were acquired using time correlated photon counting techniques and accumulated with a multi-channel analyzer prior to transfer to a PDP 11/23 computer. Analysis of the fluorescence decays which exhibited beats was accomplished by convoluting the experimental data with the system response function to obtain the best least squares fit to a single exponential decay, and subsequently Fourier transforming the unweighted residual.

§5.3 *Results*

Even at the reduced internal temperatures as produced in a free jet expansion, the spectroscopy of trans-stilbene is complicated by the presence of several low frequency carbon-phenyl torsional and carbon(ethylene)-phenyl torsional and phenyl bending modes. In addition to these modes which have previously been calculated (8) and observed (9) we also see evidence for vibrations at 16 cm^{-1} and 28 cm^{-1} in the free jet expansion. The frequencies and assignments for the ground and excited state vibrations are presented in Tables 1 and 2, respectively. The

excited state vibrations have only been included up to 300 cm^{-1} and mainly serve to demonstrate the congested level structure which exists at even low excess energies. Above 500 cm^{-1} the spectrum becomes very congested even with 0.25 A° resolution and therefore single vibronic level excitation would be compromised. The prominent low frequency excited state vibrations which we observe appear at 70, 83, 94, 174, 186, 194, 223, 228, 282, and 295 cm^{-1}. The 40 cm^{-1}, 70 cm^{-1}, and 94 cm^{-1}, vibrations probably correspond to the calculated phenyl torsional modes of a_u and b_u symmetry. The other transitions may be assigned to combination bands of the torsional fundamentals, however, in this case they exhibit anomalously large intensities, being comparable to that of the fundamentals.

The energy resolved fluorescence spectra reflect the large number of low frequency modes. In figure 1, the energy resolved fluorescence spectra for excitation to a number of vibronic levels between 0 cm^{-1} and 1342 cm^{-1} of excess energy above the first excited, ^1B_u*, singlet state are presented. The spectra are characterized by a combination of unrelaxed and relaxed fluorescence components beginning at S_1+182 cm^{-1}, until upon excitation to S_1+1342 cm^{-1}, only relaxed fluorescence features are observed. In comparison, completely relaxed fluorescence is not observed in anthracene until excitation around 3500 cm^{-1} above the S_1 origin. The apparent increasing contribution of a broad fluorescence component with increasing excitation energy appears to be a consequence of spectral congestion and insufficient spectral resolution. Throughout this excess energy region the fluorescence decay rate for the relaxed component was similar to that of the S_1 origin, being 370 MHz (2.7± 0.1 nsec). Above ~1200 cm^{-1} the fluorescence decay rate continuously increases and is

interpreted as being indicative of the onset for the isomerization process (7).

Quantum beats were observed in the energy resolved fluorescence upon excitation to specific vibrational modes corresponding to excess energies between 500 cm^{-1} and 1200 cm^{-1} above the first excited singlet $^1B_u^*$ state origin. The energies of the transitions above S_1 are, 491 cm^{-1}, 747 cm^{-1}, 804 cm^{-1}, 847 cm^{-1}, 978 cm^{-1}, 1055 cm^{-1}, and 1189 cm^{-1}. The respective energy resolved fluorescence spectra are presented in figure 1. Quantum beats only appeared on features associated with the unrelaxed fluorescence component corresponding to progressions built on the (0,1) transition. The (0,1) transition which appears at the excitation wavelength and is equivalent to what will be termed the resonance fluorescence. Many transitions in the energy resolved fluorescence for which quantum beats were observed occurred in the region which exhibited features associated with both the relaxed and the unrelaxed fluorescence component. Definite assignment of these transitions was prevented by the combination of spectral congestion and low spectral resolution. Nevertheless, oscillatory fluorescence decays were only observed, if at all, on sharp spectral features. The beat modulation depth was always largest for the resonance fluorescence.

The time resolved emission for the resonance fluorescence component at a number of excitation energies is presented in figure 2. The quantum beat pattern is essentially defined by the system response function, figure 3. The modulation depth of the quantum beats depends upon the internal vibrational and rotational temperature, figure 4, and is explained by the fact that at lower temperatures the number of states which lead to destructive interference of the oscillatory component is

reduced. An example of the best fit to a single exponential decay, and the Fourier transform of the residual is presented in figure 5. Except for the 804 cm^{-1} excitation which exhibited a dominant Fourier component at 1309 MHz (763 psec), the major oscillatory frequency was 734 MHz (1.36 nsec). For excitation and detection at an energy corresponding to S_1+624 cm^{-1}, a single exponential decay was observed and is presented for comparison with the quantum beat patterns. Single exponential fluorescence decays were documented for excitation to many transitions appearing in this excess energy region, and therefore, the interference effects are not ubiquitous, but must reflect specific properties of the vibronic and radiative intrastate coupling associated with the optically prepared states. The excitation energies (relative to the S_1 origin), possible assignments, and the characteristic beat frequencies are presented in Table 3. The 1166, 1038, 961, 846, and 748 cm^{-1} vibrations correspond to previously observed and calculated (8,9) frequencies for totally symmetric C-C-H and C-C-C bending motions of the phenyl ring. The 804 and 491 cm^{-1} transitions have previously been assigned (9) as combination bands according to (2×298 + 208 cm^{-1}) and (283 + 208 cm^{-1}), respectively. In view of the large number of low frequency torsional modes in trans-stilbene, it is not unreasonable to expect many combination bands to be quasi-energetic with these specific vibrations. Although it is therefore not surprising that the excited state vibrations for which quantum beats were observed are separated by frequencies characteristic of the ethylene-phenyl torsional vibrations (40, 70, and 94 cm^{-1}) and combinations thereof, this fact suggests that common vibrational properties of the excited levels are associated with the interference effects.

With reference to figure 2, the fluorescence decay rates are seen to

be slower for transitions which do not exhibit deeply modulated beat patterns. The fluorescence decay rates are presented in table 4. Below 600 cm^{-1} the decay rate is relatively constant at 380 MHz. Above 1200 cm^{-1} the decay rate increases dramatically, achieving values on the order of 500 GHz at 3000 cm^{-1} of excess vibrational energy (5). The values for the decay rates in the excess energy region around 1000 cm^{-1} reflect the quasi-discrete nature of the energy level structure. For a given excitation energy the fluorescence decay rate was independent of the detection wavelength, except in the region for which quantum beats were observed. For these transitions the decay rate of the resonance fluorescence was faster than that of transitions embedded within the region of the relaxed fluorescence despite the presence of oscillatory components. When quantum beats were observed on discrete transitions appearing in the congested spectral region of the relaxed emission component, the modulation depth was always less than that observed for the resonance fluorescence. This is attributed to the fact that within the detection bandwidth contributions from non- interfering states with apparently slower fluorescence decay rates are observed and serve to obscure the quantum interference effects. A slower decay rate for the relaxed fluorescence may reflect the mixed singlet-triplet character of the eigenstates.

For excitation to the S_1+780 cm^{-1} transition, quantum beats with a frequency of 1309± 10 MHz were observed on many transitions in the energy resolved fluorescence. These transitions and the time resolved decays are presented in figure 6. It can be seen that the beats are only observed on major transitions. The most intense transitions correspond to fundamentals of totally symmetric C-C-C and C-C-H bending vibrations localized on the phenyl ring. Although the modulation depth does change,

the beat frequency remains constant. The change in the beat modulation depth with the detection wavelength can be attributed to variable contributions to the fluorescence which arise from the non-interfering states.

§5.4 *DISCUSSION*

§5.41 *Spectral Features, Relaxation Rates, and Quantum Beats*

The observations which were previously emphasized serve as a basis for understanding the vibrational relaxation process in trans-stilbene. Several theoretical treatments of intramolecular vibrational redistribution dynamics which can be used as a context in which to discuss the vibrational relaxation mechanisms in trans-stilbene appear in the literature (10). The presence of quantum beats in the fluorescence implies that trans-stilbene dynamics should be discussed in terms of intermediate case level structure reflecting the quasi-discrete nature of the molecular eigenstates. The resolved fluorescence spectra are characterized by three distinct features: 1) direct, unrelaxed fluorescence with progressions originating at the excitation wavelength, 2) sharp, relaxed fluorescence features characterized by red-shifted progression origins, and 3) apparently broad relaxed fluorescence features. The broad component may be interpreted in terms of spectral congestion. In the context of a zero order level description, for all transitions to the intermediate excess energy region, the laser initially prepares various combination and fundamental vibronic states depending upon the specific dipole matrix elements to the electronic ground state origin. As phase and energy redistribution occur, the bath modes, distinguished by the radiative matrix elements characteristic of relaxed fluorescence features, become populated at the expense of specific excited state vibrational quanta. That the

relaxed states exhibit a non-statistical coupling with the prepared states is exemplified by the appearance of sharp features in the energy resolved fluorescence spectra. The selective nature of the intrastate coupling is best exemplified by considering the anomalous relaxation dynamics of the 780 cm^{-1} mode relative to that of nearby modes as indicated by the comparatively long lifetime (2.49 nsec) of the resonance fluorescence and the persistence of the quantum beats at 1309 MHz. In terms of the molecular eigenstates description (10) the unrelaxed fluorescence features are distinguished by the nature of the radiative properties of the molecular eigenstates which are established upon diagonalization of the zero order Hamiltonian and the intrastate coupling.

For excitation to the energies at which quantum beats were observed, the decay rate of the resonance fluorescence is faster than that for both the sharp and broad features associated with the relaxed fluorescence (table 4). In order for the fast decay observed for the resonance fluorescence to be interpreted in terms of initial dephasing in the intermediate level case, one would expect to observe a buildup in the intensity of the relaxed fluorescence prior to the longer radiative decay component. In our experiments, we do not observe a temporal evolution of the energy resolved fluorescence spectra, and therefore dephasing must be completed on a time scale which is slower than the 250 psec system response time. The fast decay rate of the resonance fluorescence must therefore be attributed to an accidental difference in the relaxation rate compared to that of the unrelaxed component.

Above 1200 cm^{-1} unrelaxed fluorescence features are no longer observed and the fluorescence decay rate increases dramatically due to an increase in the non-radiative relaxation rate. There is evidence that

the threshold for significant trans-cis isomerization appears at this excess energy (7) as the consequence of the proximity of the S_2 ^1A_g* manifold brought about by torsional rotation of the ethylene bond. It is not known specifically how the S_2 isomerization manifold becomes populated, although it is presumed to occur via coupling with torsional modes of the S_1 excited state surface (11).

The widespread distribution of quantum beats in the energy resolved fluorescence of trans-stilbene is in dramatic contrast to anthracene (1,4) where the fluorescence features which exhibit oscillatory behavior are associated only with a single excitation energy, 1380 cm^{-1} above the S1 $^1B_{2u}$+ origin. Nevertheless, it is significant that in both anthracene and trans-stilbene, the energy resolved fluorescence at the excitation energy for which interference effects are observed is characterized by a relatively small degree of relaxed fluorescence and a comparatively larger amount of unrelaxed component. For example, upon excitation between 748 cm^{-1} and 1166 cm^{-1} above the S_1 origin of trans-stilbene, weak progressions are built upon the resonance fluorescence (figure 1). The appearance of quantum beats at moderate excess energies in large polyatomic molecules can be interpreted in the following manner. This argument is independent of how one defines or partitions the effective density of states, but rather reflects the intrastate coupling mechanisms which establish the effective molecular states. Within the zero order (normal mode) oscillator strength spanned by the laser excitation bandwidth, many molecular eigenstates are simultaneously prepared. The eigenstates are generated upon coupling of many different vibronic levels which originate from lower energy electronic manifolds. Each pair of eigenstates exhibits an oscillatory radiative component (10). At low

excess energies, by virtue of the fact that the finite number of eigenstates possess similar radiative dipole matrix elements to a common ground state and therefore the multiple oscillatory components destructively interfere, to produce single exponential emission decays. At very high excess vibrational energies, the large number of effective eigenstates ensures that coherence effects will be obscured. At intermediate excess energies, however, the eigenstates can be partitioned into a set which is radiatively coupled directly to the larger set which exhibits different radiative propensities. The intramolecular dynamics effectively projects out a set of eigenstates which are distinguished by, for example, unique anharmonic coupling or symmetry. Therefore, with appropriate excitation and detection conditions the potential for observing interference effects will be greater for the set of eigenstates defined by the unrelaxed fluorescence.

§5.4.2 *Quantum Beats and Vibrational Motion*

The most notable feature of the quantum beats which we would like to discuss in terms of the identification of the energy levels which are responsible for the interference phenomena in the frequency resolved fluorescence decay of trans-stilbene is the similarity of the Fourier components irrespective of the vibronic level which is initially prepared by the laser pulse. With the exception of excitation to S_1+780 cm^{-1}, all other states which exhibit beats, reflect a frequency of 734 MHz (figure 2 and table 3). Although the density of vibrational states originating from the first excited singlet manifold (assuming harmonic overtones (7)) rapidly increases from approximately 7 states/cm^{-1} to 300 states/cm^{-1} between 500 and 1200 cm^{-1} of excess energy, the dominant Fourier components of the beat pattern remain essentially unchanged. The fact that quantum

beats are only observed on features associated with the unrelaxed fluorescence component, suggests that the mutually interfering eigenstates arise from specific vibrational and/or rotational states which are initially prepared upon laser excitation and not as the result of subsequent redistribution processes which occur in the excited state manifold prior to radiative relaxation. The persistence of the 734 MHz Fourier component for several different transitions spanning a wide range of excess energies suggests that specific properties of vibrational or rotational modes could be responsible for the interference phenomena. We are inclined to develop an explanation in terms of the specific nature of the initially prepared vibrational states, as opposed to rotational states, for two reasons. First, the quantum beats do not appear consistently for all transitions which are excited in the pertinent excess energy region, and the magnitude and frequencies of the Fourier components are not identical. In large molecules, one would expect the rotational levels associated with a given vibrational mode to exhibit similar coupling and relaxation properties. Secondly, and more importantly, at these excess energies, the rotational density of states is very large. The rotational constants for trans-stilbene are on the order of 1 GHz and hence with a laser bandwidth of 0.5 A°, the excitation spans approximately 60 rotational states of a single vibrational level. Considering the large number of rotational states which are originally prepared by the laser pulse, it seems unlikely that their mutual interaction could be responsible for the regularity of the quantum beat pattern. The large number of oscillatory terms in the fluorescence would lead to destructive interference and effective single exponential decay.

By far the largest contribution to the vibrational density of states in

the first excited singlet state manifold of trans-stilbene is the low frequency phenyl torsional and bending modes. In addition to the previously documented (8,9) optically active modes at 40 cm^{-1} (C-phenyl torsion), 70 cm^{-1} (C_e-phenyl oop) and 94 cm^{-1} (C_e-C_e-phenyl bend), we observe transitions at 18 cm^{-1} and 28 cm^{-1} (table 3). The latter vibrations have been observed in low temperature (4.2 °K) Raman spectra (12). Considering the states between 1200 cm^{-1} and 700 cm^{-1} for which beats were observed, the energy difference between the various states is similar to the energies of the ethylene-phenyl torsional and bending modes and combinations thereof. Although this is perhaps not a unique designation, considering the large number of possible quasi-energetic states, it does at least suggest the association of ethylene-phenyl motion with the quantum beats. Whereas the absorption spectra are dominated by the large number of transitions to ethylene-phenyl torsional and bending modes of a_u and b_u symmetry, the energy resolved fluorescence is characterized by transitions primarily to a_g, C-C-C and C-C-H bending vibrations of the phenyl group. As shown in figure 6, quantum beats were only observed on transitions with frequencies corresponding to bending motions of the phenyl group.

Within the context of establishing the vibrational properties of the states which are responsible for the appearance of quantum beats in trans-stilbene, there are several consistent explanations which incorporate the interaction of the internal torsional motion of the two phenyls with respect to the ethylene plane. Both electron diffraction (13,14) and Raman (4,15) studies have established that in the vapor phase, trans-stilbene is non-planar and hence possesses C_2 symmetry. The non-planarity apparently results from a 30 degree orientation of the two

phenyl groups with respect to the ethylene bond, in addition to a departure from planarity of the ethylene double bond itself. The large degree of vibrational anharmonicity implied by the low symmetry suggests that combination bands are able to acquire substantial oscillator strength from association with the optically active fundamentals. This is confirmed by the large degree of spectral congestion which appears in the fluorescence excitation spectrum. Furthermore, as previously mentioned, the motional characteristics of the low frequency vibrations reflect torsional and bending motions of the phenyl group with respect to the ethylene double bond. It is therefore posssible that combination bands comprised of phenyl torsional and bending modes are quasi-degenerate with and couple to the optically active a_g, C-C-C bending and C-C-H bending vibrations. In this regard a theoretical approach has been developed for treating the interaction of internal rotation with other molecular vibrations (16).

In this interpretation, the potential energy surface for the internal phenyl rotation will be a function of the torsional coordinates. In trans-stilbene, the hindered rotation is stabilized by interaction with the twisted ethylene bond and not by the steric interactions between the ethylene hydrogens and the ortho phenyl hydrogens (12,13). Mixing of the wavefunctions in the resulting double minimum potential will cause an energy splitting of the torsional modes. Refinements to the degree of interaction between the two states will result from coupling between the two phenyl rotors. Studies have shown that methyl tops are significantly coupled even when they are removed by a single bond length form one another (17,18).

Unfortunately, the lack of a permanent dipole moment for trans-

stilbene and its analogues prevents the direct investigation of the torsional splittings using the techniques of microwave spectroscopy, and hence measurements of the magnitudes of the splittings and the barrier heights for the torsional potentials have been obtained using the less sensitive techniques of infrared and Raman spectroscopy. Such investigations have been confined to studies of ground state properties. This is because, although the potential for much better spectral resolution inherent for the UV energies necessary for investigating the excited state frequencies, the large number of states and large anharmonic coupling would make spectral assignments for large molecules difficult. Although the infrared and Raman spectra of trans-stilbene have been obtained in the liquid and solid (12,19,20), to our knowledge, corresponding spectra have not been observed for trans-stilbene in the gas-phase. Major low frequency torsional modes have been identified at 40.5, 64.7, and 125.0 cm^{-1} in the Raman spectrum of trans-stilbene at 4.2 °K (12). Furthermore, complex spectral regions were interpreted in terms of combination bands arising from the highly anharmonic low frequency fundamentals at 8 cm^{-1} and 25 cm^{-1} (12). Splittings in these fundamentals and their respective combination bands were not observed with 1 cm^{-1} spectral resolution. This is understandable since the linewidths are intrinsically broad due to solvent or solid interactions. Analogues of trans-stilbene have been studied in the gas phase and interpretation of their spectra can provide information concerning the magnitude for the energy of the torsional splitting as well as estimates for the potential barrier height for internal rotations.

Considerable experimental (18) and theoretical (21) work has been undertaken in an effort to understand the internal torsional dynamics of

molecules with two C_{3v} rotors in contrast to the dual C_{2v} rotors of trans-stilbene. Trans-2-butene represents the relevant structural analogue of trans-stilbene. The infrared (22) and Raman (17,22) spectroscopy of gaseous trans-2-butene reveals several low frequency transitions which have been attributed to torsional motion of the methyl groups. Transitions at 147 cm^{-1} and 305 cm^{-1} (156.9+147.0 cm^{-1}) exhibit splittings which are assigned to the 3,0← 2,0 and 3,0← 1,0 transitions, respectively. The splittings of the 147 cm^{-1} transition are easily resolved and found to be approximately 2 cm^{-1}. The investigators were unable to resolve the splittings of the 305 cm^{-1} transition with 0.25 cm^{-1} resolution although the presence of a splitting was inferred from the linewidth. The presence of the observed splittings was attributed to the proximity of the common 3,0 energy level to the barrier for torsional motion. Analysis using a semi-rigid two top model (21) established the barrier height for methyl torsion to be approximately 713 cm^{-1} (17).

Another structurally similar molecule which can be compared in order to gain an insight into the torsional dynamics of trans-stilbene is styrene. The internal torsional motion in styrene involves the rotation of a single phenyl ring with respect to the ethylenic plane. Infrared (23) and Raman (24) studies of gaseous styrene have failed to reveal resolvable energy level splittings of the ground state torsional modes. The potential barrier to internal rotation, however, has been estimated to be 623 cm^{-1}.

This correspondence of potential barriers to internal rotation and the resultant splitting of the ground state torsional modes in molecules which are structurally analogous to trans-stilbene lends support to the postulate that a similar splitting in a torsional mode of trans-stilbene is responsible for the quantum interference effects. The splittings observed

in the ground state vibrational modes for these molecules was on the order of 2 cm^{-1} (60 MHz) or less in comparison to the spacing implied by the Fourier components for our quantum beat spectra which are on the order of 1 GHz. It is probable that an altered excited state geometry, as compared to that of the ground state, would significantly influence the potential barriers to internal rotation. It is therefore possible to interpret the quantum beats which are observed upon excitation to moderate excess energies of the first excited singlet state as originating from the energy splitting of a single hindered internal torsional rotation which is incorporated in several combination bands. The dominant contribution of a single torsional mode would insure a constant energy splitting between eigenstates with similar radiative properties. A possible complication of this scheme is the presence of other low frequency torsional modes as previously discussed, which by increasing the complexity of the level structure would dissipate the interference effects. It may be however, that the radiative dipole matrix element for a single torsional mode is such that only certain states are projected in the unrelaxed emission component.

An alternative explanation for the nature of the states which are responsible for the quantum interference phenomenon in trans-stilbene can be made in terms of in-phase and out-of-phase combinations of the localized rotation of the two phenyl rings (25). Evidence supporting this interpretation comes from the observation that in the infrared and polarized Raman spectra of trans-stilbene (19,20), the a_g and b_u fundamentals appear in nearly degenerate pairs. The splitting between the two modes is, if measurable, on the order of 2 cm^{-1} or less. The inability to resolve the two components for many transitions may explain the anomalous

values for the depolarization rations obtained from Raman experiments (20). Again, an explanation for the consistency of the beat frequency is complicated by the large number of low frequency vibrations. Since the low frequency 16 cm^{-1}, 41 cm^{-1} and 115 cm^{-1} modes appear in the energy resolved fluorescence of trans-stilbene, a distortion form planarity in the excited state is implied. Considering the low C_2 symmetry, substantial anharmonic coupling among quasi-energetic states can be expected. It is, however, possible to conceive of a single torsional mode which is subject to parity induced splitting as being predominantly responsible for the consistency of the observed beat pattern.

In the previous arguments we have discussed the manifestations of the quantum interference effects observed for trans-stilbene in terms of their resulting from the hindered internal rotation of the phenyl groups with respect to the ethylenic bond. Estimates for the rotational barrier of similar molecules have been variously estimated to be on the order of several wavenumbers. A serious inconsistency arises when invoking this argument as an explanation for the quantum beats of trans-stilbene as the consequence of the identical beat frequency which persists despite the increasing excess excitation energy. In contrast, for a low potential barrrier to internal torsion, the beat frequency (reciprocal energy of the eigenstate separation) should decrease as a function of the excess energy, analogous to the prototypical doubling of the ammonia spectrum (26). The excess energy independent beat frequency observed for trans-stilbene would imply a large potential barrier, and therefore the question arises as to the origin of this deep-welled potential surface. A consistent explanation might be developed by considering the phenomenon of parity inversion which is closely associated with theoretical approaches

advanced to explain the racemization process (27,28). In this sense it is necessary to consider the time evolution of both phenyl rings with respect to each other. The combined motion of the phenyl groups can be either in, or out of phase, specifically, the orientation of the rings can be either symmetric or anti-symmetric with respect to the molecular inversion center, while the parity of the phenyls removes the degeneracy of their combined motion. When the violation of parity is possible, the potential minima in which the phenyl groups rotate is no longer symmetric. The coherent laser excitation apparently selects a single isomer, i.e. only one parity is optically active, since otherwise an initial phase relationship would not be established and consequently interference effects would not be observed. Optical selection of a parity specific isomer is not inconsistent with optical selection rules. In this manner the parity would be a property of the molecular system and independent of individual eigenstates. Along these lines, the racemization mediated by internal rotation of hindered biphenyls has been calculated to be on the order of 8000 cm^{-1} (29). It is also intriguing to consider that the tunneling may be along the potential surface responsible for isomerization.

In the current view (30) the barrier to isomerization in trans-stilbene arises from a crossing of the S_1 and S_2 surfaces, where the latter is predicted to have a minimum energy at a 90 degree orientation of the two C_e-phenyl bonds (30). The barrier to isomerization has recently been estimated to be approximately 1200 cm^{-1} above the S_1 surface based upon the observation of a rapid increase in the fluorescence decay rate at this excess energy (7). Considering that the region for which we observe quantum beats (500 $cm^{-1} \rightarrow 1200$ cm^{-1}) is near to the threshold, one would expect to observe an excess energy dependent change in the beat fre-

quency reflecting the proximity to the barrier. However, since the ethylene torsional modes are responsible for isomerization, while the totally symmetric C-C-C and C-C-H bending vibrations of the phenyl groups are the dominant, optically active modes, a transfer of energy subsequent to excitation of the initially prepared phenyl vibrations to the ethylene and phenyl torsions is implied. In this manner the optically active phenyl vibrations which exhibit interference effects in the energy resolved fluorescence would not be directly involved with the isomerization, but nevertheless might be perturbed by the crossing from the S_1 to S_2 surfaces.

The previous discussion has emphasized the interpretation of quantum beats in terms of their manifestation of essentially high resolution spectroscopy; in this case, specifically torsional mode splittings. The appearance of quantum beats in the time resolved fluorescence decay of large molecules also can be used to understand the underlying level structure of the molecular eigenstates which influence the intramolecular vibrational energy redistribution (4). Since dephasing is completed within the 50 psec time resolution of our experiments as supported by our failure to observe a rise-time in the energy resolved fluorescence decay, the spectral and temporal features which are monitored reflect the properties of the molecular eigenstates of the system and not the initially prepared zero-order levels. The fact that we observe quantum beats for spectral features of the unrelaxed fluorescence only, indicates that the energy deposited within the molecule becomes partitioned into separate ensembles of eigenstates which exhibit different and independent radiative properties which become manifest at long times in the frequency and temporally resolved fluorescence. For a given excess energy,

the eigenstates can exhibit properties of either discrete or continuum level structure. For trans-stilbene, the region of quasi-discrete level structure occurs between 500 and 1200 cm^{-1} of excess energy in the first excited singlet state as implied by the observation of quantum beats in the resolved fluorescence upon excitation to these energies. The upper limit for quasi-discrete structure coincides with the onset of significant trans-cis isomerization. On the other hand, the lower boundary appears at an energy where the average separation between vibrational states (200 GHz) becomes such that any resulting interference effects could not be observed with the 50 psec temporal resolution of these experiments. In this intermediate excess energy region, the majority of the energy which is initially deposited within the molecule becomes randomly redistributed among the vibrational and rotational modes as reflected in the predominant, congested relaxed fluorescence component. That the fluorescence is an accurate monitor of vibrational energy redistribution in trans-stilbene is implied by the near unity quantum yield for fluorescence. As in anthracene, it is interesting to find that coherence effects can be observed despite the high rotational density of states, thereby indicating that rotational coupling with the initially prepared states is much less important than vibrationally mediated energy redistribution.

§5.5 *Conclusion*

In view of the recent demonstration of quantum beats in anthracene, and the additional results presented in this paper on trans-stilbene, an understanding of the origin of quantum interference effects should provide insight into the mechanisms responsible for intramolecular energy and phase dynamics. We have discussed the quantum beats in trans-stilbene in terms of phenyl torsional motion and photoisomerization, in

an effort to explain the persistence of a single beat frequency upon excitation over a wide range of excess energies in the first excited singlet manifold. Clearly, a complete interpretation will require further experimental work including high resolution fluorescence excitation spectra and the study of substitution effects. In this regard, it will be important to search for quantum beats in other molecules which exhibit hindered internal motion and isomerization processes. Nevertheless, the data presented here should emphasize the potential of quantum interference effects to elucidate the dynamics of intramolecular vibrational energy and phase redistribution in isolated large molecules.

In addition, the evidence indicates that the quantum beats in large isolated molecules can be observed for well defined experimental conditions on a time scale which is readily accessible with current pulsed picosecond laser technology. As in anthracene, the appearance of quantum beats in the time and frequency resolved fluorescence is not compromised by the simultaneous preparation of many vibrational and rotational levels within the excitation bandwidth. The generality of this statement is suggested by the observation of quantum beats in anthracene and trans-stilbene which reflect, at least ostensibly, substantially different vibrational structure and relaxation mechanisms.

REFERENCES

1. W.R. Lambert, P.M. Felker and A.H. Zewail, J. Chem. Phys., **75,** 5958 (1981).

2. P.M. Felker, W.R. Lambert and A.H. Zewail, Chem. Phys. Lett., **89,** 309 (1982).

3. J. Chaiken, M. Gurnick and J.D. McDonald, J. Chem. Phys., **74,** 106 (1981).

4. W.R. Lambert, P.M. Felker and A.H. Zewail, to be published.

5. N.J. Turro, *Modern Molecular Photochemistry*, Benjamin, New York, 1978.

6. B.I. Greene, R.M. Hochstrasser and R.B. Weisman, J. Chem. Phys., **71,** 544 (1979).

7. J.A. Syage, W.R. Lambert, P.M. Felker, A.H. Zewail and R.M. Hochstrasser, Chem. Phys. Lett., **88,** 266 (1982).

8. A. Warshel, J. Chem. Phys., **62,** 214 (1975).

9. R.H. Dyck and D.S. McClure, J. Chem. Phys., **36,** 2326 (1962).

10. For example see K. Freed and A. Nitzan, J. Chem. Phys., **73,** 4765 (1980), and W. Rhodes, J. Chem. Phys., **86, 2657 (1982).**

11. G. Orlandi, P. Palmiari and G. Poggi, J. Am. Chem. Soc., **101,** 3492 (1979).

12. A. Bree and M. Edelson, Chem. Phys., **51,** 77 (1980).

13. M. Traettenberg, E.B. Fransten, F.C. Meljcroff and A. Hoekstra, J. Mol. Struct., **26,** 57 (1975).

14. A. Hoekstra, P. Meertens and A. Vos, Acta. Cryst., **B31,** 2813 (1975).

15. M. Edelson and A. Bree, Chem. Phys. Lett., **41,** 562 (1976).

16. C.R. Quade, J. Chem. Phys., **73,** 2107 (1980).

17. J.R. Durig, S.D. Hudson and W.J. Natter, J. Phys. Chem., **70,** 5747 (1979).

18. P. Groner, J.F. Sullivan and J.R. Durig, in *Vibrational Spectra and Structure, V.9,* ed. J.R. Durig, Elsevier Scientific, New York, (1981).

19. C. Pecile and B. Lunelli, Can. J. Chem., **47,** 243 (1969).

20. Z. Meic and H. Gusten, Spectrochim. Acta, **34A,** 101 (1978).

21. P. Groner and J.R. Durig, J. Chem. Phys., **66,** 1856 (1977).

22. J.R. Durig, C.W. Hanley and J. Bragin, J. Chem. Phys., **57,** 1425 (1972).

23. W.G. Fateley, G.L. Carlson and F.E. Dickson, Appl. Spectrosc., **22,** 650 (1968).

24. L.A. Carreira and T.G. Towns, J. Chem. Phys., **63,** 5283 (1975).

25. A. Bree and R. Zwarich, J. Mol. Struct., **75,** 213 (1981).

26. C.H. Townes and A.L. Schawlow, *Microwave Spectroscopy* Dover Publications, New York, 1975.

27. R.A. Harris and L. Stodolsky, J. Chem. Phys., **74,** 2145 (1981).

28. R.A. Harris and L. Stodolsky, Phys. Lett., **788,** 313 (1978).

29. F.H. Westheimer, J. Chem. Phys., **15,** 252 (1947).

30. G. Orlandi and W. Siebrand, Chem. Phys. Lett., **30,** 352 (1975).

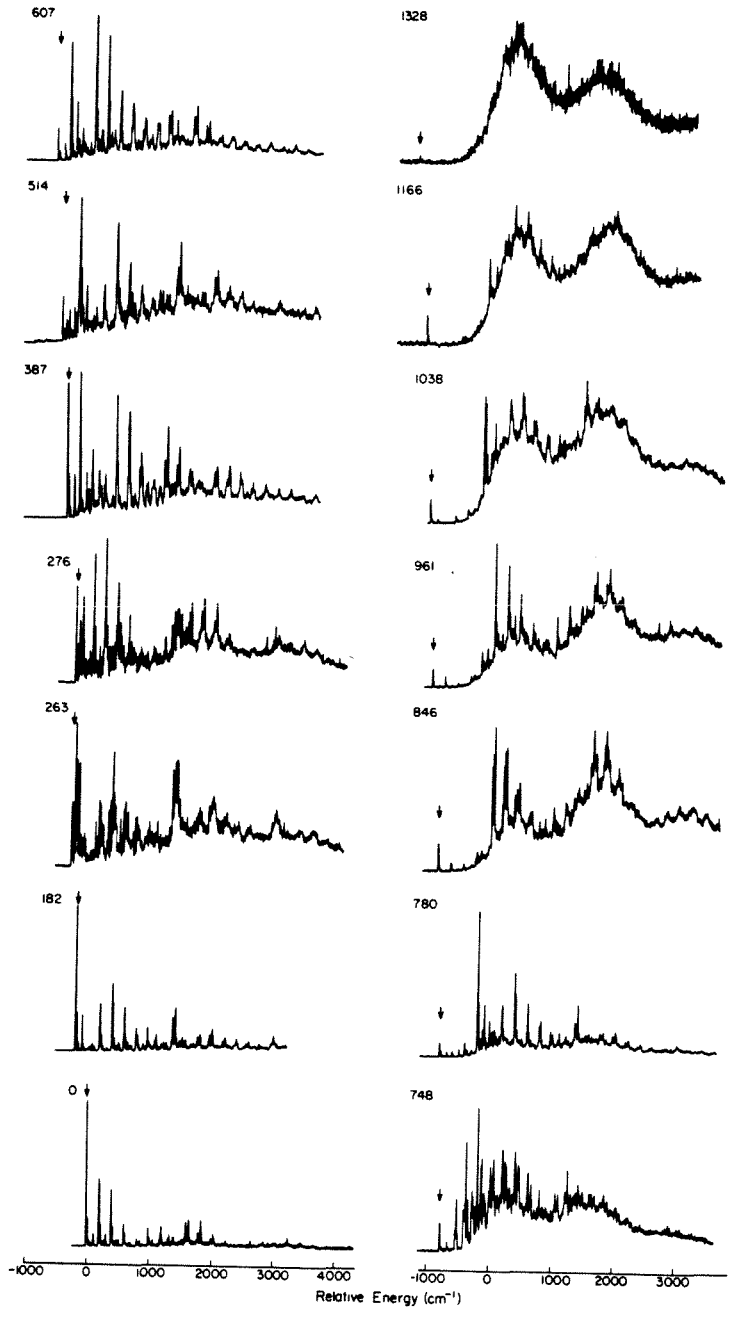

Figure 1.

Energy resolved fluorescence of trans-stilbene for excitation at different excess energies relative to the S_1 $^1B_{2u}$* origin, as indicated in the figure. The spectra show the evolution from unrelaxed to relaxed fluorescence as the excitation energy is increased. The spectral resolution was 0.25 A°. The expansion conditions were; T_0=350 °K, P_0 = 40 psi neon, D = 150 microns and X = 5 mm. The excitation energy relative to the 0-0 origin is indicated by arrows.

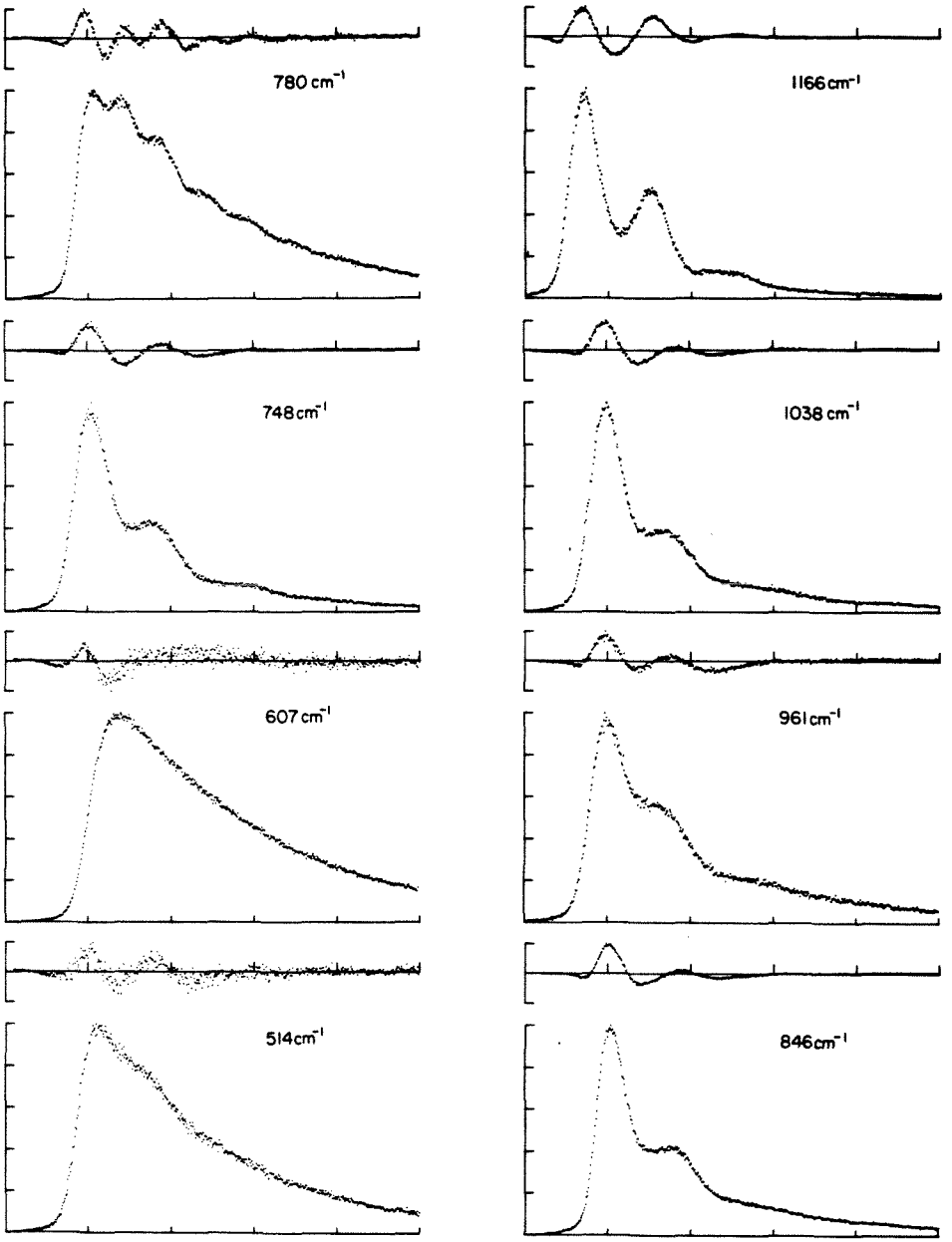

Figure 2.

Quantum beats on the resonance fluorescence ($\lambda_{det} = \lambda_{exc}$) component of trans-stilbene upon excitation to various vibronic levels in the S_1 manifold. Quantum beats are not observed for excitation to S_1 + 607 cm^{-1}, however the spectrum is included for comparison. Except for the 780 cm^{-1} transition which exhibits a beat frequency of 1309 MHz, the frequency for the other vibronic levels is independent of the excess energy, being 734 MHz. The residual obtained by subtracting the best single exponential fit from the data appears above each temporal decay. The amplitude of the residual provides a measure of the modulation depth. The system response time was 250 psec, the laser bandwidth was 0.5 A°, and the coherence width of the laser excitation was 3 cm^{-1}. The corresponding energy resolved fluorescence spectra are shown in figure 1.

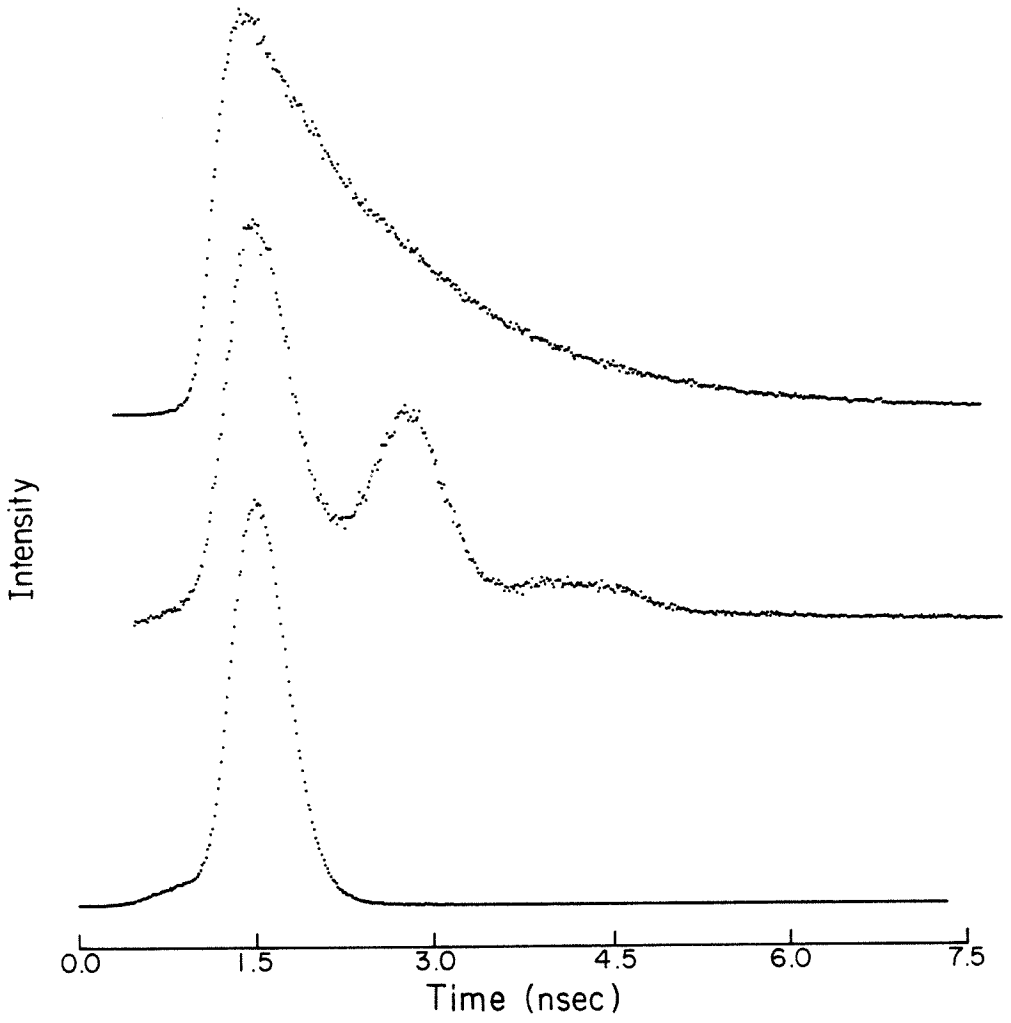

Figure 3.
The quantum beat pattern for the resonance fluorescence, for excitation to the 166 cm^{-1} vibration, is compared to a single exponential decay and the system response function (~ 500 psec). The beat pattern is seen to be defined by the system response function. The expansion conditions were the same as those indicated for figure 1.

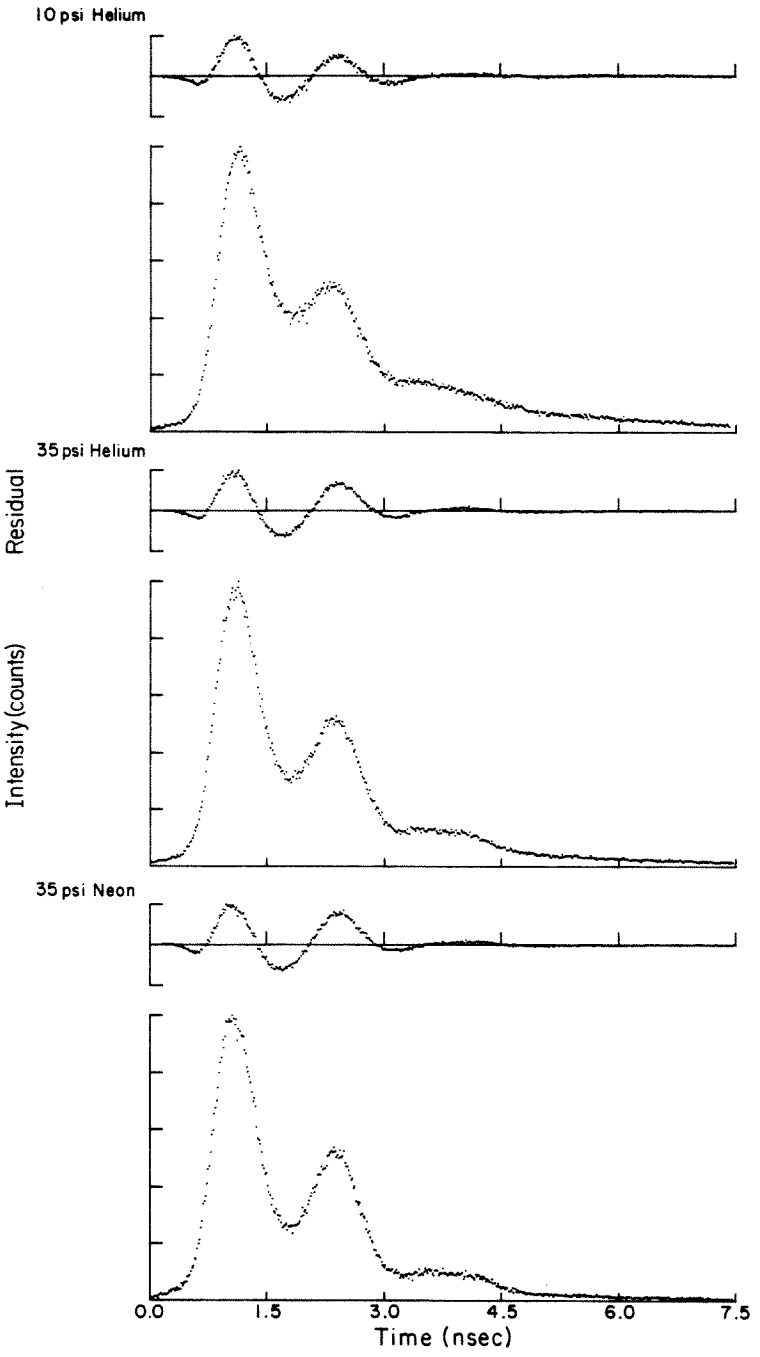

Figure 4.

The influence of the intramolecular temperature upon the modulation depth of the quantum beat pattern for trans-stilbene. The rotational and vibrational temperatures decrease with increasing backpressure and mass of the carrier gas. The increased modulation depth associated with lower internal temperatures is interpreted as reflecting the reduction in the number of vibronic levels initially prepared by the laser which contribute to destructive interference of the oscillatory component. Excitation is to the 1162 cm^{-1} vibronic level.

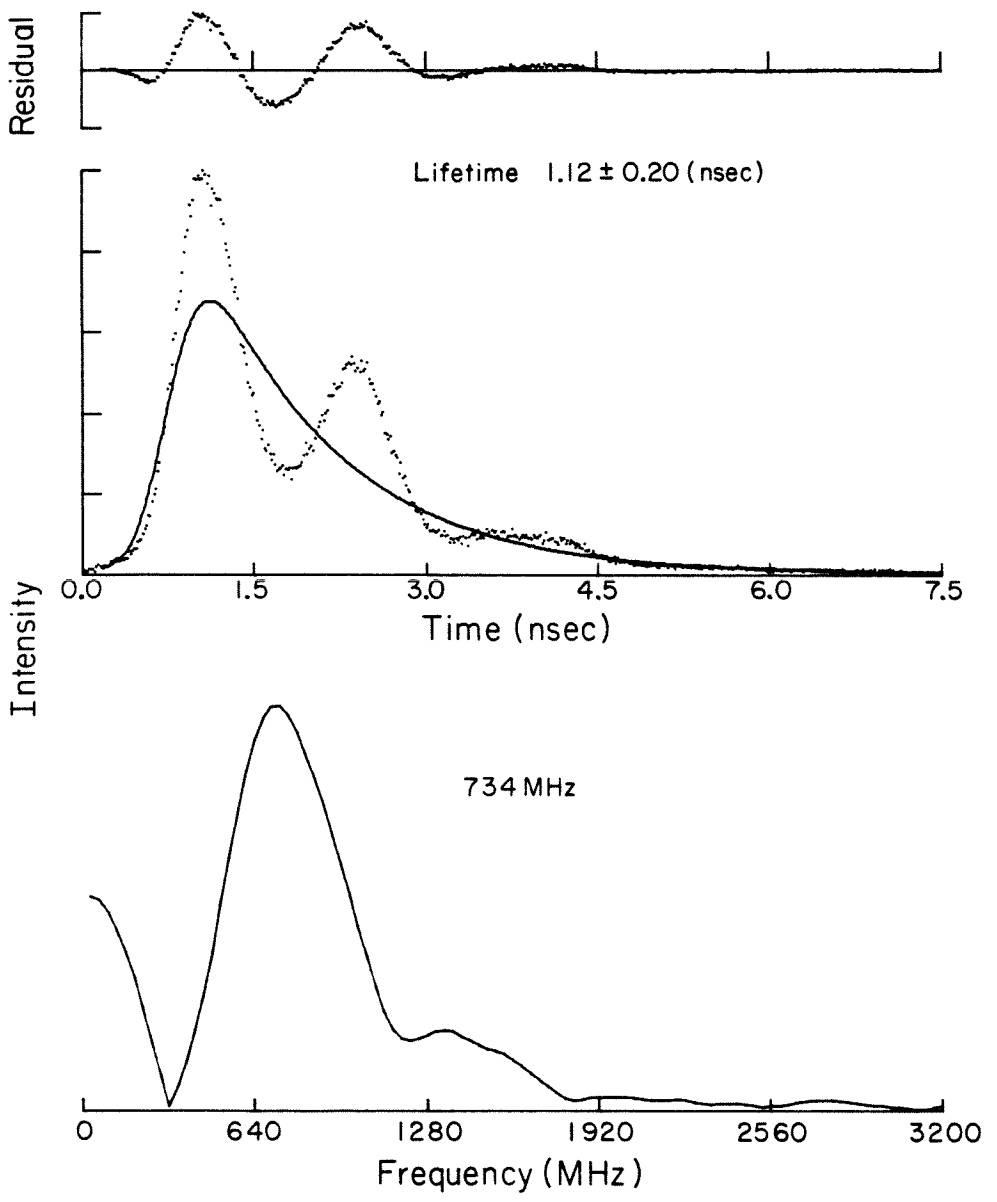

Figure 5.
An example of the fit of the quantum beat spectrum to a single exponential decay. The residual, representing the unweighted difference between the data and the fit, is Fourier transformed to generate the frequency domain spectrum. The FWHM of the Fourier component is 501 MHz.

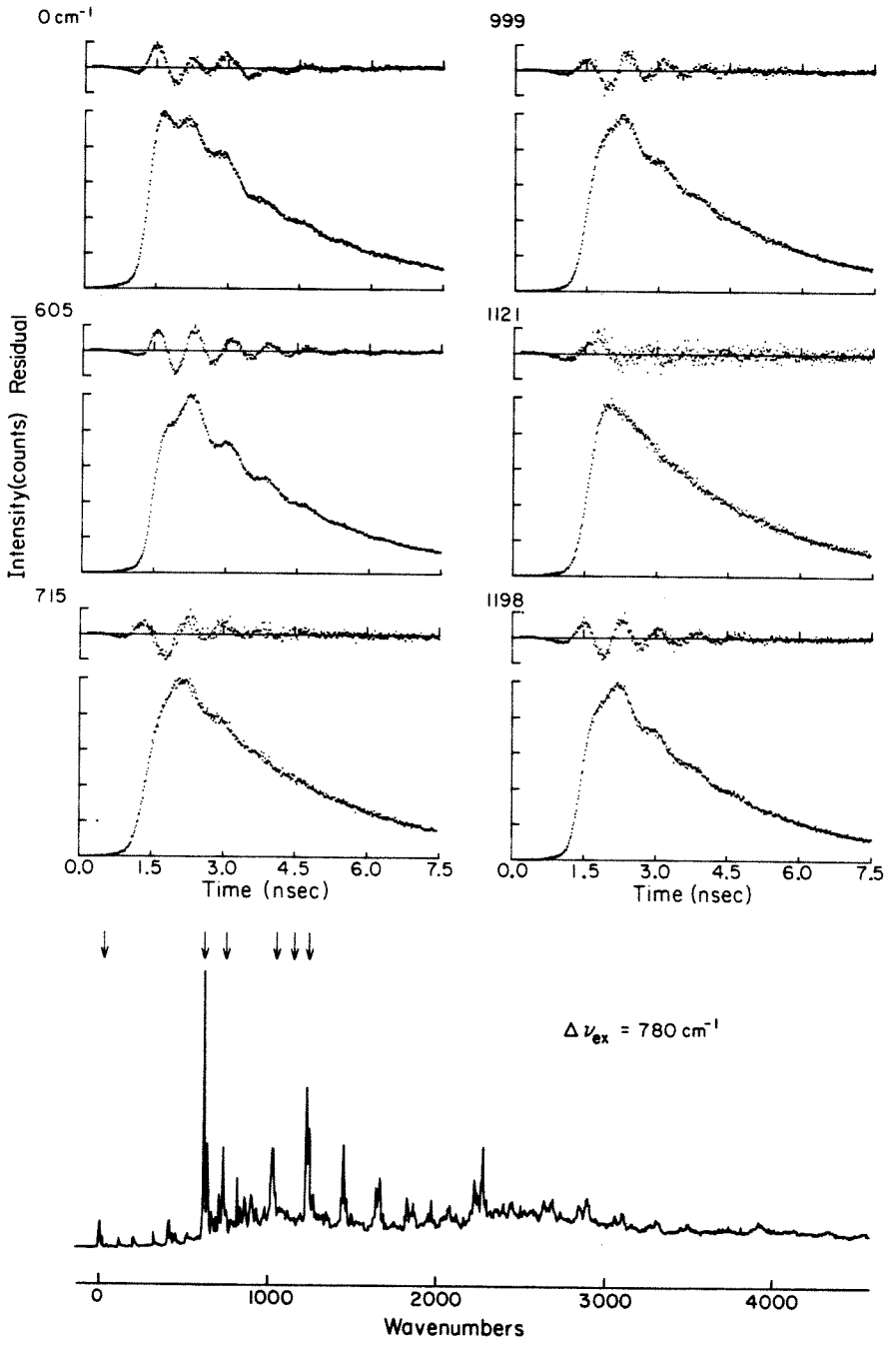

Figure 6.

Time and energy resolved fluorescence spectra for trans-stilbene upon excitation to the S_1 + 780 cm^{-1} (λ_{ex} = 3028.5 A°) vibronic state. The corresponding relative energies at which the fluorescence decays were obtained is indicated by arrows. The decays exhibit a dominant beat frequency of 1309 MHz. The decay rates are, in order of increasing detection energy: 399 MHz, 398 MHz, 352 MHz, 391 MHz, 388 MHz, and 401 ± 12 MHz. The transitions can be assigned to totally symmetric vibrations of the phenyl ring corresponding to (8): 605 cm^{-1}, CCC bend; 715 cm^{-1}, CCC bend; 999 cm^{-1}, CCH and CCC bend; 1121 cm^{-1}, relaxed fluorescence; and 1198 cm^{-1}, CCH bend.

Table 1. Ground state vibrational frequencies and assignments for trans-stilbene.

Relative Energy, cm^{-1} [a]	Relative Intensity	Assignment[a]
0	100	0-0 origin
16	28	--
41	8	a_u 38, $_C$e-φ tors
74	2	a_u 60, C_e-φ oop
115	13	b_g 121, C-φ tors
205	75	a_g 228, C_e-C_e-φ bend
222	35	(16+205)
242	13	b_g 235, C-φ tors
271	4	a_u 278, C_e-p oop
295	5	a_g 305, C_e-C-C bend
323	13	(115+205)
412	37	(2x205)
432	15	(2x205+16)
456	5	b_g 447, ring def, C_e-C_e tors
489	5	a_u 486, ring def, C_e-C_e tors
521	5	(2x205+115)
541	2	(2x205+115+16)
604	16	a_g 664, C-C-C bend
640	4	a_u 630, C-C-C bend
700	3	a_u 713, ring def
723	3	b_g 719, C-H oop
739	3	(723+16)
822	8	b_g 826
838	4	(822+16)

865	6	(822+41)
884	2	(822+16+41)
908	2	b_g 919
994	17	a_g 997, C-C-H bend
1009	6	(993+16)
1036	3	(993+41)
1060	5	(993+74)
1094	2	a_g 1085, C-C-H bend
1110	3	(993+115)
1148	4	a_g 1153, C-C-H bend
1198	16	(994+205)
1213	9	(994+205+16)
1236	9	(994+205+16)
1274	5	(994+205+74)
1316	8	(994+205+115)
1335	10	a_g 1337, C_e-C_e-H bend
1354	5	(1148+205)
1388	9	(1198+205)
1404	9	(1213+205)

a. Energies of the vibronic bands observed in the energy resolved fluorescence relative to the $S_1\ ^1B_u{}^+ \leftarrow S_0\ ^1A_g$ origin at 32239.3 cm^{-1}. Relative accuracy is ± 5 cm^{-1}.

b. The assignments are based on those indicated in references 6 and 7. Combination bands are indicated considering likely progression intensities.

Table 2. Frequencies and assignments for the low energy excited state vibrations of trans-stilbene.

Relative Energy[a], cm^{-1}	Assignment[b]
18	--
28	--
40	a_u 41, C_e-φ tors
70	a_u 60, C_e-φ oop
83	(2×40)
94	b_u 88, C_e-C_e-φ bend
108	(70+40)
120	--
132	(94+40)
147	--
154	(70+83)
160	(94+70)
174	(2×40+94)
186	(2×94)
194	a_g 231, C_e-C_e-φ bend
217	(194+18)
223	(194+28)
228	--
236	(194+41)
248	--
260	--
264	(194+70)
271	--
278	(2×40+194)

282	a_g 283 C_e-C-C bend
289	--
295	(194+70+28)
307	(194+70+40)
313	(282+28)
321	(282+40)

a. Energies observed in the fluorescence excitation spectrum of trans-stilbene relative to the S_1 $^1B_2 \leftarrow S_0$ ^1A_g origin at 32239.3 cm^{-1}. The relative accuracy is ± 5 cm^{-1}. Only low frequency vibrations are included due to the spectral congestion at higher excess energies. The relative intensities are not included since the spectra were not normalized to the laser power.

b. The assignments were made base on comparison with those given in references 6 and 7.

Table 3. Quantum beat frequencies observed in the energy resolved fluorescence of trans-stilbene.[a]

Excitation Energy[b]	Beat Frequency, MHz[c] Resonance Fluorescence	Unrelaxed Fluorescence
298	--	--
491	734	--
624	--	--
748	702	--
780	1309	1309
846	734	--
961	734	734
1038	734	--
1166	734	817

a. The corresponding energy and time resolved fluorescence spectra are presented in figures 1 and 2, respectively.

b. The energy is relative to the $^1B_u \leftarrow {}^1A_g$ origin at 32239.3 cm^{-1}. The excitation bandwidth was 0.5 A° and the coherence width was 3 cm^{-1}.

c. The dominant beat frequencies for the various transitions is given in MHz. The resonance fluorescence refers to detection (bandwidth = 0.5 A°) at the excitation wavelength. Quantum beats were also observed on some features corresponding to the unrelaxed fluorescence components (progressions built upon the 0-0 origin, commensurate with ground state vibrational frequencies).

Table 4. Fluorescence decay rates for the energy resolved fluorescence of trans-stilbene at intermediate excess energies.[a]

Excitation Energy[b]	Fluorescence Lifetime, nsec.[c]	
	Resonance Fluorescence	Unrelaxed Fluorescence
298	2.53	--
404	2.58	--
491	2.40	--
624	2.74	2.74
748	1.46	2.59
780	2.49	2.49
846	1.68	2.49
961	1.90	2.70
1038	1.41	2.15
1166	1.24	2.24

a. The corresponding energy and time resolved fluorescence spectra are presented in figures 1 and 2, respectively.

b. The energy is relative to the $^1B_u \leftarrow {}^1A_g$ origin at 32239.3 cm^{-1}.

c. The definition of the resonance and unrelaxed fluorescence components are given in table 3.